UNIVERSITY OF ALBERTA

PREDICTION OF VENTILATION, HEAT TRANSFER AND MOISTURE TRANSPORT IN ATTICS

BY

IAIN STUART WALKER

A thesis submitted to the Faculty of Graduate Studies and Research in partial fulfilment of the requirements for the degree of Doctor of Philosophy.

DEPARTMENT OF MECHANICAL ENGINEERING

Edmonton, Alberta
Spring 1993

Abstract

The attic space of most residential buildings is well insulated from the house below, and therefore experiences extreme temperature conditions on seasonal and diurnal cycles. This can cause moisture entering the attic through the ceiling from the house, or through other leaks from outside, to accumulate in or on interior wood surfaces. This moisture accumulation leads to structural degradation and the growth of micro-organisms.

An attic simulation model has been developed for this study as a practical method of examining attic moisture problems. The model was validated using measured data from the Alberta Home Heating Research Facility. After validation the attic simulation model was used in parametric simulations over a wide range of ambient weather conditions to examine strategies for moisture control. The new methods of attic simulation and the other important contributions of this study are:

- the development of a two zone attic ventilation model that calculates the house, attic and interzonal (ceiling) flow. The ventilation model calculates wind shelter using a new wind shadow method and calculates the shelter and wind pressure coefficients as continuous functions of wind direction.
- the coupling of heat transfer and ventilation models.
- the use of a complete transient mass balance for the attic moisture that includes the wood surfaces.
- the use of combined ventilation heat transfer and moisture transport models.
- calculation of ventilation rates, temperatures and moisture levels using envelope leakage, indoor temperature and relative humidity, and ambient weather conditions
- the development of a comprehensive data base of measurements for evaluating attic models and identifying important parameters for attic moisture accumulation.

The results of the simulations have shown that increased attic ventilation rates are not always a useful strategy for controlling moisture problems and that appropriate strategies are dependent on climate and attic construction. At low ventilation rates the capacity for moisture removal is small and at high ventilation rates the additional cooling of the attic causes more moisture deposition. The optimum ventilation rate for a maritime climate has been found using the model developed for this study.

Acknowledgements

The author would like to thank Dr. T.W. Forest and Dr. D.J. Wilson for their encouragement, guidance and support throughout this project. The author is also grateful to the examining committee of Dr. J.T. Ryan, Dr. J.D. Wilson and Dr. R.W. Besant for their time and consideration of this thesis and their advice concerning improvements made to this thesis.

Financial support was provided by the R.M. Hardy Engineering Enrichment Fund (University of Alberta), Canada Mortgage and Housing Corporation, Energy, Mines and Resources (Canada), and the Natural Sciences and Engineering Research Council.

I would also like to thank Mark Ackerman, Wayne Pittman and John Foy for their technical and moral support, as well as the Department of Mechanical Engineering machine shop staff and technicians for their high quality of workmanship and technical assistance.

Table of contents

Page

List of Tables

List of Figures

Nomenclature

a - Exponent for wake mean velocity decay
A - Surface area [m^2]
A_i - Area of Surface i [m^2]
A_{in} - House internal surface area [m^2]
$A_{\Delta P}$ - Leakage area at ΔP pressure difference [m^2]
A_{L4} - Four Pascal leakage area [m^2]
B_1 - Constant for wake mean velocity decay
B_2 - Constant for wake mean velocity decay
B_3 - Constant for evaluating wood moisture content [°C]
B_4 - Constant for evaluating wood moisture content
B_5 - Constant for evaluating wood moisture content
B_6 - Constant for evaluating wood moisture content
B_7 - Constant for evaluating wood moisture content
Bi - Biot number
Bi_{H2O} - Biot number for water vapour mass transfer
C - Flow coefficient [$m^3/(sPa^n)$]
C_c - Distributed building leakage coefficient for the ceiling [$m^3/(sPa^n)$]
C_d - Distributed building leakage coefficient [$m^3/(sPa^n)$]
$C_{d,a}$ - Distributed attic leakage coefficient [$m^3/(sPa^n)$]
C_f - Distributed building leakage coefficient at floor level [$m^3/(sPa^n)$]
$C_{f,i}$ - Distributed building leakage coefficient at floor level, below wall i [$m^3/(sPa^n)$]
C_F - Flue flow coefficient [$m^3/(sPa^n)$]
C_{ref} - Reference leakage coefficient [$m^3/(sPa^n)$]
$C_{s,i}$ - Soffit or gable end leakage coefficient above wall i [$m^3/(sPa^n)$]
C_V - Vent leakage coefficient [$m^3/(sPa^n)$]
$C_{w,i}$ - Distributed building leakage coefficient in the i^{th} wall [$m^3/(sPa^n)$]
C_r - Pitched roof surface coefficient [$m^3/(sPa^n)$]
C_{sh} - Specific heat [J/KgK]
$C_{sh,\alpha}$ - Specific heat of air [J/KgK]
$C_{sh,i}$ - Specific heat of node i [J/KgK]
$C_{sh,W}$ - Specific heat of wood [J/KgK]
$C_{sh,\delta}$ - Specific heat of drywall [J/KgK]
Cp - Wind pressure coefficient

Cp_F - Wind pressure coefficient for furnace flue

Cp_i - Wind pressure coefficient for i^{th} wall of the building

$Cp_{r,i}$ - Wind Pressure coefficient for i^{th} pithced roof surface

Cp_f - Wind pressure coefficient for a crawlspace

Cp_{fan} - Wind pressure coefficient for a fan

Cp_V - Wind pressure coefficient for a vent

Cp(i) - Wind pressure coefficient for wind normal to wall i

d - Distance between downwind wall of obstacle and upwind wall of building [m]

D_F - Diameter of furnace flue [m]

D_L - Largest building dimension [m]

D_Y - Smallest building dimension [m]

D_W - Diffusion coefficient for moisture in wood [m^2/s]

E_b - Black body emissive power [W/m^2]

$E_{b,i}$ - Black body emissive power for surface i [W/m^2]

$E_{b,g}$ - Black body emissive power of ground and clouds

$E_{b,sky}$ - Black body emissive power of the sky [W/m^2]

F - Switching function parameter for pitched roof surface pressure coefficients

F_{i-j} - Radiation view factor from surface i to surface j

F_{r-g} - Radiation view factor from the pitched roof sheathing surface to the ground and clouds

F_{h-sky} - Radiation view factor from horizontal surface to the sky

F_{r-sky} - Radiation view factor from pitched roof sheathing surface to the sky

F_{7-in} - Radiation view factor for house interior

g - Gravitational acceleration [m/s^2]

G - Total incident radiation on the surface [W/m^2]

G_i - Incident radiation on surface i [W/m^2]

Gr - Grashof Number

h_U - Forced convection heat transfer coefficient [$W/(m^2K)$]

$h_{U,i}$ - Forced convection heat transfer coefficient for node i [$W/(m^2K)$]

h_T - Free convection heat transfer coefficient [$W/(m^2K)$]

$h_{T,i}$ - Free convection heat transfer coefficient for node i [$W/(m^2K)$]

$h_{R,i-j}$ - Radiation heat transfer coefficients from surface i to j [$W/(m^2K)$]

$h_{R,i-g}$ - Radiation heat transfer coefficient from roof surface i to the ground and clouds [$W/(m^2K)$]

$h_{R,i-sky}$ - Radiation heat transfer coefficient from roof surface i to the sky [$W/(m^2K)$]

$h_{R,7\text{-}in}$ - Radiation heat transfer coefficient from ceiling to the house [W/(m^2K)]
h_v - Mass transfer coefficient for water vapour [m/s]
$h_{v,i}$ - Mass transfer coefficient for water vapour at node i [m/s]
h_{gs} - Latent heat of sublimation for water [KJ/Kg]
H_b - Height of bottom of window or door opening above grade [m]
H_t - Height of top of window or door opening above grade [m]
H_e - Eaves height of building above grade [m]
H_{fan} - Height of fan above grade [m]
H_f - Height of floor level leakage above grade [m]
H_F - Height above grade of top of furnace flue [m]
H_{met} - Height of measurement of meteorological wind speed measurement above grade [m]
H_{NL} - Height of neutral pressure level above grade [m]
$H_{NL,i}$ - Height of neutral pressure level above grade on the i^{th} wall [m]
$H_{NL,r}$ - Height of neutral pressure level above grade on pitched roof [m]
H_p - Height of roof peak above grade [m]
H_{ref} - Reference height for correcting meteorological wind speeds [m]
H_s - Height of soffit above grade [m]
H_V - Height of vent above grade [m]
J - Total radiation leaving surface [W/m^2]
J_i - Total radiation leaving surface i [W/m^2]
k - Thermal conductivity [W/mK]
k_Σ - Thermal conductivity of snow [W/mK]
k_W - Thermal conductivity of wood [W/mK]
K - Window and door orifice coefficient
K_D - Orifice discharge coefficient
L - Length scale for convection heat transfer [m]
Le - Lewis number
L_b - Chacteristic building dimension [m]
L_i - Length of i^{th} wall [m]
L_r - Perimeter length of building [m]
L_S - Length of sheltered wall [m]
L_w - Length of wall [m]
m_v - Mass of water at a node [Kg]
m_r - Total mass of water condensed at a node [Kg]

m_w - Mass of wood [Kg]
$m_{w,i}$ - Mass of wood at node i [Kg]
M - Mass flow rate [Kg/s]
M^i - Mass flow rate at time i [Kg/s]
M_a - Attic ventilation rate [Kg/s]
M_c - Mass flow rate through ceiling [Kg/s]
M_τ - Condensed mass change [Kg/s]
$M^j_{\tau,i}$ - Condensed mass change at node i at time j [Kg/s]
M_{fan} - Mass flow rate through a fan [Kg/s]
$M_{fan,a}$ - Mass flow rate through an attic fan [Kg/s]
M_f - Mass flow rate through crawlspace leaks [Kg/s]
$M_{f,i}$ - Mass flow rate through floor level leaks below wall i [Kg/s]
M_F - Mass flow rate through the furnace flue [Kg/s]
M_r - Mass flow rate through pitched roof surface [Kg/s]
$M_{r,in}$ - Mass flow rate in through pitched roof surface [Kg/s]
$M_{r,out}$ - Mass flow rate out through pitched roof surface [Kg/s]
$M_{s,i}$ - Mass flow rate through the i^{th} attic soffit [Kg/s]
M_{ss} - Source or sink term for attic air mass balance [Kg/s]
M_V - Mass flow rate through house vent [Kg/s]
$M_{V,a}$ - Mass flow rate through attic vent [Kg/s]
M_v - Mass flow rate of water vapour [Kg/s]
$M_{v,i}$ - Mass flow rate of water vapour at node i [Kg/s]
$M_{w,i}$ - Mass flow rate through wall i [Kg/s]
$M_{w,i,in}$ - Mass flow rate in through wall i [Kg/s]
$M_{w,i,out}$ - Mass flow rate out through wall i [Kg/s]
M_{in} - Mass flow into building [Kg/s]
M_{out} - Mass flow out of building [Kg/s]
$M_{in,a}$ - Mass flow into attic [Kg/s]
$M_{out,a}$ - Mass flow out of attic [Kg/s]
n - Flow exponent
n_c - Flow exponent for ceiling leakage
n_d - Flow exponent for distributed house leakage
$n_{d,a}$ - Flow exponent for distributed attic leakage
n_f - Flow exponent for floor level leakage
n_F - Flow exponent for furnace flue

n_r - Flow exponent for pitched roof slope leakage

n_V - Flow exponent for a vent

$n_{w,i}$ - Flow exponent for wall i

N - Number of injections per hour in the attic

Nu - Nusselt number

p - Power law exponent for atmospheric wind velocity profile at the building site

p_{met} - Power law exponent for atmospheric wind velocity profile at the meteorological station

p_{fan} - Power law exponent for fan flow

P - Pressure [Pa]

P_a - Pressure inside attic [Pa]

P_{in} - Pressure inside house [Pa]

P_∞ - Atmospheric pressure [Pa]

P_o - Wind stagnation pressure [Pa]

$P_{in,z}$ - Pressure on inside surface of building [Pa]

$P_{out,z}$ - Pressure on outside surface of building [Pa]

P_v - Water vapour pressure [Pa]

$P_{v,i}$ - Water vapour pressure at node i [Pa]

$P_{v,in}$ - Water vapour pressure inside house [Pa]

P_v^j - Vapour pressure at time j [Pa]

P_{vs} - Saturation vapour pressure [Pa]

$P_{vs,i}$ - Saturation vapour pressure at node i [Pa]

P_U - Wind reference pressure [Pa]

P'_T - Pressure gradient from indoor-outdoor temperature differences [Pa/m]

$P'_{T,a}$ - Pressure gradient from attic-outdoor temperature differences [Pa/m]

P_b - Window and door flow coefficient at bottom of opening [m^2/s^2]

P_t - Window and door flow coefficient at top of opening [m^2/s^2]

Pr - Prandtl number

q - Heat transfer rate [W]

q_K - Conduction heat transfer rate [W]

q_R - Radiation heat transfer rate [W]

$q_{R,i}$ - Net radiation heat transfer rate for surface i [W]

$q_{R,i-j}$ - Rate of radiant heat leaving surface i reaching surface j [W]

q_U - Forced convection heat transfer rate [W]

q_T - Free convection heat transfer rate [W]

q_{ss} - Source or sink heat transfer rate for attic air [W]
Q - Volume Flow rate [m^3/s]
Q_a - Attic volume ventilation rate [m^3/s]
$Q_{a,n}$ - Normalised attic ventilation rate
Q_{180} - Mean normalised attic ventilation rate for south winds
Q_{rated} - Rated fan flow rate [m^3/s]
R - Thermal resistance [m^2K/W]
R_i - Thermal resistance of node i [m^2K/W]
R_χ - Insulation thermal resistance [m^2K/W]
R_A - Drywall thermal resistance [m^2K/W]
R_Σ - Thermal resistance of snow [m^2K/W]
R_c - Total thermal resistance of ceiling [m^2K/W]
R_W - Wood thermal resistance [m^2K/W]
R_{H2O} - Gas constant for water vapour [J/KgK]
R_{R22} - Gas constant for R22 [kJ/KgK]
Re - Reynolds number
RH - Relative Humidity
RH_a - Relative humidity in the attic
RH_{in} - Relative humidity in the house
RH_{out} - Relative humidity outdoors
S - Distance from building to upwind obstacle [m]
S_C - Fraction of sky covered by cloud
S_{up} - Distance from obstacle to wall 1 [m]
S_{down} - Distance from obstacle to wall 2 [m]
S_U - Wind shelter factor
$S_U(i)$ - Wind shelter factor for winds normal to wall i of the building
$S_{U,CL}$ - Wind shelter factor on wake Centre Line
$S_{U,fan}$ - Wind shelter factor for a fan
$S_{U,F}$ - Wind shelter factor for the furnace flue
$S_{U,V}$ - Wind shelter factor for a vent
$S_{U,i}$ - Wind shelter factor for i^{th} wall of the building
t - Time [s]
t_{avg} - Averaging time for standard deviation of wind direction [s]
t_{avg1} - Averaging time for standard deviation of wind direction [s]
T - Temperature [K]

T^j - Temperature at timestep j [K]
T_{ave} - Average indoor-outdoor temperature difference [C]
T_a - Attic air temperature [K]
T_{in} - Temperature of inside air [K]
T_ϵ - Film temperature [K]
T_F - Heated flue gas temperature [K]
T_{out} - Temperature of outdoor air [K]
T_{ref} - Reference temperature [K]
T_{sky} - Sky temperature [K]
T_i - Temperature of surface i [K]
T_1 - Temperature of the attic air [K]
T_2 - Temperature of the underside of the north sheathing [K]
T_3 - Temperature of the outside of the north sheathing [K]
T_4 - Temperature of the underside of the south sheathing [K]
T_5 - Temperature of the outside of the south sheathing [K]
T_6 - Temperature of mass of wood in joists and trusses [K]
T_7 - Temperature of the ceiling inside the house [K]
T_8 - Temperature of the attic floor [K]
T_9 - Temperature of the inside of the gable end walls [K]
T_{10} - Temperature of the outside of the gable end walls [K]
U - Reference eaves height wind speed [m/s]
U_{CL} - Wind speed on wake centre line at eaves height [m/s]
U_F - Wind speed at flue top [m/s]
U_{in} - Inflow velocity at height z for flow through doors and windows [m/s]
U_{rms} - Root mean square of turbulence velocities [m/s]
$U_{rms,o}$ - Root mean square of additional turbulence provided by an obstacle [m/s]
U_S - Effective sheltered wind speed [m/s]
U_U - Attic internal convection velocity [m/s]
V - Volume [m^3]
V_i - Volume of node i [m^3]
V_{inj} - Average volume or R22 released per injection [m^3/injection]
V_a - Attic volume [m^3]
W_{MC} - Wood moisture content [% or mass H_2O/mass of wood]
$W^j_{MC,i}$ - Wood moisture content for node i at time step j [%]
W - Width of door or window opening [m]

Y_T - Free convection heat transfer parameter [$W/(m^2K^{4/3})$]

z - Height above grade level [m]

Greek Symbols

α - Radiation absorbtivity

α_i - Radiation absorbtivity of surface i

β - Angle of tilted surface from horizontal [degrees]

β_T - Volume coefficient of thermal expansion

Γ - Dummy variable for integration of wall and window/door flows

δ_z - Area averaged height of surface roughness elements [m]

ΔP - Pressure difference [Pa]

ΔP_T - Pressure difference due to temperature effect [Pa]

$\Delta P_{T,a}$ - Pressure difference due to temperature effect for the attic [Pa]

ΔP_U - Pressure difference due to wind effect [Pa]

ΔP_c - Pressure difference across the ceiling [Pa]

ΔP_e - Pressure difference at eaves height above grade [Pa]

ΔP_{fan} - Pressure difference across a fan [Pa]

$\Delta P_{fan,a}$ - Pressure difference across an attic fan [Pa]

ΔP_f - Pressure difference across crawlspace leakage [Pa]

$\Delta P_{f,i}$ - Pressure difference across the i^{th} floor level leak [Pa]

ΔP_F - Pressure difference across furnace flue [Pa]

ΔP_I - Internal house pressure difference [Pa]

$\Delta P_{I,a}$ - Internal attic pressure difference [Pa]

ΔP_p - Pressure difference at roof peak [Pa]

ΔP_r - Pressure difference across pitched roof surface [Pa]

$\Delta P_{s,i}$ - Pressure difference across soffit above wall i [Pa]

ΔP_V - Pressure difference across a fan [Pa]

$\Delta P_{V,a}$ - Pressure difference across an attic fan [Pa]

$\Delta P_{w,i}$ - Pressure difference across i^{th} wall [Pa]

ΔP_v - Water vapour pressure difference [Pa]

ΔP_b - Pressure difference at the bottom of the wall [Pa]

ΔP_t - Pressure difference at the top of the wall [Pa]

ΔP_{rated} - Rated pressure for a fan [Pa]

ΔT - Temperature difference [K]

ΔU - Wind velocity deficit in the wake [m/s]

ΔX - Distance between nodes for heat and mass transport [m]

ΔX_I - Wood inner layer thickness [m]
ΔX_S - Wood surface layer thickness [m]
ΔX_W - Total wood thickness [m]
ΔX_Σ - Snow thickness [m]
$\Delta \Omega_{H2O}$ - Wood moisture concentration difference across distance ΔX [Kg/m^3]
ϵ - Emissivity of a surface
ϵ_Ω - Error in concentration of R22 [ppm]
ϵ_N - Error in number of injections
ϵ_Q - Error in volume flowrate [m^3/s]
$\epsilon_{V,inj}$ - Error in injection volume [m^3]
θ - Wind direction [degrees]
λ - Thermal diffusivity coefficient [m^2/s]
μ - Dynamic viscosity [Kg/ms]
υ - Kinematic viscosity [m^2/s]
ρ - Density of air [Kg/m^3]
ρ^j - Density of air at time j [Kg/m^3]
ρ_a - Density of attic air [Kg/m^3]
ρ_{in} - Density of inside air [Kg/m^3]
ρ_{out} - Density of outdoor air [Kg/m^3]
ρ_F - Density of heated flue gas [Kg/m^3]
ρ_Σ - Density of snow [Kg/m^3]
ρ_W - Density of wood [Kg/m^3]
σ - Stephan-Boltzmann constant = $5.669*10^{-8}$
σ_θ - Standard deviation of wind direction [degrees]
τ - Time constant [s]
ψ - Angle of pitched roof surface measured form horizontal [degrees]
ω - Humidity ratio
Ω^a_{SF6} - Attic volume concentration of SF_6 [ppm]
Ω^{in}_{SF6} - House volume concentration of SF_6 [ppm]
Ω^a_{R22} - Attic volume concentration of R22 [ppm]
Ω^{in}_{R22} - House volume concentration of R22 [ppm]
Ω_{H20} - Concentration of water in wood [Kg/m^3]

Chapter 1. Introduction

The attic space of most residential buildings is well insulated from the house below. The house contains conditioned air that is maintained at a relatively constant temperature. Attics are left unconditioned and therefore experience extreme conditions on seasonal cycles (hot in summer and cold in winter) and diurnal cycles (hot during the day and cold at night). The increase in insulation levels between houses and attics has increased the amplitude of diurnal and seasonal temperature cycles in recent years. The extremes of temperature experienced by an attic can cause moisture entering the attic through the ceiling from the house or through other leaks from outside to accumulate in or on interior attic wood surfaces. This moisture accumulation leads to structural degradation and the growth of micro-organisms. Temperatures in the range of 2°C to 38°C and wood moisture contents above fibre saturation (30%) are the required conditions for micro-organism growth as given by the Wood Engineering Handbook (1982), p.17-3.

An estimate of the magnitude of attic moisture problems has been made by NRC (1984). Between 1973 and 1981 the Canada Mortgage and Housing Corporation was involved in the construction of approximately 689,000 houses (about 35% of the total number of houses constructed in Canada during that time). Of these houses 10,260 were reported to suffer from moisture problems. The rate of occurrence of moisture problems was found to be worst in Newfoundland, where 27% of the houses had moisture related problems. Moisture problems occurred in attics in 5390 (53%) of the problem houses. The remainder of the houses had moisture accumulating in walls and around windows.

To prevent these problems simple cost-effective strategies are required that can be applied over a wide range of climates and building construction. Current building code (National Building Code of Canada (1990)) specification requires ventilation of the attic by having a total vent area equal to 1/300th of the attic floor area. There is no provision for mechanical ventilation or variation of the code depending on different climates. The effectiveness of the code will depend on how much ventilation this leakage area provides (which depends on the configuration of the attic leaks) and whether or not this is the right amount of ventilation for preventing moisture problems.

The main objective of this study is to develop a method for predicting attic moisture levels by modelling heat and mass transport in attics. In addition, attic

ventilation strategies will be investigated in order to identifying the significant parameters for attic moisture accumulation so that recommendations can be made for building codes.

Full scale experiments are too expensive and time consuming if all the variables in climate and attic construction are to be considered. The experiments performed for the validation process in this study have shown that the large amount of scatter in measured full scale data means that experiments must run for at least a year in each configuration being tested. Performing the experiment for at least a year also means that a large range of temperatures, solar radiation gains, windspeeds, wind shelter factors and cloud cover are represented. The temperature and solar radiation varies seasonally as well as diurnally and taking a year of data is required to capture these seasonal changes. In Edmonton, where the experiments were performed for this study, these parameters have the following ranges:

- The outdoor temperature varies from -40°C to +30°C from winter to summer.
- The solar radiation gains on the pitched roof surface vary from a peak of about 60 W/m^2 to 1050 W/m^2 from winter to summer. Cloudy skies can reduce the peak radiation on a south facing surface by up to a factor of five.
- Windspeeds range from an hourly average of about 0.5 m/s to about 10 m/s.
- The wind shelter due to nearby buildings and trees depends on wind direction. To cover the complete range of possible wind sheltering effects all wind directions must be represented.

Prediction of attic moisture problems over these large ranges of parameters requires a mathematical model of the processes involved that will simulate the ventilation, thermal and moisture dynamics in attics. These simulations can then be used to find strategies for preventing attic moisture accumulation.

The attic ventilation rate is important because it removes moisture from the attic by advection. The attic is ventilated through intentional leakage sites such as soffits and ridge vents and distributed leakage in the small gaps and cracks due to the attic construction. Air flows through these cracks due to pressures from the wind, indoor-outdoor temperature differences and ventilation fans. The thermal aspects of attics can be simulated by modelling the conduction, convection and radiation heat transfer for the components of the attic. In addition, the attic heat balance includes the mass flows of air into and out of the attic. The moisture dynamics of attic spaces considered in this study are internal wood diffusion, wood-air surface exchange and moisture convected in and out of the attic by ventilation. The contribution of

moisture in porous attic insulation was not included in this study due to the small total mass of water associated with the equilibrium moisture content of glass fibre insulation. However, future developments of the attic model developed here will include the effect of attic insulation on the moisture balance. The mass balance for water in an attic is highly temperature dependent because the equilibrium wood moisture vapour pressure is a strong function of temperature. Saturation vapour pressure for the wood and the attic air is also temperature dependent and this effects mass condensation in the attic.

1.1 Previous studies

Previous simulations of the thermal performance of attics have been developed by Wilkes (1989), Abrantes (1985) and Peavy (1979). Moisture models for attics have been developed by Gorman (1987), Ford (1982), Cleary (1985) and Burch and Luna (1980). These moisture models included thermal models because the mass transfer processes in moisture models are strong functions of temperature. These models have been limited in application due to the following assumptions.

- **Attic ventilation and ceiling flow.**

The attic ventilation and ceiling flow rates have been either a specified user input (usually constant) or must come from measurements. Since the heat transfer and moisture transport in the attics is strongly dependent on ventilation rates the above models are limited when trying to simulate seasonal performance of an attic.

- **Wood moisture content and surface condensation.**

Burch and Luna did not consider wood moisture content and assumed that condensation occurred when the attic vapour pressure was above the saturation pressure for the underside of the sheathing. Ford assumed that the wood was always at the saturation vapour pressure (corresponding to its temperature) and all mass transported to the wood appeared as surface condensation. Gorman calculated wood moisture contents but assumed no condensation until the wood reached fibre saturation (approximately 30% moisture content). In this study condensation is assumed to occur when there is mass transported to the wood surface when the surface is already at its saturation pressure, which depends on the surface moisture content and temperature. In terms of structural integrity and microorganism growth the wood moisture content must be known and should be included in the modelling.

- **Steady-state solutions.**

Of the three moisture models above, only Ford considers the transient thermal response by including the rate of change of temperatures in the attic heat balance.

The other models assume that the attic is at steady-state and the temperatures are not changing with time. All of the models assume steady-state moisture transport which means that there are no terms accounting for the rate of change of moisture content of the wood with time. The diurnal dynamics of heat and moisture transport due to solar gains and night time radiative losses and the effects of changing ventilation rates mean that the attic is rarely at steady-state and this assumption has large effects on moisture predictions.

- **Mass balance for water vapour.**

Previous models have performed a mass balance on the attic air water vapour only (see Cleary (1985)). The air was considered to gain and lose moisture due to attic ventilation, flow through the ceiling and by diffusion through the attic envelope. The mass transfer to the attic wood was then calculated based on the resulting estimation of attic vapour pressure. A more accurate water vapour mass balance must include the mass transferred to the wood surfaces and simultaneously solve a set of equations to determine vapour pressures in both the air and the wood. For the air the driving force for vapour transport is the water vapour pressure but the wood surfaces are solid and cannot explicitly have a water vapour pressure. This problem has prevented previous researchers from performing a true water mass balance.

1.2 Present study

The present study consists of three parts: model development, field validation and simulations.

1.2.1 Model development.

The moisture prediction model developed in the present study will provide a broader application by addressing the above four points. The model requires inputs of the ambient weather conditions, house and attic leakage, and heat transfer parameters. The model will then provide predictions of attic and house ventilation rates (including flows through the ceiling), attic temperatures, attic wood moisture contents, and the amount of mass condensed on attic surfaces.

The components of the attic simulation model.

The transport of moisture in the attic depends on ventilation rates and the temperatures of the attic components, which are found using separate models. The complete moisture model is divided into three components as follows.

- **A ventilation model** to calculate attic, house and ceiling air flows.
- **A heat transfer model** to calculate attic component temperatures.
- **A moisture model** that uses the predictions of the ventilation and heat transfer

models as inputs to find wood moisture content, condensed mass, attic vapour pressure and relative humidity.

The interactions of the three components are illustrated in Figure 1-1. The ventilation and heat transfer models are coupled by the ceiling flow rate and the attic air temperature. This coupling requires an iterative solution because the attic air temperature changes the driving pressures and air density for attic ventilation and the ceiling flow rate changes the total energy balance for the attic. This iterative solution for the combined ventilation and heat transfer modelling is solved first. The attic envelope and ceiling flowrates from the ventilation model and the temperatures from the heat transfer model are then used in the moisture model to find wood moisture contents and condensed masses. It is assumed that the small rates of vapour transfer are not a significant part of the thermal balance for the attic so that the heat transfer and moisture models do not have to have an iterative solution. The four weaknesses of previous models will be dealt with in this study as follows:

Attic ventilation and ceiling flow.

Ventilation rates will be estimated using a ventilation model that calculates the air mass flow rates through every attic and house leak. The model developed for this study is called ATTICLEAK-1. In ATTICLEAK-1 the house and attic are treated as separate zones and interact through the ceiling flow, which can be an important parameter in the moisture balance on the attic as in winter this flow transports high moisture content air into the attic. An earlier single zone version that modelled the house only, LOCALEAKS-2, has been used previously by Wilson and Walker (1991a) and Wilson and Walker (1992) in studies of passive ventilation. ATTICLEAK-1 separates distributed background leakage from known ventilation leaks such as furnace flues, fans (using a fan performance curve) and roof vents. The pressure difference across each leak is estimated from stack (indoor-outdoor temperature difference) and wind pressures and the internal pressure that acts to equate mass flows in and out of the structure. The internal pressure is the only unknown and is solved for iteratively rather than analytically due to the non-linear relationship between this pressure and the flow balance. This model's improvements over previous single and multizone ventilation models are the use of different pressure-flow relationships for each leakage site, rather than assuming orifice flow, and improving the estimated inputs to the model. The use of different pressure-flow relationships means that furnace flues and ventilation pipes behave like orifices and the distributed building leakage uses a power law relationship. The greatest

Figure 1-1 Model Interactions

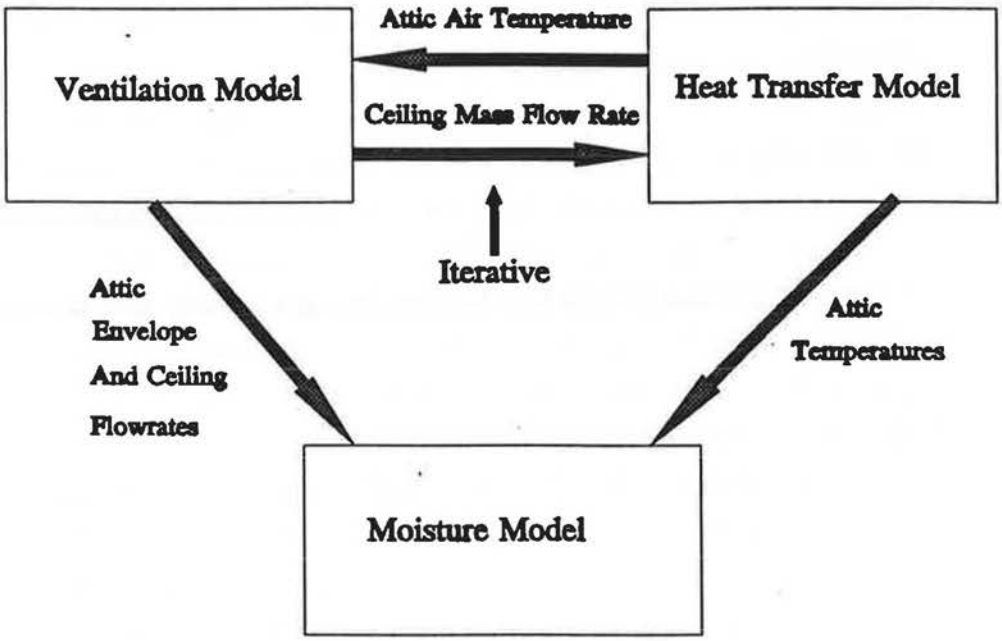

improvement in input values has been in the area of estimating surface pressure coefficients using wind tunnel data with harmonic interpolation functions for varying wind direction and in estimating wind shelter using a wind shadow technique combined with self preserving wake theory.

Wood moisture content and surface condensation.

Unlike previous work by other authors the moisture balance model developed in this study includes the amount of wood moisture in the wood in the total moisture balance for the attic. To do this a relationship is required between the wood moisture content and the vapour pressure for the wood that is used to calculate the mass of moisture transferred at the wood surface. The moisture balance model is expressed in terms of vapour pressures. To relate wood moisture content to vapour pressure an empirical relationship is used which was developed by Cleary (1985) from data in the Wood Engineering Handbook (1982) that relates wood moisture content to equilibrium vapour pressure and temperature. This equation also fits other data found in Siau (1984) from the USDA Forest Services.

Surface condensation is assumed to occur when mass is transferred to a wood surface already at its saturation pressure. The total condensed mass is tracked so that condensed mass may evaporate (or sublime) away from the surface when the surface has a higher vapour pressure than the attic air. Until all the condensed mass is gone the wood will be at the saturation pressure corresponding to the temperature of the surface. The wood sections of the attic are modelled as a separate thin surface and inner bulk wood as in Gorman (1987). This allows the surface wood to have rapid exchange with the attic air and relatively high moisture contents while the inner wood is effectively decoupled from the attic air and exchanges moisture only by diffusion to and from the surface layer.

Including time response.

A lumped heat capacity analysis is used for the heat transfer model so that the heat capacity of the attic components can be included. The sum of the heat fluxes at a node in the attic is then equal to the rate of change of thermal energy at the node. This has a significant effect on predictions of attic wood temperatures when ambient conditions are changing rapidly. Including the time response means that the attic will warm up less rapidly in the morning and cool less rapidly in the evening in response to diurnal changes in outdoor temperature and solar gain.

The moisture model uses the wood moisture content, vapour pressure and temperature relationship from Cleary to find a finite difference approximation for the

rate of change of mass of water with time for the attic wood. This means that the wood surface is not forced to be at equilibrium with the attic air. The rate of change of water vapour in the attic air is calculated by assuming that the air is an ideal gas. The sum of the moisture fluxes at a node is then equal to the rate of change of mass of water at the node.

Mass balances.

Mass conservation is applied in both the ventilation and moisture transport models. The ventilation model balances the mass flows in and out of the attic. The moisture transport model includes the moisture transferred to wood surfaces together with masses of water vapour advected in and out of the attic by the ventilation flows.

1.2.2 Field Validation.

Each of the three models has been validated using measured data from the Alberta Home Heating Research Facility (AHHRF). This research facility consists of six houses each of different construction in terms of airtightness and thermal insulation. The houses are located at the University of Alberta Farm at Ellerslie, about 30 kilometres south of Edmonton, Alberta, Canada, and have been monitored continuously since 1981 for air infiltration rates, temperatures, relative humidities and heat fluxes. Two attics have also been monitored from 1990 to 1992. This test facility has produced much more data than previously available on house and attic ventilation rates over a wide range of weather conditions, building shelter and envelope leakage and distributions. Details of this test facility can be found in Gilpin et. al. (1980). The models and the measurements have been used to identify the following important parameters for prediction of attic moisture levels:

- The attic ventilation rate depends most strongly on windspeed, wind shelter, attic leakage area and leakage distribution. In addition, the direction of flow through the leaks is important as flow into the attic through the ceiling can provide a large moisture load that is not present when this flow is reversed.
- The temperatures in the attic are dependent on attic ventilation rate, solar radiation gains during the day, night-time radiative cooling of the sheathing (both of which are strongly dependent on cloud cover) and heat transfer through the ceiling from the house below. There is only a weak interaction between ventilation rates and temperatures because the ventilation rate is a very weak function of attic temperature (although the attic temperature is a strong function of ventilation rate).
- The outdoor climate has diurnal and seasonal variation of temperature and

relative humidity.

The field measurements have been compared with the model predictions to show that the models have the correct variation with the above parameters.

1.2.3 Simulations.

After validation and identification of significant parameters, the attic simulation model has been used in parametric simulations to examine some strategies for moisture control. The model has been run with two simulated climates - prairie and maritime winters. The prairie climate was cold and dry and the maritime climate was warm and damp. The radiation gains and losses for the attic were varied diurnally and included changing cloud cover. The simulated windspeed was varied from calm (0.5 m/s) to windy (6 m/s) producing low and high ventilation rates.

The results of the simulations have shown that increasing attic ventilation rates is not always a useful strategy for controlling moisture problems and that appropriate strategies are strongly dependent on climate and attic construction (which determines ventilation rates). The two extremes that can produce moisture problems are low ventilation rates where the capacity for moisture removal by convection is small and high ventilation rates where additional cooling of the attic surfaces and attic air can cause more condensation. This suggests that there may be some optimum ventilation rate for a given climate. Some simulations examined the effects of fan ventilation of attic spaces because the fan guarantees a minimum ventilation rate. These simulations showed that fan sizes (flowrates) need to be optimized and that supply fans are more effective than exhaust fans.

1.3 Major contributions made by this study

The new methods of attic simulation and the other important contributions of this study are:

- the development of a two zone attic ventilation model that calculates the house, attic and interzonal (ceiling) flow. The ventilation model calculates wind shelter based on a new wind shadow method, in addition, the shelter and pressure coefficients are continuous functions of wind direction.
- the coupling of heat transfer and ventilation models.
- the use of a complete transient mass balance for the attic moisture that includes the attic wood.
- the use of combined models. Ventilation and heat transfer models are used to calculate ventilation flows and temperatures for the moisture model.
- calculation of ventilation rates, temperatures and moisture levels using

envelope leakage, indoor temperature and relative humidity, and outdoor temperature, relative humidity, wind speed, wind direction, and solar radiation.

- the development of a large data base of measurements for evaluating attic models and identifying important parameters for attic moisture accumulation.

Chapter 2. ATTICLEAK-1 Ventilation Model

2.1 Introduction

The ATTICLEAK-1 ventilation model was developed for this study to calculate the ventilation rates for attics and houses. The attic ventilation rate is used by the heat transfer model in the heat balance for the attic air and in calculating heat transfer coefficients. The moisture transport model also requires the attic ventilation rate as an input because the flow of air through the attic carries water vapour in and out of the attic. The ventilation model developed here is a two zone model. The two zones are the attic and the house below it and they interact through the ceiling flow. Both zones use the same type of flow equations and solution method. The total building and attic leakage is separated into components and a flow equation is developed for each leakage site. The individual flow components are illustrated in Figure 2-1. The flow at each leakage site is determined by a non-linear pressure - flow relationship. This relationship has a flow coefficient, C, that determines the magnitude of the flow and an exponent for pressure difference, n, that determines how the flow through the leak varies with pressure difference. For each zone the total leakage is divided into distributed leakage that consists of the small cracks inherent in the building construction and are intentional openings (e.g. furnace flues and open windows). Following the work of Sherman and Grimsrud (1980) the distributed envelope leakage is further divided into specific locations based on the height of the leak (i.e. floor, ceiling and walls). The building is assumed to have a rectangular planform with a user specified length, width and height. The attic has the same floor plan as the house and a pitched roof with soffits and gable ends. A simplified single zone model of the house only has been used by Wilson and Walker (1992) to examine the effects of passive ventilators on house ventilation rates. The ventilation rate is found by determining the internal pressure for the zone that balances the mass flows in and out. Because the relationship between mass flow and pressure is non-linear, the solution is found by iteration.

ATTICLEAK-1 uses entered values of building and attic leakage area and distribution to calculate the flowrates produced by natural and fan pressures. The natural pressures are due to wind and stack (temperature) effects. For the wind effect the model requires the windspeed, wind direction and shelter by surrounding obstacles to be entered. For the stack effect the ambient and house interior temperatures must be entered in the model. The attic temperature is found iteratively by the attic heat transfer model that uses the calculated ventilation rates.

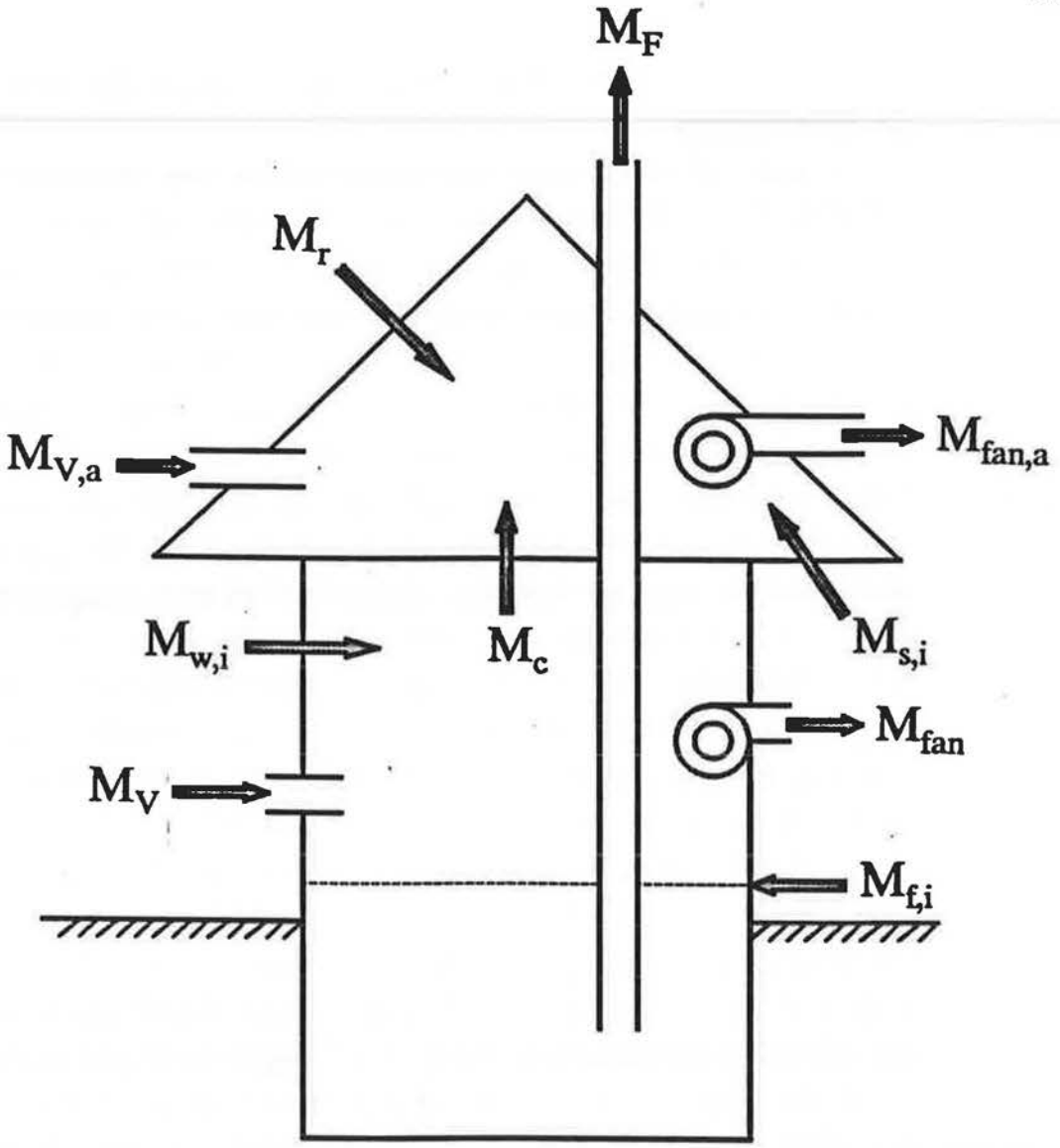

Mass flow rates [Kg/s]

M_c	- through ceiling
M_F	- through the furnace flue
M_V	- through house vent
M_{fan}	- through a fan
$M_{f,i}$	- through floor level leaks below wall i
$M_{w,i}$	- through wall i
$M_{fan,a}$	- through an attic fan
M_r	- through pitched roof surface
$M_{s,i}$	- through the attic soffit above wall i
$M_{V,a}$	- through attic vent

Figure 2-1. Individual components of mass flow balances for house and attic.

2.2 Differences from previous work

The ventilation model developed here falls between extremely complex multizone models (e.g. COMIS from Feustal and Raynor-Hoosen (1990)) that require a great deal of input data that is difficult to determine and simple single zone models that have distributed leakage only. Walker and Wilson (1990b) have shown how including a single localised leak (a furnace flue) in a model with distributed leaks can have a significant effect on calculated ventilation rates. ATTICLEAK-1 allows both the attic and the house to have localised leakage sites (e.g. a furnace flue, attic vents and combustion air inlets) with their own wind shelter, wind pressure coefficients and a specified height for stack effect. This allows more specific modelling of ventilation flows than models with distributed leakage only. Previous single zone models (e.g. Sherman and Grimsrud (1980) and Walker (1989)) have calculated wind and stack effect pressures separately and then used various superposition methods to combine the resulting flowrates. Walker and Wilson (1993) discuss superposition techniques in more detail. ATTICLEAK-1 does not separate the stack and wind effects because they are not independent of each other. The stack and wind effects are not independent because they must share the same internal pressure to balance the total mass flows. ATTICLEAK-1 has been developed to capture as much of the physics of building ventilation as possible whilst remaining simple enough for practical applicability.

Previous heat and moisture transport analyses for attics have used either values specified by the user (Gorman (1987)) or simple empirical data correlations (Peavy (1979)) to find attic ventilation rates. In this work the attic ventilation is modelled as a function of the ambient weather conditions and attic leakage. ATTICLEAK-1 is used to predict attic ventilation rates that are used in the attic heat balance to determine attic temperatures and in the attic moisture balance to find moisture transport rates. The attic ventilation rate changes the attic temperatures directly due to convection of air from outside and from the house through the ceiling and by changing the surface convection heat transfer coefficients. The attic moisture balance is also a function of the ventilation rate due to convection of outside and house air through the attic space.

The major differences from previous ventilation models are listed below:

- Wind pressure coefficients are given as a continuous function of wind angle. Different pressure coefficient values are used for houses in a row to account for the change in flow pattern around the building.

- Shelter is based on a wind shadow wake method which gives numerical values of effective windspeed reduction for each building surface.
- Mass flows are balanced instead of volume flows.
- Distributed leakage is combined with localised leakage to include the effects of furnace and fireplace flues and ventilators.
- Large openings such as doors and windows may have two-way counterflow with interfacial mixing.
- Fans are included using a fan performance curve so that if large natural pressures due to wind and stack effect occur at the fan location then the fan flow will change.
- The coupling of the attic and the house yields the interzone flow through the ceiling that is important for moisture loads on attics.

2.3 General flow equation

The general flow equation for each leak is given by

$$M=\rho C\Delta P^{n} \tag{2-1}$$

where M = Mass flow rate [kg/s]

ρ = Density of air flow [Kg/m^3] which is ρ_{in}, the density of indoor air for outflow, ρ_{out}, the density of outdoor air for inflow, ρ_F, the density of flue gasses, or ρ_a , the density of attic air.

C = Flow coefficient [m^3/(sPa^n)]

ΔP= Pressure difference across the leak [Pa]

n = Flow exponent

The value of n varies from 1 for laminar flow to 1/2 for turbulent orifice flow. The flow direction is determined by ΔP where a positive ΔP produces inflow and a negative ΔP produces outflow. A density and viscosity correction factor may be applied to C for building and attic leaks to account for changes due to the temperature of the air flow. Kiel, Wilson and Sherman (1985) used dimensional analysis to show that

$$C\propto\frac{\rho^{n-1}}{\mu^{2n-1}} \tag{2-2}$$

where μ is the viscosity of the air. To make this relationship easier to use it is

assumed that air behaves as an ideal gas and that over the range of application of the model viscosity is a linear function of temperature only. Neglecting atmospheric pressure changes Equation 2-2 may be written in terms of temperature

$$C=C_{ref}\left(\frac{T}{T_{ref}}\right)^{3n-2} \qquad (2\text{-}3)$$

where T_{ref} is the absolute reference temperature at which C_{ref} was measured, and T is the temperature of the airflow, which is T_{in} for outflow and T_{out} for inflow. For many buildings and attics the distributed background leakage has n~2/3, which means that this correction is unity. For simplicity this temperature correction was therefore not applied to distributed leakage. For localised leakage sites including furnace flues, passive vents and attic vents n is typically 0.5 and this correction can become significant and therefore it is included in the ventilation calculations.

2.4 Pressure Differences For Flow Through House and Attic Leaks

The pressures driving flows through the leaks result from two natural effects. These are the surface pressures due to airflow around the building and due to the density differences caused by temperature differences between indoor and outdoor air.

2.4.1 Wind Pressures

To find the outside surface pressure on a house or attic a wind pressure coefficient, Cp, is used. The wind speed, U, used to normalise pressure coefficients in most studies is the eaves height wind speed. Because the pressure coefficients for ATTICLEAK-1 are taken from wind tunnel studies the eaves height wind speed will be used as the reference wind speed in ATTICLEAK-1. The wind pressure coefficient is positive on upwind surfaces due to flow stagnation and negative on downwind surfaces due to flow separation and is defined as

$$Cp=\frac{\Delta P_U}{\frac{\rho_{out}U^2}{2}} \qquad (2\text{-}4)$$

where ΔP_U is the difference between the pressure on the surface of the building due to the wind and the atmospheric reference pressure P_{∞}.

ρ_{out} is chosen as the reference density for pressures. This is because pressure

coefficients are measured in terms of the external flow and the outdoor air density is used to calculate pressure coefficients from measured surface pressures.

U is the windspeed which must correspond to the windspeed used to calculate the wind pressure coefficients. This windspeed has been measured at different heights in different studies. In this thesis all pressure coefficients are corrected to the eaves height windspeed, which has been used by the majority of previous authors.

P_∞ is the pressure in the atmosphere far away from of the building where the building does not influence the flow field. The building exterior wind pressures are measured relative to this pressure.

Real buildings can be surrounded by various obstacles that impede the air flow around the building e.g. other houses, trees and fences. This is accounted for in ATTICLEAK-1 by using a shelter factor, S_U, that multiplies the wind speed. Thus Equation 2-4 for a sheltered building can be written as

$$\Delta P_U = \rho_{out} Cp \frac{(S_U U)^2}{2} \qquad (2\text{-}5)$$

where S_U is the shelter factor. This is a windspeed multiplier that accounts for windspeed reductions due to upwind obstacles. $S_U = 1$ implies no shelter and $S_U = 0$ implies complete shelter and there is no wind effect. Because each leak has a different Cp and S_U it is convenient to define a reference wind pressure P_U as

$$P_U = \rho_{out} \frac{U^2}{2} \qquad (2\text{-}6)$$

and then Equation 2-5 can be written in terms of P_U:

$$\Delta P_U = Cp S_U^2 P_U \qquad (2\text{-}7)$$

This definition of P_U will be used later in the equations for the flow through each leak.

2.4.2 Indoor-Outdoor Temperature Difference Pressures (Stack effect)

The change in hydrostatic pressure in a fluid with depth is given by Equation 2-8.

$$\frac{dP}{dz} = -\rho g \qquad (2\text{-}8)$$

where P is the static pressure

z is the height above a reference (grade level) [m]

ρ is the fluid density [Kg/m^3]

g is gravitational acceleration (9.81 [m/s^2]).

Using Equation 2-8 to calculate the pressure differences across the building envelope by using a single density indoors and outdoors assumes that there are no indoor or outdoor temperature gradients. This assumption implies that the inside and outside air are homogeneous and well mixed. i.e. the air in either the house or the attic is a single well mixed zone. Measurements performed in a house by Dale and Ackerman (1993) have shown that this is a good assumption because all the change in temperature in indoor air occurs in the thin boundary layers on the walls, the floor and the ceiling that are about 5% or less of the total room height. Dale and Ackerman found that this was true for both forced air and radiant floor heating, which shows that a forced air system is not a requirement for the assumption of a single indoor air temperature. The inside and outside of a building will generally have air at different densities. This means that the pressure gradient defined in Equation 2-8 will be also be different inside and outside. This results in a differential pressure across the building envelope, ΔP_T. ΔP_T is the outside pressure minus the inside pressure. This convention is applied so that positive pressures result in flow into the building. Equation 2-8 can then be written in terms of ΔP_T.

$$\frac{d\Delta P_T}{dz} = -(\rho_{out} - \rho_{in})g \qquad (2\text{-}9)$$

Assuming that air is an ideal gas allows the restating of Equation 2-9 in terms of temperatures

$$\frac{d\Delta P_T}{dz} = -g\rho_{out}\left(\frac{T_{in} - T_{out}}{T_{in}}\right) \qquad (2\text{-}10)$$

where ρ_{out} is chosen as the reference density to match the wind pressure reference density.

T_{in} = inside temperature [K]

T_{out} = outside temperature [K]

Equation 2-10 is integrated to find ΔP_T as a function of height. The limits of integration are from z=0 at grade level to z=h.

$$\Delta P_T(z) = -zg\rho_{out}\left(\frac{(T_{in}-T_{out})}{T_{in}}\right) \qquad (2\text{-}11)$$

Equation 2-11 implies that there is no stack effect pressure difference at grade level. There may still be a pressure difference at grade level due to either wind effect or the pressure that acts to balance the flowrates, ΔP_I. Each leak is at a different height, z , above grade, and so for convenience in writing the mass flow equations P'_T is defined as follows:

$$P'_T = g\rho_{out}\left(\frac{(T_{in}-T_{out})}{T_{in}}\right) \qquad (2\text{-}12)$$

P'_T is the pressure gradient and is multiplied by the height of each leak above grade to find the stack effect pressure difference at that location. Substituting Equation 2-12 in 2-11 gives:

$$\Delta P_T(z) = -zP'_T \qquad (2\text{-}13)$$

2.4.3 Pressure Difference Across the Building Envelope

The total pressure difference is due to a combination of the wind and indoor-outdoor temperature difference effects. The pressures outside, inside and across the wall are shown in Figure 2-2. On the outside surface of the building $P_{out,z}$ is generally a function of height as shown in Equation 2-14.

$$P_{out,z}(z) = P_\infty(z=0) + CpS_U^2\rho_{out}\frac{U^2}{2} - \rho_{out}gz \qquad (2\text{-}14)$$

The reference pressure, $P_\infty(z=0)$, is defined to be at grade level i.e. z=0. This is for convenience in calculating the hydrostatic pressure changes. The wind pressures are independent of this reference height.

Similarly, the pressure on the inside surface $P_{in,z}$ may also be found using Equation 2-15.

$$P_{in,z}(z)=P_{\infty}(z=0)-\rho_{in}gz-\Delta P_I \qquad (2\text{-}15)$$

where ΔP_I is the difference between the inside pressure and P_∞ at grade level (z=0). Because positive pressure is defined as P_{out} - P_{in}, ΔP_I appears negative in Equation 2-15. The general pressure difference, ΔP, for a surface on the building envelope at height z can then be written as

$$\Delta P=P_{out,z}-P_{in,z}=CpS_U^2\rho_{out}\frac{U^2}{2}-gz(\rho_{out}-\rho_{in})+\Delta P_I \qquad (2\text{-}16)$$

The reference pressure, P_∞, cancels out of the pressure difference equation and only the net effect of wind, density difference and the flow balancing pressure, ΔP_I, remain.

Substituting Equations 2-7 and 2-11 into Equation 2-16 results in

$$\Delta P=\Delta P_U+\Delta P_T+\Delta P_I \qquad (2\text{-}17)$$

Equation 2-17 may also be written in terms of the reference wind pressure (Equation 2-6) and the reference temperature pressure (Equation 2-12) as follows

$$\Delta P=CpS_U^2P_U-zP_T'+\Delta P_I \qquad (2\text{-}18)$$

Equation 2-18 is applied to every leak for the building and the attic with the appropriate values of Cp, S_U and z. ΔP_I acts to balance the inflows and outflows and is the only unknown in this equation.

The linear change in pressure, ΔP, with height, z, due to the stack effect term in Equation 2-18 means that when inflows and outflows are balanced there is a location where there is no pressure difference. This is called the neutral level, H_{NL}. The location of the neutral level is shown in Figure 2-2, where $\Delta P = 0$. For $T_{in} > T_{out}$ flow is in below H_{NL} and out above H_{NL}, and the flow directions are reversed for $T_{out} > T_{in}$. In general the neutral level is different for each wall due to the inclusion of wind pressures which can drive H_{NL} above the ceiling or below the floor. In those cases there is one way flow through the wall. The neutral level is found for the i^{th}

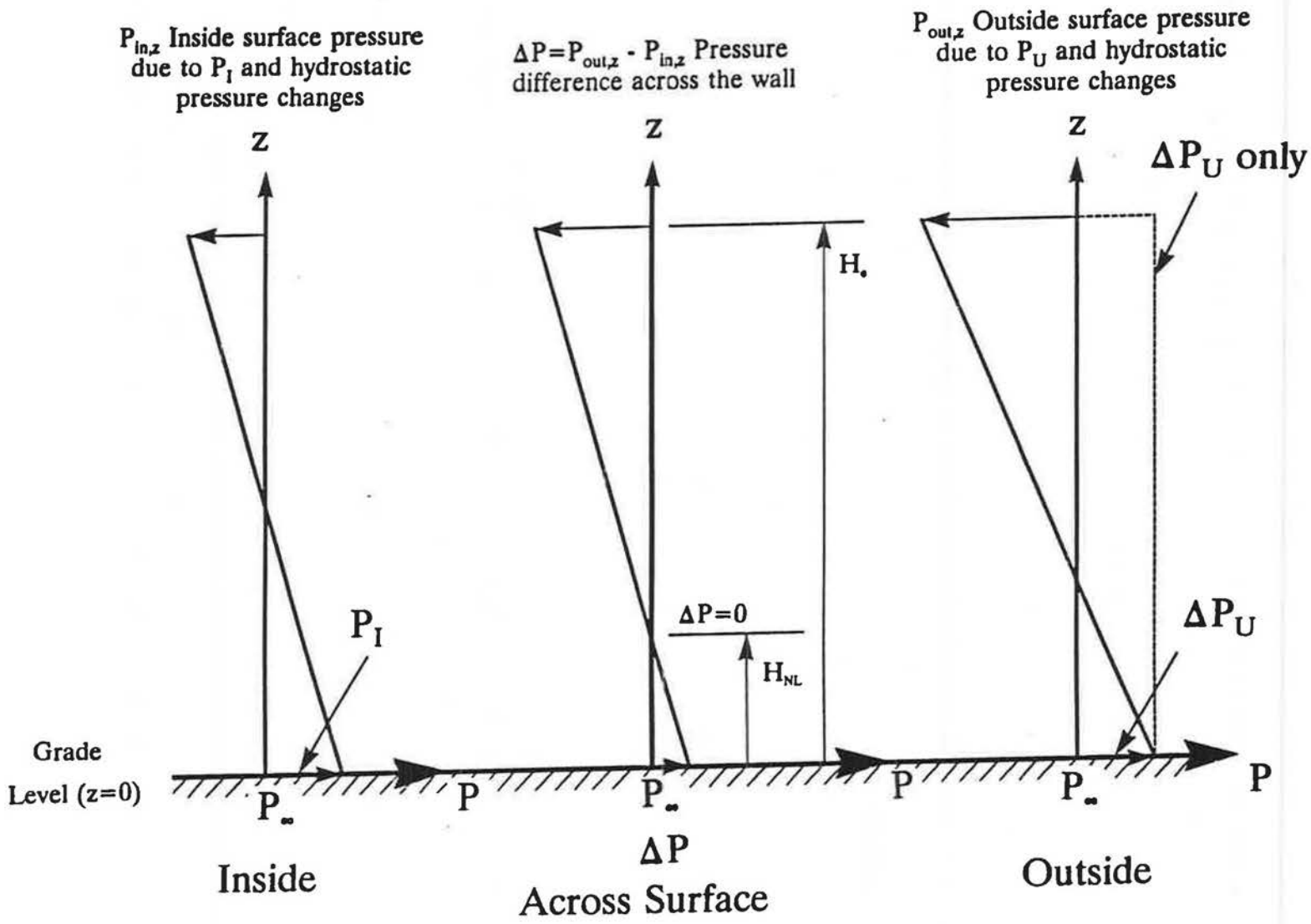

Figure 2-2. Pressures driving ventilation flows across a wall.

wall by setting $\Delta P = 0$ in Equation 2-18 and solving for $z = H_{NL,i}$:

$$H_{NL,i} = \left(\frac{\Delta P_I + S_{U,i}^2 Cp_i P_U}{P_T'} \right) \qquad (2\text{-}19)$$

2.5 Wind Pressure Coefficients

2.5.1 Wind Pressure Coefficients For the house

Wind pressure coefficients for this model are taken from wind tunnel tests. The wind pressure coefficients used in this model are wall averaged because the wall leakage is assumed to be evenly distributed over the walls. The model also assumes that there is no specific horizontal location for a leak on a wall and so extremes of pressure coefficients occurring at corner flow separations, for example, are not included. The wind pressure coefficients depend on the wind direction and this variation is included in ATTICLEAK-1.

The most comprehensive wind tunnel tests to date that cover many different wind directions have been presented by Akins, Peterka and Cermak (1979). They measured surface pressures on a cube rather than a model house but their values of Cp are within the range of values presented elsewhere (ASHRAE (1989), Chapter 14, Liddament (1986) and Wiren (1985)) for isolated buildings. Akins, Peterka and Cermak also covered the most comprehensive set of wind directions and thus their data is most useful in developing correlations of pressure coefficient with wind angle. The only adjustment to these pressure coefficients in this model is a change of side wall pressure coefficient. For an isolated building the side wall is about Cp = -0.65 based on Akins, Peterka and Cermak's measurements. For houses in a row with the wind along the row, the upwind houses change the flow pattern around the building so that large flow separations do not occur on the sidewalls. This requires a reduction in magnitude of the side wall pressure coefficient to about Cp = -0.2. This value was found by Wiren in tests of row house shelter and is suggested by model errors in passive ventilation studies performed by Wilson and Walker (1991a). Analysis of Wiren's data by Walker (1992) has shown that for a house to be considered to be in a row only one upwind house is necessary because the closest obstacle dominates the wind flow pattern. Table 2-1 contains the wall averaged wind pressure coefficients used for the house by the ventilation model for wind perpendicular to the upwind wall. For the closely spaced row, the wind is blowing

along the row of houses.

Table 2-1. Wall averaged wind pressure coefficients for a rectangular building with the wind normal to upwind wall (data from Akins, Peterka and Cermak (1979) and Wiren (1985)).

Shelter Configuration	Cp, Wind Pressure Coefficient		
	Upwind Wall	Side Walls	Downwind Wall
Isolated House	+0.60	-0.65	-0.3
In-Line Closely-Spaced Row	+0.60	-0.2	-0.3

When the wind is not normal to the upwind wall these pressure coefficients do not apply. An harmonic trigonometric function was developed in the present study to interpolate between these normal values to fit the variation shown by Akins, Peterka, and Cermak and Wiren. For each wall of the building the harmonic function for Cp was empirically developed in the following form:

$$Cp(\theta)=\frac{1}{2}[(Cp(1)+Cp(2))(\cos^2\theta)^{\frac{1}{4}}+(Cp(1)-Cp(2))(\cos\theta)^{\frac{3}{4}} \\ +(Cp(3)+Cp(4))(\sin^2\theta)+(Cp(3)-Cp(4))\sin\theta] \qquad (2\text{-}20)$$

where Cp(1) is the Cp when the wind is at 0° (+0.60)
Cp(2) is the Cp when the wind is at 180° (-0.3)
Cp(3) is the Cp when the wind is at 90° (-0.65 or -0.2)
Cp(4) is the Cp when the wind is at 270° (-0.65 or -0.2)
and θ is the wind angle measured clockwise from the normal to the wall.
This function is shown in Figure 2-3 together with data from Akins et. al. for a cube. The error bars on the data points in Figure 2-3 represent the uncertainty in reading the measured values from the figures of Akins, Peterka and Cermak. Equation 2-20 fits the measured data within about Cp = ±0.02 except at about 150° and 210° (which are the same by symmetry) where the equation overpredicts the Cp by about 0.1. Figure 2-4 shows Equation 2-20 with Cp's from another data set from ASHRAE (1989)(Chapter 14) which it also fits well. The function in Equation 2-20 was chosen

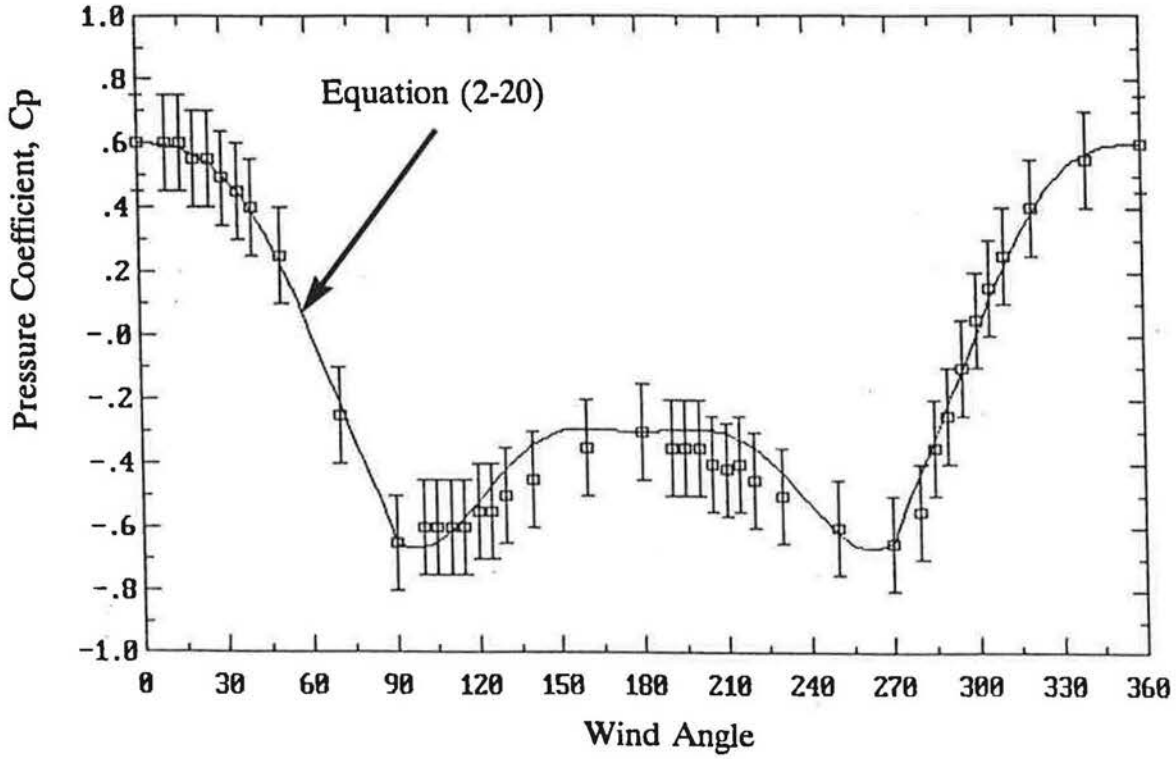

Figure 2-3. Wind angle dependence of measured (data from Akins et. al. (1979)) and predicted wall pressure coefficients for isolated buildings

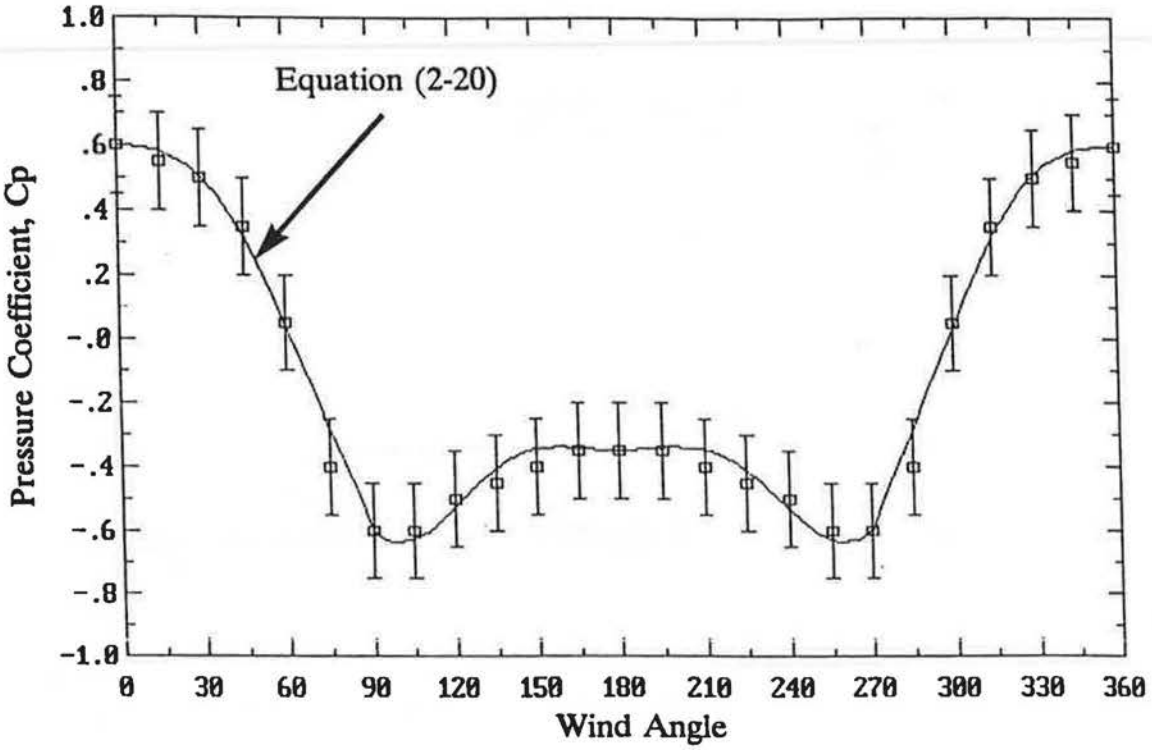

Figure 2-4. Wind angle dependence of measured (data from ASHRAE (1991)) and predicted wall pressure coefficients for isolated buildings

to have the above form so that if a different data set were to be fitted then only the values for when the wind is normal to one wall are required and the function will estimate the intermediate values for different wind directions. Equation 2-20 assumes that the upwind wall always has the same pressure coefficient. For less regular shaped buildings the pressure coefficients on the upwind wall depend on if it is the longer or shorter wall. Because of these geometry effects on flow around a building, the application of this interpolation function is limited to buildings that are of rectangular plan form (e.g. not L-shaped) with the longest wall less than three times the length of the shortest wall. Equation 2-20 collapses to give the values in Table 2-1 when the wind is perpendicular to each wall, as shown in Figure 2-3. Equation 2-20 is shown in Figure 2-5 for the row pressure coefficients where the sidewall Cp is -0.2. There are no intermediate measured values but this figure shows that Equation 2-20 produces reasonable pressure coefficients for this case.

2.5.2 Wind Pressure Coefficients For the Attic

The complete attic simulation model has been developed for a gable end attic with two pitched roof surfaces. The Cp's for gable ends or soffits are assumed to be the same as those on the walls below them and are calculated using the same procedure as for house walls. The pitched roof surfaces have Cp's that are also a function of roof slope. Table 2-2 gives values of Cp measured by Wiren (1985) for upwind and downwind pitched roof surfaces with wind normal to the upwind surface for different roof pitches. For a flat roof both surfaces are in a separation zone and experience large negative pressures. Steeper roofs of higher pitch have some stagnation on the upwind surface but still have negative Cp's for the downwind surface in the separation zone. In the same way as wall Cp's, the roof pressure coefficients are averaged over the whole pitched surface. For wind flow parallel to the roof ridge Cp's change in the same way as for houses with Cp = -0.6 for an isolated building and Cp = -0.2 for row houses for both roof pitched surfaces. The Cp is independent of roof pitch for flow parallel to the roof ridge.

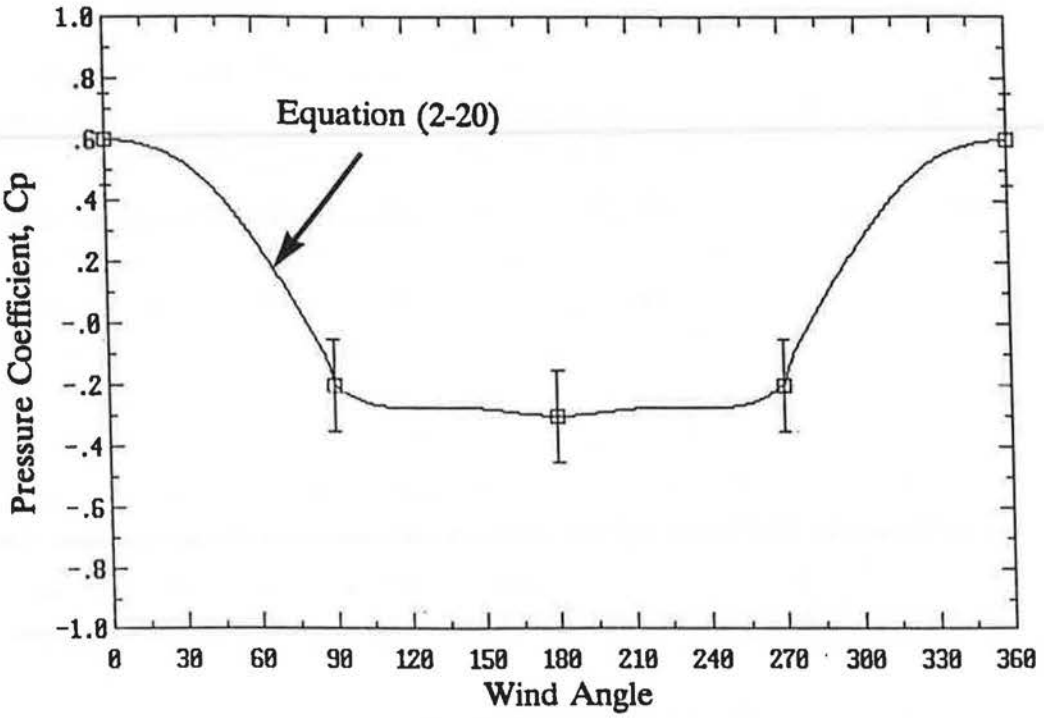

Figure 2-5. Wind angle dependence of row house wall pressure coefficients

Table 2-2. Pitched roof wind pressure coefficients for wind normal to the upwind surface (data from Wiren (1985))

Roof Pitch	Cp, Wind Pressure Coefficient	
	Upwind Surface	Downwind Surface
<10°	-0.8	-0.4
10° to 30°	-0.4	-0.4
>30°	+0.3	-0.5

To account for the variation on roof Cp with wind angle a similar empirical relationship to that for houses (Equation 2-20) has been developed for this study. Equation 2-20 then becomes the following for each roof surface

$$Cp(\theta)=\frac{1}{2}[(Cp(1)+Cp(2))\cos^2\theta+(Cp(1)-Cp(2))F \\ +(Cp(3)+Cp(4))\sin^2\theta+(Cp(3)-Cp(4))\sin\theta] \qquad (2\text{-}21)$$

where Cp(1) is the Cp when the wind is at 0°
Cp(2) is the Cp when the wind is at 180°
Cp(3) is the Cp when the wind is at 90°
Cp(4) is the Cp when the wind is at 270°
θ is the wind angle measured clockwise from the normal to the roof surface.
F is a switching function to account for changes in roof pitch.

To include the change of Cp with different roof pitches shown in Table 2-2, an empirical switching function, F, has been developed and has been found to have the form shown in Equation 2-22.

$$F=\frac{1-(|\cos\theta|)^5}{2}\left(\frac{28-\psi}{28}\right)^{0.01}+\frac{1+(|\cos\theta|)^5}{2} \qquad (2\text{-}22)$$

where ψ is the roof pitch in degrees measured from horizontal. Equation 2-22 acts like a switch with F ~ 1 up to ψ = 28° and F ~ cosθ when ψ > 28°. The switching function, F is illustrated in Figure 2-6, for cosθ = 0.5 which shows how rapidly it changes from unity to 0.5. One degree before and after the switch point of 28° this

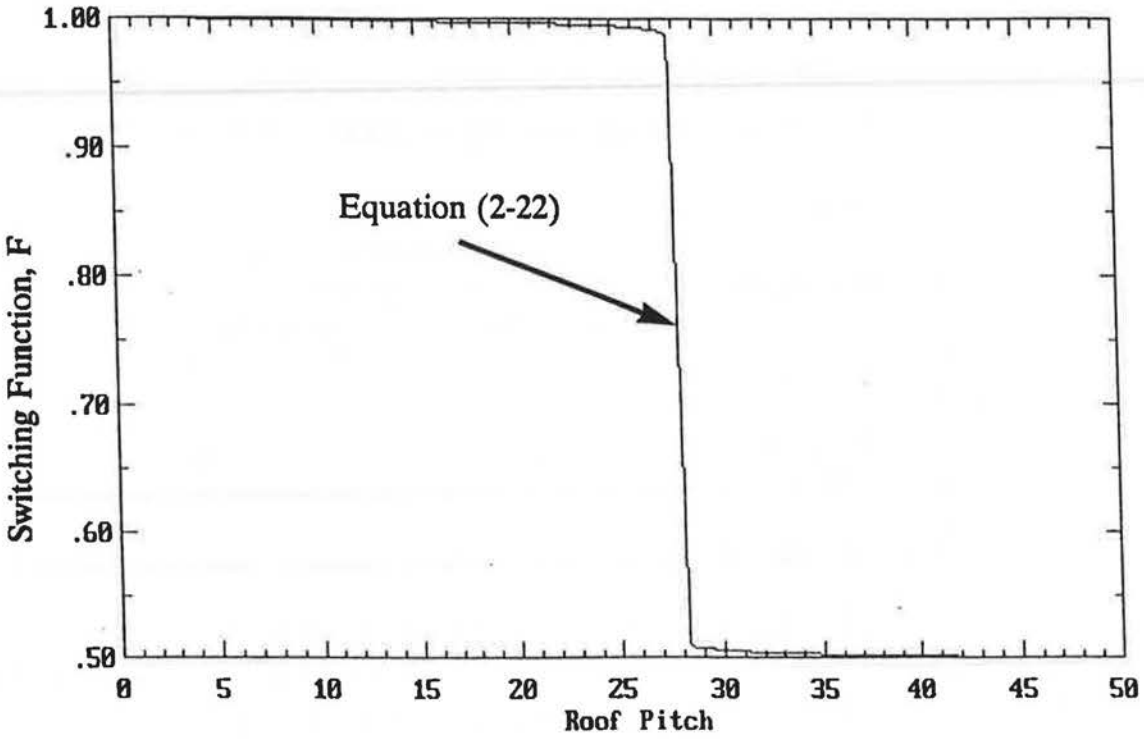

Figure 2-6. Roof pressure coefficient roof pitch switching function, F.

function is within a couple of percent of the values between which it switches. The switch point of 28° is chosen so that this relationship produces the same results as in Table 2-2. Equation 2-22 is not used to change the pressure coefficients shown in Table 2-2, but it changes the functional form Equation 2-21 so that the interpolation fits the measured pressure coefficients.

Equation 2-21 is compared with pitched roof Cp's from Liddament (1986) in Figures 2-7 through 2-9 for roof pitches >30°, 10° to 30°, and <10° respectively. In each case the equation fits the data well, typically within Cp = ±0.01. The exception is for ψ >30° at 45° and 315° (the same by symmetry) where the maximum difference of about Cp = 0.1 occurs.

2.5.3 Converting Meteorological Wind Speed Measurements to the Building Location

For most wind tunnel tests the wind pressure coefficient, Cp, is calculated using a reference wind speed at eaves height, H_e. Most meteorological data is measured at greater heights and must be converted to the eave height to account for the change in windspeed with height in the atmospheric boundary layer. Walker and Wilson (1990a) show how meteorological windspeeds measured remotely from the building site can be converted to an eaves height windspeed at the building assuming a power law boundary layer wind velocity profile. Wieringa (1980) recommended using the wind speed at the top of the constant shear surface layer when converting wind speeds from one location to another. Wieringa estimated this height to be about 80m plus the area averaged height of the roughness elements between the two locations (δ_z). The wind speed at the meteorological site, U_{met}, measured at H_{met} is converted to the wind speed at 80m+δ_z. The power law relationship is used at the meteorological site to move up the atmospheric boundary layer wind profile. At the building site this wind speed at 80m+δ_z is used to calculate the eaves height windspeed after coming down the power law wind profile. Combining these two wind speed conversions gives the following relationship as a first approximation for finding building wind speeds from meteorological measurements.

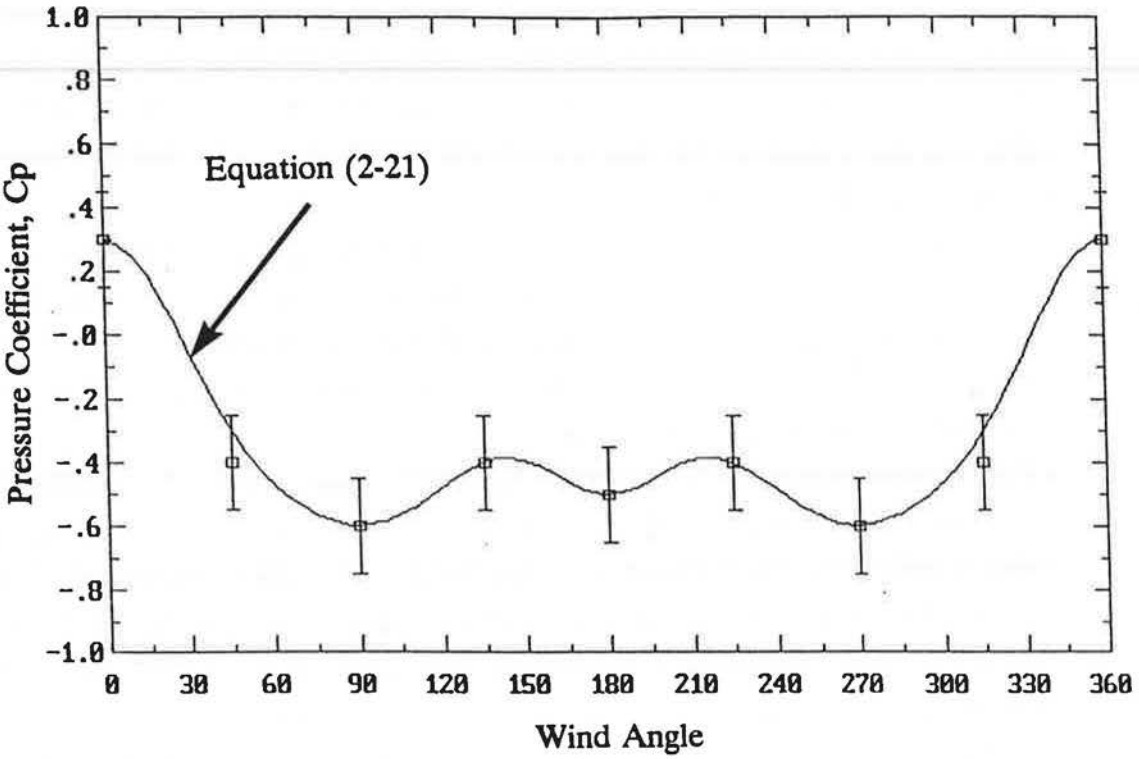

Figure 2-7. Wind angle dependence of measured (data from Liddament (1986)) and predicted pressure coefficients on a pitched roof surface for a roof pitch greater then 30 degrees.

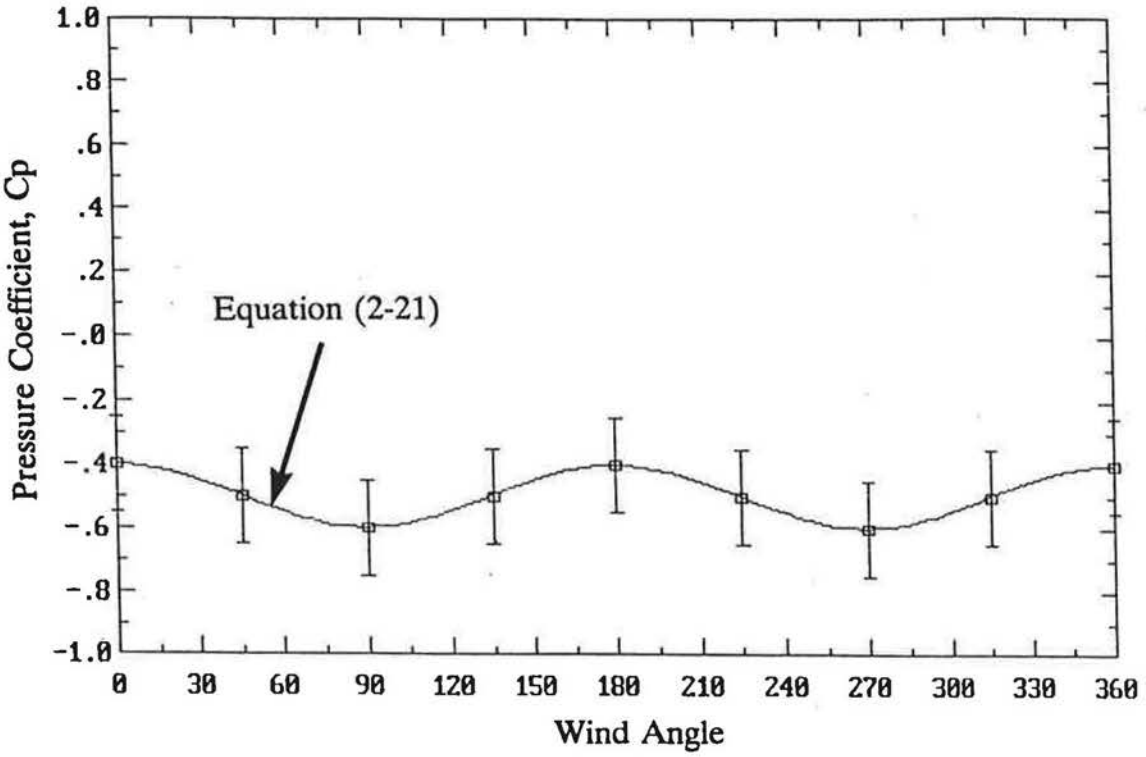

Figure 2-8. Wind angle dependence of measured (data from Liddament (1986)) and predicted pressure coefficients on a pitched roof surface for a roof pitch of 20 degrees.

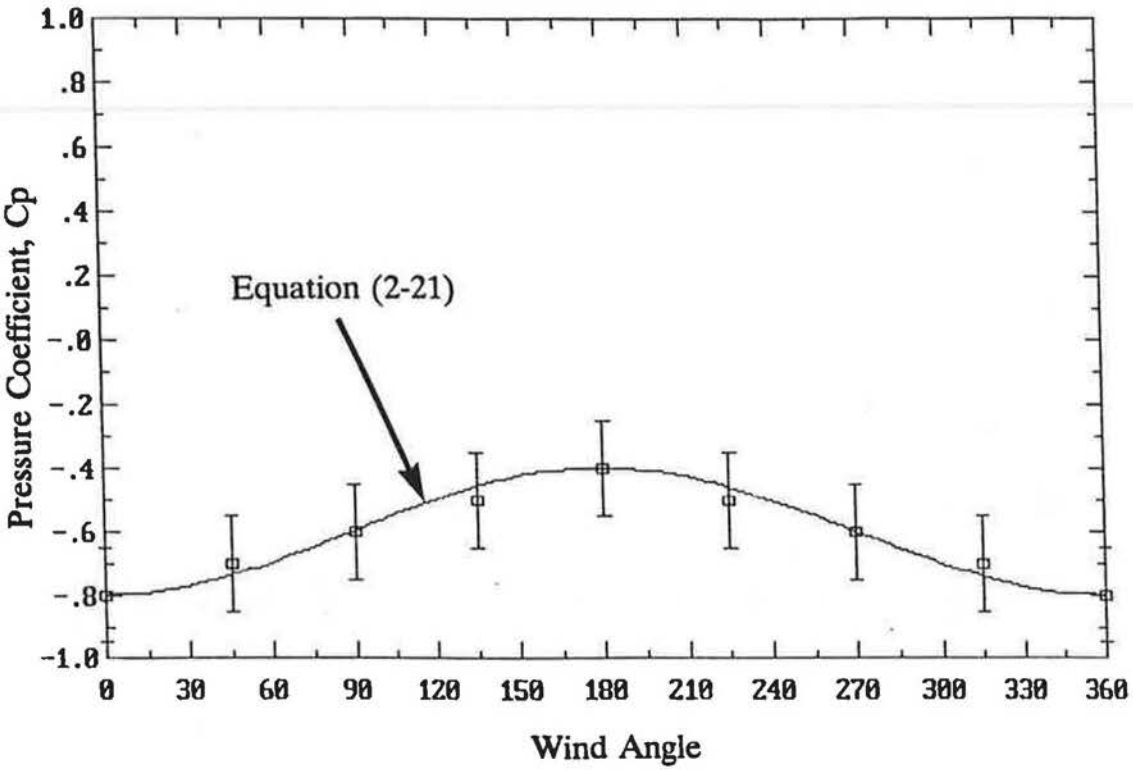

Figure 2-9. Wind angle dependence of measured (data from Liddament (1986)) and predicted pressure coefficients on a pitched roof surface for a roof pitch of less than 10 degrees.

$$U=\left(\frac{80+\delta_z}{H_{met}}\right)^{p_{met}}\left(\frac{H_e}{80+\delta_z}\right)^{p}U_{met} \qquad (2\text{-}23)$$

where p_{met} and p are the power law exponents at the meteorological station and the building site respectively. p and p_{met} depend on windspeed, ground roughness, solar insolation and atmospheric stability. Irwin (1979) gives values of p from 0.12 to .47 for a wide range of conditions. For typical urban housing p ~ 0.3, and for meteorological stations located at airports or other exposed sites p ~ 0.15. For the data used in validating the models the wind speed is measured at the building site. Therefore $p = p_{met}$ and Equation 2-23 collapses to the standard power law boundary layer relationship for a single location.

2.6 Wind Shelter

Local wind shelter provided by other buildings, trees, fences, bushes etc. is difficult to quantify and it has a significant effect on the surface pressures active in ventilation. Previous ventilation models have included shelter in broad classes with sharp changes from class to class. For example, Sherman and Grimsrud (1980) used a look-up table with five classes of shelter described in words such as "Light local shielding with few obstructions". This shelter was assumed to be the same for all wind directions. Ventilation rates measured for the present study have shown reductions in ventilation rates of up to a factor of three when the wind changed direction from perpendicular to parallel to the row. Some of these results have been reported in Wilson and Walker (1991b). Wilson and Walker recommended estimating wind shelter for winds perpendicular to each side of the building and then using an interpolation function to find the wind shelter for intermediate wind angles.

$$\begin{aligned} S_U=\frac{1}{2}[&(S_U(1)+S_U(3))\cos^2\theta+(S_U(1)-S_U(3))\cos\theta \\ &+(S_U(2)+S_U(4))\sin^2\theta+(S_U(2)-S_U(4))\sin\theta] \end{aligned} \qquad (2\text{-}24)$$

This function has the same functional form as Equation 2-20 so that for each wall where S_U is the windspeed multiplier

$S_U(1)$ is the S_U when the wind is at 0°

$S_U(2)$ is the S_U when the wind is at 90°

$S_U(3)$ is the S_U when the wind is at 180°

$S_U(4)$ is the S_U when the wind is at 270°

and θ is the wind angle measured clockwise from the normal to the upwind wall.

In this ventilation model shelter effects are separated from the effects of changing Cp's with wind direction and flow field changes. The windspeed multiplier, S_U, acts to reduce the effective windspeed generating surface pressures in Equations 2-5 and 2-6 on the building such that

$$U_S = S_U U \qquad (2\text{-}25)$$

where U is the free stream windspeed with no sheltering effects.

S_U has the limits where $S_U = 1$ implies no shelter and $S_U = 0$ implies total shelter and there are no wind pressures on the building.

U_S is the effective windspeed used for calculating surface pressures.

U_S is not necessarily the wind speed that would be measured by an anemometer in the wake, but is correct for finding the surface pressures. As will be shown later, the coefficients used to find U_S and S_U are based on measured surface pressures and not on measured wake velocities.

2.7 Wind Shadow Wake Shelter

To improve shelter estimates the wind shadow shelter method was developed to calculate numerical values for the reduction in velocity caused by an upwind obstacle. The shelter method is based on a method developed by Wilson and Walker (1991a). The present study has significantly extended and refined this shelter model. The reduction in windspeed in the shadow is assumed to be proportional to the decrease in velocity at eave height on the centreline of a wake. Applying this change in velocity assumes that all velocities in the wake scale in this manner. In order to apply self-preserving wake theories (and keep the problem simple) the shelter model assumes that the downwind building is far enough downstream that it does not affect the wake flow structure generated by the upwind obstacle.

In addition to the wind speed reduction the amount of surface covered by the projection of the wake will change the wall averaged shelter, S_U. Assuming that the sheltering effect is uniform with height for a wall of length L_w of which L_s is sheltered, S_U is given by

$$S_U = 1 - (1 - S_{U,CL})\left(\frac{L_s}{L_w}\right) \qquad (2\text{-}26)$$

For a notch wake velocity profile this equation has the correct limits where $S_U = 1.0$ for $L_s = 0$ (no part of wind shadow wake on the wall) and $S_U = S_{U,CL}$ for $L_s = L_w$ (all of the wall in shadow).

Figure 2-10 illustrates how to find L_w, L_s and the downwind distance, S. The calculation of these values is purely geometric. For each wind angle the values of S and L_s change for each wall and must be recalculated using the geometry of the upwind obstacle and the building being sheltered. The upwind building walls do not shelter downwind building walls on the same building as this is accounted for in Cp's, i.e. wall 1 does not shelter wall 3 in Figure 2-10. The wind shadow shelter model assumes that downwind building walls (e.g. wall 2 in Figure 2-10) are still sheltered by upwind obstructions and are just further away than the upwind walls and experience less shelter effect. This is further illustrated in Figure 2-11 that shows the wake velocity recovery as a function of distance. The downwind wall of a sheltered building is further downstream ($S_{down} > S_{up}$) and so experiences less sheltering effect and less velocity deficit, ΔU, i.e. $\Delta U(up) > \Delta U(down)$. This means that the downwind wall has a higher effective windspeed for producing wind pressures.

The change in windspeed is found by using the scaling laws of self-preserving wakes and is a function of downstream distance from the obstacle, S, and a characteristic building dimension, R_B, defined by Wilson (1979) as

$$R_B \equiv D_Y^{\frac{2}{3}} D_L^{\frac{1}{3}} \qquad (2\text{-}27)$$

where D_Y is the smallest building dimension and D_L is the largest building dimension of projected width or projected height as shown in Figure 2-12b. Equation 2-27 makes the smallest building dimension be the dominant scale. Thus for short buildings the height determines wake geometries and velocities while for tall thin buildings it is the width that is dominant. The physical basis for using R_B as a scaling length is that for a short and wide building the momentum transfer into the wake is mainly from above, and the sides of the wake have little effect. For a tall thin building the momentum transfer is mainly in the sides of the wake and the width of the building is the relevant scaling dimension. To think of this another way; if the wake always scaled with building height then the wakes of high rise buildings would

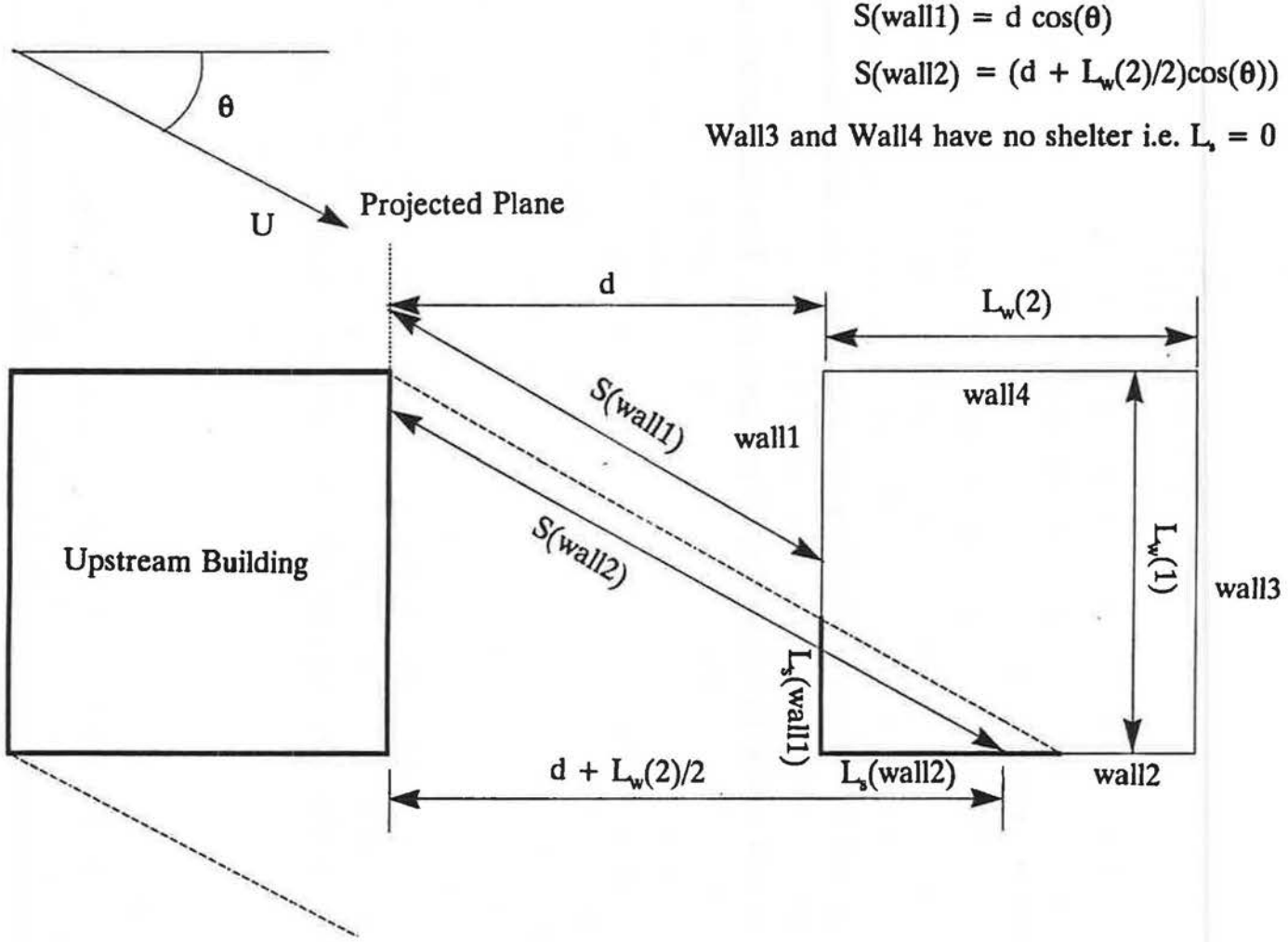

Figure 2-10. Illustration of geometry for finding sheltered wall length, L_s, and distance to upstream building, S.

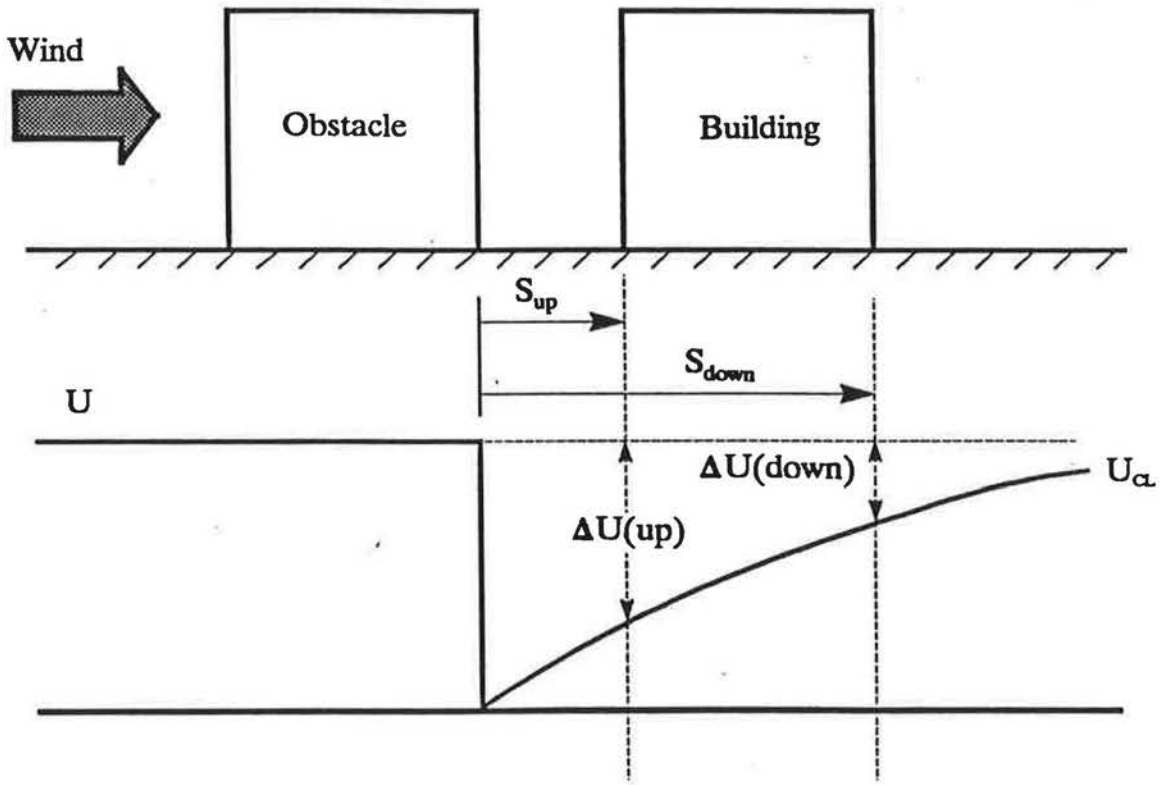

Figure 2-11. Velocity recovery downwind of an obstacle.

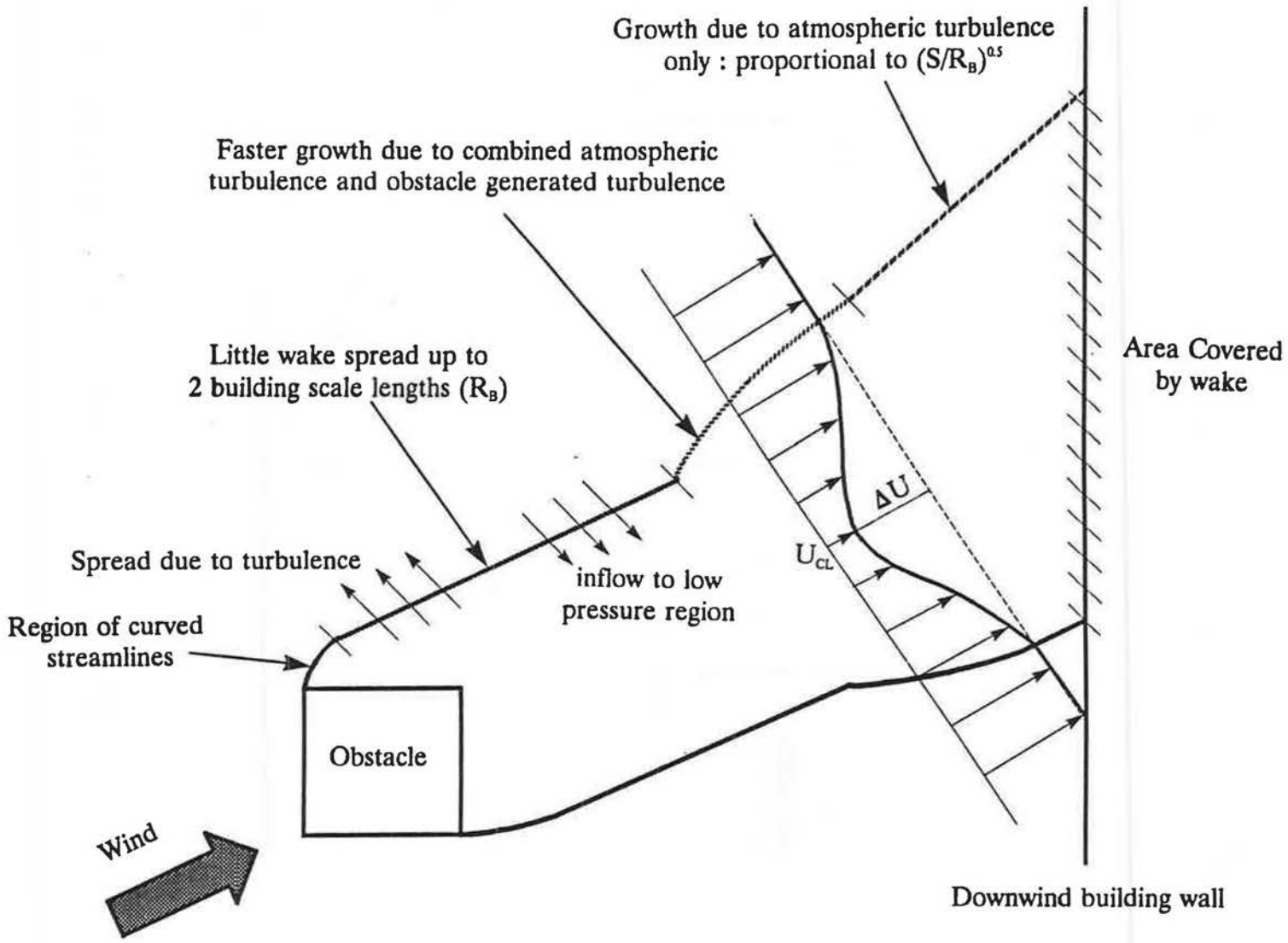

Figure 2-12a. Plan view of real near wake spread behind an obstacle.

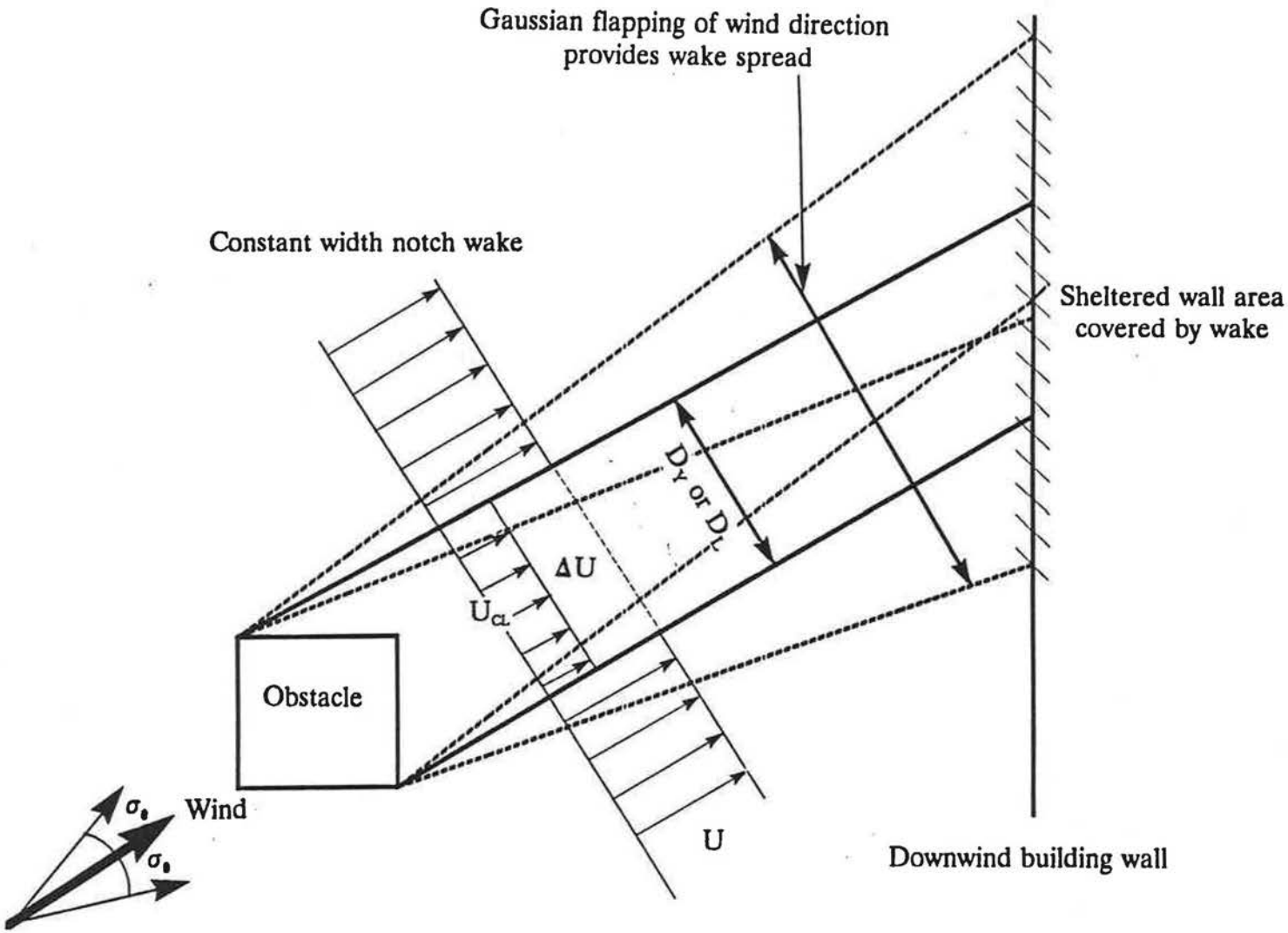

Figure 2-12b. Plan view of the near wake spread for the wind shadow model flapped notch wake behind an obstacle.

extend the same number of building heights downstream as shorter buildings and would thus have extremely large wakes. The experimental results of Hunt, Abell, Peterka and Woo (1978) have shown that this is not the case. Other investigators performing wind tunnel measurements of building wakes have used the building height as the scaling length. This is because many wake studies have been for two dimensional wakes so that the obstacle height is the only scaling length. For this study the results of other investigators that were expressed in terms of building height have been converted to R_B.

The shelter factor for the wake centreline, $S_{U,CL}$ is given by

$$S_{U,CL} = \frac{U_{CL}}{U} \qquad (2\text{-}28)$$

where U_{CL} is the centreline velocity in the wake as shown in Figures 2-12a and 2-12b. U_{CL} is the velocity that is used to calculate surface pressures, i.e. $U_S = U_{CL}$. The velocity deficit in the wake, ΔU can be defined as

$$\Delta U \equiv U - U_{CL} \qquad (2\text{-}29)$$

The velocity deficit in the wind shadow wake is assumed to be constant across the wake with a step change to the external flow velocity at the wake boundary and thus the wake looks like a notch cut out of the surrounding flow. The wind shadow is determined by projecting this wake from an upstream obstacle onto the building of interest as if it were casting a shadow of reduced windspeed.

2.8 Crosswind and Vertical Spread of Wakes

The development of the wake behind a real building is shown in Figure 2-12a. This figure illustrates the factors effecting wake growth. The present study has concentrated on the near field wakes that are typical of houses in a row. The houses used for model validation in this study are in an east - west row with a separation distance $S/R_B = 0.35$ and the wind shadow model has been developed to give the best results in this region. This is the most important region for shelter effects for most buildings because further downstream the velocity reductions are small and wind shelter is not a significant effect. Figure 2-12b shows the model of the wake used in the wind shadow notch wake technique. There are four sections of the wake that can be identified as having different factors governing the growth of the wake.

2.8.1 Region of Curved Streamlines ($S/R_B < 0.1$)

The region closest to the obstacle where accelerating flow around the obstacle

causes streamline curvature and rapid wake growth. This area is very small and is not included in the model due to the complexity of calculating the amount of wake spread in this region (that is a function of wind angle and obstacle geometry). In addition, this region has a very small effect on the total wake growth.

2.8.2 Notch-Like Wake Region ($0.1 < S/R_B < 2$)

Up to about two obstacle dimensions, R_B, downstream the measurements of wake cross section velocities by Peterka, Meroney and Kothari (1985) show little wake growth. The wake width stays at approximately the obstacle width with a uniform velocity profile until $S/R_B \approx 2$ then the wake spreads to a smooth velocity profile further downstream as illustrated in Figure 2-13. This is due to a balance of the wake spreading due to turbulence and convective flow into the low pressure region behind the obstacle. This is the region where the notch model wake is most realistic and also where shelter is most important.

2.8.3 Region of Growth due to Combined Atmospheric and Building Generated Turbulence ($2 < S/R_B < 3$)

After the low pressure region behind the obstacle has returned to the ambient pressure the wake spread is governed by turbulence effects. Additional turbulence is created by the obstacle that results in more rapid wake growth than due to atmospheric turbulence alone. The additional obstacle turbulence has been shown in Hunt's (1974) theory and in the measurements of Peterka, Meroney and Kothari (1985) to decay rapidly proportional to $(S/R_B)^2$. This means that at $S/R_B = 3$ the additional root mean square (rms) turbulence is at about 10% of its initial value immediately behind the building and thus it is a relatively weak effect by this point. After this point, which is only $S/R_B = 1$ downstream from the end of the previous constant width region, the effect of this additional turbulence is small.

The magnitude of the excess turbulence immediately downstream of an obstacle is not well known. The results of Peterka, Meroney and Kotharis' (1985) experiments cannot be used because their hot wire anemometer could not measure flow reversals. This results in overprediction of mean velocities and underprediction of turbulence because the negative velocity measurements are sensed as positive. Castro and Robbins (1977) used a pulsed hot wire anemometer that is sensitive to flow direction for measuring wake velocities. Castro and Robbins do not present sufficient data to make systematic estimates of the turbulence and in some areas of the wake the measurements show reduced turbulence intensities compared with the

R_B is the characteristic Obstacle dimension

S is down wind distance

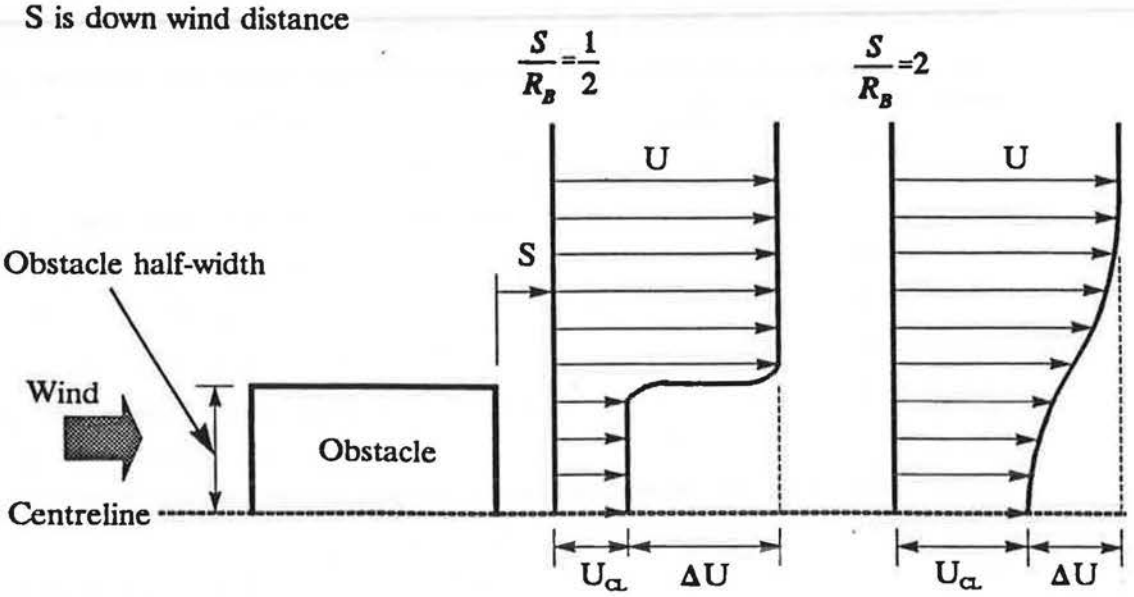

Figure 2-13. Plan view sketch of the change from a Notch to a Smooth velocity profile across a wake based on the measurements of Peterka, Meroney and Kothari (1985). In this plan view only one half of the obstacle and wake is shown due to symmetry.

undisturbed flow. The uncertainty in the amount of turbulence generated by the obstacle makes it impractical to include this in the model.

The effect of additional turbulence from the obstacle is neglected in the notch wake model because it acts over a small distance and thus has only a small effect on the total wake spread.

2.8.4 Far Wake Region ($S/R_B > 3$)

The spread of the far wake is dominated by atmospheric turbulence. In this region the effect of the obstacle geometry is negligible and only momentum deficit is important. Theoretical predictions by Hunt (1974) and Lemberg (1973) combined with measurements by Peterka, Meroney and Kothari (1985) and Lemberg (1973) have shown that the wake width increases proportional to $(S/R_B)^{0.5}$ for $S/R_B>3$. This rate of wake spread is the same for a two dimensional (long row of trees) or a three dimensional (house) obstacle in a shear flow (see Counihan, Hunt and Jackson (1974) and Hunt (1974)). This further spreading of the wake is accounted for by flapping the wind shadow notch wake over a range of wind angles as shown in Figure 2-12b, i.e. varying the wind angle about its mean value. The amount of flapping depends on atmospheric turbulence. The wind shadow model applies a gaussian weighting to ΔU over a range of wind angles about the mean wind direction, so that more extreme angles have less effect and shelter is reduced further from the wake centreline as shown in Figure 2-13 in the smooth far wake velocity profile. The standard deviation for the gaussian distribution, σ_θ, has been estimated using the mean wind speed and the atmospheric turbulence (typically about 20% in urban surroundings) by vectorially summing the along wind (mean) and cross wind (turbulent) wind components. The angle between the mean direction and the vector sum is taken to be the standard deviation of wind direction such that

$$\sigma_\theta = \arctan\left(\frac{U_{rms}}{U}\right) \qquad (2\text{-}30)$$

where σ_θ is the standard deviation of wind direction and U_{rms} is the root mean square of the turbulent velocities. The effect of the gaussian weighting on the shelter coefficient, S_U, will be calculated later.

If the turbulence generated by the obstacle were known, then in the rapid growth region where building and atmospheric turbulence are combined the standard deviation of wind direction could be estimated using

$$\sigma_\theta = \arctan\left(\frac{(U_{rms}+U_{rms,o})}{U}\right) \qquad (2\text{-}31)$$

where $U_{rms,o}$ is the rms of the additional turbulence created by the obstacle. This is further complicated by $U_{rms,o}$ decaying rapidly proportional to $(S/R_B)^2$.

2.8.5 Vertical Wake Spread

The above four points examine only horizontal wake spread. The wake also spreads vertically in a similar fashion. The measurements and theoretical predictions of Lemberg (1973) and the measurements of Peterka, Meroney and Kothari (1985) show that vertical wake spread is the same as horizontal wake spread and is proportional to $(S/R_B)^{0.5}$. This is a surprising result because the vertical spread of the wake is into higher momentum flow due to the increase in velocity with height in the atmospheric boundary layer. The wake spread in the far field (where the results of Hunt et. al. (1978) were measured) is dependent on the atmospheric turbulence only and should result in the same spreading velocity horizontally and vertically. As the wake spreads vertically the higher advective velocities compared with those for the horizontal spread would be expected to result in the vertical wake dimension being smaller at a given down wind location. The results of Hunt et. al. and Lemberg may be due to an increase in turbulent velocities with height that increases the rate of vertical wake spread approximately in proportion to the change in along wind velocity.

Vertical wake spread is dealt with the wind shadow model by allowing the wake to flap vertically, increasing the wake effective height above the height of the obstacle. This is an important consideration only if a short obstacle is sheltering a taller building and the vertical wake spread determines how much of the tall building is covered by the wake or if the wake spread is sufficient for the tall building to be completely immersed in the wake.

2.9 Velocities and Pressures in Wakes

The change in pressure in a wake effects the momentum balance but not the surface pressures directly. Wake theories e.g. Hunt (1974), Lemberg (1973) and Counihan, Hunt and Jackson (1974) use the assumption of constant static pressure in their momentum balances. These theories are only applied far downstream of an obstacle where this assumption is reasonable. The drop in pressure at the rear of an obstacle is what produces negative pressure coefficients on the downwind surfaces. A typical measured value is Cp = -0.2 (see Table 2-1). The rate of pressure recovery

in the wake is very difficult to measure due to the highly turbulent flow in this region and there is very little discussion of this in the literature. Measurements by Lemberg (1973) found no change in static pressure in the flow field. This seems to indicate that the pressure recovery is rapid but Lemberg does not give a detailed enough description of the measurements to be certain of this. In this study it is assumed that the pressure recovers rapidly enough that the velocity recovery predicted by the theories of Hunt (1974) and measurements of Peterka, Meroney and Kothari (1985) can be applied to the near wake.

The velocity recovery in the wake behind an obstacle was illustrated in Figure 2-11. The velocity returns to its upstream value as a function of the distance downstream. As shown in the figure a building in the wake of an obstacle will experience these changes in velocity thus changing the pressures driving ventilation. Most theories and measurements for velocity recovery have concentrated on the centreline velocity as this shows the greatest reduction and the slowest recovery. The velocities at the edge of the wake recover faster as they are closer to the high momentum fluid in the external flow and turbulent diffusion of momentum also has an effect. This can be seen in the data presented by Peterka, Meroney and Kothari (1985) for horizontal and vertical wake velocity profiles.

The flow in the recirculation region behind the obstacle is extremely complex as has been shown in many flow visualisation experiments (e.g. Davies, Quincey and Tindall (1980), Woo, Peterka, and Cermak (1977) and Peterka, Meroney and Kothari (1985)). The flow has three dimensional vortex structures and turbulence effects that are strongly dependent on wind direction and building geometry. These effects are too complex for the simple wind shadow model developed here, and the present model will concentrate on the centreline wake velocity.

For the notch wake shown in Figure 2-14 the centreline velocity is applied across the whole wake. This figure illustrates the lower velocity deficit at the edges of a real wake, and the flow acceleration outside the wake. From the measurements of Peterka, Meroney and Kothari (1985) this local acceleration is a relatively small effect (less than 10% of the velocity deficit) and is neglected in the wind shadow wake model.

From the theory of self-preserving velocity profiles in wakes, Hunt (1974) has shown that for a three dimensional turbulent wake in a boundary layer flow

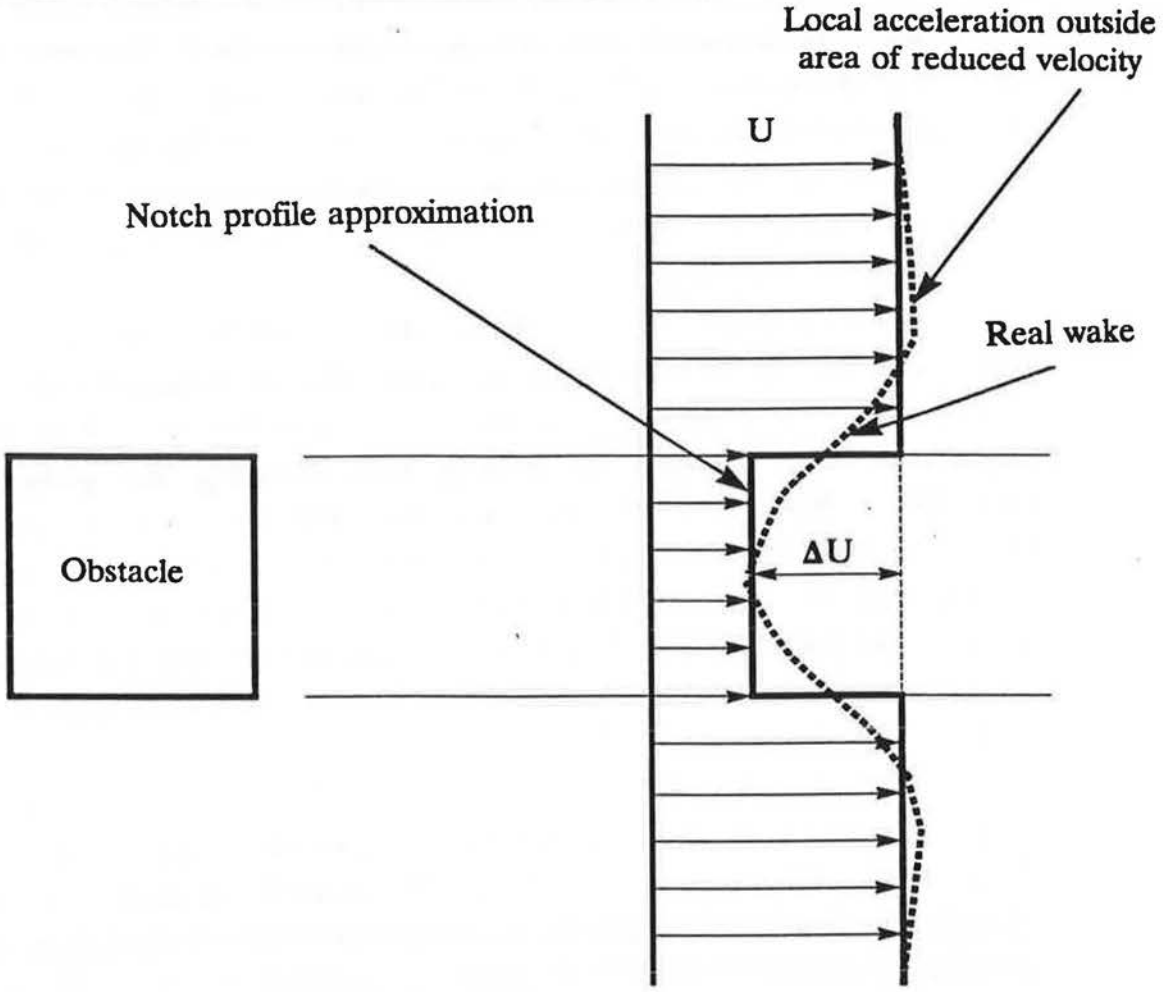

On the centreline ΔU for a real wake = ΔU for a notch wake

Figure 2-14. Plan view of comparison of velocity profiles across real and notch wakes in the far field ($S/R_B > 3$).

$$\frac{\Delta U}{U} \propto \left(\frac{R_B}{S}\right)^a \qquad (2\text{-}32)$$

where S is the distance downstream of the obstacle and

$$a = \left(\frac{3+p}{2+p}\right)$$

where p is the power law exponent of the boundary layer mean velocity profile (see section 2.5.3). For typical values of p of 0.12 to 0.47, "a" has a narrow range of values : $1.5 > a > 1.4$. Wind tunnel measurements in wakes behind structures in simulated atmospheric turbulent boundary layers by Peterka, Meroney and Kothari (1985) and Lemberg (1973) show that $a \approx 1.5$. Lemberg (1973) predicts $a = 1.5$ from his theory that determined wake centreline velocities based on the variable eddy viscosity model of Sforza and Mons (1970) and Hunt (1971). Because the range of a is small, for simplicity the wind shadow wake model will use a single value of $a = 1.5$. This corresponds to uniform flow with $p=0$ in Equation 2-32.

The separation distance, S, shown in Figure 2-10 is the distance from the centre of the surface being sheltered to the obstacle along a line parallel to the wind direction. If this line does not strike the obstacle then S is the distance to the projected plane of the nearest wall of the obstacle as shown in Figure 2-10. The shelter factor on the wake centreline, $S_{U,CL}$, is calculated individually for each wall as they each have a different distance to the obstacle. This is most important when the shielding obstacle is close to the building being studied. The assumption of self preservation means that all the velocity profiles measured downstream of an obstacle all have the same form when appropriately non-dimensionalised. This means that a single functional relationship between velocity and downstream distance, S, can be used to describe the wake. This is only true in the far field (where the wake decay has become independent of the obstacle geometry) which is at least three obstacle heights downstream for a three dimensional turbulent wake as shown by the results of Peterka, Meroney and Kothari (1985). In many cases shelter is provided by obstacles closer than three heights away. To account for this a virtual origin displacement can be introduced by rewriting Equation 2-32 as

$$\frac{\Delta U}{U}=\left(\frac{B_1}{\frac{S}{R_B}+B_2}\right)^a \qquad (2\text{-}33)$$

Combining Equations 2-28,2-29 and 2-32 yields the following relationship for the shelter factor $S_{U,CL}$:

$$S_{U,CL}=1-\left(\frac{B_1}{\frac{S}{R_B}+B_2}\right)^{\frac{3}{2}} \qquad (2\text{-}34)$$

where B_1 and B_2 must be found from measurements. Letting $B_1 \neq B_2$ accounts for possible flow reversals and non-zero velocities when S is close or equal to zero.

B_1 and B_2 have been estimated from the experimental results of Wiren (1985) who measured pressure coefficients on buildings of different separations. The value of $S_{U,CL}$ can be estimated by taking the square root of the ratio of the sheltered pressure coefficient to the unsheltered pressure coefficient. Using Equation 2-34 with the known building size and separation distance enables estimates of B_1 and B_2 to be made. Using measured pressure coefficients rather than velocities means that B_1 and B_2 will also include any static pressure changes. Given the limitations imposed by the limited quantity of data available it is reasonable to let $B_1 = B_2$. This implies that the mean windspeed is zero at the rear wall of the obstacle, which is a physically realistic assumption. The best fit to Wiren's data was found to be when $B_1 = B_2 = 3.3$. With more detailed Cp data better estimates of B_1 and B_2 could be made. A lower value of B_1 and B_2 results in a more rapid initial velocity recovery when S/R_B is small. $S_{U,CL}$ is calculated using Equation 2-35.

$$S_{U,CL}=1-\left(\frac{3.3}{\frac{S}{R_B}+3.3}\right)^{\frac{3}{2}} \qquad (2\text{-}35)$$

2.10 Accounting for Wake Spread

To account for the effect of turbulence on wake spread, as shown in Figure 2-11a and discussed earlier, a gaussian distribution of wind direction about the mean is assumed. The gaussian distribution is used to weight the calculated values of S_U

for each wind angle. This has the effect of smoothing out abrupt changes in wind shelter with wind angle that can result from the notch profile calculation of L_s and thus provides more realistic shelter estimates. To find the shelter factor for the mean wind angle θ, the shelter factors for wind angles, that deviate from θ by ϕ, are weighted by the gaussian distribution, f, given by

$$f(\phi,\theta,\sigma_\theta)=\frac{1}{\sqrt{2\pi}\sigma_\theta}\exp\left(-\frac{1}{2}\left(\frac{\phi-\theta}{\sigma_\theta}\right)\right) \qquad (2\text{-}36)$$

In the present study the standard deviation of wind direction was estimated by assuming a crosswind component atmospheric turbulence intensity of about 20%. This means that root mean square crosswind velocities perpendicular to the mean velocity are 20% of the mean velocity. This value of root mean square velocity is based on a summary of experimental results given by Panofsky and Dutton (1986) that shows that RMS crosswind velocities are typically 20%. The root mean square component of crosswind velocity from Panofsky and Dutton is for typical urban surroundings and a one hour time averaged velocities. The deviation in wind direction depends on the length of time average used. Time averages greater than about three hours should not be used because the deviation in wind direction will include the effects of changing weather systems. At shorter time averages all the scales of atmospheric turbulence may not be included. Wollenweber and Panofsky (1989) give a factor for correcting the deviation, $\sigma_{\theta 1}$, measured over the averaging time, t_{avg1}, to the deviation, σ_θ, measured over a different averaging time, t_{avg} as follows:

$$\sigma_\theta=\sigma_{\theta 1}\left(\frac{t_{avg}}{t_{avg1}}\right)^{0.2} \qquad (2\text{-}37)$$

Equation 2-37 allows for the increase in deviation with the increase in average time as a greater range of turbulent scales are included in the averaging process. The one hour time averages presented by Panofsky and Dutton are used in this study because the measured validation data was averaged over one hour and do not require the correction factor given by Equation 2-37.

For the wind shadow model the deviation in direction is found from the approximation $\sigma_\theta = \tan^{-1}(0.20)$ that is valid for small angles. This gives a standard

deviation of $\sigma_\theta \approx 11.3°$. To find S_U at the central wind direction, θ, sixty one deviations in wind angle, ϕ, are spread over $\pm 3\sigma_\theta$ (approximately one point per degree of wind angle). At each deviation angle ϕ the S_U calculated for that angle is multiplied by the weighting factor, f, calculated using Equation 2-36. The sum of the 61 points thus calculated gives S_U at the central wind direction, θ. This is an extremely tedious process requiring many trigonometric calculations for S_U and L_s.

For the validation of the ventilation model a computer programme was used to calculate S_U for all four walls of the test buildings at AHHRF every one degree of wind angle. The calculation of S_U is based on the empirically determined parameters that are summarised in Table 2-3.

Table 2-3. Summary of empirical parameters used to calculate shelter factor, S_U

Parameter	Value	Data Source
a Exponent for mean velocity decay	1.5	Peterka, Meroney and Kothari (1985) Lemberg (1973)
B_1 and B_2 Coefficients for mean velocity decay	$B_1 = B_2 = 3.3$	Based on pressure coefficients from Wiren (1985)
σ_θ Standard deviation of wind direction	11.3°	various sources listed in Panofsky and Dutton (1986)

The output of the computer programme is shown in Figures 2-15 and 2-16. When the walls are not sheltered $S_U = 1$ and complete shelter corresponds to $S_U = 0$. Figure 2-15 is for the north wall and shows the symmetry of its shelter with a maximum wind speed reduction factor of $S_U = 0.43$ for winds from 110 and 250 degrees. Figure 2-16 is for the east wall where the shelter is asymmetric since the sheltering building is much closer for east winds than west winds when the house is between the east wall and the upwind building. For east winds (90 degrees) the shelter effect is a maximum with $S_U = 0.25$. For west winds the shelter is less, with $S_U = 0.61$. Once these values of S_U are calculated they are stored in a data file as a lookup table thus reducing the calculations required by the ventilation model.

Localised leakage sites such as open windows or attic ventilators use the same Cp and S_U as the surface on which they are located. The attic surfaces (gable ends, soffits and the pitched roof slope) use the same shelter values as the house walls directly beneath them.

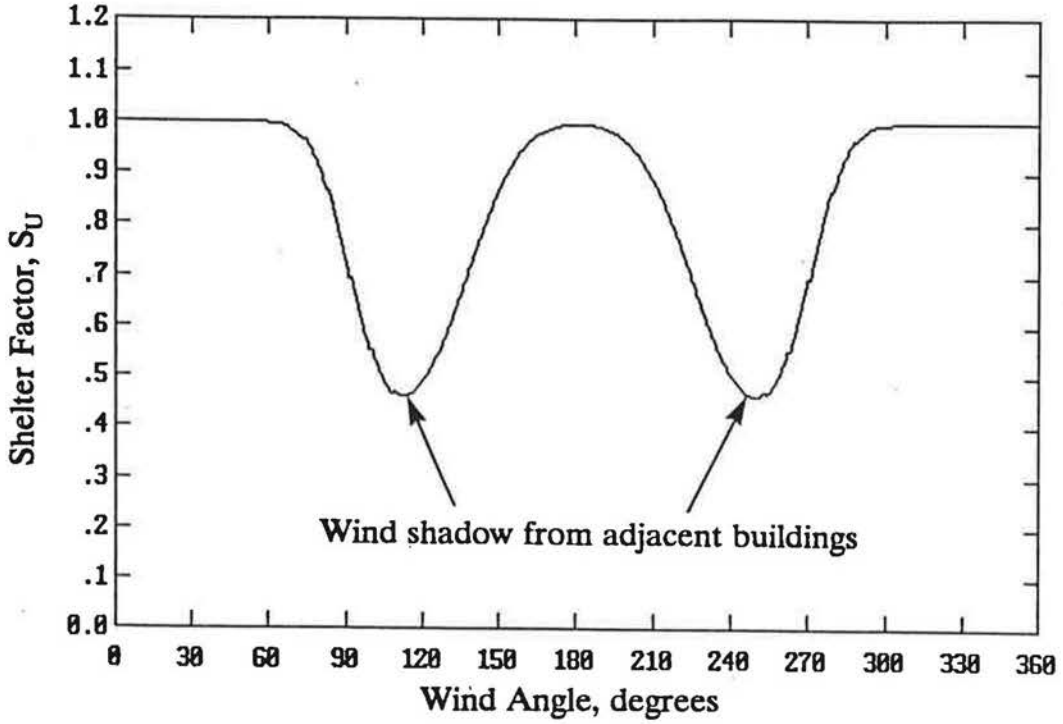

Figure 2-15. Wind angle dependence of wind speed reduction factor, S_U, for the north wall of a house at AHHRF. Calculated using data from Wiren(1985).

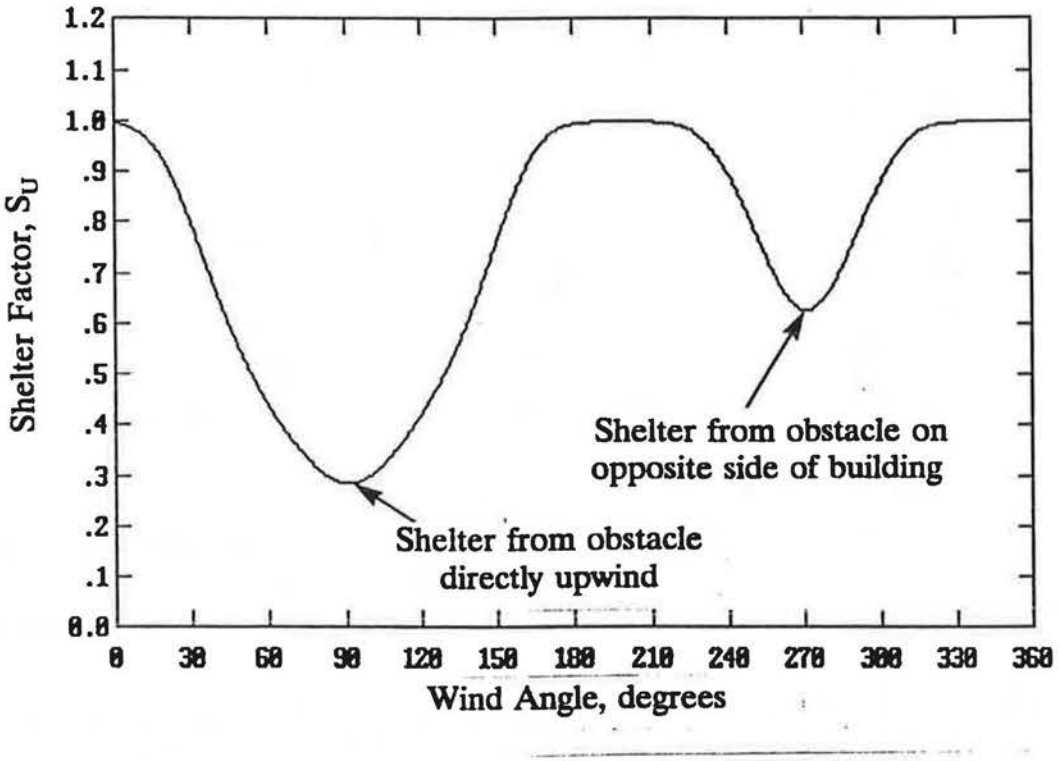

Figure 2-16. Wind angle dependence of wind speed reduction factor, S_U, for the east wall of a house at AHHRF. Calculated using data from Wiren(1985).

2.11 Combining Wakes

In some situations a building may be sheltered by more than one upwind obstacle. This complex flow situation is difficult to model using wake decay Equation 2-35 used in this study. For combined wakes, one wake is growing inside another wake. For the internal wake the external flow conditions are changing because they are a wake that is decaying. Equation 2-35 is based on the assumption that the flow external to the wake is not changing (i.e. U = constant) and therefore cannot be applied to the combined wakes. Wind tunnel studies by Wiren (1985) have shown that for multiple upwind obstacles the nearest obstacle will dominate the shelter effect. This only applies if the obstacles are of similar size. If the furthest upwind obstacle is a large building and the nearest obstacle is a lamp post then clearly the large building will have a greater sheltering effect. In this study the buildings where the measurements were made are sheltered by other buildings of the same size and the shelter is calculated based on the nearest building only, without the need to combine wakes.

2.12 Summary of Wind Shadow Shelter Model

The wind shadow shelter model has been developed to account for the sheltering effects of upwind obstacles on the surface pressures of houses and attics. The model uses a simple notched velocity profile with constant velocity deficit across the wake. For simplicity, the notch velocity profile does not include the three dimensional aspect of the wake flow including vortices and flow acceleration at the edges of the wake. The sheltering effect of the notch wake is flapped over a range of wind directions on either side of the mean wind direction with a gaussian weighting to account for wake spreading caused by atmospheric turbulence. Current wake theories only apply in the far field where velocity defects are assumed to be small and the specific geometry of the obstacle is no longer significant. The notched wake allows wake width and velocity close to the obstacle (where shelter effects are most significant) to be modelled. The model produces realistic shelter factors for a wide range of inputs and can be applied to many obstacle geometries because it relies on simple geometric construction to find the amount of shelter projected by an obstacle onto the building of interest. Static pressure changes in the wake are included indirectly in shelter factor coefficients developed from surface pressures measured by Wiren (1985).

2.13 Flow through Each Leak for the House

ATTICLEAK-1 has been developed to combine the ventilation from known ventilation sites such as fans, furnace flues, open windows and doors, and other passive vents with distributed background leakage. The distributed leakage, found from fan pressurization tests, is the unintentional leakage in a building envelope between the walls and foundation, in the ceiling, and around windows, doors and other holes in the vapour barrier. Following the work of Sherman (1980) and Sherman and Grimsrud (1980) at Lawrence Berkeley Laboratories the distributed leakage for the house is divided into user specified fractions at ceiling level, in the walls, and at floor level. This idea was modified in ATTICLEAK-1, where each of the four walls may have different amounts of leakage. As a further refinement the floor level leaks are further divided into four parts, one below each wall, for houses with basements. This allows different floor level leakage for each side of the building depending on plumbing penetrations and other leakage sites. It is assumed that the building has a rectangular floor plan so that there are four sides to the building, and that the flow exponent, n, in Equation 2-1, is the same for all distributed leaks. Because the flow exponent is assumed to be the same for all the distributed leaks, the flow coefficient, C_d, is equal to the sum of the user specified fractions. The total distributed leakage flow coefficient, C_d, and exponent, n_d, are best estimated from fan pressurization results. The flow coefficients for the ceiling, floor level leaks and walls are estimated as fractions of the total distributed leakage such that

$$C_d = \sum_{i=1}^{4} C_{f,i} + \sum_{i=1}^{4} C_{w,i} + C_c \qquad (2\text{-}38)$$

where $C_{f,i}$ is the floor level leakage below wall i, $C_{w,i}$ is the leakage in wall i and C_c is the ceiling leakage. The additional building leaks not included in C_d have different values of flow exponent so that the total building leakage cannot be found by simply adding the distributed and localised leakage coefficients.

The attic distributed leakage is divided into sloped roof pitch, soffit, gable end and attic floor areas. The attic floor leakage is the same as the ceiling leakage for the house by definition. Additional attic leakage sites include gable vents, roof vents and roof ridge vents. The flow through the attic leaks will be discussed later in section 2.14.

The following section deals with the particular flow through each leak. For

each leak C and n must be specified for use in the flow Equation 2-1, and Cp, S_U and z specified for the pressure difference Equation 2-18.

2.13.1 Furnace Flues and Fireplaces

Furnace flues and fireplaces are usually the largest openings in the building envelope and typically have a flow exponent, n_F, close to 0.5. In a previous study (Walker (1989)) the author measured the flow characteristics of a 6m length of flue made of 15cm diameter round galvanized steel, with a rain cap at one end. The results showed that $n_F = 0.54$ for both forward and backdraughting flow. The flue leakage coefficient, C_F, can be calculated from diameter, D_F, of the flue or fireplace assuming orifice flow. The values of C_F from Walker's (1989) experiments showed that the discharge coefficient of $K_D = 0.6$ should be used in the following orifice equation

$$C_F = K_D \left(\frac{\pi D_F^2}{4} \right) \sqrt{\frac{2}{\rho}} \qquad (2\text{-}39)$$

where ρ is the density of the airflow.

An estimate of the pressure coefficient to be used for furnace flues, Cp_F, can be found in Haysom and Swinton (1987). Haysom and Swinton measured Cp's at the top of flues with a range of flue caps and found a typical value of Cp = -0.5 in a uniform flow. Using this pressure coefficient, that is different from those used on other building leaks is important because the furnace flue is usually the largest single leakage site on a building. The change in wind velocity with height above grade may be significant for furnace flues that protrude above the reference eaves height. Equating the pressure produced by the increased velocity, U_F, at Cp = -0.5 to the pressure produced by the reference wind speed, U, (measured at the eaves height, H_e) and Cp_F using Equation 2-4 gives

$$U^2 Cp_F = U_F^2 (-0.5) \qquad (2\text{-}40)$$

Rewriting this equation in terms of Cp_F gives

$$Cp_F = \left(\frac{U_F}{U} \right)^2 (-0.5) \qquad (2\text{-}41)$$

The change in wind speed with height is found by assuming a power law wind velocity

such that:

$$\frac{U_F}{U}=\left(\frac{H_F}{H_e}\right)^p \tag{2-42}$$

where H_F is the height of the top of the flue above grade. The corrected Cp_F is then found by substituting Equation 2-42 in 2-41 to give

$$Cp_F=(-0.5)\left(\frac{H_F}{H_e}\right)^{2p} \tag{2-43}$$

Shelter for the flue, $S_{U,F}$, is the shelter factor at the top of the flue. If the surrounding buildings and other obstacles are below the flue height then it is assumed that $S_{U,F} = 1$. If the surrounding obstacles are higher than the flue then the flue is sheltered and $S_{U,F}$ is calculated using Equation 2-35. Now the general pressure difference Equation 2-18 can be written specifically for the furnace flue as

$$\Delta P_F=\Delta P_I-P'_T H_F+P_U S^2_{U,F} Cp_F \tag{2-44}$$

where P_U and P'_T are given by Equations 2-6 and 2-12 respectively.
The mass flow rate, M_F, for the flue is given by Equation 2-45.

$$M_F=C_F(\Delta P_F)^{n_F} \tag{2-45}$$

For a heated flue with the furnace on or a fire in the fireplace the temperature of the gas in the flue is T_F is used instead of the inside temperature, T_{in}. The flue temperature is used to find ρ_F in the mass flow rate Equation 2-1, correct C in Equation 2-3, and to change the driving pressure for flue flow. An extra term is added to Equation 2-44 that accounts for the difference in pressures between a flue full of air at T_{in} and air at T_F. The extra term is given by

$$-gH_F(\rho_{in}-\rho_F) \tag{2-46}$$

The density difference is expressed in terms of temperatures assuming that the air in the flue is an ideal gas so that

$$\Delta P_F=\Delta P_I+P_U\, S_{U,F}^2\, Cp_F-P_T'\, H_F-g\rho_{in}H_F\left(1-\frac{T_{in}}{T_F}\right) \qquad (2\text{-}47)$$

The extra term, from Equation 2-46, makes the flue flow driving pressure more negative and therefore increases the outflow through the flue. For a flue taken in isolation (with no ΔP_I or P_U) raising the flue temperature to 373K from 293K (typical T_{in}) will approximately quadruple the driving pressure and thus double the mass flow rate (with $n_F \approx 0.5$). This change in the flue temperature will also change C_F as shown by Equation 2-3.

2.13.2 Floor Level Leakage

The leakage at floor level, $C_{f,i}$, is estimated as a fraction of the total distributed leakage and n_f is the same as n for the other distributed leaks. There are two cases of floor level leakage that require different assumptions about wind pressure effects. The cases depend on house construction.

a. Basements and Slab on Grade

In this case the total floor level leakage is split into four parts, one for each side of the building. On each side the floor level leakage is given the same Cp and S_U as the wall above it. For the i^{th} side of the building

$$\Delta P_{f,i}=\Delta P_I+Cp_i\, S_{U,i}^2\, P_U-H_f\, P_T' \qquad (2\text{-}48)$$

where H_f is measured from grade level. For a house with a basement this is the height of the main level floor above grade and the leakage coefficient, $C_{f,i}$ includes the leakage around basement windows, dryer vents etc.

The mass flow rate for these floor level leaks is given by Equation 2-49.

$$M_{f,i}=C_{f,i}(\Delta P_{f,i})^{n_f} \qquad (2\text{-}49)$$

b. Crawlspaces

As an estimate of the wind pressure in a crawl space the shelter and pressure coefficients for the four walls of the building are averaged. The average is weighted for non square plan buildings by the length of each side, L_i, so that for the i^{th} side.

$$Cp_f=\sum_{i=1}^{4} S_{U,i}^2 Cp_i\left(\frac{L_i}{L_\pi}\right) \qquad (2\text{-}50)$$

where L_T is the perimeter of the building (the sum of the L_i's) and then the pressure across the crawlspace is given by

$$\Delta P_f = \Delta P_I + Cp_f P_U - H_f P_T' \quad (2\text{-}51)$$

The mass flow rate through the crawlspace leakage is given by Equation 2-52

$$M_f = C_f (\Delta P_f)^{n_f} \quad (2\text{-}52)$$

In the present study the houses where the measurements were made all had full basements and so the floor level leakage is divided into four parts and Equations 2-48 and 2-49 were used to find the floor leakage pressure differences and mass flow rates, respectively.

2.13.3 Ceiling Leakage

The ceiling flow coefficient C_c is estimated from the total distributed leakage and n_c is the same as n for the other distributed leaks. There are no wind pressures acting on the ceiling except indirectly through ΔP_I and $\Delta P_{I,a}$ as the ceiling is completely sheltered from the wind. $\Delta P_{I,a}$ is the equivalent of ΔP_I for the attic zone. The pressure across the ceiling includes the difference in attic and house buoyancy pressures

$$\Delta P_c = \Delta P_I - \Delta P_{I,a} - \rho_{out} g H_a \left(\frac{T_{in} - T_{out}}{T_{in}} - \frac{T_a - T_{out}}{T_a} \right) \quad (2\text{-}53)$$

When $T_a = T_{out}$ the buoyancy term is the same as for a house with no attic. When $T_a = T_{in}$ the buoyancy term vanishes and only the difference in internal pressures due to wind forces is acting across the ceiling.

The mass flow rate through the ceiling is given by Equation 2-54.

$$M_c = C_c (\Delta P_c)^{n_c} \quad (2\text{-}54)$$

2.13.4 Wall Leakage

For the i^{th} wall $C_{w,i}$ is estimated from the total distributed leakage and the flow exponent, n, for each wall is n_d, the same as for the other distributed leaks. The linear change in pressure with height due to stack effect means that when inflows and outflows are balanced there is a location where there is no pressure difference. This is called the neutral level, H_{NL} and is given by Equation 2-19. The location of the neutral level is shown in Figure 2-2, where $\Delta P = 0$. For $T_{in} > T_{out}$ flow is in below

H_{NL} and out above H_{NL}, with the flow directions reversed for $T_{out} > T_{in}$. If there is no stack effect and $P'_T = 0$, then the pressure is constant over the wall and H_{NL} is undefined. In this case the pressure difference across wall i is given by

$$\Delta P_{w,i}=\Delta P_I+S_{U,i}^2 Cp_i P_U \tag{2-55}$$

When $T_{in} \neq T_{out}$ the total flow through each wall must be found by integration because the pressure difference varies with height. This change in pressure and the change in mass flow rate with height is illustrated in Figure 2-17. The limits of integration for pressure are found at the top, ΔP_t, and bottom, ΔP_b, of the wall and are

$$\Delta P_t=\Delta P_I+S_{U,i}^2 Cp_i P_U-H_e P_T' \tag{2-56}$$

$$\Delta P_b=\Delta P_I+S_{U,i}^2 Cp_i P_U-H_f P_T' \tag{2-57}$$

The change in pressure with height, z, is given by Equation 2-18 such that

$$\Delta P_{w,i}(z)=\Delta P_I+S_{U,i}^2 Cp_i P_U-zP_T' \tag{2-58}$$

Thus the flow through the wall is also a function of height which must be integrated to find the total mass flow in and out of wall i.

$$M_{w,i}=\int dM_{w,i}(z)dz \tag{2-59}$$

where

$$dM_{w,i}(z)=\rho dC_{w,i}(\Delta P_{w,i}(z))^{n_i} \tag{2-60}$$

where $\Delta P_{w,i}(z)$ is given by Equation 2-58. Assuming evenly distributed leakage allows easy integration over the wall because the fractional leakage $dC_{w,i}$ is given by

$$dC_{w,i}=C_{w,i}\frac{dz}{(H_e-H_f)} \tag{2-61}$$

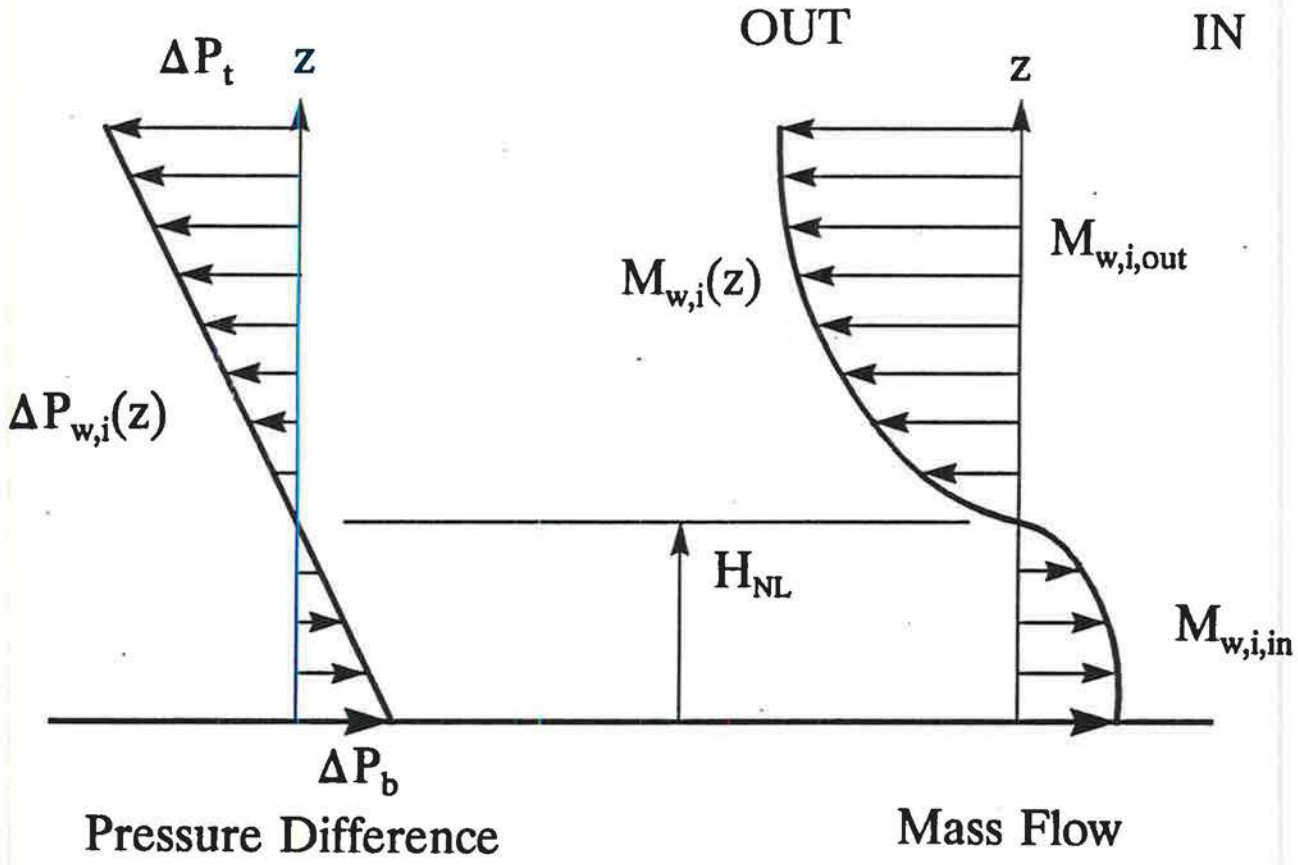

Figure 2-17. Variation of pressure difference and mass flows with height for a wall.

Substituting Equations 2-60 and 2-61 in 2-59 gives

$$M_{w,i}=\frac{\rho C_{w,i}}{(H_e-H_f)}\int \Delta P_{w,i}^{n_d} dz \qquad (2\text{-}62)$$

where the limits of integration depend on the neutral level height, H_{NL}, that is found for each wall using Equation 2-18. The next section shows how the limits of integration change depending upon H_{NL}. When H_{NL} is on the wall there is flow both in and out of the wall and upon integrating Equation 2-62 the masses flowing in and out are kept separate. This important for the total mass balance and for keeping track of all the flows through the building envelope.

There are six cases of wall flow, each with different integration limits, for Equation 2-62. There can be inflow, outflow or two-way flow for the wall with the flow direction determined by T_{in} and T_{out}. All of the cases are given in appendix A including an example derivation of Equation 2-63 and 2-64. The example case given here is for $T_{in} > T_{out}$ with H_{NL} on the wall with flow in below H_{NL} and flow out above H_{NL}, such that

$$M_{w,i,out}=\frac{\rho_{in} C_{w,i} \Delta P_t^{n_d+1}}{(H_e-H_f)P_T' (n_d+1)} \qquad (2\text{-}63)$$

$$M_{w,i,in}=\frac{\rho_{out} C_{w,i} \Delta P_b^{n_d+1}}{(H_e-H_f)P_T' (n_d+1)} \qquad (2\text{-}64)$$

2.13.5 Fan Flow

There can be multiple fans at different locations on the house envelope. Each fan may have its own fan characteristics of rated flow, Q_{rated}, and pressure difference, ΔP_{rated}. Fans at different locations will have different wind and stack pressures. Because the flowrate through a fan depends on the pressure difference across it the flow through a fan is found by using a fan performance curve. The operating point on the curve is determined by the pressure across the fan due to the wind, stack and internal pressure difference pressures. The stack and wind pressures across each fan are found by specifying which wall the fan is on and its height above grade, H_{fan}. Cp_{fan} and $S_{U,fan}$ are the same as the wall they are located in. The pressure difference across the fan is then given by

$$\Delta P_{fan}=\Delta P_I+S_{U,fan}^2 Cp_{fan} P_U-H_{fan} P_T' \quad (2\text{-}65)$$

A fan performance curve is used to find the effect that ΔP_{fan} has on the flowrate through the fan. Figure 2-18 shows a schematic of a fan curve illustrating this principle. The rated flowrate for the fan is Q_{rated} with no pressure drop and the maximum pressure that the fan can provide is ΔP_{rated} at no flow. Approximating the fan performance curve by a power law using p_{fan} gives the following equation for mass flow through the fan:

$$M_{fan}=\rho Q_{rated}\left(\frac{\Delta P_{rated}+\Delta P_{fan}}{\Delta P_{rated}}\right)^{p_{fan}} \quad (2\text{-}66)$$

where ρ is equal to ρ_{in} for outflow and ρ_{out} for inflow.

The flow direction is determined by the sign of the pressure term. A positive term means inflow and a negative term means outflow. ΔP_{rated} is positive for a supply fan and negative for an exhaust fan. The power, p_{fan}, depends on the type of fan being used. For the centrifugal fans used in this study it is assumed that $p_{fan} = 0.3$.

2.13.6 Vent Leakage

The vent leakage is attributed to deliberately installed leakage sites that are separate from the background leakage. These vents are assumed to be horizontal so that the temperature of air inside them does not change the pressure across the leak. ATTICLEAK-1 allows multiple vents to be installed, each with their own flow characteristics and each at a different location on the house envelope. Furnace and fireplace flues are treated separately as they may contain heated air that would produce a stack effect for that leak only. The flow characteristics, C_V and n_V must be known for each vent. These vents are assumed to exit through the walls at a height, H_V, with the same exterior shelter and pressure coefficients, S_U and Cp, as the wall they are located in. Vents exiting through the roof use the same Cp and S_U as the furnace flue. The pressure difference across a vent is

$$\Delta P_V=\Delta P_I+S_{U,V}^2 Cp_V P_U-H_V P_T' \quad (2\text{-}67)$$

Q_{rated} = Maximum fan flowrate

ΔP_{rated} = Maximum fan pressure

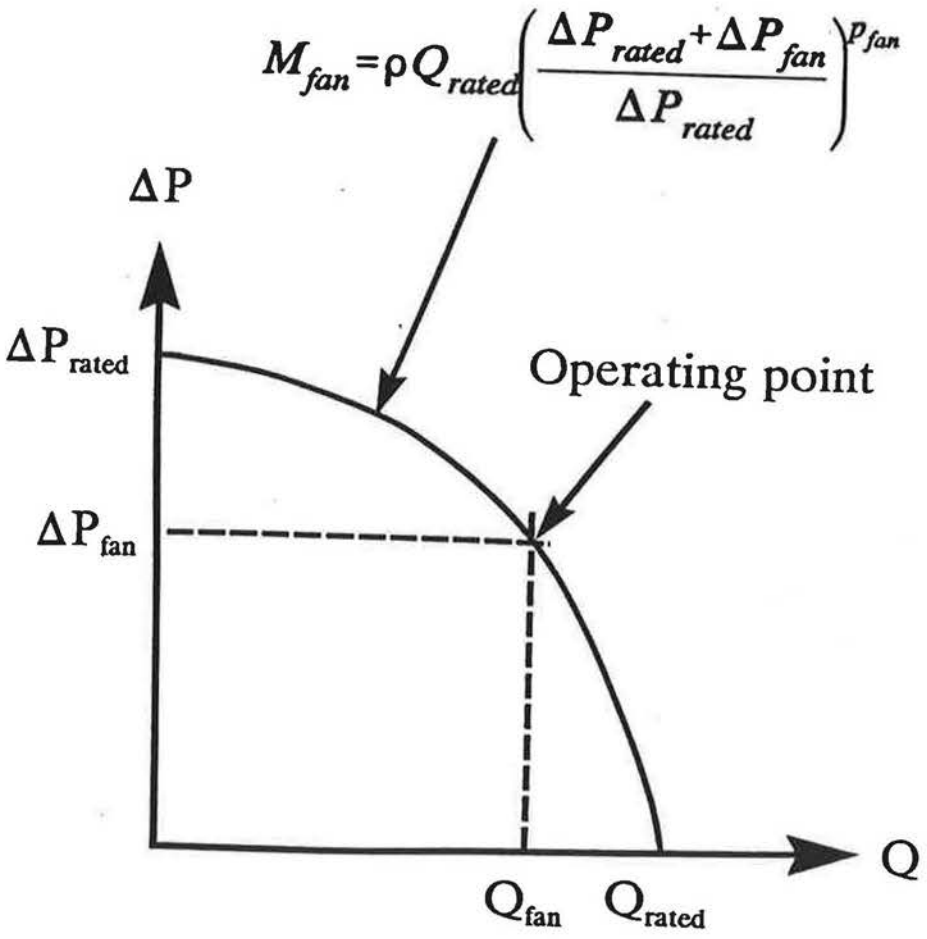

Figure 2-18. Schematic of fan performance curve

The mass flow through each vent is given by Equation 2-68.

$$M_V = C_V(\Delta P_V)^{n_V} \tag{2-68}$$

2.13.7 Flow through open Doors and Windows

Open doors and windows are both modelled the same way: as rectangular openings in the building envelope. The effect of specific door or window geometry (e.g. sliding windows or hinged windows) has been neglected for simplicity. Previous studies of flow through windows have concentrated on flows dominated by either temperature differences or wind effects, but little has been done with the combination of the two. Brown and Solvason (1962) developed flow relationships assuming stack effect only, and they assumed that exactly half of the opening area had inflow and half had outflow which implies equal volume flowrate and not equal mass flow. Shaw and Whyte (1974) studied the effects of additional forced airflow into a room combined with flow through an opening due to stack effect. They too assumed that exactly half of the opening area had inflow and half had outflow, which is unlikely for a room that is pressurized or depressurized due to forced ventilation.

The effects of wind pressure have been examined for flow through a single opening by Crommelin and Vrins (1988) and Cockroft and Robertson (1976). A major complication in determining flowrates due to wind pressure is the turbulent nature of the wind. Both the turbulence intensity and the energy spectra of the turbulence effect the flowrates. The various turbulent scales interact in different ways with both the building and the specific window geometry, e.g. the opening angle of hinged windows. Crommelin and Vrins found that the ventilation rates varied by a factor of two depending on the orientation of the open window to wind direction. An exact relationship is more complex as it depends on which turbulent scales are dominant in the atmospheric boundary layer. Cockroft and Robertson showed that a higher turbulence intensity resulted in greater ventilation rates and that a reasonable estimate of the amount of air entering a single opening that mixes completely with the internal air is approximately 1/3. This result applies to a building with a single opening in one wall with no net flow through the opening so that the air exchange is due to turbulence only. In a real building there will always be some net flow through the opening and this situation will not arise.

The mechanisms of ventilation outlined above are not well understood even for this simple single opening cases and are not included in this model. The factors neglected in estimating flow through open windows or doors in this model are:

• Window and door opening geometry. Crommelin and Vrins (1988) looked at the effect of hinged external windows on flow rate through the opening. Vertically hinged windows were tested by Crommelin and Vrins with the opening facing upwind and downwind. Their results showed increases in ventilation of up to a factor of three compared with the opening with no external hinged window. For sliding windows as used in the present study this effect does not occur.

• Interaction of turbulent scales in the wind with building and opening geometry. The mechanism of interaction is complex depending on the relationship between atmospheric turbulent scales, building scales and opening scales. This has been studied by Haghighat, Rao and Fazio (1991) for buildings with one and two openings. The two opening case is most like a real building with other leaks elsewhere on the building envelope. For the two opening case Haghighat et al. found that the turbulent flow through an opening was 84% of the mean flow.

The flowrates through door and window openings are determined by integrating the flow velocity profiles found by applying Bernoulli's equation along streamlines passing through the opening as shown by Kiel and Wilson (1986). For convenience the following parameters are defined

$$P_b = CpS_U^2U^2 - 2gH_b\left(\frac{T_{in}-T_{out}}{T_{in}}\right) + \frac{2\Delta P_I}{\rho_{out}} \qquad (2\text{-}69)$$

$$P_t = CpS_U^2U^2 - 2gH_t\left(\frac{T_{in}-T_{out}}{T_{in}}\right) + \frac{2\Delta P_I}{\rho_{out}} \qquad (2\text{-}70)$$

where Cp and S_U are for the surface that the opening is in

H_b = Height above grade of the bottom of the opening

H_t = Height above grade of the top of the opening

As with the integrated wall flows the mass flows in and out depend on H_{NL}, T_{in} and T_{out}. Figures 2-19a to 2-19c show the three different cases of neutral level location and flow pattern for $T_{in} > T_{out}$. All of the possible cases for flow above and below H_{NL} are given in appendix A. Appendix A also contains a derivation for the flow in below H_{NL} for the case where H_{NL} falls in the opening and $T_{in}>T_{out}$, such that

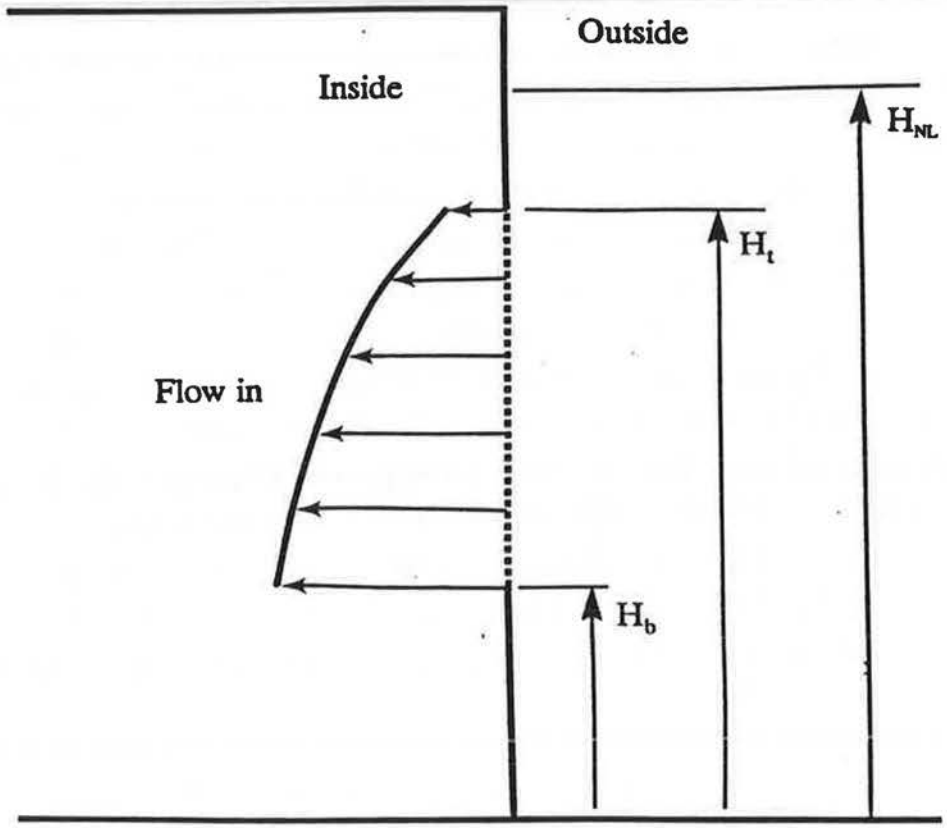

Figure 2-19a. Flow through window or door opening with the neutral level, H_{NL}, above the top of the opening, H_t, and all flow in.

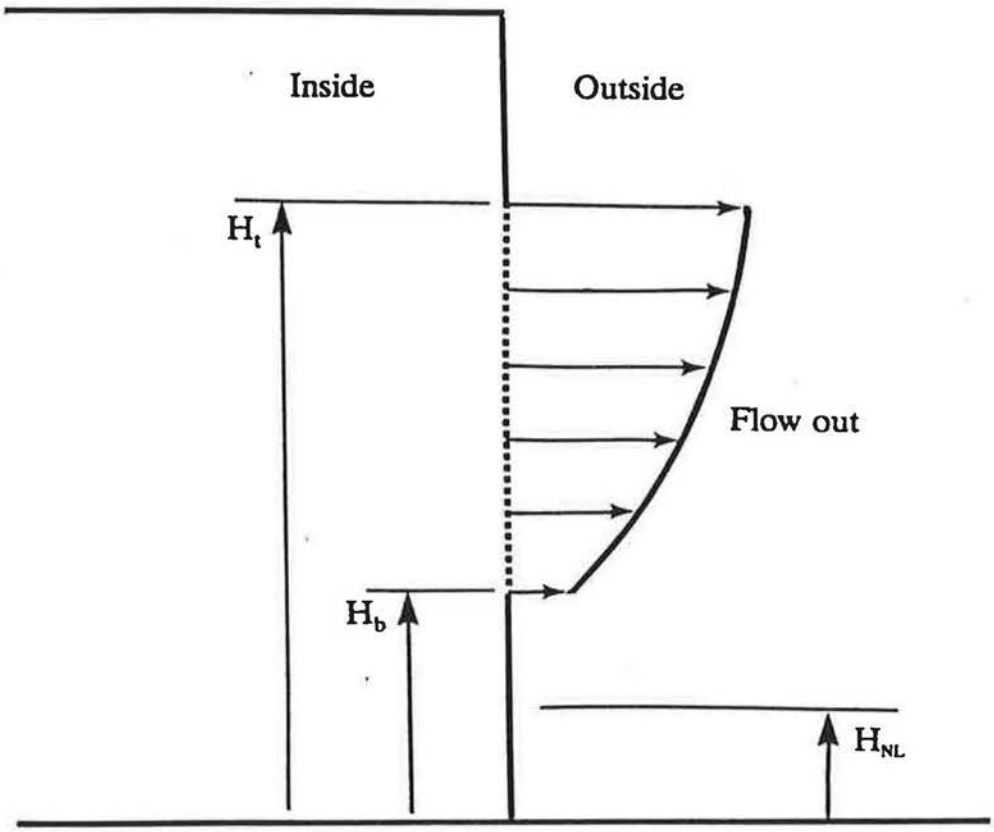

Figure 2-19b. Flow through window or door opening with the neutral level, H_{NL}, below the bottom of the opening, H_b, and all flow out.

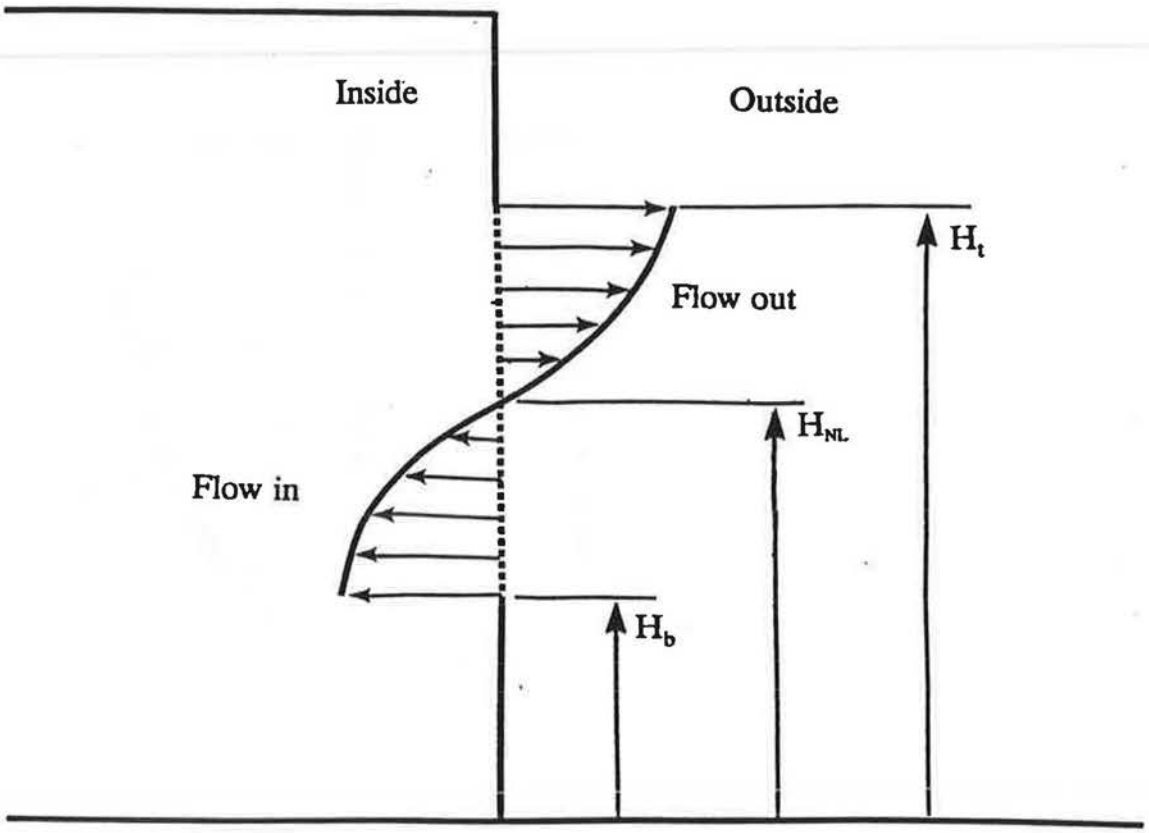

Figure 2-19c. Flow through window or door opening with the neutral level, H_{NL}, between the top, H_t, and the bottom of the opening, H_b. Flow is out above H_{NL} and in below H_{NL}.

$$M_{out}=(\rho_{out}\rho_{in})^{\frac{1}{2}}\frac{KWT_{in}}{3g(T_{in}-T_{out})}P_t^{\frac{3}{2}} \quad (2\text{-}71)$$

$$M_{in}=\rho_{out}\frac{KWT_{in}}{3g(T_{in}-T_{out})}P_b^{\frac{3}{2}} \quad (2\text{-}72)$$

2.13.8 Window and Door Flow Coefficient, K

The flow coefficient, K, accounts for reduction in flow due to flow contraction, viscous losses and interfacial mixing. An estimate for K that accounts for the variation in K due to interfacial mixing generated by atmospheric turbulence is given by Kiel and Wilson (1986) as

$$K=0.400+0.0045|T_{in}-T_{out}| \quad (2\text{-}73)$$

The flow coefficient must be altered when the interface is near the top or the bottom of the opening so that the iterative solution of flow for the whole building does not have the neutral level oscillating just above and below the top or bottom of the opening. A first order approximation is to let K vary linearly in the top and bottom 10% of the opening between the value of K with the neutral level at 10% or 90% of the opening height and K = 0.6 at the edges of the opening. This is physically realistic because when the interface is near the top or the bottom of the opening the edges of the opening will interfere with the interfacial mixing process. This will make the flow look more like one way flow with an assumed orifice discharge coefficient, K_D = 0.6.

2.14 Flow Through each Leak for the Attic

The attic ventilation section of ATTICLEAK-1 uses the same approach as for the house. The total leakage is divided into distributed leakage and localised leakage. The flow through each leak is then calculated using the pressure difference across each leak. The pressure difference uses the same relationship (Equation 2-18) as the house but with T_a replacing T_{in} in P'_T. For wind pressures, P_U is used together with the Cp's and S_U's for each leak location. The general pressure difference equation for attic leaks is given by

$$\Delta P(z)=CpS_U^2\rho_{out}\frac{U^2}{2}-gz(\rho_{out}-\rho_a)+\Delta P_{I,a} \qquad (2\text{-}74)$$

where $\Delta P_{I,a}$ is the internal pressure difference for the attic and is the equivalent of ΔP_I for the house.

Equation 2-74 can be written in terms of P_U and $P'_{T,a}$

$$\Delta P(z)=CpS_U^2P_U-zP'_{T,a}+\Delta P_{I,a} \qquad (2\text{-}75)$$

where

$$P'_{T,a}=\frac{\rho_{out}g(T_a-T_{out})}{T_a} \qquad (2\text{-}76)$$

The total distributed leakage flow coefficient $C_{d,a}$ and exponent $n_{d,a}$ are best estimated from fan pressurization results. All the distributed leakage sites are assumed to have the same flow exponent. The flow coefficients for the roof and soffit must be estimated as fractions of the total distributed leakage such that

$$C_{d,a}=\sum_{i=1}^{4}C_{s,i}+C_r \qquad (2\text{-}77)$$

where C_r is the total leakage in the two pitched roof surfaces and $C_{s,i}$ is the leakage in the soffit or gable ends above each wall. For the houses used in this study the north and south sides have soffits and the east and west sides have gable ends.

2.14.1 Pitched roof Leakage

The pitched roof leakage is treated the same way as house walls. The two pitched roof surfaces are assumed to have equal leakage. Therefore there is $C_r/2$ leakage in each surface. C_r is estimated from the total distributed leakage in the attic and n_r is the same as the n for the other distributed leaks. C_r is assumed to be evenly distributed over the pitched roof surfaces in the same way as wall leakage is evenly distributed. The same method of integrating the pressure difference over the height of the roof pitch can then be used to find the total mass flow. Equation 2-62 can be used with Equation 2-75 for attic pressure difference in place of the house pressure difference (Equation 2-58), and with $C_r/2$ in place of $C_{w,i}$.

Cp for the pitched roof surfaces is found using Equation 2-21 and Table 2-2. The pitched roof is assumed to have the same shelter factor as the furnace flue. This

means that if the surrounding obstacles are not higher than the flue top (which is close to roof peak height) then the pitched roof surfaces have no shelter and S_U = 1. If the surrounding obstacles are taller than the building in question then S_U for the pitched roof surfaces is estimated to be the same as the wall below them. For example, a south facing roof pitch would then have the same S_U as calculated for the south facing wall below it. For the attic roof the neutral level,$H_{NL,r}$, is calculated for the two roof pitches using the appropriate Cp and S_U values in

$$H_{NL,r}=\left(\frac{\Delta P_{I,a}+S_U^2 Cp P_U}{P'_{T,a}}\right) \tag{2-78}$$

There are several different cases of flow through the pitched roof surfaces depending on the location of $H_{NL,r}$, T_a and T_{out}. The same combination of cases exist as for flow through walls. All of the cases are given in appendix A. The pressure differences at the eave height, ΔP_e, and at the roof peak, ΔP_p, are defined as follows and are convenient to use when calculating the mass flow rates.

$$\Delta P_p=\Delta P_{I,a}+S_U^2 Cp P_U-H_p P'_{T,a} \tag{2-79}$$

$$\Delta P_e=\Delta P_{I,a}+S_U^2 Cp P_U-H_e P'_{T,a} \tag{2-80}$$

An example case given by Equations 2-81 and 2-82 is for $T_a > T_{out}$ with $H_{NL,r}$ somewhere on the pitched roof surface between the eave height, H_e, and the peak height H_p. There is two way flow through the roof surface in this case with flow in below $H_{NL,r}$ and flow out above $H_{NL,r}$:

$$M_{r,out}=\frac{\rho_a \frac{C_r}{2}\Delta P_p^{(n_r+1)}}{(H_p-H_e)P'_{T,a}(n_r+1)} \tag{2-81}$$

$$M_{r,in}=\frac{\rho_{out} \frac{C_r}{2}\Delta P_e^{(n_r+1)}}{(H_p-H_e)P'_{T,a}(n_r+1)} \tag{2-83}$$

2.14.2 Soffit and Gable Leakage

The soffit and gable leakage are treated identically. The soffit and gable leakage is split into four parts, one for each side of the building. $C_{s,i}$ is the estimated fraction of the total attic distributed leakage in the soffit or gable on the i^{th} side of the building. H_s is the height of the leakage above grade and usually $H_s = H_e$ for soffits. For the gable leakage H_s can be assumed to be H_e plus half of the attic height (H_p - H_e). The wind pressure coefficient (Cp_i) and shelter factor ($S_{U,i}$) are assumed to be the same as for the wall below each soffit or gable. This simplifying assumption is made due to lack of data for wind pressure coefficients on soffits. There is little data because the additional complexity added to the building by including eave overhangs makes systematic wind tunnel measurements extremely time consuming. The pressure difference across each soffit or gable above wall i is then given by

$$\Delta P_{s,i}=\Delta P_{I,a}+Cp_i\ S_{U,i}^2\ P_U-H_s P'_{T,a} \tag{2-83}$$

The flow through each soffit or gable is given by

$$M_{s,i}=C_{s,i}(\Delta P_{s,i})^{n_r} \tag{2-84}$$

2.14.3 Attic Vent Leakage

Attic vents provide extra ventilation leakage area over the background distributed leakage. There can be multiple attic vents at different locations on the attic envelope, each with their own C_V and n_V. C_V and n_V are user specified leakage characteristics of each vent. Usually the vent can be assumed to act like an orifice with $n_V = 0.5$. In that case C_V can be estimated from the vent area multiplied by the discharge coefficient, K_D. The vent area should be corrected for any blockage effects e.g. by insect screens. $S_{U,V}$ and Cp_V for each vent are the same as for the attic surface they are on, either the gable ends (which have the same S_U and Cp as the wall below them) or the roof pitches. H_V is the height above grade of the vent and the pressure difference across each attic vent is given by

$$\Delta P_{V,a}=\Delta P_{I,a}+S_{U,V}^2\ Cp_V\ P_U-H_V\ P'_{T,a} \tag{2-85}$$

$\Delta P_{V,a}$ is calculated for each attic vent and the flow through each attic vent is given by

$$M_{V,a}=C_V\,(\Delta P_{V,a})^{n_V} \tag{2-86}$$

2.14.4 Attic Floor Leakage

The mass flow rate through the attic floor is calculated by the house zone part of the ventilation model in Equation 2-54. The resulting $\Delta P_{I,a}$ from balancing the mass flows for the attic zone is returned to the house zone to be used in Equation 2-53 to calculate pressure across the ceiling, and then to recalculate the mass flow through the attic floor.

2.14.5 Ventilation Fans in Attics

Fans are included in the same way as for the house zone by using a fan performance curve. The operating point on the curve is determined by the pressure across the fan. The stack and wind pressures across each fan are found by specifying which attic surface the fan is located in and its height above grade, H_{fan}. Cp_{fan} and $S_{U,fan}$ are the same as the surface the fan is are located in. There can be multiple fans each with their own rated flowrates, Q_{rated}, and rated pressure differences, ΔP_{rated}. The pressure difference across each attic fan, $\Delta P_{fan,a}$, is given by

$$\Delta P_{fan,a}=\Delta P_{I,a}+S_{U,fan}^2 Cp_{fan} P_U - H_{fan} P'_{T,a} \tag{2-87}$$

Approximating the fan performance curve by a power law using p_{fan} gives the following equation for mass flow through each fan:

$$M_{fan,a}=\rho Q_{rated}\left(\frac{\Delta P_{rated}+\Delta P_{fan,a}}{\Delta P_{rated}}\right)^{p_{fan}} \tag{2-88}$$

where ρ is equal to ρ_a for outflow and ρ_{out} for inflow.

The flow direction is determined by the sign of the pressure difference term. A positive term means inflow and a negative term means outflow. ΔP_{rated} is positive for a supply fan and negative for an exhaust fan. The power, p_{fan}, depends on the type of fan being used. For the centrifugal fans used in this study it is assumed that $p_{fan} = 0.3$.

2.15 Solution Method

2.15.1 For Each Zone

All of the flow equations for the house contain the difference between the inside and outside pressure, ΔP_I, that is the single unknown (or $\Delta P_{I,a}$ for the attic).

To find ΔP_I all of the flow equations are combined into one equation that is the mass balance for air in the house

$$\sum M = M_F + M_f + M_c + \sum_{i=1}^{4} M_{w,i} + M_V + M_{fan} = 0 \qquad (2\text{-}89)$$

where M_f is the mass flow rate through all the floor level leaks, M_V is the mass flow rate through all of the vents and M_{fan} is the sum of the mass flow rates through all of the fans. This equation for mass balance is highly non-linear in ΔP_I. A Newton-Raphson iterative technique was used to attempt to solve this equation using the partial derivatives of all the flow equations with respect to ΔP_I. Unfortunately the shape of the solution curve of ΔP_I and ΣM makes this method unstable. A more robust iterative bisection technique was adopted because it is unaffected by the non-linearity of the function. This bisection search technique assumes that $\Delta P_I = 0$ for the first iteration and the mass inflow or outflow rates are calculated for each leak. At the next iteration ΔP_I is chosen to be +1000 Pa if total inflow exceeds total outflow and -1000 Pa if outflow exceeds inflow. These large initial pressure differences mean that even large high pressure fans may be included. Succeeding iterations use the method of bisection in which ΔP_I for the next iteration is reduced by half the difference between the last two iterations, thus the third iteration changes ΔP_I by $\pm$500 Pa. The sign of the pressure change is positive if inflow exceeds outflow and negative if outflow is greater then inflow. The limit of solution is determined by the number of iterations. After 17 iterations the change in ΔP_I is < 0.01 Pa, which gives mass flow imbalances on the order of 0.001 Kg/s (or 4Kg/hour).

For the attic the mass balance equation is given by

$$\sum M = M_r + M_c + \sum_{i=1}^{4} M_{s,i} + M_{V,a} + M_{fan,a} = 0 \qquad (2\text{-}90)$$

where M_r is the sum of the in and the out flows through the pitched roof surfaces, $M_{fan,a}$ is the sum of the mass flows through all the attic fans and $M_{V,a}$ is the sum of the flows through all the attic vents. As with the house all of the components of this mass balance equation contain the single unknown, $\Delta P_{I,a}$, the attic to outdoor pressure difference. The attic zone is solved using the same bisection technique as the house zone. The two zones interact through the ceiling flow that is common to both mass balance Equations 2-89 and 2-90.

2.15.2 Coupled Zones

The house and attic zones are coupled by the flow through the ceiling and pressure difference across the ceiling. The house zone uses $\Delta P_{I,a}$ to calculate the mass flow through the ceiling. This mass flow is used in the mass flow balance by the attic zone the calculate a new $\Delta P_{I,a}$. This is an iterative procedure that continues until the change in mass flow through the ceiling from iteration to iteration is less than 0.00001 Kg/s. A typical ventilation rate of 0.2 ACH for the houses in this study can be expressed in terms of mass flow as 0.0134 Kg/s. Thus the convergence criteria is about 0.075% of the total house flow.

2.16 Summary of important aspects of ATTICLEAK-1

ATTICLEAK-1 is a two-zone ventilation model that calculates ventilation rates for houses and attics. The flow through each leakage path (and the total flow for each zone) is found by determining the internal pressure in each zone that balances the mass flow rates in and out of each zone. The house and attic interact through the pressure difference and flowrate through the ceiling of the house, and the combined solution is found iteratively. The calculated ventilation rates are used in this study as inputs to the attic heat transfer model and the attic moisture transport model. The ventilation model and the heat transfer model are coupled because the ventilation rate effects the amount of outside and house air convected through the attic (as well as convective heat transfer coefficients) and the attic air temperature changes the attic air density. This change in density changes the mass flow rates and the stack effect driving pressures for ventilation. The combined ventilation and heat transfer model solution is found iteratively, with the ventilation rate being passed to the heat transfer model which then calculates an attic air temperature. This new attic air temperature is then used in the ventilation model to recalculate ventilation rates. The initial temperature estimate for the attic air used in the first iteration for the ventilation model is the outside air temperature. Most of the time the attic air is within a few degrees of the outside air temperature and the combined ventilation and heat transfer model requires only a few iterations (fewer than 5).

Some significant limitations and assumptions for ATTICLEAK-1 are listed below:

- There is assumed to be no valving action in the building and attic leakage so that flow coefficients are independent of flow direction.
- The building has a rectangular planform. The planform must not have the

longest side greater than about three times the shorter side because the wind pressure coefficients used in the model will be incorrect. In addition, both wall and floor level leakage is distributed among four walls and non-rectangular buildings (e.g. L-shaped) have more than four sides.

- The attic has two pitched roof surfaces and gable ends. This assumption affects the leakage distribution and the pressure coefficients applied to the attic leakage sites.
- The interior of both the house and the attic are well-mixed zones so that all of the air entering is completely mixed with the interior air.
- There are no indoor or outdoor vertical temperature gradients, so that the indoor and outdoor densities are independent of location.
- Air behaves as an incompressible ideal gas. This allows density and viscosity to be functions of temperature only.
- Wall and pitched roof leakage is evenly distributed so as to allow simple integration of height dependent mass flow equations.
- All wind pressure coefficients are averaged over a surface. This means that extremes of wind pressure occurring at corner flow separations are not included.
- The notch wake model does not include the three dimensional aspect of wake flow including vortices and flow acceleration at the edge of the wake. These are localised effects that are cannot be included in the model because leaks are not given specific horizontal locations. This can be an important factor for large openings in a wall that may experience much different wind pressures than that produced by the assumption of uniform wake effects for entire walls.
- Upwind obstacles are assumed to shade the entire wall height of the downwind building when calculating wind shelter.

Chapter 3. Attic Heat Transfer Model

The purpose of developing the attic heat transfer model is to determine the temperature of the attic air and the wood in the attic. These temperatures need to be known for the moisture transport model to calculate wood moisture content and to find saturation pressures. The saturation pressures are very important because they are used to calculate attic air relative humidity and to determine if mass is condensing. The moisture and heat transfer models are assumed to be uncoupled because the mass of water vapour transported in and out of the attic is very small (less than 1% of the air mass) and thus transports a negligible amount of energy. Later in this chapter it will be shown that condensation does release significant quantities of latent heat. The attic air temperature is also used to find the attic air density used in ATTICLEAK-1 to find the attic ventilation rates. The attic ventilation rate changes the energy balance for the attic air and the surface heat transfer coefficients. Fortunately this coupling of the ventilation model and the heat transfer model is weak because attic ventilation rates are not a strong function of attic air temperature, as will be shown later.

Some previous authors (Gorman (1987) and Burch and Luna(1980)) used simple steady-state energy balances in the attic that included the attic air, attic floor and the sheathing. These steady-state approaches do not capture the strong diurnal changes in attic temperature due to daytime solar gains or rapid changes in temperatures due to changing ventilation rates. As will be shown later by the attic simulations, these effects cannot be ignored if wood moisture content and condensed mass accumulation are to be predicted. Another approach taken by Peavy (1979) and Wilkes (1989) is to use response factors that include the effect of previous temperatures and heat fluxes to calculate a time dependent response for the attic temperatures. Neither Peavy or Wilkes separated the sheathing surfaces into north and south parts that receive different solar radiation gains or included conduction heat transfer losses through gable end walls. The most comprehensive model to date is that of Ford (1982). Ford (p.104) used a first order lumped heat capacity analysis where the change in energy at each node was equal to the sum of the heat fluxes at the node. The assumption of a lumped heat capacity analysis is improved here by splitting the wood into surface and inner layers. An option for further refinement of this model is to split the wood into more layers because this will improve the assumption of using a single temperature for each node. Ford also separated the north and south sheathing so that they may have different daytime solar gains and

included heat losses through gable ends. Because Ford's model is the most thorough it will be used as the basis of the heat transfer model for this study. A few refinements and simplifications to Ford's attic heat transfer model will be made as listed below:

- An additional node is used to account for the mass of wood in joists and trusses in the attic. This node effectively increases the thermal mass of the attic air.
- Attic ventilation and ceiling flow rates are calculated instead of being a required input. This results in an iterative procedure as the attic ventilation and ceiling flow rates depend on the attic temperature.
- Forced convection heat transfer coefficients are used inside the attic. In this study the ventilation rates are found using ATTICLEAK-1 and thus forced convection heat transfer coefficients may be calculated inside the attic. Ford did not have a ventilation model and so natural convection heat transfer coefficients were used.
- Radiation heat transfer inside the attic is simplified to three nodes: the attic floor and the two pitched roof surfaces. Ford also included gable ends and eaves but these components have small view factors and are neglected for simplicity in the present study.

The energy balance for the attic is based on Ford's lumped heat capacity analysis using the nodes shown in Figure 3-1 where:

T_1 = Temperature of the attic air
T_2 = Temperature of the underside of the North Sheathing
T_3 = Temperature of the outside of the North Sheathing
T_4 = Temperature of the underside of the South Sheathing
T_5 = Temperature of the outside of the South Sheathing
T_6 = Temperature of mass of wood in joists and trusses
T_7 = Temperature of the ceiling inside the house
T_8 = Temperature of the attic floor
T_9 = Temperature of the inside of the gable end walls
T_{10} = Temperature of the outside of the gable end walls

The pitched roof sheathing is labelled north and south so that the differences in solar radiation between north and south facing surfaces may be included. The test houses used in this study were in an east-west row so that they have north and south facing sheathing surfaces.

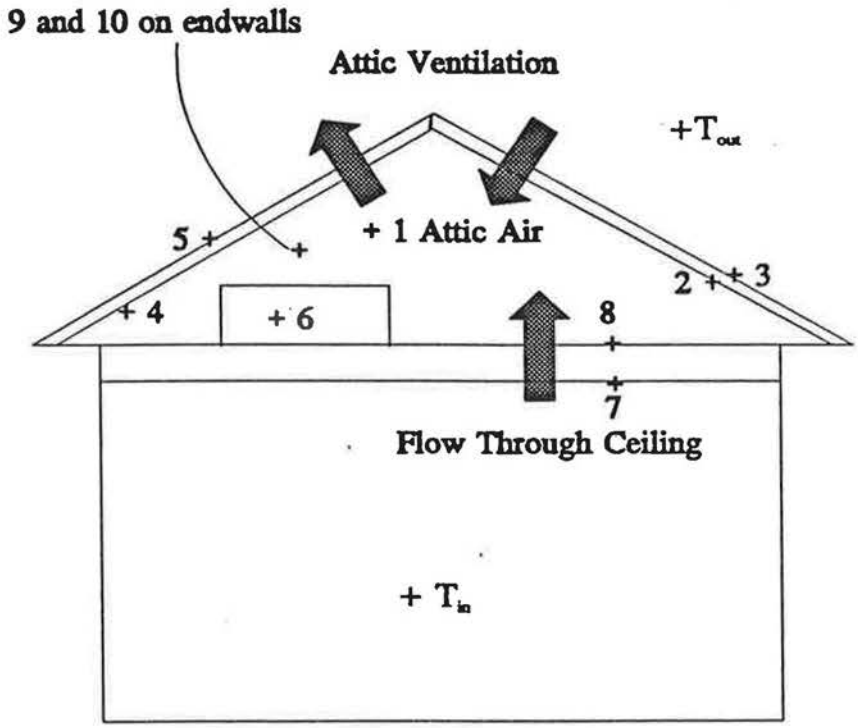

Figure 3-1. Node Locations for Heat Transfer Balance

1 = attic air
2 = underside of the North Sheathing
3 = outside of the North Sheathing
4 = underside of the South Sheathing
5 = outside of the South Sheathing
6 = mass of wood in joists and trusses
7 = ceiling inside the house
8 = attic floor
9 = inside of the gable end walls
10 = outside of the gable end walls

The rate of change of energy is equal to the sum of the heat fluxes for each node so that for node i

$$\rho_i V_i C_{sh,i} \frac{dT_i}{dt} = \Sigma q \qquad (3\text{-}1)$$

where ρ_i is the density [Kg/m^3] , V_i is the volume [m^3], $C_{sh,i}$ is the specific heat [J/KgK], T_i is temperature [K] and q are the heat fluxes [W]. The fluxes are due to convection, radiation and conduction heat transfer. The derivative in this equation is calculated using a finite difference approximation. Only the first term of the finite difference approximation is used so that the equation remains linear with temperature. This first order response assumes that temperatures change linearly with time so that the rate of change of energy with time at a node can be written as a linear equation in temperature as follows

$$\rho_i V_i C_{sh,i} \frac{T_i^j - T_i^{j-1}}{\tau} = \Sigma q \qquad (3\text{-}2)$$

were j refers to the current timestep and j-1 the previous timestep and τ is the length of the time step. Equation 3-2 is a backwards difference approximation to the derivative in Equation 3-1.

The error in approximating the derivative by the first term of the finite difference expansion is given by James, Smith and Wolford (1977) as

$$\text{Error} = \frac{5T^i - 18T^{i-1} + 24T^{i-2} - 14T^{i-3} + 3T^{i-4}}{6\tau} \qquad (3\text{-}3)$$

Using sheathing temperatures measured for this study Equation 3-3 has been used to estimate the errors for the finite difference approximation of Equation 3-2. The sheathing was chosen to evaluate the errors because it experiences the fastest temperature changes. The largest error will be for clear days when the sheathing temperature changes the fastest due to solar radiation gains. For a clear spring day the maximum error in rate of temperature change calculated using Equation 3-3 is about 1.75°C/hour. Over 24 hours the mean error is only 0.02°C/hour and the mean absolute error (where positive and negative errors do not cancel) is 0.6°C/hour. For other nodes whose temperatures change more slowly the errors would be reduced. The maximum error is 25% of the maximum measured temperature change rate of 7°C/hour for this day. This error would make a significant difference to the energy

balance for that hour. Because the temperature is cyclic Equation 3-2 will sometimes overpredict the rate of change of temperature and sometimes under predict, and over 24 hours these effects will tend to cancel out. This is why the 24 hour averages errors are much smaller than the maximum error. The linear finite difference approximation of Equation 3-2 is used in this study for simplicity. The errors introduced by this approximation may be seen in errors in the time response of temperatures in the attic.

In the present study τ is equal to one hour because this is the time interval between measured data points. The energy balance is performed at each hour j with the previous hour's (j-1) temperatures used to calculate the rate of change of energy at each node. This results in a linear system of 10 equations and 10 unknowns (the temperatures) that can be solved using simple matrix solutions. A more complex analysis is unjustified because the rate of change of entered values such as outside temperature, T_{out}, are usually not known.

Figure 3-2 shows some typical heat transfer rates for a winter night and a winter day. The heat flows and attic air temperature were calculated during the simulations presented later in Chapter 7. The arrows indicate the direction of heat flow in each case. These results show that the heat flow through the ceiling is always an important contributor to the heat balance for the attic. During the day, when the solar gains heat the south sheathing, the ventilation flow cools the attic. At night, when the sheathing is losing heat by radiation to the night sky, the ventilation flow acts to heat the attic. This implies that it is important to include the attic ventilation rate and the external sheathing radiation exchanges in the heat transfer model.

3.1 Radiation Heat Transfer

3.1.1 Inside the Attic (Nodes 2,4 and 8)

View Factors

Ford (p.85) calculated view factors for an attic split into seven sections: floor, two gable end walls, two pitched roof surfaces and two eave overhangs (soffits). From Ford's analysis for a gable end attic the view factors from the attic floor and the pitched roof sheathing surfaces to the gable ends are about 0.03. From the pitched roof surfaces to the eaves the shape factors are about 0.11 for the eave directly below each pitched roof surface and about 0.003 for the eave across the attic from each pitched roof surface. The view factors from the pitched roof surfaces to the floor are about 0.76 and from the floor to each pitched roof surface about 0.47.

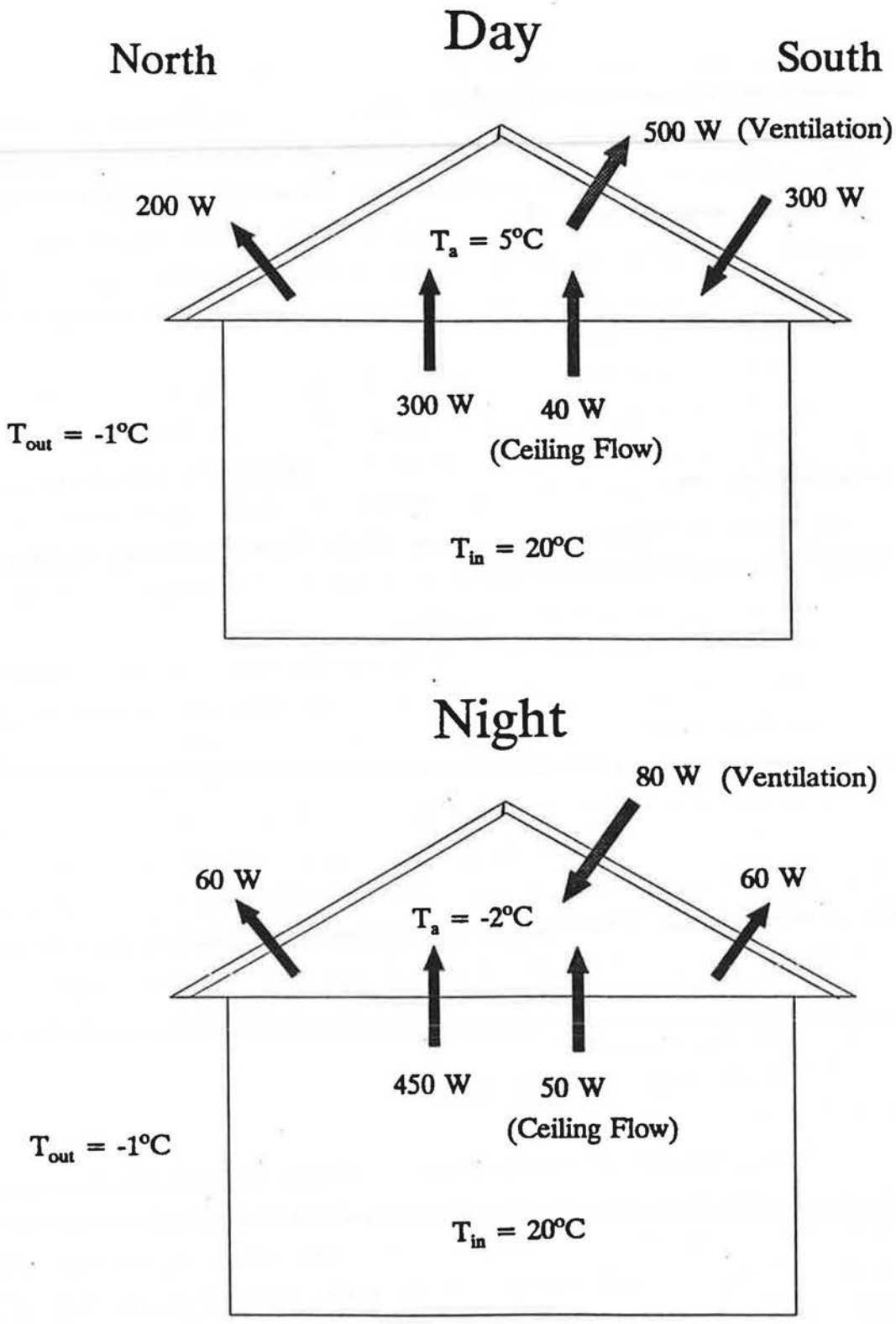

Figure 3-2. Typical attic heat fluxes for an attic with 7 ACH, clear skies, and an outdoor temperature of -1°C.

Including the fact that the pitched roof surfaces and the floor have the largest surface areas of the attic nodes means that these three nodes dominate the internal radiation heat transfer in the attic. For simplicity the model developed for this study will neglect the eave overhangs and the gable ends because they have only a small area and the view factors for the floor and pitched roof surfaces are the largest. This reduces internal attic radiation heat transfer to a three surface problem that does not require numerical integration to find the view factors, F_{i-j}. The subscript i on the view factor indicates the surface that the radiation leaves and the subscript j the surface that the radiation reaches. The three surfaces are

1. Floor, node 8
2. Inner north sheathing, node 2
3. Inner south sheathing, node 4

and the node locations are illustrated in Figure 3-1. The following analysis does not use the complex numerical integration technique used by Ford (p.88) to find the view factors. For the simple three surface model used in this study the view factors have be determined as follows.

For a the test houses at AHHRF the roof slope is 1:3 and the attic floor is almost square (7.3m x 7.8m) if the eaves are included. From symmetry, the view factors for radiation between the floor and each of the two sheathing surfaces are the same. In addition, using a three surface model assumes that the floor only has radiant exchange with these two surfaces so that

$$F_{8-2}=F_{8-4}=0.5 \tag{3-4}$$

The calculated areas of the three surfaces (A_2, A_4 and A_8 where the subscripts refer to the node number) are $A_2 = 30.3\ m^2$, $A_4 = 30.3\ m^2$ and $A_8 = 57\ m^2$. Using the reciprocity theorem and using these calculated areas the view factors for radiation from the sheathing (nodes 2 and 4) to the floor (node 8) are given by

$$F_{4-8}=F_{8-4}\frac{A_8}{A_4}=0.5\frac{57}{30.3}=0.94=F_{2-8} \tag{3-5}$$

The sum of the radiation view factors for each surface is unity, therefore the view factors for radiation between the sheathing surfaces are

$$F_{4-2}=F_{2-4}=0.06 \tag{3-6}$$

If only the attic floor is included in A_8 (i.e. not including the eaves) then A_8 is equal to 49 m^2 and the view factors become

$$F_{4-8}=F_{2-8}=0.81 \tag{3-7}$$

$$F_{4-2}=F_{2-4}=0.19 \tag{3-8}$$

For the purposes of verifying the model a nominal attic width of 7m was used which lies between these two extremes and the view factors then become

$$F_{4-8}=F_{2-8}=0.84 \tag{3-9}$$

$$F_{4-2}=F_{2-4}=0.16 \tag{3-10}$$

Radiation for Three Attic Surfaces

The calculation of radiation exchange inside the attic is based on heat exchange between non-blackbodies from Holman (1981, p.330-332). The final form of the internal attic radiation heat transfer to be used in the present study is given by Equations 3-22 and 3-23. These equations represent a linearised solution to the radiant heat transfer between three bodies: i, j and k. Equations 3-11 to 3-21 are given here to show how the linearised equations were developed by Holman.

The internal surfaces of the attic are assumed to be opaque bodies with no transmission of radiation. Based on this assumption the total radiation leaving the surface can be written as

$$J=\epsilon E_b+(1-\epsilon)G \tag{3-11}$$

where J = radiosity, the total radiation leaving per unit surface area [W/m^2]

ϵ = emissivity of surface

E_b = black body emissive power per unit surface area [W/m^2]

G = Irradiation, the total incident radiation per unit surface area [W/m^2]

The net energy radiant energy, q_R, leaving the surface is the difference between the radiosity and the irradiation

$$\frac{q_R}{A} = J - G = \varepsilon E_b + (1-\varepsilon)G - G \tag{3-12}$$

where A = Area [m^2] of the surface

q_R = rate of radiant energy leaving the surface [W]

Rearranging Equation 3-11 gives the irradiation

$$G = \frac{J - \varepsilon E_b}{1-\varepsilon} \tag{3-13}$$

and substituting Equation 3-13 in 3-12 yields an equation for the rate of energy leaving the surface:

$$q = \frac{E_b - J}{\left(\frac{1-\varepsilon}{A\varepsilon}\right)} \tag{3-14}$$

Of the total radiation leaving surface i the amount that reaches j is $J_i A_i F_{i-j}$ and the radiation leaving j that reaches i is $J_j A_j F_{j-i}$. The net exchange from surface i to surface j is then given by

$$q_{i-j} = J_i A_i F_{i-j} - J_j A_j F_{j-i} \tag{3-15}$$

$A_i F_{i-j}$ is equal to $A_j F_{j-i}$ by reciprocity and Equation 3-15 can be written as

$$q_{i-j} = \frac{J_i - J_j}{\left(\frac{1}{A_i F_{i-j}}\right)} \tag{3-16}$$

Using Equation 3-11 in Equation 3-16, the net radiation leaving surface i that reaches the surface j is given by

$$q_{i-j} = \frac{E_{b,i} - E_{b,j}}{\frac{1-\varepsilon_i}{\varepsilon_i A_i} + \frac{1}{A_i F_{i-j}} + \frac{1-\varepsilon_j}{\varepsilon_j A_j}} \tag{3-17}$$

For the exchange between surfaces j and k Equation 3-17 may be written with k

substituted for j. Combining the exchange between the i and the other two surfaces j and k yields Equation 3-18.

$$q_i=\frac{E_{b,i}-E_{b,j}}{\frac{1-\epsilon_i}{\epsilon_i A_i}+\frac{1}{A_i F_{i-j}}+\frac{1-\epsilon_j}{\epsilon_j A_j}}+\frac{E_{b,i}-E_{b,k}}{\frac{1-\epsilon_i}{\epsilon_i A_i}+\frac{1}{A_i F_{i-k}}+\frac{1-\epsilon_k}{\epsilon_k A_k}} \qquad (3\text{-}18)$$

where q_i is the net radiation heat transfer for node i. Similar equations can be written for surfaces k and j.

The emissive power of a body, E_b, is given by

$$E_b=\sigma T^4 \qquad (3\text{-}19)$$

where T is the temperature of the body and σ is the Stephan-Boltzman constant that is equal to $5.669*10^{-8}$. Substituting the relationship for emissive power, Equation 3-19, into the radiant heat exchange Equation 3-18 results in a highly nonlinear heat transfer equation with temperature to the fourth power where

$$E_{b,i}-E_{b,j}=\sigma(T_i^4-T_j^4) \qquad (3\text{-}20)$$

To keep the system of attic heat transfer equations linear so that it may be easily solved, Equation 3-20 must be linearized. By rearranging the $(T^4_i - T^4_j)$ term a linearizing approximation may be obtained from Holman (p.394)

$$(T_i^4-T_j^4)=(T_i-T_j)(T_i+T_j)(T_i^2+T_j^2) \qquad (3\text{-}21)$$

For the heat transfer model developed here the linearization term $(T_i + T_j)(T^2_i + T^2_j)$ is calculated from the previous hour's temperatures. Equation 3-18 can then be written in terms of $(T_i - T_j)$ only, thus linearizing the equation. Using the previous hour's temperatures will produce significant errors if the temperatures are changing rapidly. The worst case for attics occurs when temperatures change rapidly after the sun rises in the morning when the sheathing changes temperature the fastest. For a clear spring day that has rapid temperature changes measurements at AHHRF have shown that the North facing sheathing (node 2) changes temperature at approximately 6°C an hour and the South Sheathing (node 4) at 11°C an hour. This rapid change takes place between 10 and 11 a.m. Calculating the linearization term using 10 a.m. temperatures and then using 11 a.m. temperatures will show how much

error is induced by using 10 a.m. temperatures to linearize radiation heat transfer at 11 a.m.

Using 10 a.m. temperatures $(T_2 + T_4)(T^2_2 + T^2_4) = 7.5*10^7$

Using 11 a.m. temperatures $(T_2 + T_4)(T^2_2 + T^2_4) = 8.2*10^7$

Thus this linearization technique can produce errors up to about 9% in this linearization term. This implies the same percentage error in $(T^4_2 - T^4_4)$, $E_{b,2} - E_{b,4}$ and the total radiation heat transfer between these two nodes, q_{2-4}. For less rapid change in temperatures experienced at the other hours of the day the error is much smaller, typically 1% to 2%.

Equation 3-18 can now be written in a linearized form

$$q_i = A_i h_{R,i-j}(T_i - T_j) + A_i h_{R,i-k}(T_i - T_k) \qquad (3\text{-}22)$$

where $h_{R,i-j}$ are radiation heat transfer coefficients from node i to node j that are calculated from

$$h_{R,i-j} = \frac{\sigma(T_i + T_j)(T_i^2 + T_j^2)}{\frac{1-\epsilon_i}{\epsilon_i} + \frac{1}{F_{i-j}} + \frac{(1-\epsilon_j)A_i}{\epsilon_j A_j}} \qquad (3\text{-}23)$$

The emissivity of surfaces found in building construction is given by ASHRAE (1989)(Chapter 37). For the inside sheathing surfaces a typical value for wood is $\epsilon = 0.90$ and for the attic floor that is assumed to be covered with fibreglass insulation the typical emissivity glass (from ASHRAE (1989), Chapter 37) is used, $\epsilon = 0.94$. The emissivity of glass is also typical of diffuse surfaces, and the fibreglass insulation is a diffuse surface due to its roughness. Equation 3-23 is applied to each of the three interior attic radiation heat transfer nodes: the floor and the two pitched roof surfaces. The shape factors, F_{i-j}, are found using Equations 3-9 and 3-10.

3.1.2 Solar Radiation (Nodes 3 and 5)

Solar gain is a significant term in the energy balance because it has large peak values. For the AHHRF attic sheathing area this amounts to a peak of 15kW for 550 W/m^2 in winter when attic moisture problems are most prominent. In the summer the solar gain can be as high as 1050 W/m^2 on a clear day. These large solar gains heat the attic above the ambient temperature and thus have a large effect on moisture transport in the attic by forcing moisture out of the warm sheathing. This dries the sheathing and raises the moisture content of the attic air.

Solar gains are only applied to the external sheathing surfaces. The energy transfer due to solar radiation is

$$q_R = A\alpha G \qquad (3\text{-}24)$$

where q_R is radiation heat transfer rate [W]

A = Surface area [m^2]

α = Surface absorbtivity $\approx$ 0.90 for shingles (ASHRAE (1989) Chapter 37)

G = Total Solar Radiation [W/m^2], both direct and diffuse.

The values of G must be specified as entered data to the model and will generally be different for north and south sheathing surfaces. Values measured for this study at the AHHRF have shown south sheathing solar radiation peaks of about 550 [W/m^2] with north sheathing peaks of only 60 [W/m^2] on a clear winter day. However, on a cloudy winter day both roof surfaces receive a similar quantity of solar radiation, with peaks of about 120 [W/m^2] on both surfaces. The differences between these values show how important it can be to have good estimates of cloud cover when estimating attic temperatures.. Snow on the roof will change the absorbtivity and thus the solar gains. This effect will be examined in the simulations presented in Chapter 7.

3.1.3 Radiant Exchange of Exterior Surfaces with Sky and Ground (Nodes 3 and 5)

In addition to the daytime solar gain the outside of the pitched roof sheathing has low temperature long wave radiant exchange with the sky and the ground. This exchange is responsible for cooling of the sheathing at night as it radiates energy to the cooler sky. This nighttime temperature reduction in the sheathing is also important for moisture transport. Because the sheathing is the coldest attic surface at night it tends to have a lower vapour pressure and thus the water vapour in the attic air is transported to the inner sheathing surfaces. The cooling of the sheathing also leads to an increased quantity of condensed mass at the surface. On a cloudy night the cooling of the sheathing is reduced because the radiation exchange is with clouds that are warmer than the sky temperature. Both the clouds and the ground are assumed to be at the outside air temperature. The view factors that account for the proportion of sky, cloud or ground seen by the pitched roof surface are from Ford (1982).

Exterior Radiation Heat Transfer

The net radiation exchange for exterior pitched roof sheathing surfaces has the same form as Equations 3-22 and 3-23 for the internal radiation because this is a

three body problem involving the roof surface, the sky and the ground and the clouds (which are at the same temperature). The rate of radiation heat exchange, $q_{R,i}$, for an exterior attic surface, i, is

$$q_{R,i}=\frac{E_{b,i}-E_{b,sky}}{\frac{1-e_i}{A_i e_i}+\frac{1}{A_i F_{i-sky}}}+\frac{E_{b,i}-E_{b,g}}{\frac{1-e_i}{A_i e_i}+\frac{1}{A_i F_{i-g}}} \qquad (3\text{-}25)$$

where $E_{b,i}$ = Emissive power of surface i at T_i

$E_{b,sky}$ = Emissive power of sky = σT^4_{sky}

$E_{b,g}$ = Emissive power of ground and clouds (that are assumed to be at T_{out}) = σT^4_{out}

A_i = Area of surface

ϵ = Emissivity of surface. Emissivity of shingles is estimated to be = 0.90 from ASHRAE (1989), Chapter 37.

F_{i-sky} is the view factor from pitched roof surface i to the clear sky.

F_{i-g} is the view factor from the pitched roof surface i to the ground and the clouds.

The sky temperature T_{sky} depends on the water vapour pressure in the air and is discussed in the next section. The view factors give the fraction of exposure to the ground (and clouds) and the sky for the pitched roof surfaces. Using the same view factors for both pitched roof surfaces assumes that the cloud cover is uniformly distributed over the sky. The view factors will be discussed in detail in the following sections.

Equation 3-25 is linearized the same way as the interior radiation (see Equation 3-22) so that for exterior surface i (where i = 5 for the outside of the south sheathing and i = 3 for the outside of the north sheathing)

$$q_{R,i}=A_i h_{R,i-g}(T_i-T_{out})+A_i h_{R,i-sky}(T_i-T_{sky}) \qquad (3\text{-}26)$$

where $h_{R,i-g}$ is the radiation heat transfer coefficient from roof surface i to the ground and clouds and is given by

and $h_{R,i-sky}$ is the radiation heat transfer coefficient from roof surface to the clear sky and is given by

Effective Sky Temperature for Radiation

The sky temperature, T_{sky}, is the equivalent temperature of an imaginary

$$h_{R,i-g}=\frac{\sigma(T_i+T_{out})(T_i^2+T_{out}^2)}{\frac{1-e_i}{e_i}+\frac{1}{F_{i-g}}} \quad (3\text{-}27)$$

$$h_{R,i-sky}=\frac{\sigma(T_i+T_{sky})(T_i^2+T_{sky}^2)}{\frac{1-e_i}{e_i}+\frac{1}{F_{i-sky}}} \quad (3\text{-}28)$$

blackbody that radiates energy at the same rate as the sky. The effective sky temperature, T_{sky}, is a function of air temperature, T_{out}, and water vapour pressure P_v. Parmelee and Aubele (1952) developed the following empirical fit to measured data to estimate T_{sky} for horizontal surfaces exposed to a clear sky.

$$T_{sky}=T_{out}\left(0.55+5.68*10^{-3}\sqrt{P_v}\right)^{0.25} \quad (3\text{-}29)$$

where P_v is in Pascals and the temperatures are in Kelvin. Sample calculations show how T_{sky} can be very different from T_{out}. For example at T_{out} = 273K and 50%RH (so that P_v = 305 Pa) then T_{sky} = 245K, almost 30K difference. This effect of a reduced sky temperature becomes more pronounced at lower temperatures where even saturated air has a low water vapour pressure. Because Equation 3-29 is for horizontal surfaces fully exposed to a clear sky, Ford (1982) (p.96) developed the view factors $F_{i\text{-}sky}$ and $F_{i\text{-}g}$ to account for the amount of cloud in the sky and the slope of the pitched roof surfaces.

View Factor To Account For Cloud Cover

The view factor from a horizontal surface, $F_{h\text{-}sky}$, to the sky that accounts for cloud cover is given by

$$F_{h\text{-}sky}=(1-S_C) \quad (3\text{-}30)$$

where S_C is the fraction of sky covered by cloud that must be estimated as an input to the model. S_C = 0 means there is no cloud and S_C = 1 implies complete cloud cover.

View Factor To Account For Inclination

The fraction of the sky seen by a tilted surface, $F_{i\text{-}sky}$, is directly proportional to the angle of inclination from the horizontal, β [degrees], such that

$$F_{i\text{-}sky}=\frac{180-\beta}{180} \tag{3-31}$$

Combining Equation 3-31 with 3-30 gives the view factor, $F_{i\text{-}sky}$, from a tilted roof to a cloudy sky at T_{sky}

$$F_{i\text{-}sky}=\frac{(1-S_C)(180-\beta)}{180} \tag{3-32}$$

The pitched roof surface sees either the clouds and ground or the sky and so the two view factors must add up to unity. Assuming that the ground, cloud and air temperatures are the same then a view factor to the ground and clouds, $F_{i\text{-}g}$, can be defined as

$$F_{i\text{-}g}=1-F_{i\text{-}sky} \tag{3-33}$$

3.1.4 Radiant Exchange of the Ceiling (Node 7) with the Room Below

This is modelled as a two body enclosed system where one body is the ceiling and the other body is the interior surfaces. The interior surfaces are assumed to be all at the same temperature as the inside air, T_{in}. The same linearization as for the pitched roof surfaces and the attic floor is applied so that the radiation heat transfer, $q_{R,7}$, is a linear function of temperature. The heat transfer coefficient, $h_{R,7\text{-}in}$, is calculated based on the previous hour's temperatures. The ceiling is node 7 and so the radiation heat transfer at this node can be written as

$$q_{R,7}=A_7 h_{R,7\text{-}in}(T_7-T_{in}) \tag{3-34}$$

where the radiation heat transfer coefficient is

$$h_{R,7\text{-}in}=\frac{\sigma(T_7+T_{in})(T_7^2+T_{in}^2)}{\frac{1-\epsilon}{\epsilon}+\frac{1}{F_{7\text{-}in}}+\frac{(1-\epsilon)A_7}{\epsilon A_{in}}} \tag{3-35}$$

where A_7 = ceiling area

A_{in} = Internal house surface area

ϵ = 0.9 for interior surfaces. This is a typical value for painted surfaces, wood and paper from ASHRAE (1989) Chapter 37.

$F_{7\text{-in}}$ = 1 because all the surfaces are enclosed.

3.2 Convection Heat Transfer

3.2.1 House Internal Free Convection (Node 7)

Due to low air velocities in the house turbulent natural convection is assumed to be dominant because there is no forced convection inside the house. The heat transfer on the ceiling due to free convection is given by

$$q_T = h_T A \Delta T \tag{3-36}$$

where q_T is the free convection heat transfer rate [W]

h_T is the free convection heat transfer coefficient [W/m^{2}K]

A is the surface area

ΔT is the temperature difference

The turbulent free convection heat transfer coefficient, h_T [W/m^{2}K], is given by Holman (1981), p.285, as

$$h_T = Y_T (\Delta T)^{\frac{1}{3}} \tag{3-37}$$

where Y_T depends on surface geometry and orientation and the direction of heat flow and ΔT is the temperature difference between the surface and the surrounding air. Ford (1982) used the free convection heat transfer coefficients of Fuji and Imura(1972) for convection heat transfer (over flat plates) in both the attic and the house. Fuji and Imura found heat transfer coefficients for multiple plate orientations with the plates both heated and cooled. For the model developed here it is assumed that the house ceiling is a cooled horizontal plate facing downwards. This implies that the attic is cooler that the house which is true almost all of the time in temperate climates. Fuji and Imura used data correlations to suggest that the Nusselt number for a horizontal cooled plate facing downwards is given by

$$\frac{h_T L}{k} = 0.13(GrPr)^{\frac{1}{3}} \tag{3-38}$$

where Gr = Grashof Number

Pr = Prandtl number

k = thermal conductivity [W/mK]

L = Length Scale for convection heat transfer [m]

The Grashof number represents the ratio of buoyancy to viscous forces and is given by

$$Gr=\frac{g\beta_T\Delta TL^3}{\nu^2} \tag{3-39}$$

where β_T is the volume coefficient of thermal expansion

ν is the kinematic viscosity of the fluid [m^2/s]

g is gravitational acceleration [m/s^2].

For an ideal gas, $\beta_T = 1/T$, where T is the absolute temperature of the gas. The Prandtl number is given by

$$Pr=\frac{\nu}{\lambda} \tag{3-40}$$

where λ is the thermal diffusion coefficient [m^2/s].

Gr and Pr can be estimated for air given typical values of λ and ν. For air Pr is typically 0.71, k is about 0.02624 [W/mK] and Gr is approximately $2084L^3\Delta T$. The length scale, L, in Gr cancels with the L on the left hand side of Equation 3-38 and does not need to be estimated. Substituting these values into Equation 3-38 yields the following equation for free convection heat transfer coefficient

$$h_T=3.2(\Delta T)^{\frac{1}{3}} \tag{3-41}$$

To keep the heat transfer equations linear, ΔT is evaluated using the previous hours temperatures.

3.2.2 Attic Internal (Nodes 2 and 4) and External Convection (Nodes 3 and 5)

The convection inside the attic has been assumed by previous authors (e.g. Ford (1982) and Burch and Luna (1980)) to be dominated by free convection. For an enclosed space, such as an attic, the ratio of buoyancy forces (due to temperature differences) to inertial forces (due to forced air movement) determines wether the surface heat transfer is due to free or forced convection. In most attics the ventilation rates are high which results in relatively high forced air velocities. In addition, the ventilation flows close to the attic leaks, even at low ventilation rates, will act to disrupt any motion due to free convection. This means that forced

convection due to ventilation will be more important for the convection heat transfer processes on the inside surfaces of the attic. The model developed for this study uses forced convection heat transfer coefficients, h_U, whose magnitudes depend on attic ventilation rates. This is important because it makes the energy balance for the attic more dependent on the ventilation rates. In addition, the mass transfer coefficients used in the moisture model are linearly related to the convection heat transfer coefficients so that the attic ventilation rate will also change the surface mass transfer rates of moisture in the attic.

Both natural convection and forced convection inside of the attic produce heat transfer coefficients that are of the same magnitude so that assuming forced convection is not critical. Using Equation 3-41 to calculate the free convection heat transfer and Equation 3-55 (that will be developed in the following sections) for forced convection, a range of heat transfer coefficients may be estimated. For free convection the range of h_T is about 0.3 to 6 W/m^{2}K, and for forced convection the range of h_U is about 1 to 10 W/m^{2}K, corresponding to the low and high ventilation rates encountered in the attics. The following section shows how the forced convection heat transfer coefficients are calculated and how the assumptions for calculating attic air velocities due to ventilation used in this model effect the dominance of free and forced convection.

For both the internal attic surfaces and the external pitched roof surfaces the forced convection heat transfer is given by

$$q = A h_U \Delta T \tag{3-42}$$

where q_U is the forced convection heat transfer coefficient [W]

A = Surface area [m^2]

h_U [W/m^{2}K] is calculated using Equation 3-52

ΔT = Temperature difference between surface and the surrounding air.

The ratio of buoyancy to inertia forces is used to determine if natural or forced convection is dominant. The buoyancy forces are represented by Gr from Equation 3-39 and the ration of inertial to viscous forces are represented by the Reynolds number, Re

$$Re = \frac{U_U L}{\nu} \tag{3-43}$$

where U_U is the velocity of the forced flow due to attic ventilation. Based on an

order of magnitude analysis of the natural convection boundary layer equations Holman (1982) p.295 suggests the following criterion for the domination of natural convection over forced convection

$$\frac{Gr}{Re^2}>1 \tag{3-44}$$

The ratio of buoyancy forces to inertia force in Equation 3-44 is called the Richardson number, Ri. Ri is given by substituting Equations 3-39 and 3-43 into 3-44 such that

$$Ri=\frac{g\beta_T \Delta TL}{U_U^2}>1 \tag{3-45}$$

In Ri the viscosity, ν, in Gr and Re cancels so that Ri is independent of viscosity as expected for forced turbulent flows.

The dominance of free or forced convection depends on the value chosen for a typical attic forced air velocity, U_U. Previous attic heat transfer studies by Ford (1982) and Burch and Luna (1980) calculated U_U by assuming a plug flow model of air flow through the attic so that

$$U_U=\frac{Q_a L}{3600s} \tag{3-46}$$

where Q_a = attic ventilation rate in air changes per hour [ACH] and L [m] was assumed by Ford and Burch and Luna to be the length of attic in flow direction. For typical values measured in this study for Q_a equal to 5 ACH and L equal to 7m then, from Equation 3-46, U_U is approximately $1*10^{-2}$ m/s. Using this estimate of velocity in Equation 3-45 with a typical attic length scale for convection flows of 1m yields

$$Ri=380\Delta T \tag{3-47}$$

This ratio of buoyancy to inertial forces implies natural convection is dominant even at very low temperature differences.

The plug flow model for attic ventilation is unrealistic because when air enters or leaves the attic it does so through a combination of small cracks (the distributed leakage) and localized leakage sites. The flow velocity through these leaks is much higher than the plug flow model indicates. To estimate this velocity the ventilation

rate of the attic is divided by the area that it flows through. The flow area is the leakage area of the attic A_{LA} [m^2]. A_{LA} is the area of an orifice that would have the same flow rate as the attic at 4 Pa and is found by equating orifice flow to the general flow Equation 2-1.

$$A_{LA}=C_{d,a}\sqrt{\frac{\rho_a}{2}}\Delta P^{0.5-n_{d,a}} \qquad (3\text{-}48)$$

where $C_{d,a}$ and $n_{d,a}$ are the distributed leakage coefficient and power for the attic, ρ_a is the density of the attic air and $\Delta P = 4$ Pa. The A_{LA} calculated using Equation 3-48 is the total attic leakage area of which about half will have inflow and half will have outflow. The flow area used to estimate velocities will then be half of the total A_{LA}. This would overestimate the flow velocity because further from the leaks the velocity will be lower. This implies that there are different heat transfer coefficients for different parts of the attic depending on the distance from the leakage sites. What is required is a typical advection velocity that can be applied to all interior attic surfaces. As a first approximation U_U is calculated for this study by dividing the velocity by four. This factor could be adjusted to provide better approximations of the heat transfer coefficients but will not be changed here due to lack of measured data for attic heat transfer coefficients and flow velocities. The velocity, U_U, can then be estimated by

$$U_U=\frac{M_a}{\rho_a\frac{A_{LA}}{2}}\frac{1}{4} \qquad (3\text{-}49)$$

where M_a [Kg/s] is the attic ventilation rate and A_{LA} is divided by 2 in Equation 3-49 as an estimate of the inflow area and 1/4 is the velocity reduction factor. An estimate of U_U using Equation 3-49 can be made using the same attic ventilation rate as for the plug flow model of 5 ACH. The volume of the attics used in this study is 61 m^3 and A_{LA} is about 1500 cm^2 (as will be shown later in Chapter 5). Substituting these values into Equation 3-49 gives U_U equal to 0.3 m/s. This is thirty times larger than the results of the plug flow estimate (Equation 3-46) suggesting that the plug flow model may not be a good estimate of attic air velocities for heat transfer calculations.

Using U_U equal to 0.3 m/s the Richardson number (Equation 3-45) is

$$Ri = 0.4\Delta T \qquad (3\text{-}50)$$

At typical attic air to surface temperature differences of 5K or less (from measurements made for this study at AHHRF) this result for Ri implies that neither free or forced convection is dominant inside the attic. Because Ri is inversely proportional to U^2_U small changes in U_U will make Ri much smaller and increase the likelihood of forced convection being dominant. However free convection could still occur for extreme conditions in the middle of clear days with low ventilation rates when U_U is small and ΔT is large. Measurements made for this study at AHHRF (see Chapter 5) have shown that sheathing surfaces can be up to 5K hotter than the attic air under these conditions. Because extreme conditions are required for free convection to occur it is assumed that forced convection should be used for the internal attic surfaces. In addition, the ventilation flows act close to the attic surfaces since all the leaks are in the surfaces and they also act to break up any natural convection cells within the attic space. These factors also suggest that forced convection gives a better estimate of the surface heat transfer.

The most important effect of the forced convection method is that the heat transfer is a function of the ventilation rate. This is important because this effect was not included by the free convection assumed in previous studies. Making the convection heat transfer coefficients functions of ventilation rate also has an effect on the moisture transport model because it uses the convection heat transfer coefficients to calculate mass transfer coefficients for the interior attic surfaces. Another advantage of using forced convection heat transfer coefficients is that they are the same for every surface. For free convection the heat transfer coefficients change depending on surface orientation (horizontal, vertical, at an angle and facing up or down) and direction of heat transfer. Using forced convection coefficients eliminates these complications.

The above analysis showed that neither free or forced convection is always dominant in an attic. A future refinement of this heat transfer model is to use a combination of heat transfer coefficients. When ventilation rates are high the forced convection coefficient would be used and at low ventilation rates with high temperature differences between the wood surfaces and attic air, the free convection coefficient would be used. This combination was not examined here because the method by which the two cases combine for attics requires further experiments that are beyond the scope of this study.

The following section shows how the forced heat transfer coefficients were estimated. For turbulent forced convection over a flat plate Holman (1981), p.202, gives a relationship for the Nusselt number, Nu, (ignoring the initial laminar region)

$$Nu=\frac{h_U L}{k}=0.037Re^{\frac{4}{5}}Pr^{\frac{1}{3}} \tag{3-51}$$

and substituting for Re and Pr gives

$$\frac{h_U L}{k}=0.037\left(\frac{U_U L}{\nu}\right)^{\frac{4}{5}}\left(\frac{\nu}{\lambda}\right)^{\frac{1}{3}} \tag{3-52}$$

where λ is the thermal diffusion coefficient and ν,λ and k are all functions of temperature. Ford (1982) linearized the temperature dependence of Equation 3-52 over the range of 250K (-23°C) to 300K (27°C) to obtain

$$h_U=(6.940-0.0344T_e)U_U^{\frac{4}{5}}L^{-\frac{1}{5}} \tag{3-53}$$

where T_e = Film Temperature (in degrees Celsius from Ford) at which ν, α_T and k are evaluated, and is the mean temperature of the surface, T_i, and the attic air, T_a:

$$T_e=\frac{(T_i+T_a)}{2} \tag{3-54}$$

T_e is calculated using the previous hour's temperatures so that the overall heat transfer equation remains linear in temperature.

Ford found that h_U calculated from Equation 3-53 matches the measured data of Burch (1980b) and McAdams (1954) with L equal to 0.5m. This is a purely empirical value for L and does not have any physical significance. This value of L only means that convective heat transfer coefficients calculated using Equation 3-53 will match the measured data of Burch and McAdams. Including this length scale and converting from °C to K, Equation 3-53 can be written as

$$h_U=(18.192-0.0378T_a)U_U^{\frac{4}{5}} \tag{3-55}$$

where h_U is the turbulent forced convection heat transfer coefficient [W/m^{2}K], U_U is determined from Equation 3-49 and T_e is found from Equation 3-54. Equation 3-55

is used in Equation 3-42 to calculate the internal attic forced convection heat transfer. Ford (1982) used Equation 3-53 for external surfaces only because the internal surfaces were assumed to have free convection.

For the outside sheathing the flow velocity, U_U is equal to the ambient wind velocity, U. Because U is typically ten times greater than U_U, forced convection is always dominant on the exterior surfaces of the attic. For the exterior pitched roof sheathing surfaces Equation 3-55 is used to find h_U with U_U equal to U, the external wind speed.

The expressions for forced (Equation 3-55) and free (Equation 3-38) heat transfer coefficients can be used to find how the ventilation flow velocity determines which is dominant. The ratio of forced to free convection heat transfer coefficients (ignoring coefficients) is given by

$$\frac{h_U}{h_T} \propto \frac{Re^{\frac{4}{3}} Pr^{\frac{1}{3}}}{(RiRe^2)^{\frac{1}{3}} Pr^{\frac{1}{3}}} \qquad (3\text{-}56)$$

where Gr has been replaced by ($RiRe^2$). Pr cancels in Equation 3-56 which can then be written in terms of Ri and Re only

$$\frac{h_u}{h_T} \propto \frac{Re^{\frac{2}{13}}}{Ri^{\frac{1}{3}}} \qquad (3\text{-}57)$$

To find this ratio in terms of velocity the following substitutions are used : Re is proportional to U and Ri is proportional to U^{-2}. The ratio of forced to free heat transfer coefficients is then given by

$$\frac{h_U}{h_T} \propto U^{\frac{4}{3}} \qquad (3\text{-}58)$$

This means that the forced convection heat transfer coefficient becomes more dominant with increasing velocity.

3.3 Conduction Heat Transfer

Conduction occurs through the ceiling of the house, the pitched slope roof surfaces and the gable ends. The conduction is assumed to be one dimensional

because each surface has only one node. The general equation for one dimensional conduction is given by Holman (1981), p.2., as follows

$$q_K = \frac{A}{R}\Delta T \qquad (3\text{-}59)$$

where q_K = heat conducted between nodes [W]

A = Surface area over which ΔT acts [m^2]

R = Thermal Resistance between nodes [m^2K/W]

ΔT = Temperature difference between nodes [K].

The thermal resistance depends on the thickness and material properties. The inside and outside of the pitched roof surfaces and (nodes 2,3,4 and 5) and the gable end walls (nodes 9 and 10) are assumed to have the same thickness of wood sheathing. The thermal resistance of the sheathing is given by

$$R = \frac{\Delta X}{k_W} \qquad (3\text{-}60)$$

where ΔX = sheathing thickness [m]. For the attics tested in this study ΔX = 0.01m.

k_W = thermal conductivity of wood ≈ 0.1 [W/mK], ASHRAE (1989), Chapter 37.

Substituting these values into Equation 3-60 gives the thermal resistance of the sheathing as 0.1 m^2K/W. The sheathing thermal resistance is increased if there is snow on the roof. This effect is considered later in Chapter 7. Heat conduction through the ceiling occurs between the ceiling of the house (node 7) and the attic floor (node 8). The thermal resistance of the ceiling is modelled as the insulation and joist thermal resistances in parallel with the drywall resistance in series with this parallel combination. The total thermal resistance of the ceiling, R_c, is given by

$$R_c = R_A + \frac{1}{\frac{1}{R_X} + \frac{1}{R_W}} \qquad (3\text{-}61)$$

where R_A = Drywall resistance [m^2K/W]

R_X = Insulation resistance [m^2K/W]

R_W = Joist (Wood) resistance [m^2K/W]

In this study the joist spacing was 61cm (24 inches) with 10cm insulation depth so that R_c = 2.3 m^2K/W. For thicker insulation the resistance increases. For example

with 15cm insulation depth, R_c = 3.4 m^2K/W. R_c is used as R in Equation 3-59 to find the heat conducted through the ceiling.

3.4 Accounting for Thermal Storage

In order to remove the assumption of steady-state, an estimate must be made for the rate of change of thermal energy at each node. A simple method is to use a lumped heat capacity analysis which assumes a uniform temperature for each node. This is only valid if internal conduction is more rapid than the surface heat transfer. Holman (1982), p.113, gives a criteria for the limits of a lumped heat capacity analysis using the Biot number which estimates the ratio of surface heat transfer to internal conduction, such that:

$$Bi = \frac{h_U \left(\frac{V}{A}\right)}{k} < 0.1 \qquad (3\text{-}62)$$

where h_U = surface heat transfer coefficient [W/m^2K]

A = Surface area [m^2]

V = Volume [m^3]

k = thermal conductivity [W/mK]

This is only a rough estimate of the applicability of lumped heat capacity analysis and Holman (p.114) gives examples of lumped heat capacity systems for Bi up to about 3.

For the same h_U and k the node with the largest V/A ratio is least likely to meet the restriction of Equation 3-62. Node 6 representing the joists and trusses in the attic is the most critical. For 5cm x 10cm (2" x 4") construction, then V/A is equal to 0.017m. To estimate h_U, the convection heat transfer coefficient from Equation 3-55 is used with typical values of U_U equal to 0.3 m/s and T_f equal to 273K. This gives a value of h_U equal to 3 W/m^2K. Using k_w equal to 0.1 W/mK then Equation 3-62 gives Bi equal to 0.5. For the sheathing Bi is approximately equal to 0.1. These results show that the lumped heat capacity analysis is applicable to the sheathing but the assumption of a single temperature for the rest of the wood in the attic may be a poor one. Holman (1981), p.122, shows how to estimate the difference between the centreline temperature of a cylinder and the external temperature as a function of Bi, time, thermal conductivity, thermal diffusivity and chacteristic dimensions. Letting V/A be the characteristic radius of a cylinder and using a time period of one hour (as used in this model), Holman shows that the

centerline temperature will only be 10% different from the exterior temperature. The data presented by Holman are responses to step changes in temperature, so the response of attic wood to more slowly changing temperatures will have errors less than 10% on the centreline. In addition, the average temperature difference for the whole of the wood will be even less than the centreline.

Because the sheathing meets the requirements for a lumped heat capacity analysis, the rest of the wood has small errors (less than 10%), and in the interests of simplicity the lumped heat capacity analysis is used for this study. As stated earlier in this chapter, the assumption of a lumped heat capacity would be further improved by dividing the wood into more nodes.

The rate of change of thermal energy at a node for a lumped heat capacity is found using a finite difference approximation to the time derivative of temperature such that (from equations 3-1 and 3-2)

$$\rho V C_{sh} \frac{(T^i - T^{i+1})}{\tau} \qquad (3\text{-}63)$$

where ρ = density of node [Kg/m_3]

V = Volume of node [m_3] so that ρV = Mass of node [Kg]

C_{sh} = Specific Heat [J/KgK]

T^i = temperature of node at time step i

T^{i+1} = temperature of node at time step i+1

τ = Time step. One hour is used in the model as this is the interval between measured data points used for verification.

Equation 3-63 assumes that the temperature changes linearly from timestep to timestep.

3.5 Latent Heat Released by Condensation.

When moisture condenses in the attic latent heat is given off which may increase the temperatures in the attic. If the heat transfer due to condensation is significant in the attic then there needs to be an iterative process between the heat transfer and moisture transport models because the moisture transport will significantly effect the heat transfer and visa-versa. The latent heat only needs to be considered when condensation is occurring. To determine if latent heat effects are significant, typical values of latent heat, radiation, convection and conduction fluxes are compared.

• **Latent Heat**

A typical mass flux from the attic air to the sheathing is 10^{-5} Kg/s calculated by the moisture transport model for the AHHRF attics with a sheathing area of 30.3m^2. The latent heat released in the transformation from vapour to solid is h_{gs} = 2834 KJ/Kg. The heat flux due to latent heat released is then approximately 1 W/m^2.

• **Solar Radiation**

Values measured for this study at AHHRF (in Edmonton, Alberta)have shown that there is a wide range of solar radiation. The range is from approximately 60W/m^2 for a cloudy winter day to 1050 W/m^2 on a clear summer day.

• **Convection**

With a convective heat transfer coefficient of 3 W/m^{2}K (as calculated in section 3.4) and a typical air to wood temperature difference measured at AHHRF of 2K (the range is from approximately zero to about 5K) a typical convective flux is about 6W/m^2.

• **Conduction**

Conduction through the sheathing is given by Equation 3-59. For the sheathing R is equal to 0.2 m^{2}K/W. Using this value of R and estimating the temperature difference between the inside and the outside of the sheathing (ΔT) as 2K, the conductive flux is about 20 W/m^2. The 2K temperature difference across the sheathing is a typical value measured in the test attics for this study as will be shown later in Chapter 6.

• **Internal Radiation**

Consider the radiation exchange between the south facing sheathing and the attic floor during the day. Measurements from AHHRF for this study presented in later (in Chapter 5) give typical daytime temperatures (for a clear spring day) of 303K for the sheathing and 298K for the attic floor. The radiation heat transfer coefficient from Equation 3-23 found using these temperatures is approximately 4.61 W/m^{2}K. Using this result in Equation 3-22 from the heat transfer rate gives a radiative heat flux of about 23 W/m^2.

These example calculations show that the heat flux due to latent heat is less than all the other heat fluxes in the attic for typical conditions. This means that ignoring the latent heat released by condensation will not have a significant effect on the attic heat transfer, and an iterative solution between the heat transfer and moisture transport models is not necessary. The heat flux due to latent heat released by condensation has been included in an attic heat transfer model by Gorman (1987),

p.30. Gorman found that its inclusion did not have a significant effect on wood moisture content predictions.

3.6 Node Heat Transfer Equations

At each of the 10 nodes the rate of change of energy (see Equation 3-1, 3-2 and 3-63) is equated to the net heat flow to the node due to radiation, convection and conduction. This results in 10 heat balance equations that must be solved simultaneously for the 10 unknown temperatures. In each of the following equations the subscript on temperature, T, refers to the node location and the superscript to the timestep.

Node 1. Attic Air

The attic air has convective (the h_U terms) heat transfer from all the interior attic surfaces - nodes 2, 4, 8, 6 and 9 as shown Figure 3-1. Although each convection term uses the same velocity, U_U, the different temperatures will change the film temperature, T_f, and thus the heat transfer coefficient. In addition the convective flows in and out of the attic, M_a, and the flow through the ceiling, M_c, transport heat in and out of the attic air. When ventilation rates are high, M_a is large and this becomes the dominant term so that the attic air has almost the same temperature as the out door air. When M_a is small, M_c and the h_U terms become more important so that solar radiation heating the pitched roof surfaces will heat the attic air. A source or sink term, q_{ss} [W], (e.g. a hot furnace flue) is also included for the heat balance on the attic air, although in the present study this term was zero.

$$\rho_a V_a C_{sh,a}\frac{(T_1^i - T_1^{i-1})}{\tau} = h_{U,8}\,A_8(T_8^i - T_1^i) + h_{U,4}\,A_4(T_4^i - T_1^i) + h_{U,2}\,A_2(T_2^i - T_1^i) \qquad (3\text{-}64)$$
$$+A_9 h_{U,9}(T_9^i - T_1^i) + M_c C_{sh,a}(T_{in}^i - T_1^i) + M_a C_{sh,a}(T_{out}^i - T_1^i) + h_{U,6}\,A_6(T_6^i - T_1^i) + q_{ss}$$

where V_a = volume of the attic [m^3] (61m^3 for the AHHRF test houses)

$C_{sh,a}$ = specific heat of air. This assumed to be independent of temperature and is equal to 1000 J/KgK

$h_{U,2}$ = forced convection heat transfer coefficient from Equation 3-55

$h_{U,4}$ = forced convection heat transfer coefficient from Equation 3-55

$h_{U,6}$ = joist and truss forced convection heat transfer coefficient from Equation 3-55

$h_{U,8}$ = forced convection heat transfer coefficient from Equation 3-55

$h_{U,9}$ = end wall forced convection heat transfer coefficient from Equation 3-55

$A_2 = A_4$ = sheathing surface area

A_9 = end wall surface area. Both end walls are assumed to be identical and so this is the area of both endwalls combined

A_6 = area of joists and trusses

M_c = mass flow rate through the ceiling from ventilation model

M_a = mass flow rate through the attic from ventilation model.

Node 2. Inside North Sheathing

The inside of the sheathing exchanges heat with the attic air by convection (h_U) and with the outside of the sheathing by conduction (A/R). In addition there is radiant exchange with the attic floor and the inside of the south sheathing (the h_R terms).

$$\rho_W V_2 C_{sh,W} \frac{(T_2^i - T_2^{i-1})}{\tau} = h_{U,2}\, A_2 (T_1^i - T_2^i) + \frac{A_2}{R_2}(T_3^i - T_2^i) + h_{R,2\text{-}8}\, A_2 (T_8^i - T_2^i) + h_{R,2\text{-}4}\, A_2 (T_4^i - T_2^i) \qquad (3\text{-}65)$$

where ρ_W = density of wood, approximately 400Kg/m^3

V_2 = half of the north sheathing volume

A_2 = surface area of north roof pitched surface

R_2 = thermal resistance of sheathing from Equation 3-60

$h_{R,2\text{-}8}$ = radiation heat transfer coefficient from Equation 3-23

$h_{R,2\text{-}4}$ = radiation heat transfer coefficient from Equation 3-23

Node 3. Outside North Sheathing

The outside pitched roof sheathing surface has radiant exchange with the ground and the clouds, $h_{R,3\text{-}g}$, the sky, $h_{R,3\text{-}sky}$ and daytime solar gain, G_3. The radiant exchange to the sky is important on clear nights because this reduces the sheathing temperature and makes it prone to moisture condensation. There is also convective exchange with the outside air, $h_{U,3}$, and conduction through the sheathing to the inner sheathing (A/R). The separation of sheathing into north and south allows the two pitched roof surfaces to have different solar gains. The test houses used in this study were in an east-west row with one sheathing surface facing south and the other facing north.

$$\rho_W V_3 C_{sh,W} \frac{(T_3^i - T_3^{i-1})}{\tau} = h_{U,3}\, A_3 (T_{out}^i - T_3^i) + \frac{A_3}{R_3}(T_2^i - T_3^i) + A_3 G_3 \lambda_3 + h_{R,3\text{-}sky}\, A_3 (T_{sky}^i - T_3^i) + h_{R,3\text{-}g}\, A_3 (T_{out}^i - T_3^i) \quad (3\text{-}66)$$

where $V_3 = V_2$, $A_3 = A_2$, $R_3 = R_2$,

$h_{U,3}$ = exterior forced convection heat transfer coefficient from Equation 3-55, with the ambient wind speed, U, substituted for the internal attic velocity, U_U.

λ_3 = absorbtivity of shingles which is approximately 0.9 from ASHRAE (1989), Chapter 37

G_3 = solar radiation on north sheathing

$h_{R,3\text{-}sky}$ = radiation heat transfer coefficient from roof to sky from Equation 3-28

$h_{R,3\text{-}g}$ = radiation heat transfer coefficient from roof to ground and clouds from Equation 3-27.

To include the effect of the thermal mass of the shingles outside the sheathing, the thermal mass of this node is doubled by doubling the effective volume. The actual thermal mass of the shingles is much larger (by a factor of 15) but calculations performed later for model verification (in Chapter 6) have shown that the attic temperature predictions are insensitive to changing the effective mass of the sheathing.

Node 4. Inside South Sheathing

The inside of the south sheathing has the same heat transfer contributions as the inside north sheathing.

$$\rho_W V_4 C_{sh,W} \frac{(T_4^i - T_4^{i-1})}{\tau} = h_{U,4}\, A_4 (T_1^i - T_4^i) + \frac{A_4}{R_4}(T_5^i - T_4^i) + h_{R,4\text{-}8}\, A_4 (T_8^i - T_4^i) + h_{R,4\text{-}2}\, A_4 (T_2^i - T_4^i) \quad (3\text{-}67)$$

where $V_4 = V_2$, $A_4 = A_2$, $R_4 = R_2$

$h_{R,4\text{-}8}$ = radiation heat transfer coefficient from Equation 3-23

$h_{R,4\text{-}2}$ = radiation heat transfer coefficient from Equation 3-23

Node 5. Outside South Sheathing

The outside of the south sheathing has the same heat transfer contributions as the outside north sheathing.

$$\rho_W V_5 C_{sh,W} \frac{(T_5^i - T_5^{i-1})}{\tau} = h_{U,5}\, A_5 (T_{out}^i - T_5^i) + \frac{A_5}{R_5}(T_4^i - T_5^i) \qquad (3\text{-}68)$$
$$+ A_5 G_5 \lambda_5 + h_{R,5\text{-}sky}\, A_5 (T_{sky}^i - T_5^i) + h_{R,5\text{-}g}\, A_5 (T_{out}^i - T_5^i)$$

where $V_5 = V_2$, $A_5 = A_2$, $R_5 = R_2$

$h_{U,5}$ = exterior forced convection heat transfer coefficient from Equation 3-60, with the ambient wind speed, U, substituted for the internal attic velocity, U_U. this is not necessarily equal to $h_{U,3}$ because the sheathing surfaces may be at different temperatures.

G_5 = solar radiation on south sheathing

λ_5 = surface absorbtivity $\approx$ 0.9 for shingles

$h_{R,5\text{-}sky}$ = radiation heat transfer coefficient from roof to sky from Equation 3-28

$h_{R,5\text{-}g}$ = radiation heat transfer coefficient from roof to ground and clouds from Equation 3-27

The increased thermal mass contributed by the sheathing is dealt with in the same way as for the outside of the north sheathing i.e. the thermal mass of this node is doubled by doubling the effective volume.

Node 6. Attic Joists and Trusses

The joists and trusses only exchange heat with the attic air by convection, therefore they act to increase the thermal mass of the attic air.

$$\rho_W V_6 C_{sh,W} \frac{(T_6^i - T_6^{i-1})}{\tau} = h_{U,6}\, A_6 (T_1^i - T_6^i) \qquad (3\text{-}69)$$

where V_6 = Volume of joists and trusses

A_6 = Surface Area of joists and trusses.

Node 7. Underside of House Ceiling

The underside of the ceiling has radiant exchange with the inside surfaces of the house that are assumed to be at T_{in}, i.e. the same temperature as the air in the house. The house is assumed to have internal free convection and so the ceiling exchanges heat with the house air. There is also conduction through the ceiling to

the floor of the attic.

$$\rho_7 V_7 C_{sh,7}\frac{(T_7^i - T_7^{i-1})}{\tau} = h_{U,7}\, A_7(T_{in}^i - T_7^i) + h_{R,7\text{-}in}\, A_7(T_{in}^i - T_7^i) + \frac{A_7}{R_7}(T_8^i - T_7^i) \quad (3\text{-}70)$$

where ρ_7 = Average Density of ceiling drywall, joist and insulation

V_7 = 1/2 volume of ceiling drywall, joist and insulation

$C_{sh,7}$ = specific heat of node 1. For the wood - $C_{sh,W}$ = 1100 J/KgK and for the drywall - $C_{sh,\delta}$ = 1080 J/KgK so use C_{sh7} = 1100 J/KgK

τ = timestep = 3600s for all nodes

$h_{U,7}$ = convective heat transfer coefficient from Equation 3-41

A_7 = ceiling area

$h_{R,7\text{-in}}$ = radiation heat transfer coefficient from Equation 3-35

R_7 = ceiling conduction resistance from Equation 3-61

Node 8. Attic Floor

The attic floor exchanges heat by radiation to the pitched roof surfaces, forced convection with the attic air and by conduction through the ceiling form the house below. The radiation terms are important because during high daytime solar gains the warm sheathing can raise the attic floor temperature above the attic air and reduce heat loss through the ceiling. Conversely cooler attic sheathing on clear nights will make the attic floor colder.

$$\rho_8 V_8 C_{sh,8}\frac{(T_8^i - T_8^{i-1})}{\tau} = h_{U,8}\, A_8(T_1^i - T_8^i) + \frac{A_8}{R_8}(T_3^i - T_8^i) + h_{R,8\text{-}4}\, A_8(T_4^i - T_8^i) + h_{R,8\text{-}2}\, A_8(T_2^i - T_8^i) \quad (3\text{-}71)$$

where $\rho_8 = \rho_7$, $V_8 = V_7$, $A_8 = A_7$, $R_8 = R_7$,

$C_{sh,8} = C_{sh,7}$

$h_{R,8\text{-}4}$ = radiation heat transfer coefficient from Equation 3-23

$h_{R,8\text{-}2}$ = radiation heat transfer coefficient from Equation 3-23

Node 9. Inside both Endwalls

Both the endwalls (east and west) are assumed to be identical and are lumped together. The inside of the endwalls exchanges heat with the attic air by forced convection and with the outside of the endwalls by conduction. The end walls are another path for heat to enter or leave the attic. The effective resistance of this path is governed by the surface forced convection heat transfer coefficients on the inside

and the outside of the endwalls and by their conductive resistance.

$$\rho_W V_9 C_{sh,W}(T_9^i - T_9^{i-1}) = h_{U,9}\, A_9(T_1^i - T_9^i) + \frac{A_9}{R_9}(T_{10}^i - T_9^i) \qquad (3\text{-}72)$$

where V_9 = 1/2 total end wall volume

$R_9 = R_4$ assuming same thickness of wood for endwalls and pitched roof sheathing.

Node 10. Outside both Endwalls

The outside of the endwalls exchanges heat with the outside air by forced convection and with the inside of the endwalls by conduction. The external forced convection heat transfer coefficient, $h_{U,10}$, uses the same outside wind speed as the pitched roof surfaces.

$$\rho_{wood} V_{10} C_{shwood}(T_{10}^i - T_{10}^{i-1}) = h_{conv,10} A_{10}(T_{out}^i - T_{10}^i) + \frac{A_{10}}{R_{10}}(T_9^i - T_{10}^i) \qquad (3\text{-}73)$$

where $V_{10} = V_9$, $R_{10} = R_9$

$h_{U,10}$ = exterior forced convection heat transfer coefficient from Equation 3-55 with U substituted for U_U.

3.7 Solution of the Attic Heat Transfer Equations

At each node Equation 3-63 is equated to the sum of the heat fluxes due to radiation, convection and conduction. This results in the above set of equations that are linear in temperature and must be solved simultaneously. This simultaneous solution is found using gaussian elimination. When the temperatures have been calculated the attic air temperature (Node 1) is returned to the attic ventilation model so that a new attic ventilation rate can be calculated. This new ventilation rate is then used in the thermal model at the attic air node to calculate temperatures. This iterative process is continued until the attic air temperature changes by less than 0.1°C. Because the attic ventilation rates are relatively insensitive to the attic air temperature usually fewer than five iterations between thermal and ventilation models are required.

3.8 Summary of Attic Heat transfer Model

The attic heat transfer model uses a multi-node lumped heat capacity analysis to determine the temperatures at ten attic locations shown in Figure 3-1. The heat transfer between the nodes is by radiation, conduction and convection. These

temperatures are used by the moisture transport model to calculate saturation pressures, vapour pressures and wood moisture contents. The heat transfer model is coupled to the attic ventilation model through the temperature of the attic air. The air temperature is used to calculate air densities in the attic which changes the mass flow rates and the driving pressures for ventilation. In turn the attic ventilation rate has a large effect on the attic air temperature and thus the two models are coupled and require an iterative procedure to solve the combined problem. Because the attic ventilation rate is not a very strong function of attic air temperature the models are only weekly coupled and only a few iterations are required for convergence.

The major assumptions of the heat transfer model are:

- The temperature at each node location is uniform so that the lumped heat capacity analysis can be used.
- The flow velocities inside the attic are uniform and are proportional to the attic ventilation rate so that heat (and mass) transfer coefficients are functions of attic ventilation rate.
- Latent heat released by condensing moisture is not included as it does not have a significant effect. Therefore the heat transfer model is not coupled to the moisture transport model.
- The end walls of the attic do not receive any external solar radiation gains and do not have any internal radiation heat transfer.

The major differences from previous attic heat transfer models (e.g. Ford (1982)) are

- An additional node is used to account for the mass of wood in joists and trusses in the attic. This effectively increases the thermal mass of the attic air.
- Attic ventilation and ceiling flow rates are calculated instead of being a required input. This results in an iterative procedure as the attic ventilation and ceiling flow rates depend on the attic temperature.
- Forced convection heat transfer coefficients are used inside the attic. In this study the ventilation rates are found using ATTICLEAK-1 and thus forced convection heat transfer coefficients may be calculated inside the attic. Previous authors have not had a ventilation model to calculate ventilation rates and so they used natural convection heat transfer coefficients. These heat transfer coefficients are important as they make the heat transfer model more dependent on the ventilation model and because the mass transfer coefficients are linearly dependent on the heat transfer coefficients.

• Radiation heat transfer inside the attic is simplified to three nodes: the attic floor and the two pitched roof surfaces. Ford (1982) also included gable ends and eaves but these components have small view factors and are neglected for simplicity in the present study.

Chapter 4. Moisture Transport in Attics

4.1 Introduction

The moisture transport model is based on a mass balance of water in the attic. The mass of water in the attic is assumed to be located at the seven nodes shown in Figure 4-1. The model makes the mass change rate at each node equal to the sum of the fluxes at that node and solves for the vapour pressures at each node that will give this balance. The fluxes include ventilation flows, wood surface exchange and diffusion within the wood. The mass balance is performed simultaneously for all the nodes. The ceiling is assumed to be impermeable to water vapour as most residential buildings will have a vapour retarder in the ceiling. The flow of vapour through the ceiling is only that due to convective flows through gaps in the vapour barrier. It is also assumed that no water vapour is exchanged with the outside air through the shingles on top of the sheathing or through the endwalls which are usually painted. This is due to the relatively low vapour permeability of these surfaces (see ASHRAE Fundamentals (1989), Chapter 37). Thus the outer surfaces of the sheathing are assumed to be impermeable and have zero mass flux.

Figure 4-2 shows the order of magnitude of moisture fluxes for a typical winter day. This is for the same conditions shown for heat transfer rates in Figure 3-2. These moisture fluxes were taken from the results of simulations discussed later in Chapter 7. There is a large range of moisture fluxes from 10^{-9} Kg/s for diffusion within the wood to 10^{-3} Kg/s for the ventilation flows. The internal wood diffusion has a small effect on the total attic moisture balance compared with the ventilation and wood surface convection moisture fluxes. These results show the importance of using the correct ventilation rate and including the wood surface flux directly in the moisture mass balance for the attic air.

The attic air is assumed to be well mixed so that the air vapour pressure is the same at all attic locations. This is the same assumption as used in the thermal and ventilation models where the attic air is treated as a single node. The water vapour in the wood and the mixture of water vapour and attic air are assumed to act as ideal gasses. This is a standard assumption for psychometric calculations. Moisture flow through the ceiling is assumed to mix completely with the attic air. This assumption neglects the possible deposition of moisture in the insulation above holes in the ceiling. The interaction of thermal and moisture models due to heat transport by water vapour and latent heat released by condensation is neglected. The effect of latent heat was discussed in Chapter three and shown to be insignificant. Because

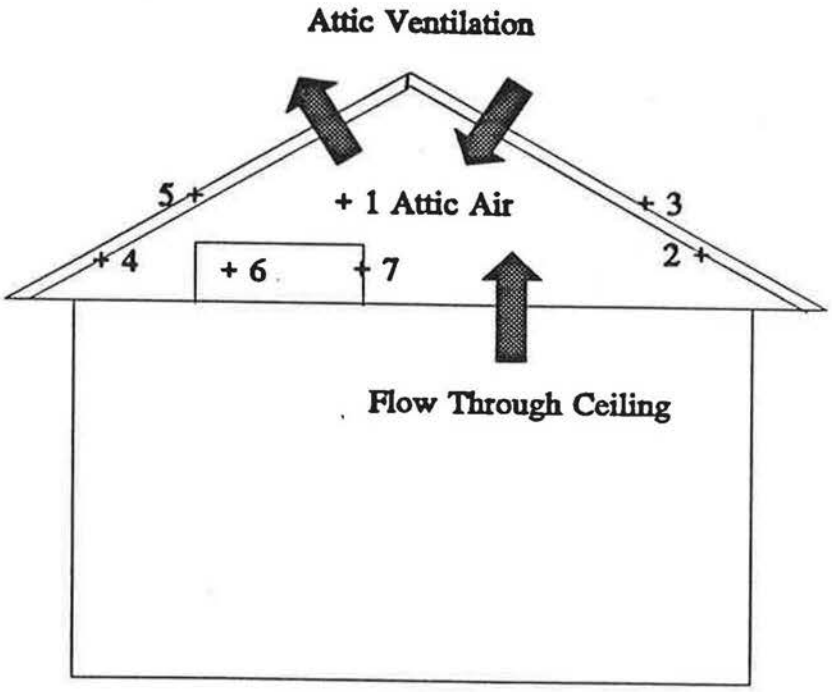

Figure 4-1. Node locations for moisture transport mass balance.

1. Attic air
2. North sheathing surface
3. North sheathing interior
4. South sheathing surface
5. South sheathing interior
6. Truss and joist surface
7. Truss and joist interior

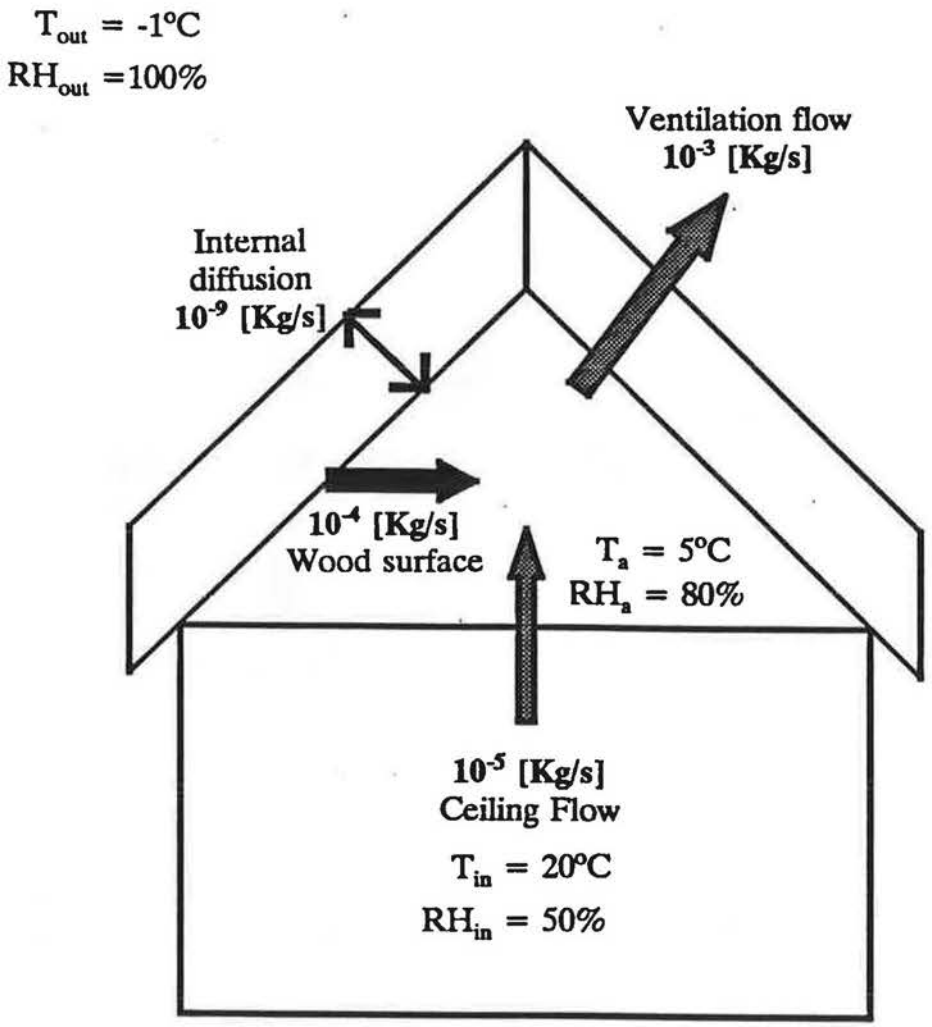

Figure 4-2. Typical attic moisture fluxes [Kg/s] in a maritime climate, with a clear sky and an attic ventilation rate of 7 ACH.

the mass fraction of water vapour in the attic air and the air flowing through the attic is small (always less than half a percent) the contribution of the water vapour to heat transfer is neglected.

The deposition of moisture in the insulation above holes in the ceiling was neglected because the deposition is limited to a small volume above each hole. Although the local moisture content of the insulation is high, the total volume is small and so the contribution of this moisture to the total attic balance is ignored. However, localised deposition of this nature may lead to localised moisture problems in the ceiling of the house. This important study of the three dimensional combined heat, air and moisture transport through these leaks is a topic for future research. The solution to this complex problem is beyond the scope of this study. One dimensional studies of this problem have been carried out by Tao, Besant and Rezkallah (1990) and Ogniewicz and Tien (1981).

The porous insulation on the attic floor can exchange moisture with the attic air. The total mass of insulation in the attic is significant (about 250 Kg in the attics used for this study with a 10cm layer of insulation), however, the moisture concentration is low if condensation is not included. A typical moisture concentration (corresponding to the plateau value of the sorption isotherm) is about 0.2% (Besant (1993), private communication) resulting in a total mass of about 0.5 Kg in the insulation. The surface wood nodes described later in this chapter have a total mass of about 50 Kg, and at 20% moisture content they contain 10 Kg of moisture. These simple calculations show that the wood has more moisture capacity than the insulation so that ignoring the moisture content of the insulation will not introduce large errors into the attic moisture balance. It would be possible to include the insulation in future developments of this model by treating the insulation the same way as the attic wood, i.e. dividing the insulation into an active surface layer that exchanges moisture by convection with the attic air, and an inner insulation layer. Dividing the insulation in this way would make the total mass in the active surface layer of insulation even less, and thus reduce its effect on the attic moisture balance. Another reason why it is not critical to include the insulation in the moisture balance is that it remains at a relatively constant temperature because the house below the ceiling remains at a constant temperature compared to the sheathing and the attic air. Because the insulation is warmer than the wood and attic air in winter (when moisture problems occur) than the insulation the equilibrium moisture content of the insulation will be lower than the wood and attic air.

The moisture transport model developed for this study uses the ventilation and heat transfer models developed in previous chapters to calculate input parameters. These input parameters are the air flow rates through the attic and the ceiling and the temperatures at each node. The air flow rates are used directly to calculate the mass balance of moisture for the attic air. The temperatures are used to calculate saturation pressures for all nodes and vapour pressures for the wood nodes. An important element in the attic moisture transport model is that the wood transfers moisture through its surface and can also store moisture internally. Choong and Skaar (1969 and 1972) and Siau (1984) have shown that the rate of moisture transfer in wood depends on the surface mass transfer and internal diffusion. Gorman (1987) accounted for these two processes by creating two nodes for each sheathing section. The sheathing was separated into a thin (3 mm) surface layer and a thicker (7 mm) inner layer. The surface layer exchanges moisture with the attic air and the inner and outer layer exchange moisture by diffusion of water vapour. This idea is used here with the inclusion of another two nodes to include the rest of the wood in the attic. The sheathing (nodes 2, 3, for north sheathing and 4 and 5 for south sheathing) and the rest of the wood in the attic (joists and trusses, nodes 6 and 7) are split into surface nodes (2, 4 and 7) and interior nodes (3, 5 and 6). Figure 4-3 illustrates the surface and inner wood layers for the sheathing. The distance between nodes used for diffusion, ΔX, is one half of the total sheathing thickness, ΔX_W. ΔX is always one half of ΔX_W independent of the surface thickness, ΔX_S, and the inner thickness, ΔX_I. This is because ΔX_S and ΔX_I must always add up to ΔX_W and ΔX is the sum of one half of ΔX_S and ΔX_I.

The mass transfer equations are written in terms of vapour pressure. Vapour pressure, P_v, is used rather than relative humidity (RH) or humidity ratio (ω) because it is easier to use in the ideal gas law that is applied in many situations in this model. The vapour pressure of wood is defined as the vapour pressure of air that would be in equilibrium with the wood at uniform temperature.

To remove the assumption of steady state it is necessary to write the rate of change of wood moisture content (W_{MC}) with time for the wood nodes in terms of vapour pressure. In this study the relationship developed by Cleary (1985) that relates wood moisture content to temperature and humidity ratio is used (as shown later in section 4.3). Cleary (1985) and Gorman (1987) have used this relationship to find water vapour pressure and humidity ratio so that mass transfer rates between attic air and the wood and within the wood could be calculated. Wood moisture

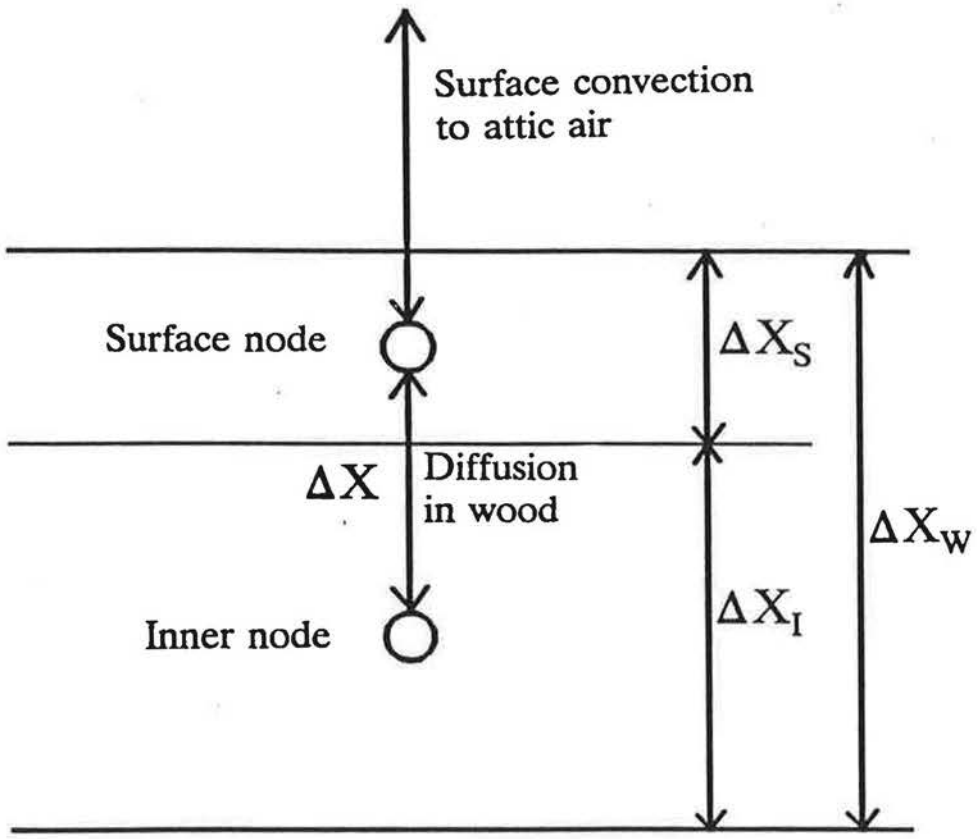

Figure 4-3. Sketch of surface and inner wood layers

contents are expressed as the mass of water as a fraction of the mass of dry wood. This water is considered to be within the cell walls. Defining wood moisture content to be the moisture in cell walls only is important because when the cell walls becomes saturated moisture transported to the wood exists as free water within the cell. In this study this free water is considered to be a condensed mass and is not included in the wood moisture content.

In the model developed for this study condensation is assumed to occur when mass is transferred to a node that is at its saturation pressure, P_{vs}. Therefore the vapour pressure at a node is always less than or equal to the saturation pressure. This condensed mass is not included as moisture in the wood but is kept track of separately. If there is condensed mass at a node then the node remains at saturation pressure until all the condensed mass is removed from the node.

In this study the diffusion of water vapour through the ceiling and to the outside air through the rest of the attic envelope is neglected. This is because the building materials have high resistance to vapour transmission. For the same surface area and vapour pressure difference the rate of vapour transfer to the wood surface is about seven orders of magnitude greater than the rate of vapour diffusion through wood as will be discussed later (see sections 4.4.2 and 4.4.3). The convective moisture flows due to attic ventilation are even larger than the rate of vapour exchange with the wood surfaces and thus the diffusive component of moisture transport is included only to find inner wood moisture contents.

4.2 Major differences from previous attic moisture transport models

Previous attic moisture transport models have been developed by Ford (1982), Cleary (1985) and Gorman (1987). Ford's model is the simplest because wood moisture contents are not calculated. The sheathing surfaces are assumed to have ice or liquid water on them at all times (i.e. they are at saturation). This means that all moisture transported to the sheathing condenses and does not change the wood moisture content. The mass balance for water used by Ford is a single equation for the attic air only. This equation includes the rate of change of mass of water in the attic air and the ventilation flows through the attic but does not include the exchange with the wood surfaces. The amount of moisture transferred from the air to the wood surfaces is calculated from the vapour pressure of the attic air and the saturation pressure of the wood surface (that is a function of its temperature only). The temperatures for Ford's model were calculated using an attic heat balance similar to that used in this study and given in Chapter 3. The ventilation rates for the

attic and the flow rate through the ceiling were not calculated by Ford and had to be supplied by the user.

Cleary's model assumes a steady-state solution to the mass balance of moisture between inside air, attic air and the wood surface. The wood moisture content from the previous hour is used to find the humidity ratio of the wood surface using a relationship developed by Cleary (see section 4.3). Knowing the humidity ratio of the outside air and the attic ventilation rate the humidity ratio of the attic air can be found. The change in moisture content of the attic wood is then found by calculating the mass of moisture transferred to the wood surface based on the new attic humidity ratio and the wood humidity ratio from the previous hour. This new moisture content is used to find the wood humidity ratio for use in the next hour's mass balance. Cleary's model does not include moisture transferred through the ceiling which can be a significant moisture load on the attic. The temperature of the attic wood and the attic ventilation rate are both user inputs to Cleary's model. Cleary's model does not differentiate between water bound within the wood and condensed surface moisture.

Gorman's model is based on Cleary's model but includes additional nodes to account for two attic sheathing surfaces that may be at different temperatures. In addition the flow of moisture into the attic through the ceiling is included in the attic air moisture balance. Gorman made Cleary's model more sophisticated by separating the wood into a surface node that exchanges moisture with the attic air and an inner node that exchanges moisture by diffusion with the surface node. This allows rapid change of surface wood moisture content rather than distributing the moisture throughout the wood. This is important for moisture exchange with the wood because the wood surface will come to equilibrium faster than if the moisture is distributed to the bulk of the wood. The wood surface will then exchange less moisture with the attic air. Gorman also separated condensed mass from water bound within the wood. In Gorman's model a wood surface that is above it's fibre saturation point (Gorman assumed this was 28%) will experience condensation rather than a change in moisture content. The fibre saturation point is the moisture content at which the cell walls of the wood have absorbed all of the water they can hold. Any further moisture accumulation appears as free water within the cells. The temperatures for the wood and the attic air are calculated by Gorman using an attic heat balance similar to that in Chapter 3. The attic ventilation flows were a required user input to Gorman's model.

The following are the major differences between the moisture transport model developed for this study and those discussed above.

• For the mass balance, the model developed for this study solves for all the nodes shown in Figure 4-1 simultaneously. Previous models by Ford (1982), Cleary (1985), and Gorman (1987) balance the air flow mass transfers to find the attic air mass content which is used separately to calculate mass transferred to and from the wood surfaces.

• The model developed here does not assume steady state. Gorman and Cleary assume a steady state solution for all the nodes. Ford did not assume a steady-state solution for the attic air but did not calculate wood moisture contents. The model used in this study uses the same ideal gas relationship as Ford for the rate of change of attic air moisture with time. A relationship for the rate of change of wood moisture content with time has been developed for this model so that the wood nodes are not assumed to be at steady state. This is very important if the moisture content of interior attic surfaces is to be calculated each hour because this moisture content can change rapidly. This, in turn, effects the amount of mass that is condensed.

• The air flow through the attic to and from outside and the flow through the ceiling are different for each hour and are calculated using the attic ventilation model shown in Chapter 2. Previous models have either assumed a constant ventilation and ceiling flow rate or required them to be measured inputs. Using the correct ventilation rate is important not only for the mass balance of water vapour, but also because the attic temperatures and surface heat and mass transfer coefficients are functions of the ventilation rate as will be shown later (see section 4.6).

• Mass condenses at the wood surfaces and appears as free water as well as being absorbed by the wood. Previous attempts to calculate the condensed mass have been based on simple assumptions. Ford (1982) assumed that the wood was always saturated so that any mass flow to the wood appeared as condensation, and wood moisture contents were not calculated. Gorman (1987) assumed that there was no condensation until the wood reached fibre saturation. A more sophisticated approach is assumed in this model that uses the wood moisture content, temperature and vapour pressure relationship developed by Cleary (1985). This relationship is used to estimate an equivalent wood vapour pressure (including the saturation pressure) from wood moisture content and temperature. Condensation is assumed to occur when mass is transferred to a node that is at saturation pressure. This condensed mass is not included as moisture in the wood but is kept track of separately. If there

is condensed mass at a node then the node remains at saturation pressure until all the condensed mass is removed from the node. This process assumes that Cleary's relationship gives the correct vapour pressure over the full range of temperatures experienced in attics. Often the attic is below the temperature range that Cleary's relationship was developed for and the relationship is extrapolated to these lower temperatures. The uncertainty in this extrapolation has not been determined due to lack of measured data. The next section discusses this relationship in greater detail.

4.3 Relating vapour pressure to wood moisture content and temperature

Cleary (1985) took data from the Wood Handbook (1982) to develop a relationship between humidity ratio, ω, temperature, T, and wood moisture content, W_{MC}, as follows

$$\omega = \exp\left(\frac{T}{B_3}\right)(B_4 + B_5 W_{MC} + B_6 W_{MC}^2 + B_7 W_{MC}^3) \qquad (4\text{-}1)$$

where B_3 through B_7 were found by fitting to measured data. Cleary determined the following values for these constants:

B_3 = 15.8°C, B_4 = -0.0015, B_5 = 0.053, B_6 = -0.184 and B_7 = 0.233.

Humidity ratio is defined as the ratio of the mass of water vapour to the mass of dry air in a given volume. Wood moisture content is defined as the ratio of the mass of water to the mass of dry wood in a given sample. The data used by Cleary was found by determining the equilibrium humidity ratio for a measured wood moisture content at several different temperatures. This means that Equation 4-1 should be applied to equilibrium conditions. It is assumed here that the air layer nearest the wood surface is in equilibrium with the surface so that this equation may be applied. Without more data it is difficult to estimate the effect on Equation 4-1 for non-equilibrium conditions. The lowest temperature used to find the coefficients in Equation 4-1 was about -1°C (30 °F). Below this temperature there may be some uncertainty in using this equation. This is important because attic temperatures in winter can be as low as -40°C and Equation 4-1 leads to predictions of low wood moisture contents of about 5% (even at saturation pressure) for these conditions. More detailed measurements at lower temperatures are required to validate Equation 4-1.

Equation 4-1 has some important effects for moisture transport in attics. Figure 4-4 shows how Equation 4-1 gives the relationship between equilibrium wood

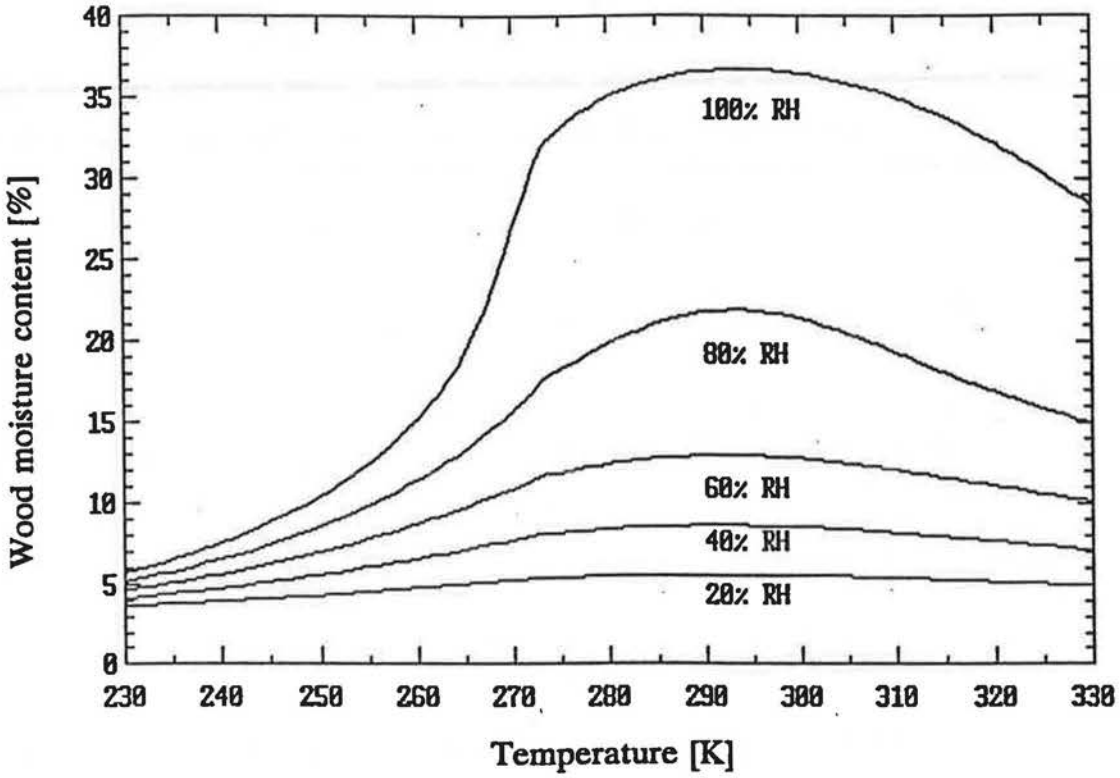

Figure 4-4. Equilibrium wood moisture content (relationship from Cleary(1985)) for a range of relative humidities (RH).

moisture content, temperature and humidity ratio, which is expressed in Figure 4-4 as relative humidity (RH). This figure shows that when the water vapour pressure in the wood is close to saturation (about 98% RH) the wood moisture content is a strong function of temperature. From Siau (1984), p.124, the fibre saturation point is reached when the relative humidity of the air above the surface of the wood (that the wood is in equilibrium with) is about 98%. Above this relative humidity the wood becomes saturated and the cells within the wood fill with free water. If this free water is included in the calculation of wood moisture contents then wood moisture contents of up to about 180% can be found using the equation given by Siau (1984)(p.29, Equation 1-20).

For simplicity the model developed here assumes that no moisture condenses until the wood reaches saturation (100% RH). At typical Canadian winter temperatures of -20°C (253 K) the maximum wood moisture content given by Equation 4-1 is only about 10%. If moisture is transferred to a wood surface at saturation it will not increase the wood moisture content but is assumed for this model to appear as free surface moisture that is condensed. If a wood surface at 0°C (273 K) and 15% wood moisture content is cooled, as happens for winter nights, the vapour pressure in the wood reaches saturation at about -13°C (260 K). Further cooling will force moisture to be condensed out of the wood as the vapour pressure cannot go above saturation. This production of condensed mass by cooling of the wood is an important factor in calculating mass condensation on attic surfaces for the moisture transport model developed here, but is only true if the assumption that Equation 4-1 can be extrapolated to lower temperatures is valid.

The maximum moisture content calculated using Equation 4-1 is about 35% at 22°C (295 K). This is at the high end of estimated values for fibre saturation limit. Typical estimates of fibre saturation point for wood in Siau (p.20, 124 and 125) are about 30% but higher values have been measured depending on the measurement method used. Due to this uncertainty in estimating fibre saturation for wood no upper limit will be placed on wood moisture content as used by other authors and wood moisture contents will be calculated using Equation 4-1, with no other limits. The highly non-linear nature of Equation 4-1 is illustrated in Figure 4-5 which shows equilibrium vapour pressure as a function of wood moisture content and temperature. At high wood moisture contents (above 15%) at a constant temperature the wood moisture content changes very rapidly with vapour pressure. At low wood moisture content the wood moisture content changes very little with vapour pressure, and

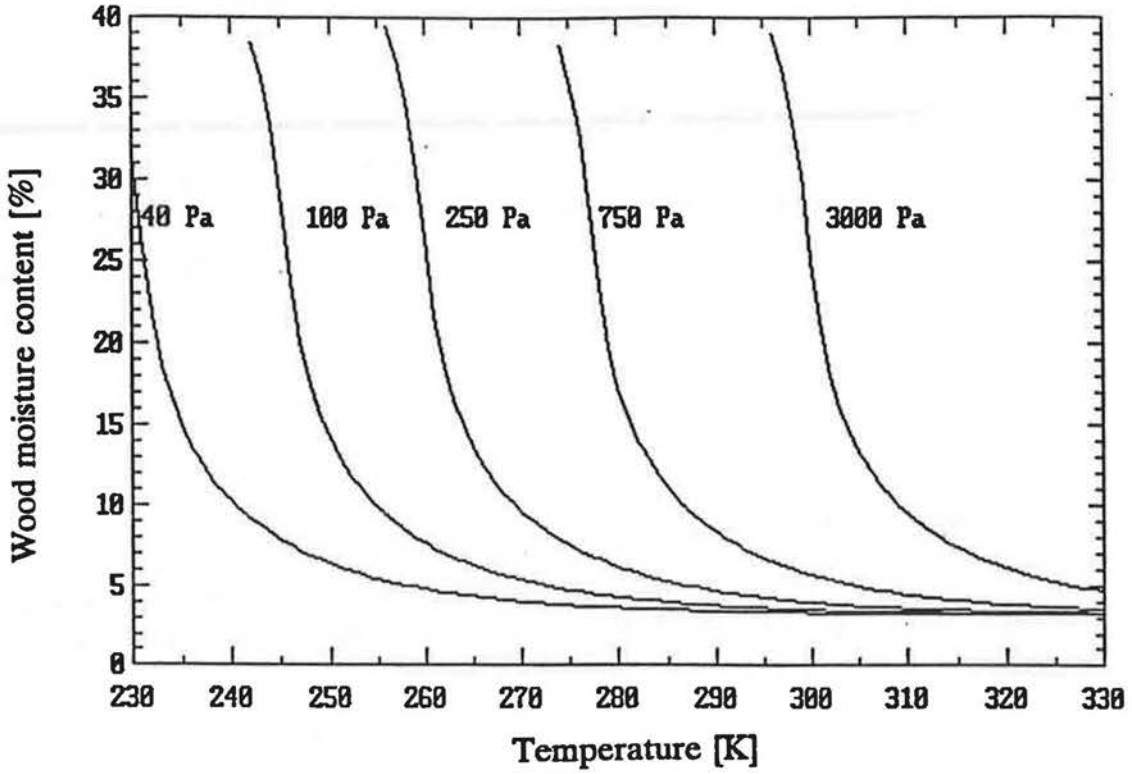

Figure 4-5. Equilibrium Wood Moisture Content (relationship from Cleary (1985)) for a range of Vapour Pressures.

equilibrium vapour pressure for the wood is almost temperature independent. A lower limit of wood moisture content of 3.2% is determined by the values of the fitted coefficients in Equation 4-1 when vapour pressure and humidity ratio are zero. This artificial lower limit is set so that vapour pressure and humidity ratio are not calculated to be negative.

4.4 Development of nodal equations

For each of the nodes shown in Figure 4-1 the rate of change of mass of moisture at the node with time is set equal to the sum of the fluxes at each node. The equations are written in terms of vapour pressure with the direction of moisture transport from high to low pressure. For the attic air the rate of change of mass is expressed in terms of vapour pressure using the ideal gas law. For the wood nodes the procedure is more complex because the vapour pressure is based on the wood moisture content and the temperature as shown in the next section, 4.4.1. The fluxes of vapour transport within the wood are by diffusion as shown in section 4.4.2. At the wood surfaces a heat transfer-mass transfer analogy is used to estimate the rate of mass transport as will be shown later in section 4.4.3. All of these terms are combined for each node in the mass balances for each node outlined in section 4.4.4.

4.4.1 Estimating the rate of change of mass of water at a wood node with time

The rate of change of mass of water at a node is given by

$$\frac{dm_v}{dt} = \frac{d(m_w W_{MC})}{dt} = m_w \frac{dW_{MC}}{dt} \qquad (4\text{-}2)$$

where m_v is the mass of water at the node, m_w is the mass of dry wood at the node and W_{MC} is the moisture content of the node. The mass of wood is a known input and does not change with time. The rate of change of mass of water at the node is then only a function of wood moisture content. To estimate the rate of change of wood moisture content Equation 4-1 is used to convert wood moisture content to vapour pressure and temperature. This must be done because the mass transport equations are functions of vapour pressure and not wood moisture content.

Because Equation 4-1 is in terms of humidity ratio, ω, the following relationships are used to convert ω to vapour pressure. Assuming an ideal gas mixture ASHRAE (1989), p.6.4, gives

where P_a is atmospheric pressure. Because atmospheric pressure is about 100kPa and vapour pressure is typically 2 to 3 orders of magnitude below this, Equation 4-3

$$\omega = 0.622 \frac{P_v}{P_\infty - P_v} \tag{4-3}$$

may be approximated as

$$\omega = 0.622 \frac{P_v}{P_\infty} \tag{4-4}$$

Substituting Equation 4-4 into 4-1 gives

$$P_v = \frac{P_\infty}{0.622} \exp\left(\frac{T}{B_3}\right)(B_4 + B_5 W_{MC} + B_6 W_{MC}^2 + B_7 W_{MC}^3) \tag{4-5}$$

now the time rate of change of wood moisture content in Equation 4-2 can be expressed as

$$\frac{dW_{MC}}{dt} = \frac{\partial W_{MC}}{\partial P_v}\frac{dP_v}{dt} + \frac{\partial W_{MC}}{\partial T}\frac{dT}{dt} \tag{4-6}$$

The dP_v/dt and dT/dt terms will be determined later using a finite difference approximation. $\partial(W_{MC})/\partial P_v$ and $\partial(W_{MC})/\partial T$ are found from Equation 4-5 as follows. $\partial(W_{MC})/\partial P_v$ is found by differentiating Equation 4-5 with respect to wood moisture content to give

$$\frac{\partial P_v}{\partial W_{MC}} = \frac{P_\infty}{0.622} \exp\left(\frac{T}{B_3}\right)(B_5 + 2B_6 W_{MC} + 3B_7 W_{MC}^2) \tag{4-7}$$

The inverse of Equation 4-7 can be used in Equation 4-5. To find $\partial(W_{MC})/\partial T$ Equation 4-5 is rearranged to express temperature in terms of wood moisture content and the following substitution used to keep the equations compact

$$fn(W_{MC}) = (B_4 + B_5 W_{MC} + B_6 W_{MC}^2 + B_7 W_{MC}^3) \tag{4-8}$$

then

$$T = B_3 \ln\left(\frac{P_v}{0.622\, P_\infty fn(W_{MC})}\right) \tag{4-9}$$

The partial derivative of Equation 4-9 with respect to wood moisture content is

$$\frac{\partial T}{\partial W_{MC}} = B_3\left(\frac{0.622\,P_{\infty} fn(W_{MC})}{P_v}\left(-\frac{P_v}{0.622\,P_{\infty}(fn(W_{MC}))^2}\frac{d\,fn(W_{MC})}{dW_{MC}}\right)\right) \qquad (4\text{-}10)$$

Inverting this relationship and substituting the derivative of Equation 4-8 gives

$$\frac{\partial W_{MC}}{\partial T} = \left(-\frac{B_3}{fn(W_{MC})}(B_5+2B_6W_{MC}+3B_7W_{MC}^2)\right)^{-1} \qquad (4\text{-}11)$$

Equations 4-7 and 4-11 are now substituted in Equation 4-6 so that the rate of change of moisture content with time is given by

$$\begin{aligned}\frac{dW_{MC}}{dt} = &\left(\frac{P_{\infty}}{0.622}\exp\left(\frac{T}{B_3}\right)(B_5+2B_6W_{MC}+3B_7W_{MC}^2)\right)^{-1}\frac{dP_v}{dt} \\ &+\left(\frac{-B_3(B_5+2B_6W_{MC}+3B_7W_{MC}^2)}{(B_4+B_5W_{MC}+B_6W_{MC}^2+B_7W_{MC}^3)}\right)^{-1}\frac{dT}{dt}\end{aligned} \qquad (4\text{-}12)$$

As in the thermal model in Chapter 3 the time derivatives are found using a finite difference approximation so that at the i^{th} hour

$$\frac{dT^i}{dt} = \frac{T^i - T^{i-1}}{\tau} \qquad (4\text{-}13)$$

$$\frac{dP_v^i}{dt} = \frac{P_v^i - P_v^{i-1}}{\tau} \qquad (4\text{-}14)$$

where the temperatures are found from the heat transfer model and P_v^i is the unknown to be found from the mass balance equation. The time step, τ, is one hour, the same as for the heat transfer model.

The partial derivatives of wood moisture content with respect to vapour pressure and temperature must be evaluated at each hour for the finite difference scheme. Because wood moisture content is not known for the current hour (i) the moisture content from the previous hour (i-1) and the temperatures for the previous hour are used in Equations 4-11 and 4-7. For node j at hour i the partial derivatives are approximated by

$$\frac{\partial W^i_{MC,j}}{\partial P^i_{v,j}} = \left(\frac{P_\infty}{0.622} \exp\left(\frac{T^{i-1}_j}{B_3} \right) (B_5 + 2B_6 W^{i-1}_{MC,j} + 3B_7 (W^{i-1}_{MC,j})^2) \right)^{-1} \qquad (4\text{-}15)$$

$$\frac{\partial W^i_{MC,j}}{\partial T^i_j} = \left(\frac{-B_3 (B_5 + 2B_6 W^{i-1}_{MC,j} + 3B_7 (W^{i-1}_{MC,j})^2)}{B_4 + B_5 W^{i-1}_{MC,j} + B_6 (W^{i-1}_{MC,j})^2 + B_7 (W^{i-1}_{MC,j})^3} \right)^{-1} \qquad (4\text{-}16)$$

These partial derivatives are substituted into Equation 4-2 together with the finite difference approximations for change of temperature and vapour pressure (Equations 4-13 and 4-14). This gives the finite difference approximation for the rate of change of mass of water at node j.

$$m_W \frac{dW^i_{MC,j}}{dt} = m_W \left(\frac{\partial W^i_{MC,j}}{\partial P^i_{v,j}} \left(\frac{P^i_{v,j} - P^{i-1}_{v,j}}{\tau} \right) + \frac{\partial W^i_{MC,j}}{\partial T^i_j} \left(\frac{T^i_j - T^{i-1}_j}{\tau} \right) \right) \qquad (4\text{-}17)$$

4.4.2 Diffusion Coefficient for Moisture in Wood

The diffusion coefficient for moisture in wood relates the flux and concentration gradient of wood moisture. The diffusion coefficient is defined under steady-state and isothermal conditions by Siau (1984), p.151, as

$$D_W = \frac{M_v}{A} \frac{\Delta X}{\Delta \Omega_{H2O}} \qquad (4\text{-}18)$$

where D_W is the diffusion coefficient for moisture in wood [m^2/s], M_v is the mass flow rate of water [Kg/s], ΔX is the distance in the flow direction [m], and $\Delta\Omega_{H2O}$ [Kg/m^3] is the concentration difference across distance ΔX.

Siau (1984), Chapter 6, has shown that the diffusion coefficient depends on temperature, moisture content, wood type and directional properties (where diffusion is parallel or perpendicular to the wood grain). For simplicity and because there is only a single node for each wood section, a constant diffusion coefficient is used in this study. The variation in diffusion coefficient with temperature and wood moisture content is about one order of magnitude (Siau (1984), p.158). Neglecting this effect

in the present study does not introduce large errors in the attic moisture balance calculations because the amount of water vapour transported by diffusion is several orders of magnitude less than the other transport terms. Experiments by Choong and Skaar (1969 and 1972) to separate surface resistance from internal resistance for moisture transfer through wood showed differences of approximately a factor of 2 in diffusion coefficient for flows parallel or perpendicular to the wood grain. The separation of surface and internal diffusion resistance is important since most experiments to determine permeability include both effects. As the samples become thicker the internal diffusion term becomes more dominant. Choong and Skaar tested two samples of different thicknesses dried under identical conditions and used theoretical relationships from Newman (1931) to isolate the diffusion term. This yielded diffusion coefficients on the order of 10^{-9} to 10^{-8} m^2/s for the woods they tested which were yellow poplar and sweetgum. More recent work by Cunningham (1990) gives an estimate of $D_W = 3*10^{-10}$ m^2/s for pine. This value by Cunningham is used in this moisture transport model as pine is more typical of wood used in attic construction. Fir and spruce are used in the plywood and trusses respectively in the attics used in this study. All of these values of diffusion coefficient are small so the exact value used is not critical for the moisture model developed in this study.

Assuming that water vapour acts as an ideal gas within the wood allows the concentration difference $\Delta\Omega_{H2O}$ to be written in terms of a vapour pressure difference, ΔP_v as follows

$$D_W = \frac{M_v}{A}\frac{\Delta X R_{H2O} T}{\Delta P_v} \qquad \textbf{(4-19)}$$

where R_{H2O} is the gas constant for water vapour (462 J/KgK), T is the temperature [K] and ΔP_v is the vapour pressure difference [Pa]. The water vapour mass flow due to diffusion within the wood from node j to node i is then given by

$$M_{v,i} = \frac{DA}{\Delta X R_{H2O} T_i}\left(\frac{T_i}{T_j}P_{v,j} - P_{v,i}\right) \qquad \textbf{(4-20)}$$

Equation 4-20 is the relationship used to determine water vapour mass flows due to internal diffusion for each wood node.

4.4.3 Mass Transfer Coefficient at Wood Surface

The rate of water vapour transfer at the wood surface is determined using a heat transfer to mass transfer analogy as shown by Holman (1981), p.492-494. Because phenomenological laws governing heat and mass transfer are similar, a relationship can be developed between heat and mass transfer at a surface. Holman (1981), p.494, shows that by equating friction factors based on heat and mass transfer coefficients for flow through pipes

$$h_v = \frac{h_U}{C_{sh,a}(Le)^{\frac{2}{3}}} \qquad (4\text{-}21)$$

where h_v = mass transfer coefficient for water vapour, m/s

h_U = heat transfer coefficient from heat transfer model, J/sm^{2}K

$C_{sh,a}$ = Specific heat of air ≈ 1000 J/KgK

Le = Lewis number

In the model developed for this study Equation 4-21 is assumed to apply to flow over the wood surfaces in the attic. A similar relationship has been used in a previous attic moisture model by Gorman (1987) to relate heat and mass transfer at the wood surface. Using a typical heat transfer coefficient of about 5 W/m^{2}K the corresponding mass transfer coefficient calculated using Equation 3-21 is about 5.3 * 10^{-3}m/s.

The Lewis number, Le, is given by the ratio of thermal diffusivity to water vapour diffusion coefficient. The ASHRAE fundamentals handbook (1989), p.5-9, gives a typical value of Lewis number for air and water vapour of 0.919. As with the internal diffusion the concentration of water vapour can be expressed assuming an ideal gas relationship such that the rate of mass transfer at the wood surface is given by

$$M_v = \frac{h_v A}{R_{H2O} T} \Delta P_v \qquad (4\text{-}22)$$

where ΔP_v is the difference in vapour pressure between the wood surface and the air flowing over it. Equation 4-22 is used for all the wood surface nodes to determine the amount of mass transferred between the surface and the attic air.

4.4.4 Mass transfer Biot number

The biot number for mass transfer is determined by the ratio of the rate of mass transfer at the surface to the internal mass transfer. For the lumped heat capacity approximation to be valid the value of Biot number must be low (<0.1). In this case the ratio is of the surface convection coefficient to the internal diffusion coefficient.

$$Bi_{H2O} = \frac{h_v\left(\frac{V}{A}\right)}{D_W}$$

where Bi_{H2O} is the mass transfer Biot number, h_v is the surface convection mass transfer coefficient, V/A is the volume to area ratio (or characteristic length) and D_W is the diffusion coefficient for moisture in wood. Using the typical value of h_v = $5.3*10^{-3}$ (as shown in the previous section), V/A is the sheathing thickness of 0.01m and a diffusion coefficient of $3*10^{-10}$ gives Bi_{H2O} of approximately $2*10_5$. This value of Bi_{H2O} shows that using a single moisture content for each wood location in the attic is a poor approximation. Even using one of the lower estimates of diffusion coefficient and making the surface layer only 1% of the total wood thickness would not produce a low enough Bi_{H2O}. This is because the rate of diffusion transport of moisture in wood is very slow and considerable moisture gradients exist in the attic wood. One method of reducing the errors from the lumped heat capacity analysis would be to further divide the wood into thinner layers. This is a possible future development for attic moisture models. The rate of moisture transport in the wood is complicated by temperature and moisture content effects, and free water above freezing may move by capillary action. In order to also include these effects, another solution to this problem is to find an appropriate surface layer thickness that provides realistic predictions of surface moisture content and condensed mass. The effect of changing the effective surface layer thickness will be examined later in the simulations in Chapter 7.

4.4.5 Mass transfer equations for moisture in attics

The mass transfer at each node is found in terms of its vapour pressure. For the wood nodes the transfer depends on diffusion within the wood and convection transfer at the surface. The attic air includes the convective mass transfer with the wood surfaces and the convective flows of outdoor and house air through the attic.

The rate of mass accumulation at a node is equated to the net flux to the node using finite difference approximation for time derivatives. All the following equations are written for the i^{th} hour and all the time derivatives are calculated using the values of vapour pressure and temperature from the previous hour. This results in a system of equations describing the mass transfer in the attic that is linear in vapour pressure. The solution of this set of linear equations with the same number of equations as unknowns is described in section 4.6. The complications arising from condensed masses where the vapour pressure at a node is limited to its saturation pressure are discussed in section 4.5. For each wood node the partial derivatives of wood moisture content, W_{MC}, are calculated using Equations 4-15 and 4-16.

Node 1. Attic air

The rate of change of moisture in the attic air, given by the left hand side of Equation 4-24, is calculated using the ideal gas law. This rate of change depends on the transfer to and from the wood surfaces, the convective flows of air through the attic and any condensed mass. An additional term, M_{ss}, is used for the attic air to account for any source or sink terms (e.g. humidifiers), although in this study this term is zero. The mass balance yields:

$$\frac{V_a(P^i_{v,1}-P^{i-1}_{v,1})}{R_{H2O}T^i_1\tau}=\frac{h^i_{v,4}A_4}{R_{H2O}T^i_4}\left(P^i_{v,4}-\frac{T^i_4}{T^i_1}P^i_{v,1}\right)+\frac{h^i_{v,2}A_2}{R_{H2O}T^i_2}\left(P^i_{v,2}-\frac{T^i_2}{T^i_1}P^i_{v,1}\right)$$
$$+\frac{h^i_{v,7}A_7}{R_{H2O}T^i_7}\left(P^i_{v,7}-\frac{T^i_7}{T^i_1}P^i_{v,1}\right)+\frac{M^i_cP^i_{v,in}}{\rho^i_{in}R_{H2O}T^i_{in}} \qquad (4\text{-}24)$$
$$+\frac{M^i_{in,a}P^i_{v,out}}{\rho^i_{out}R_{H2O}T^i_{out}}-\frac{M^i_{out,a}P^i_{v,1}}{\rho^i_aR_{H2O}T^i_1}-M^i_{\tau,1}+M_{ss}$$

Term 1 is the mass change rate of the attic air assuming an ideal gas and V_a is the attic volume and R_{H2O} is the gas constant for water vapour = 462 J/KgK

Terms 2, 3 and 4 correspond to the mass fluxes from the wood surfaces.

Term 5 accounts for mass of moisture flowing through the ceiling assuming that the flow is from the house to the attic. M_c is the mass flow rate through the ceiling calculated by the ventilation model. For reversed flow from attic to house this term becomes

$$\frac{-M_c^i P_{v,1}^i}{\rho_a^i R_{H2O} T_1^i} \qquad (4\text{-}25)$$

Term 6 is the mass flow into the attic from outside. If M_c is into the attic and M_a is the total attic ventilation rate then $M_{in,a} = M_a - M_c$, but if M_c is out of the attic then $M_{in,a} = M_a$.

Term 7 is the mass flow to outside from the attic. If M_c is into the attic then $M_{out,a} = M_a$, but if M_c is out of the attic then $M_{out,a} = M_a - M_c$.

Term 8, M_τ, is the rate of mass condensation for the attic air which is distributed to the wood surfaces and to the air leaving the attic.

The mass fluxes in terms 2, 3 and 4 contain the following variables, where

A_2 = sheathing surface area

$h_{v,2}$ = surface mass transfer coefficient from Equation 4-21.

A_4 = sheathing surface area = A_4.

$h_{v,4}$ = surface mass transfer coefficient from Equation 4-21.

A_7 = truss and joist surface area

$h_{v,7}$ = surface mass transfer coefficient from Equation 4-21.

Node 2. North sheathing surface

Node 2 exchanges moisture by diffusion with the inner node 3 and with the attic air by convection. The rate of change of mass of water at the wood nodes is given by Equation 4-17.

$$m_{W,2}\left(\frac{\partial W_{MC,2}^i}{\partial P_{v,2}^i}\frac{(P_{v,2}^i - P_{v,2}^{i-1})}{\tau} + \frac{\partial W_{MC,2}^i}{\partial T_2^i}\frac{(T_2^i - T_2^{i-1})}{\tau}\right) + M_{\tau,2}^i$$
$$= \frac{h_{v,2}^i A_2}{R_{H2O} T_2^i}\left(\frac{T_2^i}{T_1^i}P_{v,1}^i - P_{v,2}^i\right) + \frac{D_w A_2}{R_{H2O} T_2^i \Delta X_2}\left(\frac{T_2^i}{T_3^i}P_{v,3}^i - P_{v,2}^i\right) \qquad (4\text{-}26)$$

where

$m_{W,2}$ is the mass of wood at node 2, Kg

ΔX_2 = distance between sheathing nodes for diffusion of water vapour = 1/2 sheathing thickness

$M_{\tau,2}^i$ = rate of mass condensed or evaporated/sublimed during hour i. When $P_{v,2} < P_{vs,2}$ then this term is zero.

Node 3. North sheathing inner layer

The inner wood only exchanges moisture by diffusion with the surface layer because it is assumed that the outer sheathing surface is covered by impermeable shingles. As for node 2, the rate of change of mass of water at the wood nodes is given by Equation 4-17.

$$m_{W,3}\left(\frac{\partial W^i_{MC,3}}{\partial P^i_{v,3}}\frac{(P^i_{v,3}-P^{i-1}_{v,3})}{\tau}+\frac{\partial W^i_{MC,3}}{\partial T^i_3}\frac{(T^i_3-T^{i-1}_3)}{\tau}\right)+M^i_{\tau,3} = \frac{D_w A_2}{R_{H2O}T^i_3\Delta X_2}\left(\frac{T^i_3}{T^i_2}P^i_{v,2}-P^i_{v,3}\right) \quad (4\text{-}27)$$

where

$m_{W,3}$ is the mass of wood at node 3, Kg.

$M_{\tau,3}^{\ i}$ = Mass condensed or evaporated/sublimed during hour i. When $P_{v,3}<P_{vs,3}$ then this term is zero.

Node 4. South sheathing surface

The south sheathing surface has the same moisture exchange mechanisms as the north sheathing surface, node 2. It exchanges moisture by diffusion with the inner node 5 and with the attic air by convection. The rate of change of mass of water at the wood nodes is given by Equation 4-17.

$$m_{W,4}\left(\frac{\partial W^i_{MC,4}}{\partial P^i_{v,4}}\frac{(P^i_{w4}-P^{i-1}_{w4})}{\tau}+\frac{\partial W^i_{MC,4}}{\partial T^i_4}\frac{(T^i_4-T^{i-1}_4)}{\tau}\right)+M^i_{\tau,4} = \frac{h^i_{v,4}A_4}{R_{H2O}T^i_4}\left(\frac{T^i_4}{T^i_1}P^i_{v,1}-P^i_{v,4}\right)+\frac{D_w A_4}{R_{H2O}T^i_4\Delta X_4}\left(\frac{T^i_4}{T^i_5}P^i_{v,5}-P^i_{v,4}\right) \quad (4\text{-}28)$$

where

$m_{W,4}$ is the mass of wood at node 4, Kg

ΔX_4 = distance between sheathing nodes for diffusion of water vapour = 1/2 sheathing thickness

$M_{\tau,4}^{\ i}$ = rate of mass condensed or evaporated/sublimed during hour i. When $P_{v4}<P_{vs,4}$ then this term is zero.

Node 5. South sheathing inner layer

The south sheathing inner layer only exchanges moisture with the south sheathing surface layer because it is assumed that the outer surface is covered by impermeable shingles.

$$m_{W,5}\left(\frac{\partial W^i_{MC,5}}{\partial P^i_{v,5}}\frac{(P^i_{v,5}-P^{i-1}_{v,5})}{\tau}+\frac{\partial W^i_{MC,5}}{\partial T^i_5}\frac{(T^i_5-T^{i-1}_5)}{\tau}\right)+M^i_{\tau,5} = \frac{D_w A_4}{R_{H2O}T^i_5\Delta X_4}\left(\frac{T^i_5}{T^i_4}P^i_{v,4}-P^i_{v,5}\right) \quad \textbf{(4-29)}$$

where

$m_{W,5}$ is the mass of wood at node 5, Kg.

$M_{\tau,5}^{\ i}$ = rate of mass condensed or evaporated/sublimed during hour i. When $P_{v,5}<P_{va,5}$ then this term is zero.

Node 6. Inside trusses and joists

The inside of the trusses and joists only have a single path for moisture movement. This node is connected to the surface node for the joists and trusses (node 7) by diffusion.

$$m_{W,6}\left(\frac{\partial W^i_{MC,6}}{\partial P^i_{v,6}}\frac{(P^i_{w6}-P^{i-1}_{w6})}{\tau}+\frac{\partial W^i_{MC,6}}{\partial T^i_6}\frac{(T^i_6-T^{i-1}_6)}{\tau}\right) +M^i_{\tau,6}=\frac{D_w A_6}{R_{H2O}T^i_6\Delta X_6}\left(\frac{T^i_6}{T^i_7}P^i_{v,7}-P^i_{v,6}\right) \quad \textbf{(4-30)}$$

where

$m_{W,6}$ is the mass of wood at node 6, Kg.

$M_{\tau,6}^{\ i}$ = rate of mass condensed or evaporated/sublimed during hour i. When $P_{v,6}<P_{va,6}$ then this term is zero.

ΔX_6 = Distance between sheathing nodes for diffusion of water vapour = 1/2 mean wood thickness. e.g. for a 50mm by 100mm cross section ΔX_6 = 37.5mm.

Node 7. Surface of trusses and joists

The surface of the trusses and joists exchange moisture with the attic air by convection and with node 6 by diffusion.

$$m_{W,7}\left(\frac{\partial(W^i_{MC,7})}{\partial P^i_{v,7}}\frac{(P^i_{v,7}-P^{-1}_{v,7})}{\tau}+\frac{\partial(W^i_{MC,7})}{\partial T^i_7}\frac{(T^i_7-T^{i-1}_7)}{\tau}\right)+M^i_{\tau,7}$$
$$=\frac{h^i_{v,7}A_7}{R_{H2O}T^i_7}\left(\frac{T^i_7}{T^i_1}P^i_{v,1}-P^i_{v,7}\right)+\frac{D_w A_7}{R_{H2O}T^i_7\Delta X_6}\left(\frac{T^i_7}{T^i_6}P^i_{v,6}-P^i_{v,7}\right) \qquad (4\text{-}31)$$

where

$m_{W,7}$ is the mass of wood at node 3, Kg. For joists and trusses this is assumed to be the mass corresponding to a 1mm thick layer.

$M_{\tau,7}^{\ i}$ = rate of mass condensed or evaporated/sublimed during hour i. When $P_{v,7}<P_{vs,7}$ then this term is zero.

The mass of wood at each node used for the model verification and for the simulations is given by Table 4-1. These masses are different from the heat transfer model because the wood is divided into a thin surface layer and a thicker inner layer. For the heat transfer model the sheathing is divided into inner and outer surfaces that both have the same mass of 25.7 Kg and the inner and outer truss and joist masses are combined. This gives the same total masses for the moisture transport and heat transfer models.

Table 4-1. Distribution of mass of wood in the attic for model verification and attic simulations

Location	Node	Mass of Wood [Kg]
North Sheathing Surface	2	17.2
North Sheathing Inner	3	34.2
South Sheathing Surface	4	17.2
South Sheathing Inner	5	34.2
Truss and Joist Inner	6	188
Truss and Joist Surface	7	12

4.5 Calculating Condensed Mass.

4.5.1 Wood Surface Nodes.

Previous models have either assumed that all mass transferred to a wood surface condenses (Ford (1982)) or that no mass condenses unless the wood is at fibre saturation point (Gorman (1987)). The model developed for this study is more sophisticated than these previous methods because it uses Equation 4-5 to determine the water vapour pressure at the wood surface. A limiting value of $P_v = P_{vs}$ (100% RH in Figure 4-4) is applied so that water vapour pressures in the wood are never above the saturation pressure, P_{vs}, determined by the temperature of the node. As shown in Figure 4-4, Equation 4-5 limits the wood moisture content at the saturation vapour pressure at low temperatures. This is a characteristic of Equation 4-5 that was not fitted to low temperature wood moisture content data and is being extrapolated here beyond its limits. Therefore there is some uncertainty in the wood moisture content at the saturation vapour pressure. Equation 4-5 is used in the present study because there is insufficient data on low temperature wood moisture contents to develop other relationships.

If the vapour pressure from simultaneous solution of the mass transfer equations is calculated to be greater than the saturation vapour pressure for a node, then the vapour pressure is set equal to the saturation vapour pressure. A new mass balance is performed with the vapour pressure held at the saturation vapour pressure for that node. Once all the other vapour pressures are found (other nodes may also be at saturation) the rate of mass condensation, M_τ, is calculated from the mass balance equation that includes the fluxes to and from other nodes as well as mass changes due to temperature effects when the node is saturated. The effects of temperature are very important because a decrease in temperature for a node at saturation in cold winter weather implies a decrease in wood moisture content as can be seen in Figure 4-4 and as described in section 4.2.4. The mass that was included as wood moisture content now appears as condensed mass at this wood surface. Thus the temperature change at a wood node can change its wood moisture content and condensed mass even if there is no net flux to the node. If the rate of condensed mass change at a node (M_τ)is positive then mass accumulates at the node. This mass is not included in the wood moisture content (and therefore in finding the vapour pressure for the next hour) but is monitored using a separate term, m_τ, that is the total mass accumulated at the surface. If the net mass change is negative then m_τ is reduced. If this reduction makes the total accumulated mass negative then the

difference between the net mass change and the accumulated mass from the previous hour is used to reduce the wood moisture content (and the vapour pressure) of the node. Thus when all the condensed mass has been sublimed, evaporated or reabsorbed by the wood then $m_\tau = 0$, the vapour pressure is below saturation, and the mass balance for the attic must be repeated as this node is now an unknown.

4.5.2 Attic Air Node.

As with the wood surface nodes the vapour pressure is limited to the saturation vapour pressure (for this node this is determined by the attic air temperature). If there is a net mass flux to the attic air when it is saturated from the combination of attic wood surfaces and air flows then this net mass must result in condensed mass in the saturated attic air. Unlike the wood there is no surface for this mass to accumulate on. The condensed mass is assumed to be distributed to the wood surfaces and the air leaving the attic in proportion to their mass flux exchange with the attic air. Condensed attic moisture is only transferred to wood surfaces for which there is a positive flux from the attic air (at its saturation vapour pressure) to that node. This usually means positive fluxes from the attic air to colder sheathing surfaces (which are at a lower vapour pressure) which agrees with observations of frost buildup on the interior of attic sheathing. The rest of the condensed attic air moisture is advected out with the attic air ventilation flows.

At the wood nodes the additional condensed mass from the attic air is used to calculate a new wood moisture content and vapour pressure, and the mass balance for the attic is repeated with the vapour pressure for the attic air held at the saturation vapour pressure. If the mass transfer with the attic air at saturation makes the wood vapour pressure greater than its saturation vapour pressure then the procedure for considering condensed mass for the wood must also be performed (section 4.5.1). This process of finding which nodes are at saturation (then holding them at their saturation vapour pressure and recalculating the mass balance) is continued until no more nodes reach saturation.

4.6 Solution Methods

If the vapour pressure is less than saturation at all nodes then the moisture model is a system of seven mass balance equations (4-23 through 4-30) in terms of seven unknown vapour pressures. Gaussian elimination (see, for example, James, Smith and Wolford (1977), p.169-182) is used to simultaneously solve these seven equations. Problems occur because the vapour pressure has an upper limit of the

saturation pressure. If a node is at saturation then its vapour pressure is known and is determined by the node temperature. This known vapour pressure must be substituted into the remaining equations for the other nodes and one less equation has to solved. This requires changing the number of equations in the gaussian elimination scheme and becomes even more complex if more than one node is at saturation pressure.

A solution to this problem is to use an iterative technique rather than gaussian elimination to solve the equations. Gaussian elimination is still used to provide initial estimates of vapour pressure which speeds up the iterative process. With the iterative technique each node can be checked for saturation after every iteration and the appropriate vapour pressures held constant in the next iteration. The iterative technique used here makes estimates of the vapour pressure at a node by substituting the vapour pressures from the previous iteration for the other nodes. Each of the seven equations is solved consecutively. The process is speeded up by using the updated vapour pressures within each iteration as they become available. For example, after equation 1 is solved then $P_{v,1}$ is known. This vapour pressure is now substituted wherever it appears in the other six equations rather than waiting for the next iteration. Repeated estimates of vapour pressure are made by cycling through the seven equations until all the vapour pressures change by less than 0.1 Pa. Each node at each iteration is checked to see if the calculated vapour pressure is greater than saturation. If it is then this vapour pressure is set equal to the saturation vapour pressure corresponding to the temperature at that node. The mass balance is then performed with this fixed vapour pressure to find the condensed mass as outlined in sections 4.5.1 and 4.5.2. If no saturation occurs only one iteration is required since the initial estimates from the gaussian elimination method are already the solution to the set of non-saturated equations.

Once the vapour pressure is found for each node the wood moisture content is calculated for the wood nodes using Equation 4-5. To find wood moisture content from the cubic Equation 4-5, the cube root is found analytically using standard mathematical methods from Spiegel (1968).

4.7 Summary

In this chapter a moisture transport model for the attic has been developed. The model includes convective ventilation flows through the attic, the exchange of moisture at wood surfaces and the storage of moisture in the wood. The model uses

ventilation rates and temperatures calculated by the models in Chapters 1 and 2 as inputs. Surface mass transfer coefficients are calculated from the convective surface heat transfer coefficients found in the heat transfer model. Moisture movement within the wood is assumed to be by diffusion. Estimates of diffusion coefficient from other authors indicate that the diffusion process is several orders of magnitude slower than the surface moisture transport. This is important because it means that the wood nodes should be treated as if they are at a single moisture content. To examine this effect different surface layer thicknesses will be examined in the simulations in Chapter 7. The rate of change of moisture content of each node of the model is approximated using a finite difference technique with a timestep of one hour. This length of timestep was chosen because the measured data used for validation are hourly averaged values. A system of seven equations has been developed for the seven nodes shown in Figure 4-1. At each node the rate of change of moisture at the node is set equal to the sum of the fluxes at the node as shown in Equations 4-23 to 4-30. This set of linear equations is solved using an iterative scheme to find the vapour pressures, and hence wood moisture contents and attic air relative humidity. The complication of nodes at saturation where mass is condensing is dealt with by fixing the vapour pressure at these nodes at their saturation pressure. This known value of vapour pressure is then substituted into the remaining equations to be solved.

An important aspect of this model is the use of a relationship developed by Cleary (1985) between wood moisture content, temperature and vapour pressure. This relationship allows the rate of change of moisture content with time to be estimated so that the wood nodes and the attic air vapour pressures may be solved for simultaneously. This relationship is also vital in determining the amount of condensation on a wood surface. The extrapolation of this relationship to low temperatures results in wood surface nodes reaching saturation vapour pressure well below the fibre saturation point of wood (approximately 30%). This has a significant effect on the drying of wood (reduction of moisture content) in cold winter months. To improve the low temperature extrapolation of Cleary's equation more experiments need to be performed to determine the moisture content of wood at low temperatures.

Chapter 5. Measurements for model validation

To validate the attic ventilation, thermal, and moisture models described in the previous chapters field data was taken over the course of two heating seasons, 1990-91 and 1991-92 at The Alberta Home Heating Research Facility (AHHRF). This chapter describes the construction details and configurations of the two attics that were monitored. This includes the background leakage area and vent configuration of the attics and the distribution of the ceiling leakage. The instrumentation and measurement procedures are presented for attic ventilation rates and fan pressurization tests to determine leakage areas. This chapter also includes presentation of some typical results for ventilation rates, attic temperatures and wood moisture content.

There have been several previous studies monitoring ventilation, heat transfer and moisture in attics. Some studies, e.g. Wilkes (1983) and Burch, Lemay, Rian and Parker (1984), have used scale models of attic spaces inside environmental chambers. This allows direct control over the ambient conditions for the attic. However, this does not provide data on real attics exposed to the dynamics of real weather. In addition, the attic in both the above studies had forced fan ventilation with no natural wind. This provides a constant ventilation rate that does not occur in real attics. Limited full scale field testing has been carried out by previous authors. Fairey (1983) performed tests over three days on a fan ventilated attic. Fairey was only interested in heat transfer and concentrated on heat flux measurements with no ventilation, relative humidity of moisture content measurements.

For testing more specifically directed at moisture in attics the following four studies have appeared in the literature. Gorman (1987) did not measure ventilation rates but did measure relative humidity in the attic using a strip chart recorder. Gorman also took limited manual readings of sheathing moisture content and temperatures. Ford (1982) took a total of 350 hours of temperature data at multiple attic locations. In addition Ford measured relative humidities with an aspirated psychrometer (above freezing only) but took no wood moisture content or ventilation measurements. Some of the most thorough attic measurements to date have been provided by Cleary (1985). Cleary measured, temperatures, wind speed, wind direction, solar radiation, wood moisture content and air relative humidity over a six month heating season. Cleary made 24 periodic measurements of ventilation using a tracer gas decay technique and on one occasion measured the house to attic

exchange rate.

The measurements performed for this study provide significantly more information for the evaluation of attic moisture phenomena and validation of attic ventilation, heat transfer and moisture transport models. Data has been taken continuously for over two years, providing a data base of over 5000 hours. This data covers a wide range of weather conditions with outside temperatures ranging from +30°C to -40°C, wind speeds of up to 10 m/s and covering all wind directions. The complete set of wind directions is important (as will be shown later in this chapter and in the following chapter on model verification) because both wind pressure coefficients and wind shelter are highly dependent on wind direction. This study has continuously monitored ventilation rates and house to attic exchange rates that have not been systematically measured before. Ambient conditions of relative humidity, temperature, solar radiation on both pitched roof surfaces, wind speed and wind direction have been measured for use as inputs to the models developed for this study. The relative humidity and temperatures of the house and attic air have been measured and additional measurements of wood moisture content and wood temperature were performed in the attic.

5.1 Attic test facility

The field monitoring program was carried out over a period covering two heating seasons in 1990-91 and 1991-92 at The Alberta Home Heating Research Facility (AHHRF), located south of Edmonton, Alberta. The facility consists of six houses situated in an east-west row as shown in Figure 5-1. Each house has a full basement with a single storey and gable-end attic. The houses are spaced approximately 2.6 m apart. At each end of the row, false end walls were constructed about 3.7 m high but without roof gable peaks, to provide wind shelter and solar shading similar to that experienced by interior houses in the row. The attic ventilation tests were carried out in houses 5 and 6 which are the last two houses at the east end of the row. Both houses are essentially identical in construction and insulation levels and the details of the house construction are given in Table 5-1. All houses at the test site are heated electrically with a centrifugal fan which operates continuously, recirculating 4.5 house interior volumes per hour. The continuous fan operation ensures that the air inside the house is well mixed with the sulphur hexafluoride (SF_6) tracer gas used to monitor house ventilation rates. Both houses have a 6m long 15.2 cm ID flue pipe that extends through the ceiling and roof to terminate in a rain cap level with the roof ridge. This places the flue cap a little below the required height

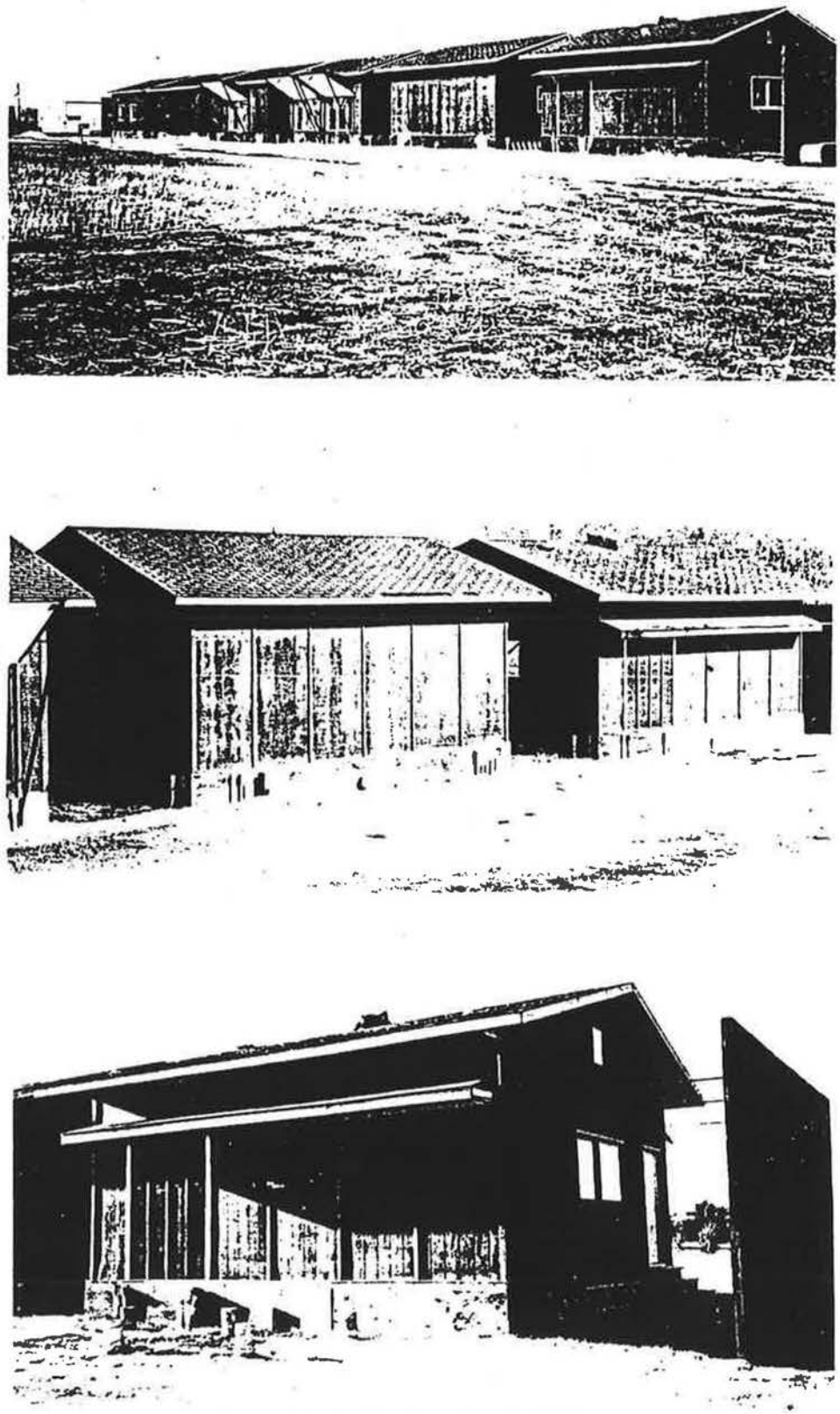

Figure 5-1. Houses 5 and 6 at AHHRF showing building orientation and false end wall.

to meet the building code (NBCC (1990)), however, because the flues are passive (i.e. not connected to a furnace) this does not present a problem. The present tests were carried out with the flue blocked to increase air exfiltration through the ceiling to provide a moisture load for the attic.

Table 5-1
Construction details of houses 5 and 6

Floor Area	6.7 m x 7.3 m (22′ x 24′)
Wall Height	2.4 m (8′)
Basement Height	2.4 m, 1.8 m below grade (8′,6′ below grade) Exterior insulation RSI 1.76 (R10) to 0.61 m (2′) below grade
Walls	9.5 mm (3/8") Prestained Plywood 64 mm (2-1/2") Glass fiber batts 51 mm x 102 mm (2" x 4") studs, 40 cm (16") o/c 4 mil poly vapour retarder 12.7 mm (1/2") drywall, painted
Wall Area/Floor Area	1.39/1
Windows	North: 99 cm x 193 cm (39" x 76") double glazed sealed South: none East : 101 cm x 193 cm (40" x 76") double glazed sealed West : same as E
Window Area/Floor Area	11.9%
Ceiling	152 mm (6") Glass fiber batts 4 mil poly vapour retarder 12.7 mm (1/2") drywall, painted
Roof	CMHC approved trusses with 76 cm (2-1/2") stub asphalt shingles 9.5 mm (3/8") plywood sheathing roof pitch 3.0:1 61 m^3 attic volume
Basement	20 cm (8") concrete wall 10 cm (4") concrete slab on 6 mil poly
Electric Furnace Capacity	12 kW

As will be shown later in this chapter, and also in the following chapter discussing model validation, wind shelter is an important factor in determining attic (and house) ventilation rates. In Chapter 2 it was shown that the closest obstacle dominates the wind shelter effect for a building. For the test houses at AHHRF their shelter is dominated by the other houses in the row and the false end walls. Other obstacles that may provide significant shelter are a storage shed and machinery building, both two storeys high, that are about 50m to the northwest of the row of test houses. For more details of the surroundings see Forest and Walker (1993).

The attics in houses 5 and 6 have the same construction. Each attic has plan dimensions of 6.7 m by 7.3 m (including the eaves makes it 7.8 m by 7.3 m) with gable end walls and a full length ridge oriented along the east-west direction. The sloped roof sections face north and south while the gable ends of the attic are vertical extensions of the east and west walls. The roof trusses are constructed of 38 mm by 89 mm spruce joists and are spaced at 61 cm intervals as shown in Figure 5-2. The sloped roof section (with a pitch of 3:1) is raised 0.67 m above the attic floor to accommodate various levels of ceiling insulation for other tests that have been conducted at AHHRF. The sloped roof was covered with 95 mm exterior plywood sheathing and brown asphalt shingles. The ceiling consisted of 12.7 mm painted drywall, 4 mil polyethylene vapour barrier, and 89 mm glass fibre batts between the trusses. The total enclosed attic volume was estimated to be 61 m^3.

The main difference between the two attics used in this study is their air tightness. Attic 5 was a "tight" attic where there were no intentional openings such as roof or soffit vents in the exterior portion on the attic envelope. The only leakage area in attic 5 was the background leakage associated with construction of the attic envelope. Attic 6 was fitted with continuous soffit vents (shown in Figure 5-3) along the north and south eaves and two flush-mounted attic vents (shown in Figure 5-4). The soffit vents were mounted on false eaves that were aligned with the floor of the attic. This was done to have the soffit leakage area in a location that was representative of conventional residential construction. The soffits on attic 6 had a gross open area of 403 cm^2 on each side of the house. The flush-mounted roof vents were commercial vents and had a gross opening area of 384 cm^2. The net area of the roof vents was reduced by a screen which was used to prevent the entry of insects.

During the second heating season, attic 6 was retro-fitted with a roof-mounted fan (Broan Model 334) as shown in Figure 5-5. The fan was designed to exhaust attic air to outdoors (depressurizing the attic). The fan was also operated in the opposite

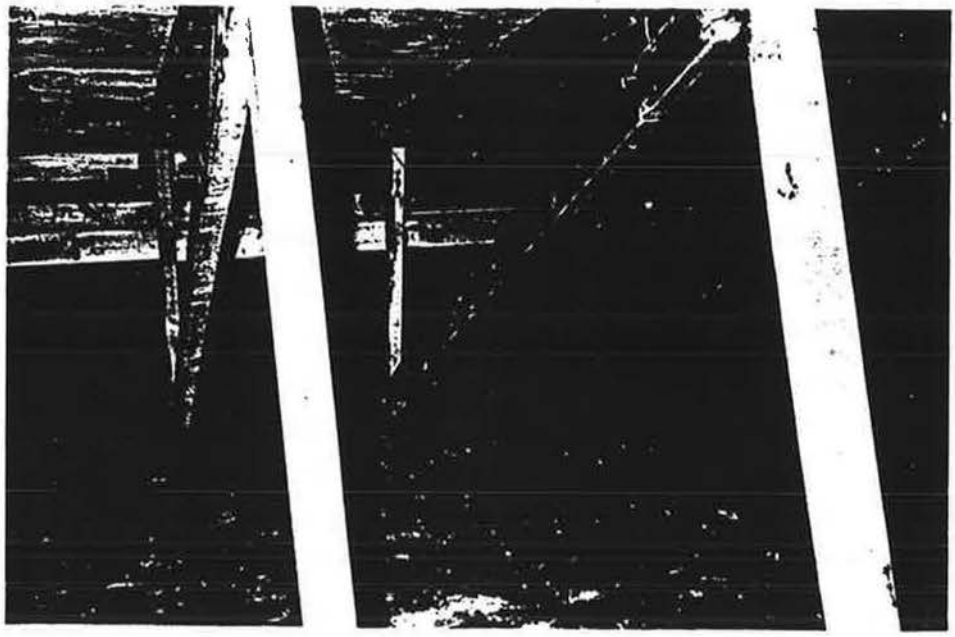

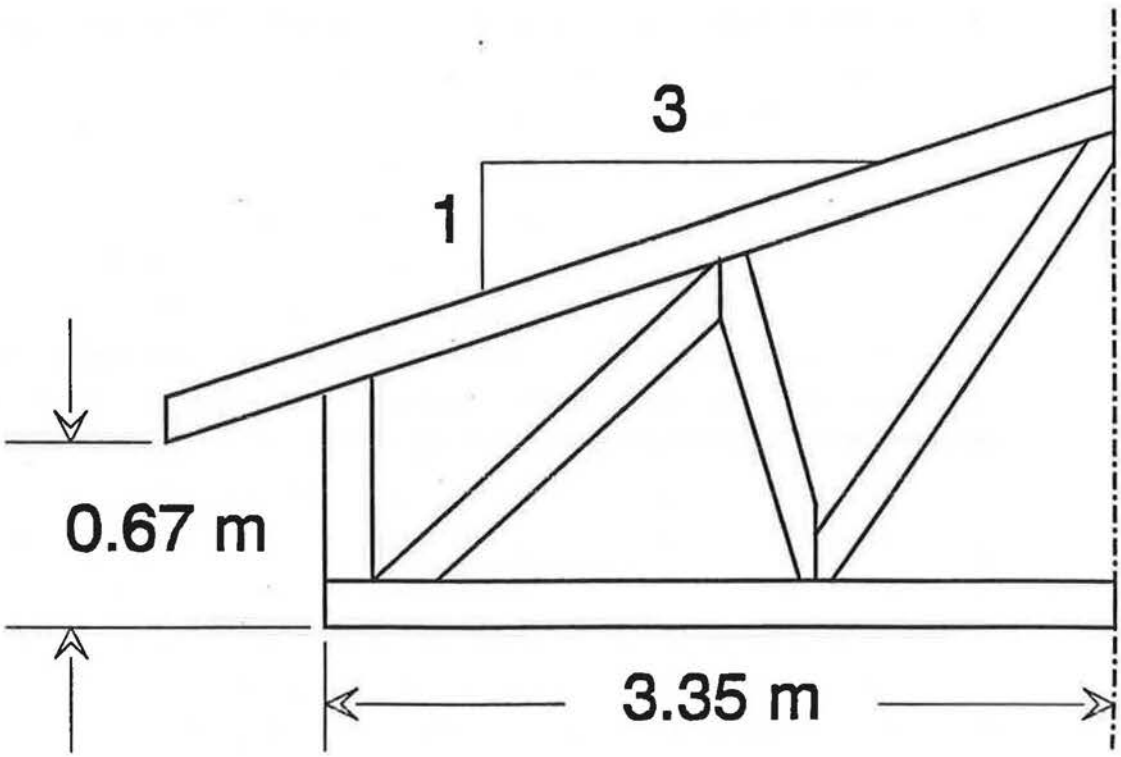

Figure 5-2. Attic interior showing detail of trusses.

Figure 5-3. False eaves on house 6.

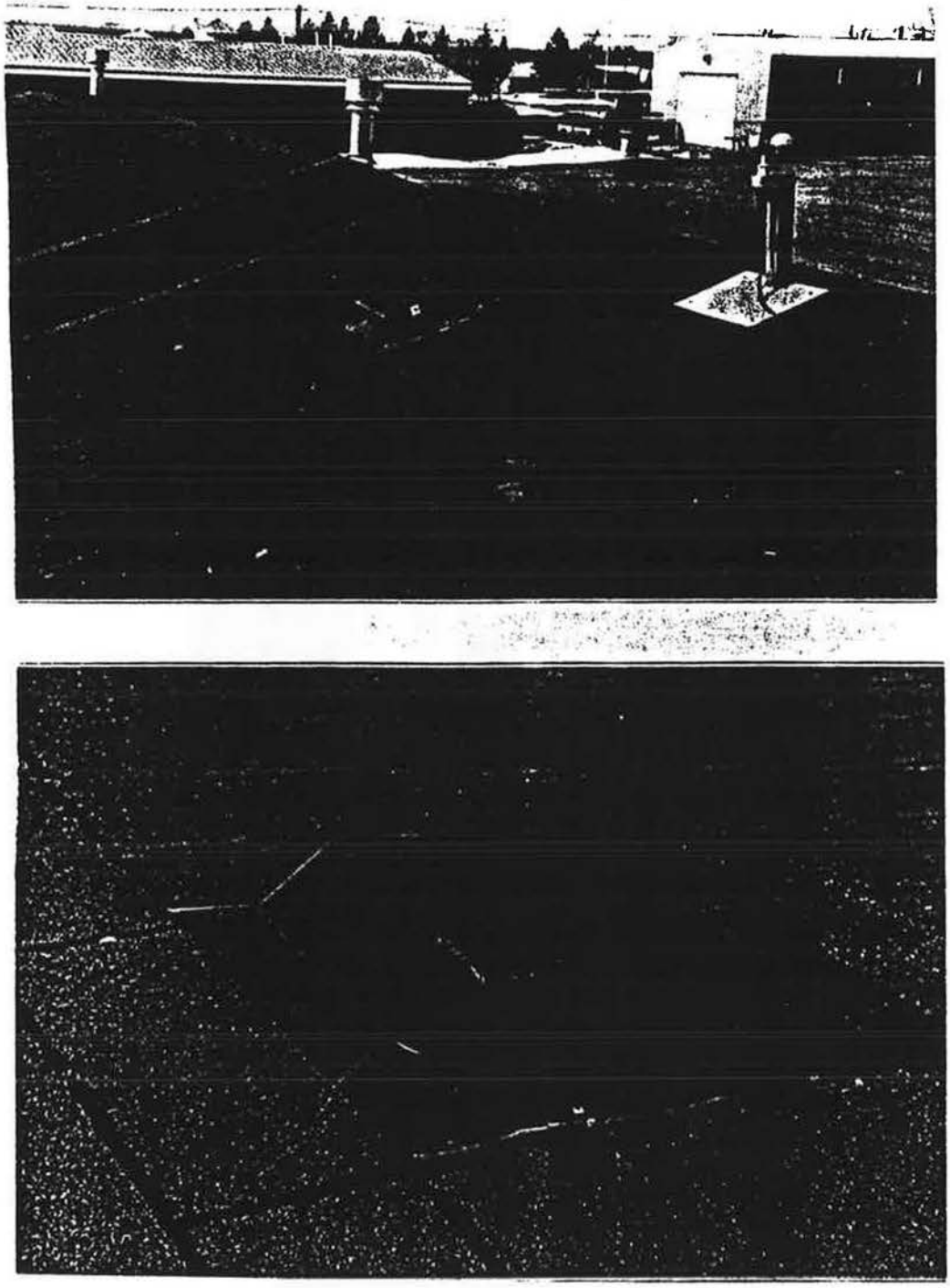

Figure 5-4. Location and installation of roof vents for attic 6.

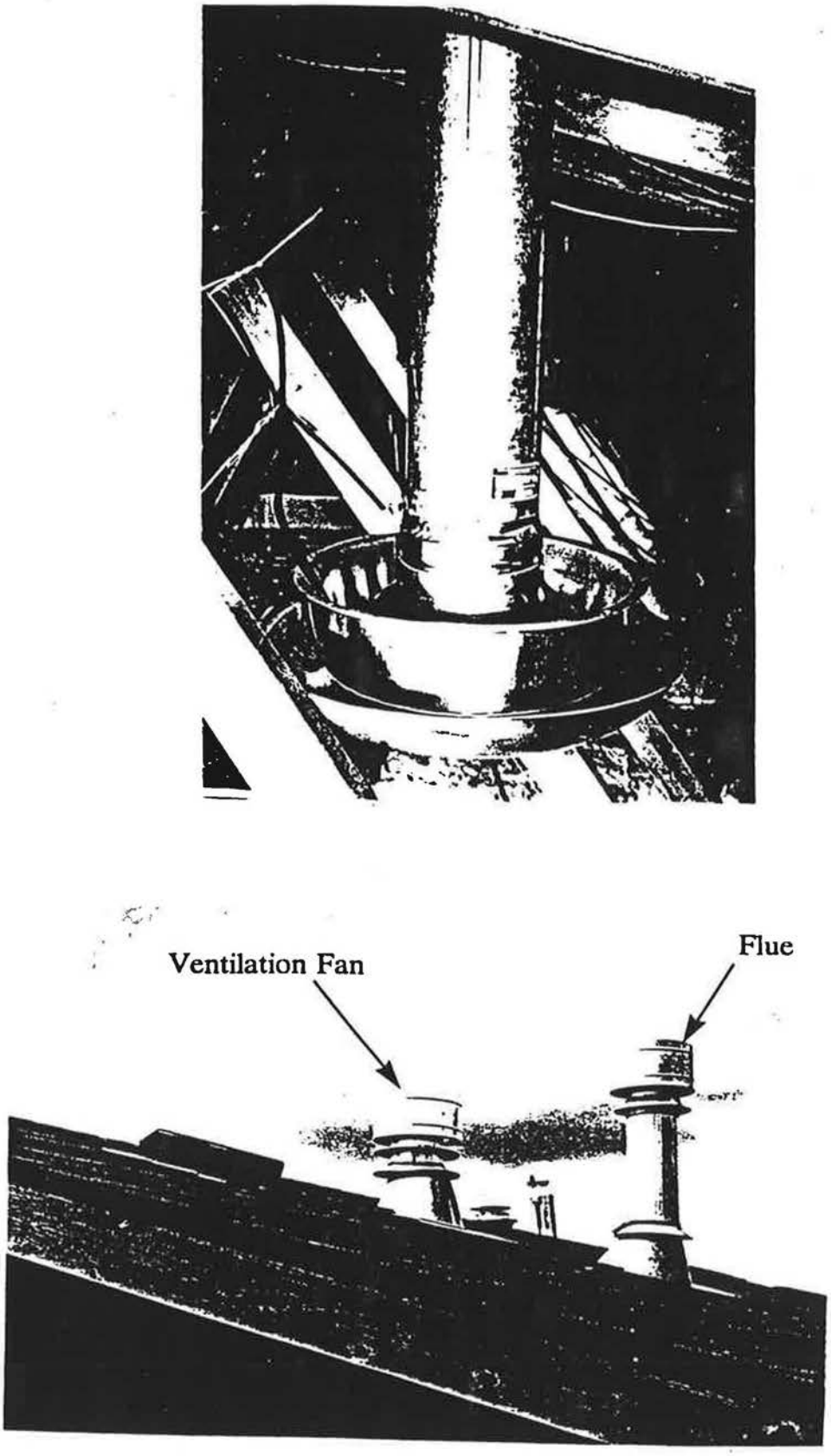

Figure 5-5. Ventilation fan in attic 6 in supply orientation showing interior view and exterior protective rain cap (same as the flue beside it).

mode with the fan blowing outdoor air into the attic (pressurizing the attic). This required that the fan be physically turned upside down in order to reverse the flow direction. This would expose the fan inlet to the outdoor environment. In order to protect the fan, a short length (1 m long) of 15 cm diameter pipe was attached to the inlet of the fan with a rain cap at the open end (the discharge side of the fan was protected by its own rain cap). It was necessary to use the fan with this inlet duct arrangement in both pressurization and depressurization modes so as to maintain the same flow characteristics of the fan in both orientations. This fan-inlet duct system was initially installed on the roof of attic 6 on November 4, 1991 and tested in the exhaust mode between November 4, 1991 and January 30, 1992. The fan was operated on a timed cycle where the fan was on between 10:00 am and 4:00 pm and off for the rest of the day. On February 1, 1992 the fan orientation was reversed and ventilation rate measurements made with the attic pressurized. Prior to installation, the fan-duct system was tested in a calibrated flow apparatus where the fan performance characteristics were measured. These measurements showed that the maximum flowrate for the fan was 0.164 m^3/s (which corresponds to an attic ventilation rate of 9.6 air changes per hour (ACH) based on an attic volume of 61 m^3) and the maximum pressure difference that the fan can generate is 175 Pa. When the fan was installed in the attic the additional flow resistances through the vents and soffits would act to decrease the flow delivered by the fan.

The leakage area in the ceiling interface between the heated interior space of the house and the attic allows air exchange between the two zones. During cold weather, indoor air exfiltrating into the attic may impose a significant moisture load on the attic. One of the main objectives of the tests performed for this study was to measure the indoor-attic exchange rate. The ceilings in houses 5 and 6 were essentially identical in construction and insulation levels. There was some unintentional leakage area, particularly around the electrical junction boxes for the two fluorescent light fixtures in each house. In addition, a 0.5 m by 0.89 m ceiling panel, shown in Figure 5-6, was placed approximately in the centre of the ceiling in both houses. A 7.6 cm diameter hole was placed in the centre of the panel to provide a large leakage site. This intentional leakage site was part of an orifice flow meter which was used to monitor the flow through this leakage area. The ceiling in house 5 had an additional ceiling panel that had three separate leakage sites, 7.6 cm, 2.5 cm, and 0.64 cm diameter respectively, which was used for a separate study on moisture accumulation in the ceiling insulation.

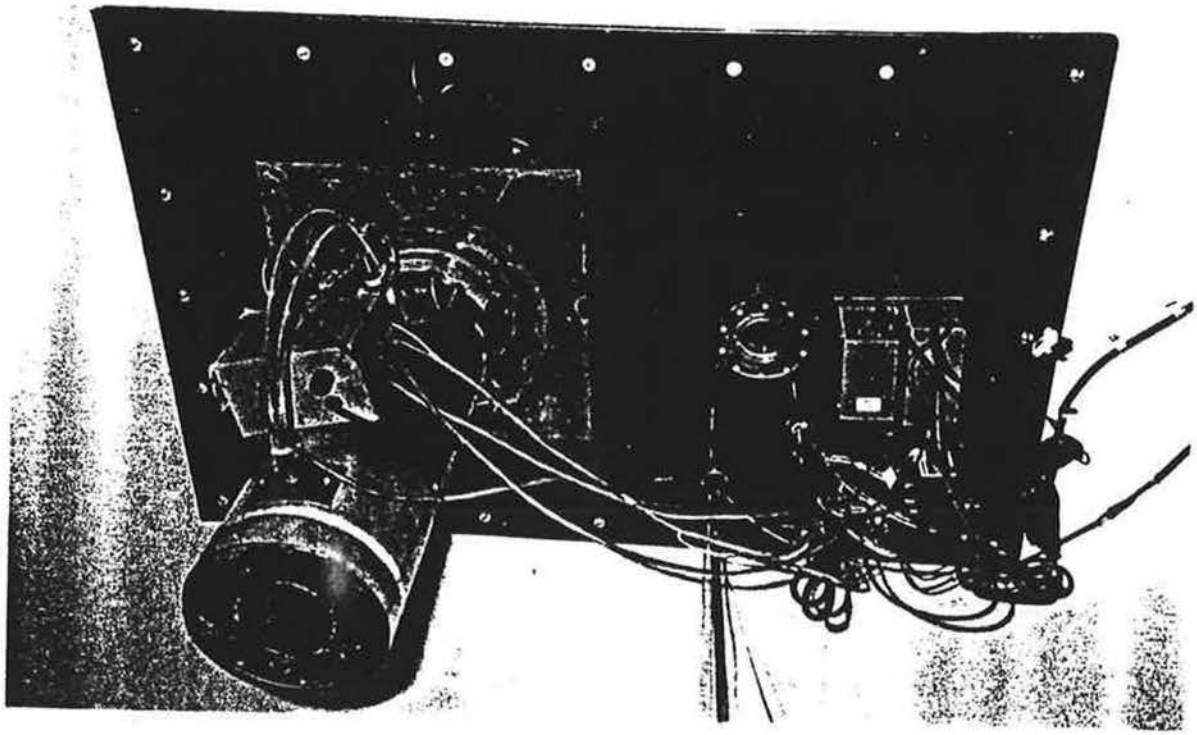

Figure 5-6. Ceiling Panel and Orifice Flow meter.

In order to provide a moisture load on the attic, the indoor air in both houses was humidified throughout the heating season. The humidification was provided by rotating-drum type humidifiers. During the first heating season (1990-91), the indoor relative humidity was maintained at approximately 40% with a variation of ±5%; during the 1991-92 heating season this level was increased to 50% in order to provide a larger moisture load on the attic. The humidifier water consumption rate was measured in the following way. Water for the humidifiers was supplied to an intermediate tank which was a 15 cm ID by 122 cm tall PVC pipe and the water from this tank was fed to the float valve on the humidifier. A pressure transducer near the bottom of the intermediate tank sensed the change in pressure caused by the change in water level as water was consumed by the humidifier. The pressure in the tank was measured by the data acquisition system at the end of each hour and the change in pressure from the previous hour was converted to the hourly water consumption rate. At the end of each 24 hour period, a pump refilled the intermediate tank up to its capacity. It was found that water consumption was highest during very cold periods because the outdoor air which infiltrates into the house contained very little moisture.

5.2 Measurement Procedure

5.2.1 Fan Pressurization Tests

Fan pressurization tests were performed to determine the leakage characteristics of the exterior envelope of the attic, the ceiling, and the houses. The attic tests were carried out using two separate fans, one connecting the attic with the interior of the house and the other connecting the interior the house with the outdoors as shown in Figure 5-7. The attic fan was connected through the plexiglass ceiling panel (shown in Figure 5-6) which had been temporally removed for these tests. The flowrate through each blower was obtained by measuring the pressure drop across a laminar flow element which was in series with the fan and pressure difference measurements were taken with calibrated diaphragm transducers (Validyne).

Because ceiling leakage is very important in calculations to find the flow of air and moisture into the attic, it was measured separately from the rest of the attic leakage. To determine the background leakage area of the exterior portion of the attic envelope (not including the ceiling) the attic was pressurized relative to the outdoors and the fan connected to the interior of the house was adjusted until the

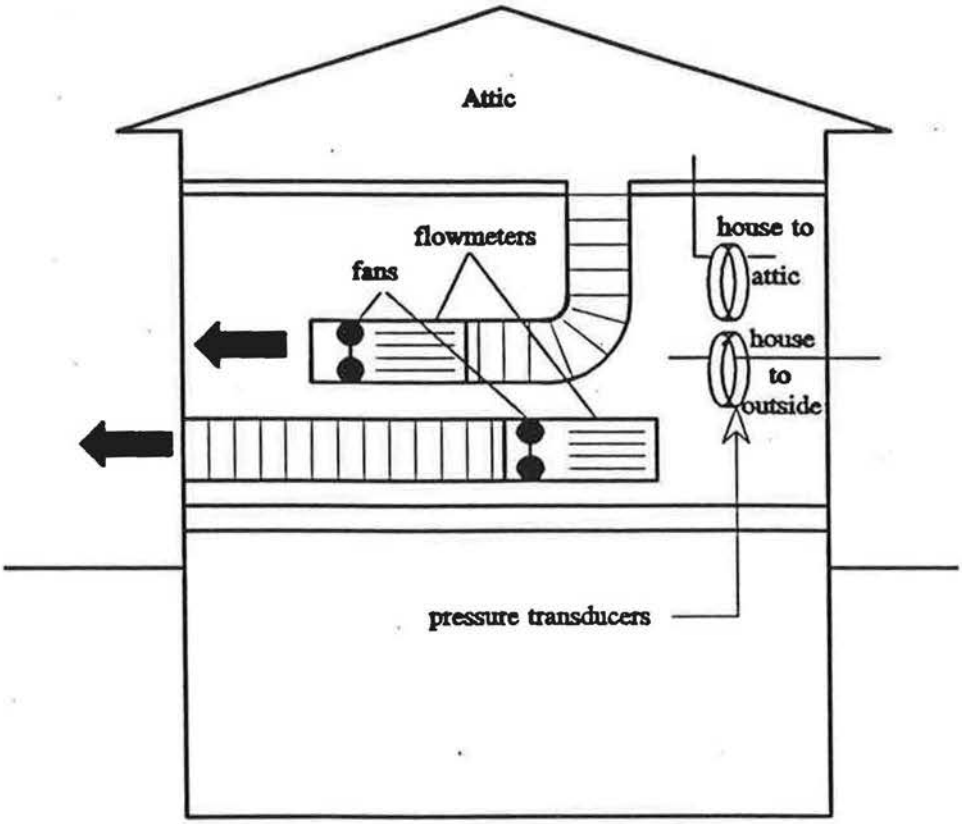

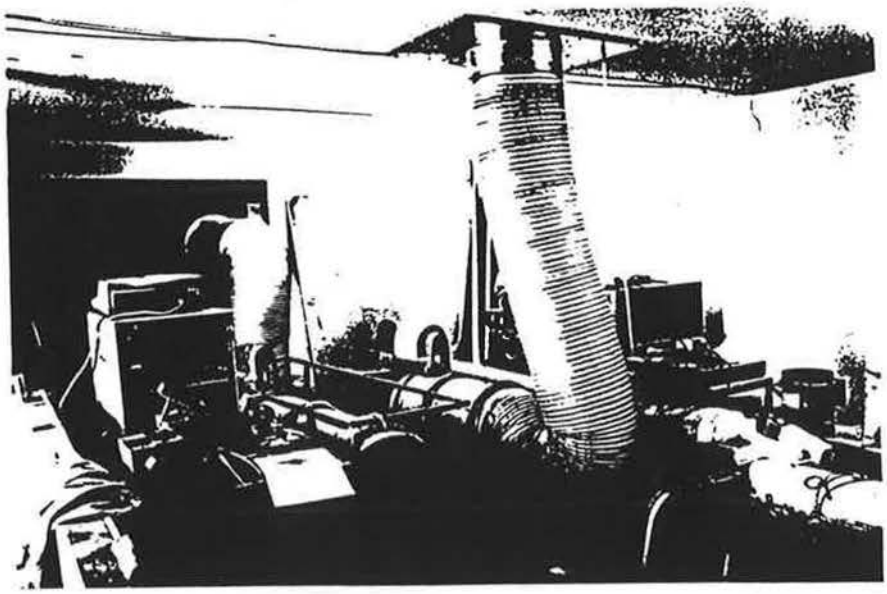

Figure 5-7. Blower Apparatus for Attic Leakage Testing.

attic-indoor pressure difference was zero. Making the pressure difference across the ceiling zero means that there will be no flow through the ceiling, in which case the measured flowrate will not include the ceiling leakage. This procedure required careful manipulation to maintain zero pressure difference across the ceiling because of fluctuations in ceiling pressure difference even at low wind speeds. The measurements were repeated at several attic to outdoor pressure differences to obtain a complete flow-pressure difference characteristic.

The results of these tests are shown in Figures 5-8A and 5-8B for attic 5 and 6 respectively. For these tests, the two roof vents on attic 6 were sealed so that only the background leakage area was being measured. In order to reduce the scatter in these data caused by wind pressure fluctuations, all fan pressurization tests were carried out only when the wind speed was less than 1 m/sec. The figures show the individual data points as well as a linear least squares fit to the data. The linearity of the data indicates that the flow characteristic follows a power law where

$$Q = C\Delta P^n \tag{5-1}$$

where Q is the flowrate [m^3/s], ΔP is the pressure difference across the attic envelope [Pa], C is the flow coefficient [m^3sPa^n] and n is the flow exponent. Building leakage is often expressed in terms of equivalent leakage area. Equivalent leakage area is the area of an orifice that would have the same flowrate as that given by Equation 5-1 at a given pressure difference. By equating 5-1 to an orifice flow relationship, Equation 5-2 may be found. Equation 5-2 is the same as Equation 3-48, but with the four pascal reference pressure substituted, and is used to convert C and n to equivalent leakage area, A_{L4}.

$$A_{L4} = C\sqrt{\frac{\rho}{2}}4^{(n-1/2)} \tag{5-2}$$

where ρ is the air density. The reference pressure of four pascals is chosen because it is the standard pressure used by ASHRAE (1989) (Chapter 23, p.14) in calculating equivalent leakage areas of building components.

The pressure difference range for attic 6 was 3 to 7 Pa whereas, attic 5 was tested from 7 to 30 Pa. These pressure ranges were dictated by the maximum flow capacity of the attic fan (approximately 0.7 m^3/s) and the leakage area of the attic. Because the leakage area of attic 6 was substantially larger than attic 5 (mainly due

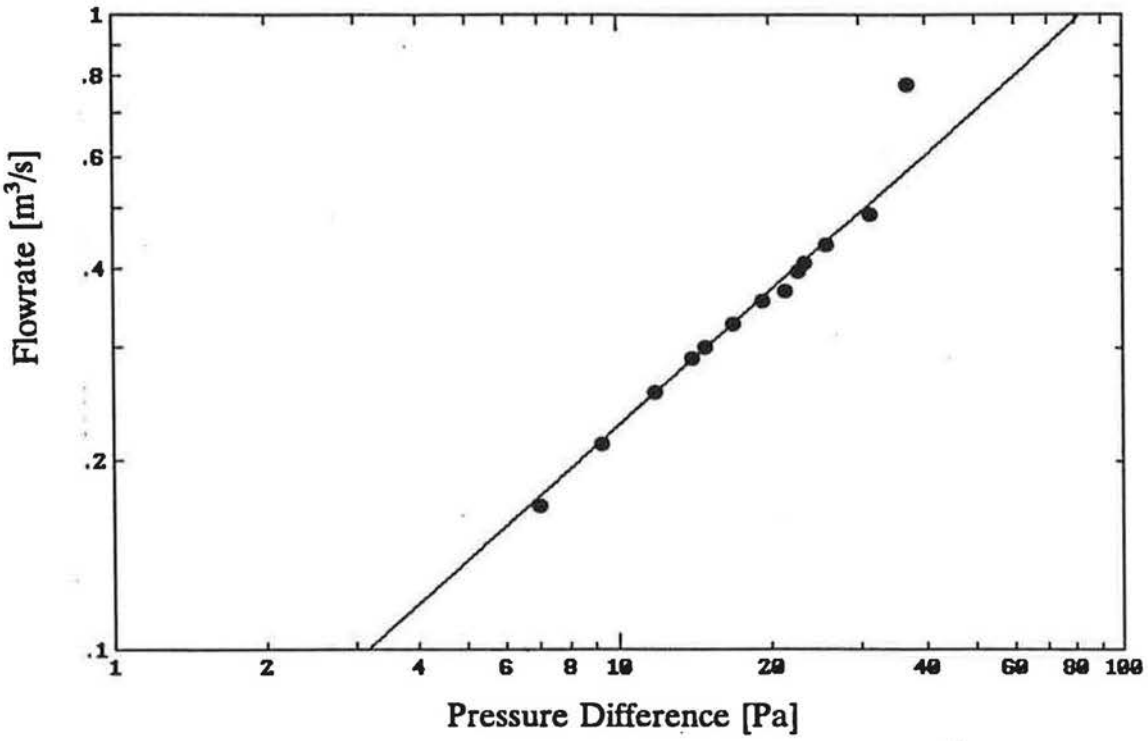

Figure 5-8A. Fan pressurization test results for attic 5.

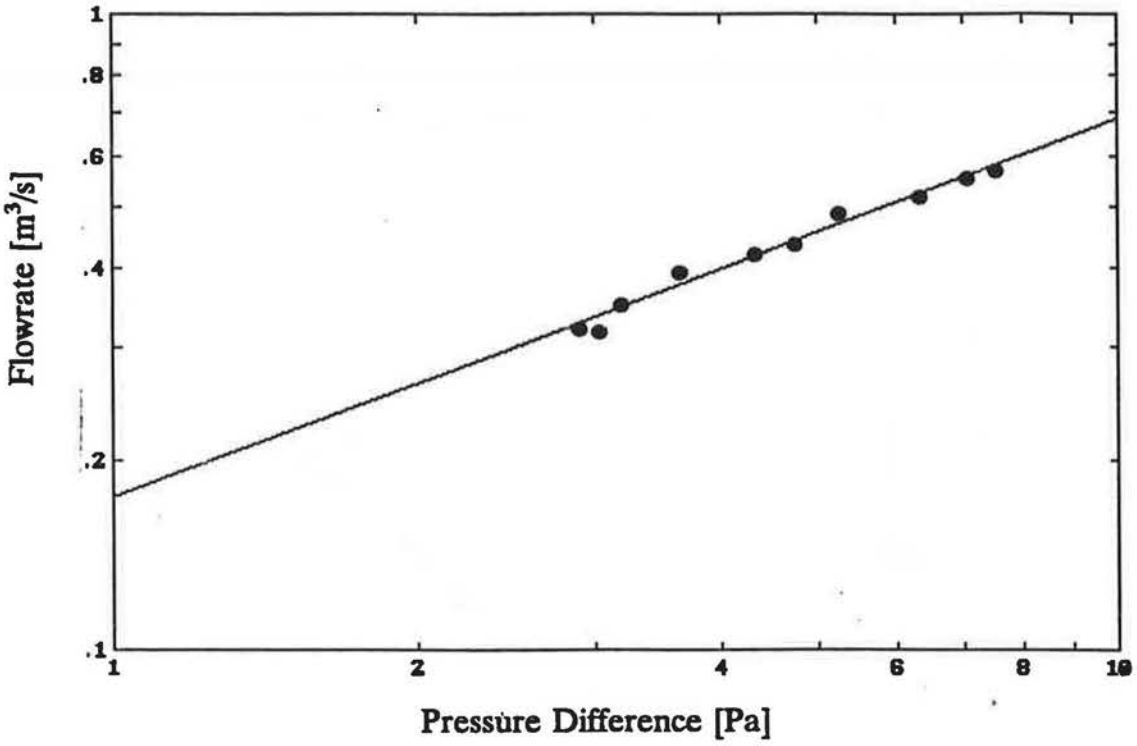

Figure 5-8B. Fan pressurization test results for attic 6.

to the soffits), the maximum pressure difference that could be reached in attic 6 was much less than in attic 5. The values of C and n found by fitting to the data (shown in Figures 5-8A and 5-8B) for the exterior portion of each attic envelope is given in Table 5-2 together with the equivalent leakage area based on a pressure difference of 4 Pa.

Table 5-2. Leakage Characteristics of Attic, House and Ceiling in Houses 5 and 6

House Zone	Flow Coefficient $m^3/sec.(Pa)^n$	Flow Exponent n	Leakage Area @ 4 Pa cm^2
Attic 5 - exterior envelope	4.416×10^{-2}	0.707	456
House 5 - ceiling uncovered	9.842×10^{-3}	0.583	85
House 5 - ceiling covered	8.446×10^{-3}	0.580	73
Attic 6 - exterior envelope	1.740×10^{-1}	0.597	1542
House 6 - ceiling uncovered	6.903×10^{-3}	0.737	74
House 6 - ceiling covered	5.730×10^{-3}	0.766	64

The results show the large difference in leakage areas of the two attics due to the extra soffit leakage in attic 6. Attic 6 has approximately four times the leakage area of attic 5. The differences in flow exponent, n, are due to the different leaks in each attic. The leakage in attic 5 is dominated by small cracks that arise from the construction of the attic envelope and flow through these cracks is probably developing flow because the cracks are short compared with their width. The value of n = 0.707 is close to values measured for the envelopes of houses. Attic 6, on the other hand, includes soffit and roof vents which behave as orifice flow (with n close to one half). The measured value of n = 0.597 for attic 6 supports this observation.

The ceiling leakage area was not included in the above set of measurements since the attic-indoor pressure difference was maintained at zero by the indoor fan. The simplest method of measuring the ceiling leakage characteristics, was to carry out a pressurization test on the interior of the house with the ceiling exposed and repeating the test with the ceiling leakage covered. For both houses 5 and 6 almost

all the ceiling leakage was concentrated in the intentional openings in the ceiling panel and the unintentional openings around the light fixtures, which made covering the ceiling leakage easy to do. In a more conventional house, there would tend to be other leakage paths (such as plumbing stacks and gaps between the flue pipe and the duct leading up to the attic) that are inaccessible and would make this method impractical. The ceiling leakage would then have to be estimated as a fraction of the total house leakage.

Fan pressurization tests on the houses were performed by an automated system that also only carried out the tests when wind speeds were below 1 m/s. A polyethylene sheet was placed over the central portion of the ceiling to seal the ceiling leakage. The sheet covered the ceiling panel and the two light fixtures and was sealed by taping along its edge. Pressurization tests were then performed over a range of pressures from 1 to 100 Pa. Depressurization tests were not performed because the plastic sheet would be blown off the ceiling even when small pressure differences are applied. The fan pressurization test system and measurement methods are described in detail by Modera and Wilson (1989). The most important features of the fan pressurization test system are as follows:

- The tests cover a large range of pressure differences from 1 to 100Pa. This more than covers the range required by ASTM (1982) and CGSB (1986) standards. Testing at windspeeds below 1m/s allows extension of the low pressure range down to 1 Pa, which is much lower than either of the above standards.
- Pressures across the envelope due to wind and stack effects are corrected by taking a reference pressure at zero flow rate for every data point. This reference pressure is the pressure measured across the envelope with the fan off and a closed damper sealing the fan duct system.
- Outdoor pressures are spatially averaged by having a pressure tap outside each of the four walls of the building.

Figures 5-9A and 5-10A show the test results with the ceiling leaks uncovered for houses 5 and 6 respectively. Figures 5-9B and 5-10B show the results of the tests with the ceiling covered for houses 5 and 6. From a least squares fit to the data (solid lines in these figures), values of C and n were obtained. From these the leakage area, A_{LA}, was calculated using Equation 5-2. The fan pressurization test results for the houses are given in Table 5-2. The fraction of leakage in the ceiling can be estimated from the difference between the house pressurization tests with the

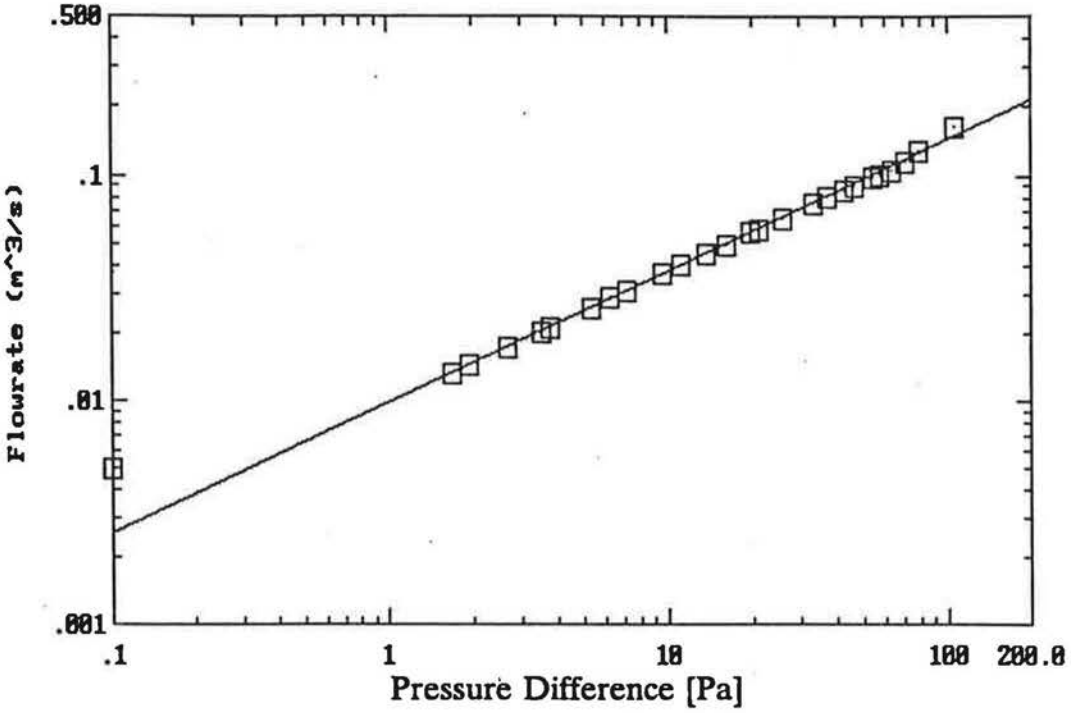

Figure 5-9A. Fan pressurization test results for house 5 with ceiling leaks uncovered.

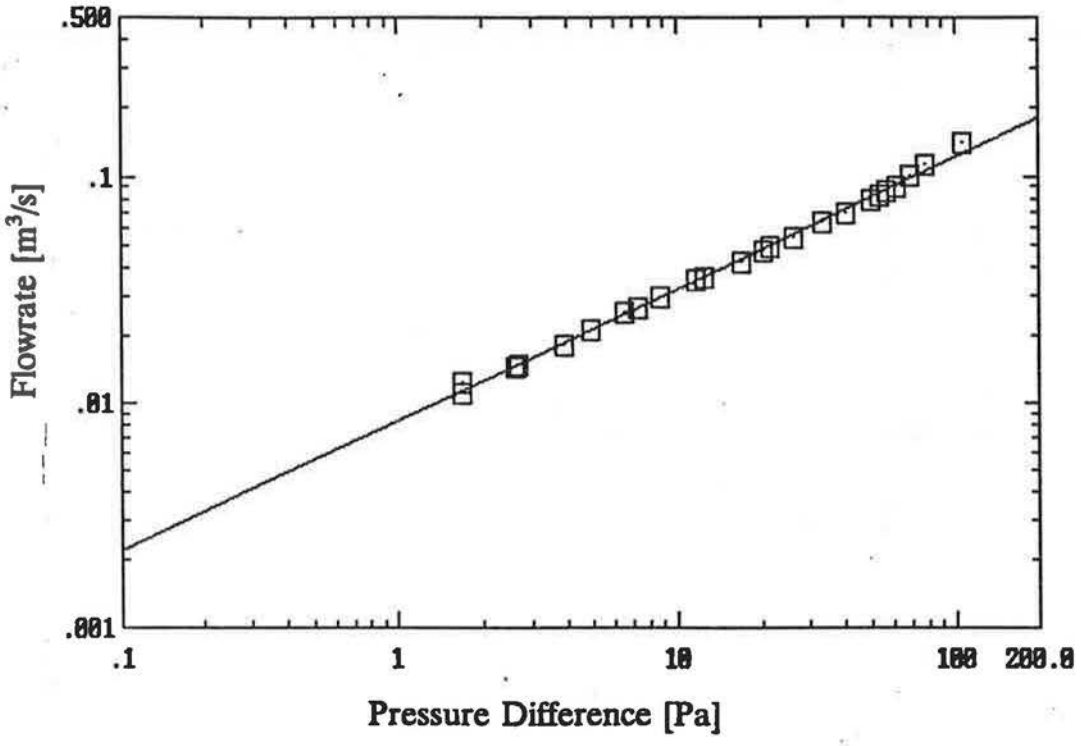

Figure 5-9B. Fan pressurization test results for house 5 with ceiling leaks sealed.

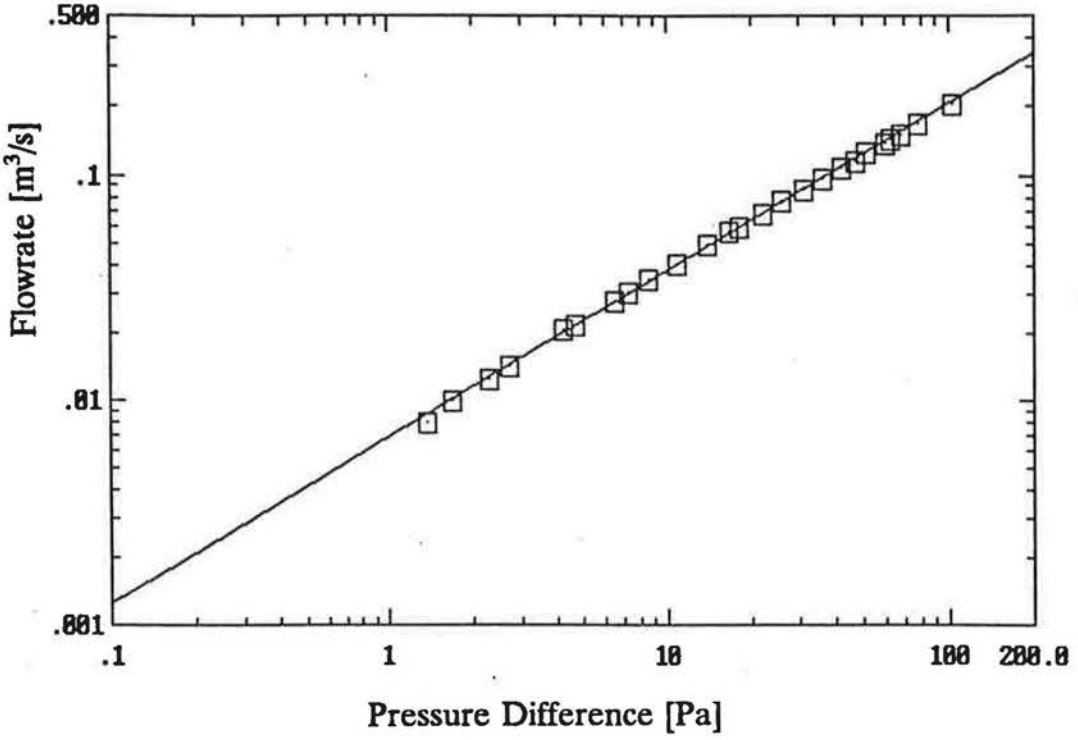

Figure 5-10A.Fan pressurization test results for house 6 with ceiling leaks uncovered.

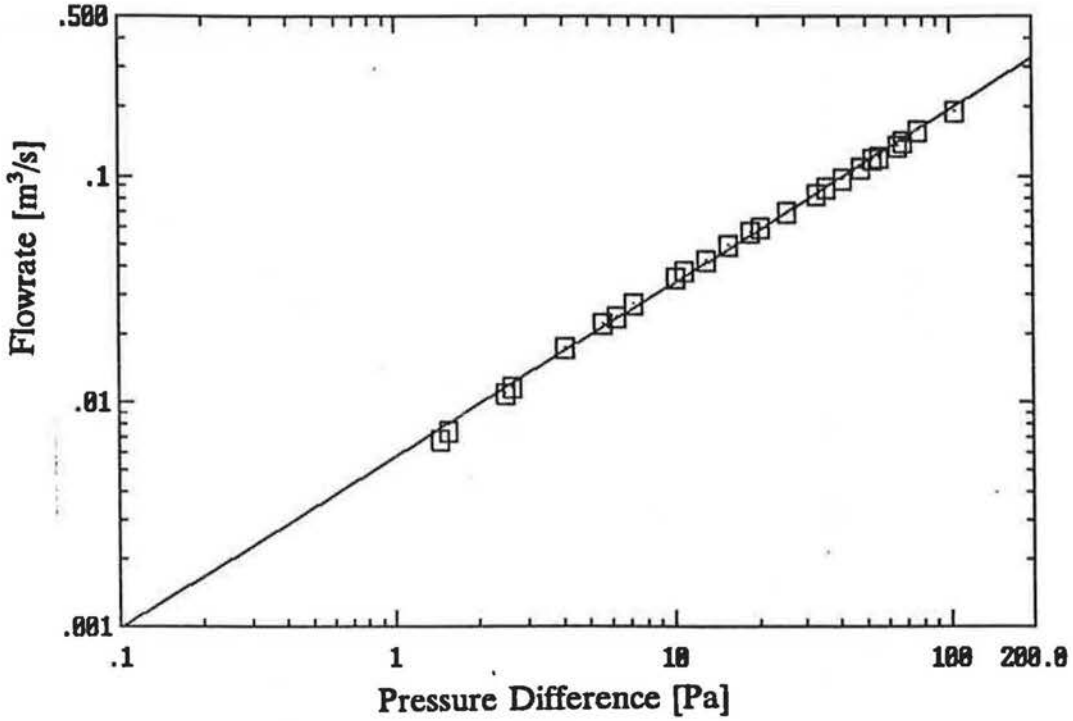

Figure 5-10A.Fan pressurization test results for House 6 with ceiling leaks uncovered.

ceiling covered and uncovered. The ceiling leakage areas (at 4 Pa) for house 5 and 6 were estimated to be 12 and 10 cm^2, respectively. These leakage areas can be compared with the area of the 7.6 diameter orifice flowmeter in the ceiling panel, which is 26.5 cm^2. This area together with the additional leakage of the light fixtures corresponds to a considerably larger gross area than the measured values. The discrepancy is due to the additional flow resistance of the 89 mm thick glass fibre batt ceiling insulation above these leaks resulting in smaller effective ceiling leakage areas. These results show that actual leakage areas are quite different from visible leakage areas and fan pressurization tests are required to accurately measure these areas.

5.2.2 Ventilation Rate Measurements

The ventilation rates of attics 5 and 6 were measured using a tracer gas injection system that measured the amount of tracer gas required to maintain a constant concentration within the attic space. The data acquisition system measured tracer gas concentrations with an infra-red gas analyzer (Wilkes MIRAN 1A) that had the capability of measuring concentration of different tracer gases by adjusting the wavelength of the infra-red radiation. This capability was necessary because two different tracer gases were used to separately measure the indoor ventilation rates (using sulphur hexaflouride SF_6) and the attic ventilation rates (using a refrigerant gas, R22). The house ventilation rates were monitored by a separate system that has been operating for the past ten years at AHHRF. In the houses computer controlled gas injections maintain the gas concentration inside the house at a nominal value of 5 ppm. Ventilation rates were calculated from the amount of gas injected into the interior space. Details of the house ventilation measurement system can be found in Wilson and Walker (1991a).

Attic ventilation rates were monitored separately from the indoor ventilation rates using R22 as the tracer gas for the attic. The R22 concentration in the attic was maintained at a nominal concentration of 5 ppm. Both attics used two small fans to mix the attic air and the tracer gas. these fans are shown in Figure 5-11. The fans provided a combined flow of approximately 10 attic air changes per hour. The mixing of the attic air is important because, as will be shown later, high attic ventilation rates above 20 ACH lead to incomplete mixing of the tracer gas that results in overprediction of attic ventilation rates. A four point sampling system and manifold was used to draw equal volumes of air from distributed locations in the attic in order to obtain a more representative average sample of the tracer gas concentration. All

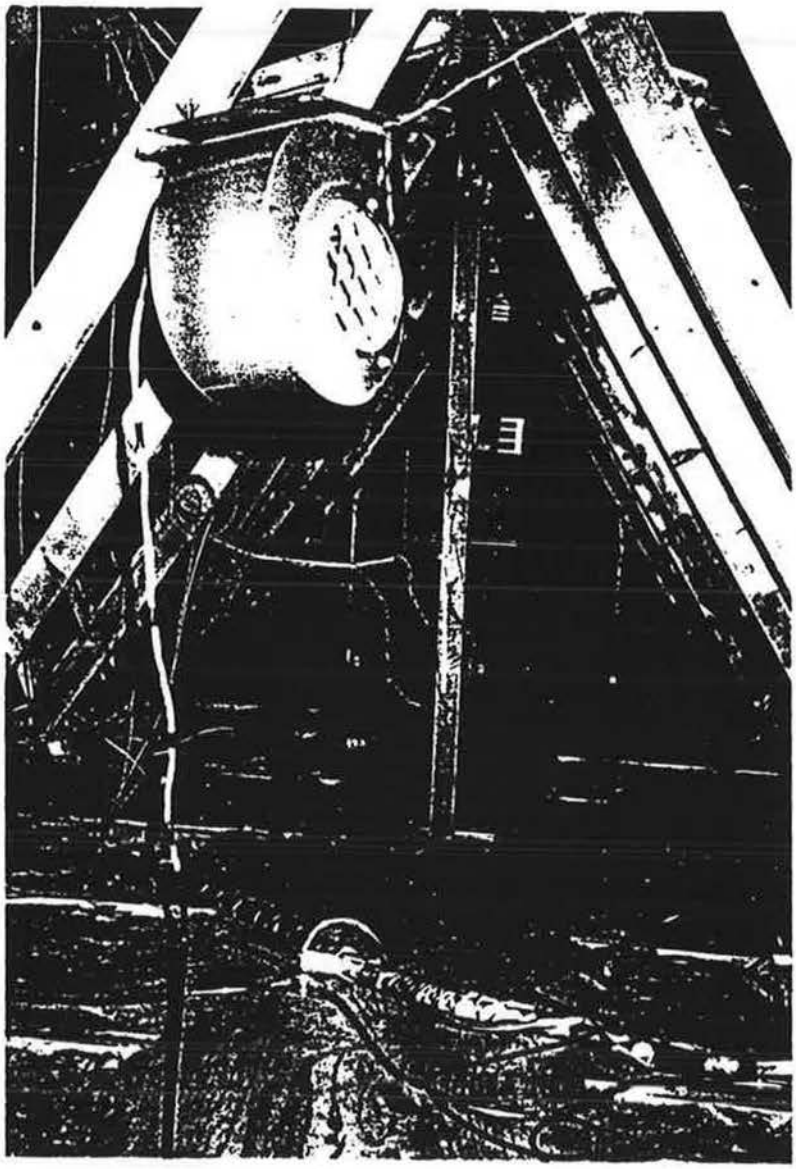

Figure 5-11. Attic interior showing mixing fans.

air samples were drawn through a heated water bath to remove the effects of the sensitivity of the gas analyzer to temperature fluctuations. The gas analyzer was used to measure the concentrations of both R22 and SF_6 in air samples drawn from both attics and both houses. By measuring concentrations of both tracer gasses, attic ventilation rates and indoor-attic exchange rates were measured. The gas analyzer was calibrated by filling it with prepared mixtures of R22 and air and SF_6 and air of varying concentrations in from 0 to 5 ppm. This calibration procedure has been repeated four times over the course of the past two heating seasons.

Tracer gas to maintain the 5 ppm nominal concentration in each attic was injected from a bottle of pure R22. Each injection was provided by pulsing a pair of closely spaced solenoid valves in series to produce puffs of tracer gas. The injector volumes, V_{inj}, for attic 5 and 6 were 5.0 and 7.4 ml of R22 gas (at room temperature and pressure) respectively. These injector volumes were calibrated by counting the number of pulses required to produce 1 litre of gas which was measured by bubbling the gas through water and collecting the gas in an inverted graduated cylinder. These injector volumes are converted to volumes at attic temperature by using the ideal gas law. The volume at attic temperature is used when calculating the attic ventilation rates (as will be shown later in Equation 5-3).

The attic system took 12 to 13 samples from each of the two attics and houses per hour. At the end of each hour, all measurements were averaged and stored by the data acquisition system. At midnight, the first 5 minutes of the hour was used to take a sample of outdoor air to provide a continuous check on the gas analyzer drift. This sample was used to monitor the drift in instrument zeros and on the presence of background contaminants (such as ammonia from fertilizers that are applied in the surrounding area during certain times of the year) that occasionally produce a false tracer gas reading.

The attic ventilation rate is calculated assuming that the tracer gas and attic air are well mixed and using the hourly mean attic and indoor temperatures. The mean attic ventilation rate for each hour is given by

$$Q_a = \frac{N\, V_{inj}}{\Omega^a_{R22}\ 3600} \frac{T_a}{T_{in}} \qquad (5\text{-}3)$$

where Q_a is the attic ventilation rate [m^3/s], N is the number of tracer gas injections during the hour [$hour^{-1}$], V_{inj} is the injector volume [m^3] and Ω^a_{R22} is the average R22 tracer gas concentration over the hour. The factor of 3600 converts the ventilation

rate to be m/^{3}s instead of m^3/hour. The ratio of the attic temperature, T_a, to the house temperature, T_{in}, corrects the injector volume from the house, where the injector solenoid pair are located, to the attic where the tracer gas is released. Neglecting the difference between house and attic pressures, which is small compared with atmospheric pressure, Equation 5-4 gives the indoor to attic exchange rate:

$$Q_c = \frac{T_{in}}{T_a} \frac{\Omega^a_{SF6}}{\Omega^{in}_{SF6}} \qquad (5\text{-}4)$$

where Q_c is the flowrate through the ceiling [m^3/s], Ω^a_{SF6}, is the hourly mean attic concentration of SF_6 [ppm] and Ω^{in}_{SF6} is the hourly mean concentration of SF_6 in the house [ppm].

The resolution of the tracer gas measuring system is due to the discrete nature of the injection system, and the resolution of the data acquisition system. For the injection system, the resolution is one injection volume which corresponds to a resolution of 0.017 and 0.025 ACH for attics 5 and 6, respectively, based on an attic volume of 61 m^3 and a nominal concentration of 5 ppm. The resolution of the data acquisition system is limited to 1 bit which corresponds to 1 mV in measuring the gas concentration. Since the voltage output of the gas analyzer at a nominal R22 concentration of 5 ppm is approximately 240 mV, the resolution of the concentration measurement (and hence, ventilation rate) is 0.4%. Thus, for each measurement of the ventilation rate, the combined error is approximately 0.6%. Other sources of error include the hourly resolution of the injection system, the quantity of R22 released per injection and the variation in mean concentration during the hour. An error analysis accounting for these factors was performed by Wilson (unpublished) for the house SF_6 tracer gas system. The same procedure has been followed in this study for the attic tracer gas system. The error analysis for the attic tracer gas ventilation monitoring system is given in detail in appendix B. An example calculation is also given in appendix B that shows that the estimated error is 6% of the measured ventilation rate.

Adequate tracer gas mixing and air sampling introduce other systematic errors. At high ventilation rates above about 20 ACH the fans in the attic can no longer mix the air completely. As shown in the results of the ventilation measurements (section 5.3.1) the samples that are taken contain air that is short circuiting the mixing fans

resulting in an artificially low mean concentration and too high a calculated ventilation rate using Equation 5-3.

5.2.3 Other measurements

Temperatures and wood moisture contents were measured at six locations in each attic. A schematic of the sensor locations is shown in Figure 5-12. Four of these measuring points were placed on the inner surface of the roof sheathing in the middle of the NE, NW, SE, and SW quadrants of the sloped roof. Two sets of thermocouples and moisture pins were placed near the large opening in the ceiling panel. One set was located on the upper end of the horizontal ceiling joist next to the opening, while the second set was placed directly above this location in the roof truss.

5.2.3.1 Wood moisture

At each measurement location a thermocouple was glued to the wood surface and wood moisture content was measured with a pair of stainless steel metal pins imbedded in the wood. The electrical resistance across the pins was measured and moisture contents inferred from the calibration of the resistance readings. The pins measured 6.4 mm in length and 3.2 mm in diameter and were spaced at a distance of 31.8 mm, centre-to-centre. The pins were inserted into pre-drilled holes so that the top of each pin was flush with the surface. The top exposed surface of each pin was sealed by applying a thin coat of epoxy glue. This was done to prevent surface condensation from creating a low resistance path between the pins and produce a false reading. In this way, each pair of pins was recording the moisture content of the underlying layer of wood. The resistances were measured with a wood moisture meter (Lignometer) which had been calibrated on small samples of roof sheathing and joist sections. These samples had been pre-soaked to known moisture contents (determined gravimetrically). In addition to the resistance measurement, the measured temperature at each location was used to correct the wood moisture content reading using the correction factors given by Pfaff and Garrahan (1986).

5.2.3.2 Temperature

Temperatures were measured using type K thermocouples. The thermocouples were epoxied to the wood surface at every wood moisture pin location. In addition the attic air, house interior air and the outside air temperature were monitored. The outside air temperature was measured inside a ventilated box on the north wall of house 6.

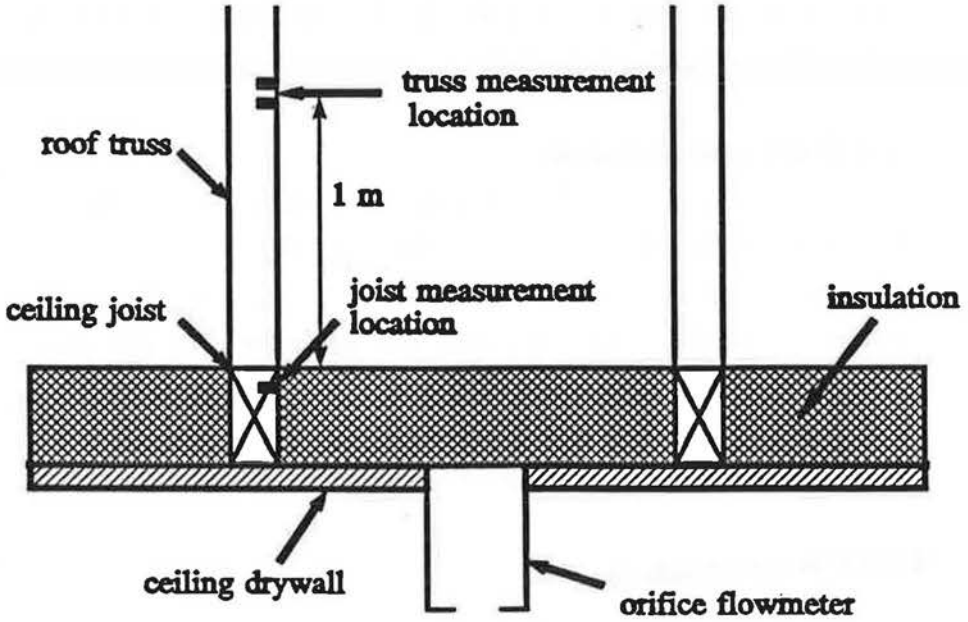

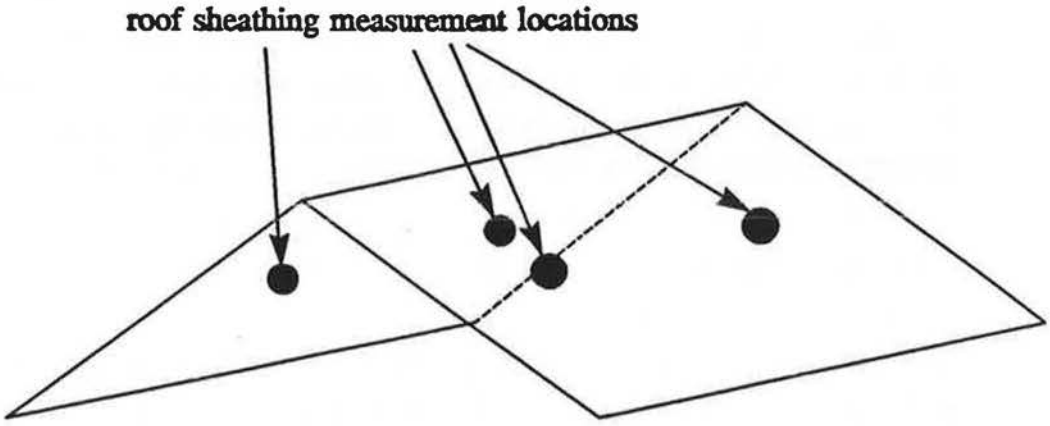

Figure 5-12. Schematic of the attic space showing locations of moisture pins.

5.2.3.3 Relative humidity

A polymer film capacitance sensor (General Eastern) was used to measure the relative humidity. Air vapour pressures were calculated based on these relative humidity measurements and the saturation pressure based on the air temperature. The relative humidity sensors were calibrated over three different saturated salt solutions which spanned a relative humidity range from 12% to 98%. The relative humidity of the air in both attics and houses was measured in addition to the outside air.

5.2.3.4 Wind speed and direction

The sensors for wind speed and direction were placed on top of a 10 m tall tower located midway along the row of houses and approximately 30 m north of the houses. Wind speed was measured with a low-friction cup anemometer which had been calibrated in a low speed wind tunnel while wind direction was measured with a rotating vane (Windflow 540 - Athabasca Research Corp.). The data acquisition system recorded the average wind speed and east and north vector components for each hour. These east and north vector components were used to calculate the true average wind direction.

5.2.3.5 Solar radiation

Incoming solar radiation on the north and south facing sections of the roof was measured with two pyranometers (Kipp and Zonen), one on each of the sloped roof sections of attic 6. One was placed on the north and the other on the south section of the pitched roof surface. The two pyranometers are oriented parallel to the roof slope so that the measured values can be entered directly to the heat transfer model without geometric conversion.

5.3 Results

Prior to presentation of a comparison of measured results and predictions (this will be done in Chapter 6), some initial results of attic ventilation rates and indoor-attic exchange rates are presented in this section in order to identify certain trends in the data.

Data binning procedure

In several of the figures presented in this chapter and the following chapter on model verification the measured and predicted data is binned so that trends may be revealed in the data that is otherwise obscured by scatter. In all cases the binning procedure is the same. For each bin the mean and standard deviation are calculated.

In the figures the measured data is represented by a square for the mean value and error bars representing ± one standard deviation. The predicted values are shown by a line connecting the mean values of each bin. The variables on both the horizontal and vertical axes are averaged so that sometimes the points representing the mean values will not appear in the centre of the bin.

5.3.1 Ventilation Rates

Attic ventilation rates were found to be dominated by wind speed, increasing as wind speed increased. Ventilation rates in attic 5 varied between 0 ACH up to approximately 7 ACH at average wind speeds of 9 m/sec, while ventilation rates in attic 6 varied from 0 ACH up to 50 ACH. With inferred ventilation rates approaching 50 ACH there may not be sufficient mixing of R22 tracer gas in the attic by the two attic fans to yield accurate values of ventilation rate. In order to investigate this effect, ventilation rates in attic 6 were plotted on a log-log scale. When the data are plotted in this way, a straight line should result i.e. there is a power law-type dependence of ventilation rate on wind speed. A power law exponent of 2n is expected because the wind driven pressure difference is proportional to wind speed squared and the flowrate is proportional to pressure difference to the power n. This assumes that leakage paths are not changed by valving action due to increased pressure differences and flowrates. If valving action increased or decreased the flow area with increasing pressure difference then the power law dependence of ventilation rate on windspeed would be obscured. In addition, a single wind direction must be chosen to reduce the effects of shelter that change wind pressures at the same wind speed. Results for attic 6 with southeast winds only (in the range of 120° to 150°) are shown in Figure 5-13 where the measured data has been binned every 1m/s and the mean value plotted with the error bars showing one standard deviation within the bin. The dashed line in Figure 5-13 simply connects the average values of ventilation rate in ascending order to compare with a straight line. The results for attic 6 generally follow a power law that is linear in this figure up to an average wind speed of approximately 6 m/sec where the mean ventilation rate is about 20 ACH. Beyond this wind speed, there is a significant deviation in ventilation rates from the power-law relation.

If the problem is one of incomplete mixing of tracer gas in the attic then more gas would be injected than is necessary to maintain a constant concentration of 5 ppm. This would yield higher inferred ventilation rates than the true values. Since

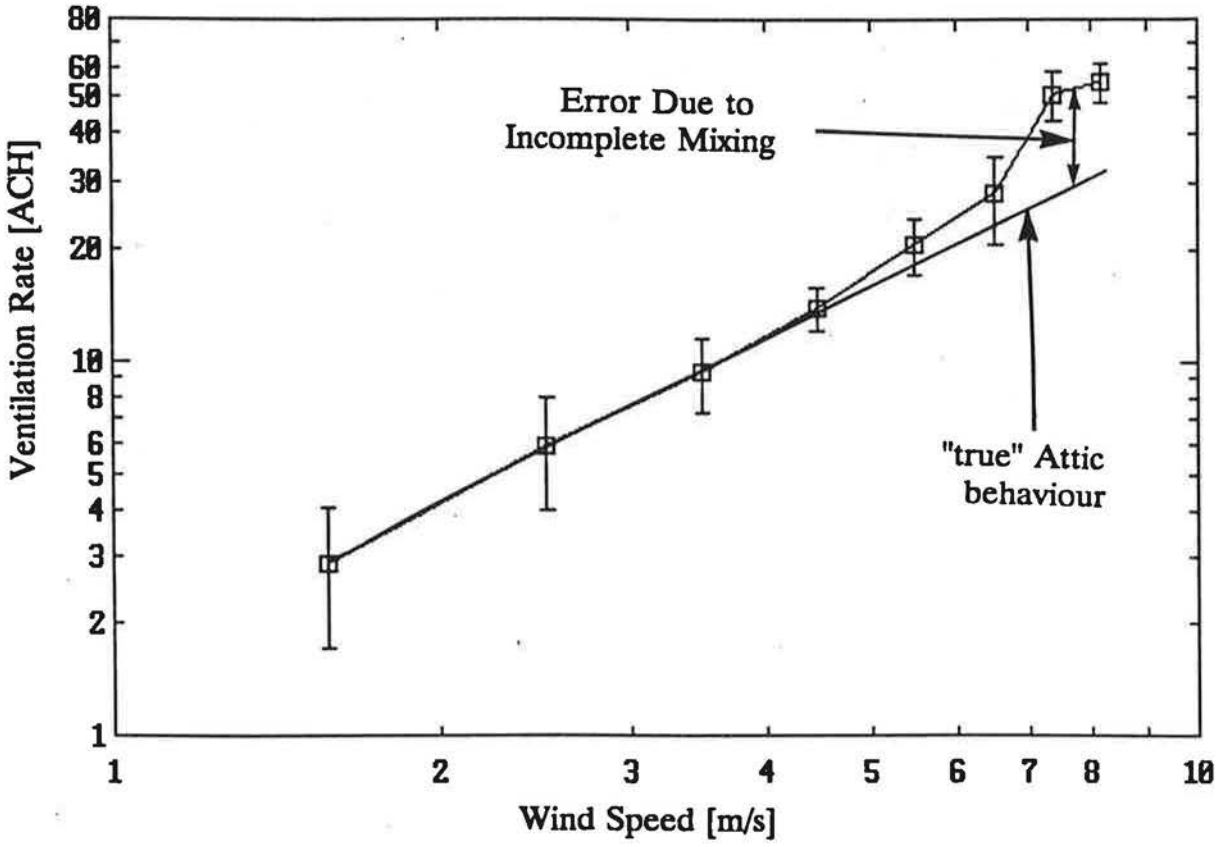

Figure 5-13. Measured ventilation rates in attic 6 as a function of windspeed for south-east winds between 120° and 150° (with 0° being north).

this is what is observed in the data and the attic leaks are not of type that would experience a valving action, the conclusion is that this must be the limit for accurately measuring ventilation rates in the attics with the current measurement technique. One possible method of increasing this limit would have been to increase the flow rate of the mixing fans in the attic. Larger fans may have created pressures on the attic interior surfaces which would affect the ventilation rate. It was decided not to alter the measurement technique but invoke a simple criterion to stop ventilation rate measurements if the wind speed was greater than 6 m/s. This corresponds to a maximum ventilation rate in attic 6 of about 20 ACH. The same criterion of a 20 ACH maximum was applied to attic 5.

The ventilation of an attic is driven by a combination of wind-induced pressures on the attic envelope and the attic stack effect that depends on the attic-outdoor temperature difference. Figures 5-14A and 5-14B show the ventilation rates in attic 5 and 6 as a function of wind speed. These figures have a large range of ventilation rates for any given wind speed because they include wind from all directions and all attic-outdoor temperature differences. For all wind speeds, the ventilation rates in attic 5 are much less than in attic 6 and reflect the difference in leakage areas. Attic 5 has approximately one quarter the leakage area of attic 6 as shown in Table 5-2. Both sets of data show a general increase in ventilation rate with wind speed although there is considerable scatter in these data. A large part of this scatter is due to the variation in wind direction which alters both the shelter and pressure coefficients on the attic envelope. Both attics are essentially unsheltered for winds from the north or south and would therefore have relatively large ventilation rates when the wind is from these directions. Strong shelter occurs for east and west winds producing lower ventilation rates. An example of this is shown in Figures 5-15A and 5-15B where attic 5 ventilation rates are shown as a function of wind speed for south and west winds, respectively. Each data set only includes wind directions $\pm 22.5°$ about the nominal direction. For west winds, the ventilation rates are about a factor of three less than for south winds showing that attic 5 is sheltered by the other houses in the east-west row.

The dependence of attic ventilation on stack effect is shown in Figures 5-16A and 5-16B for attics 5 and 6 respectively where attic ventilation rates are plotted versus the attic-outdoor temperature difference. In these two figures each point represents an hour of measured data. To show the trend in these figures more clearly the data has been binned every 5°C of attic-outdoor temperature difference. The

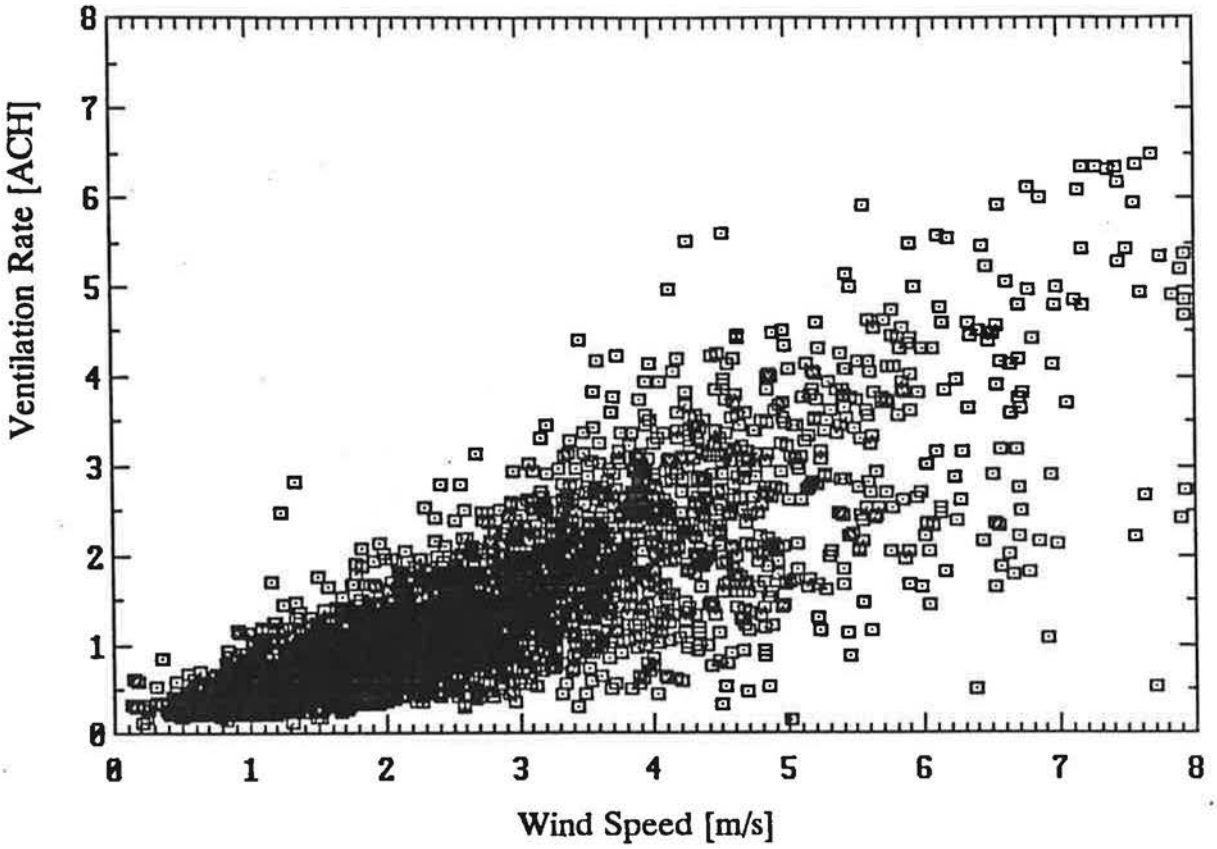

Figure 5-14A. Measured ventilation rates in attic 5 for all windspeeds and temperature differences (3758 data points).

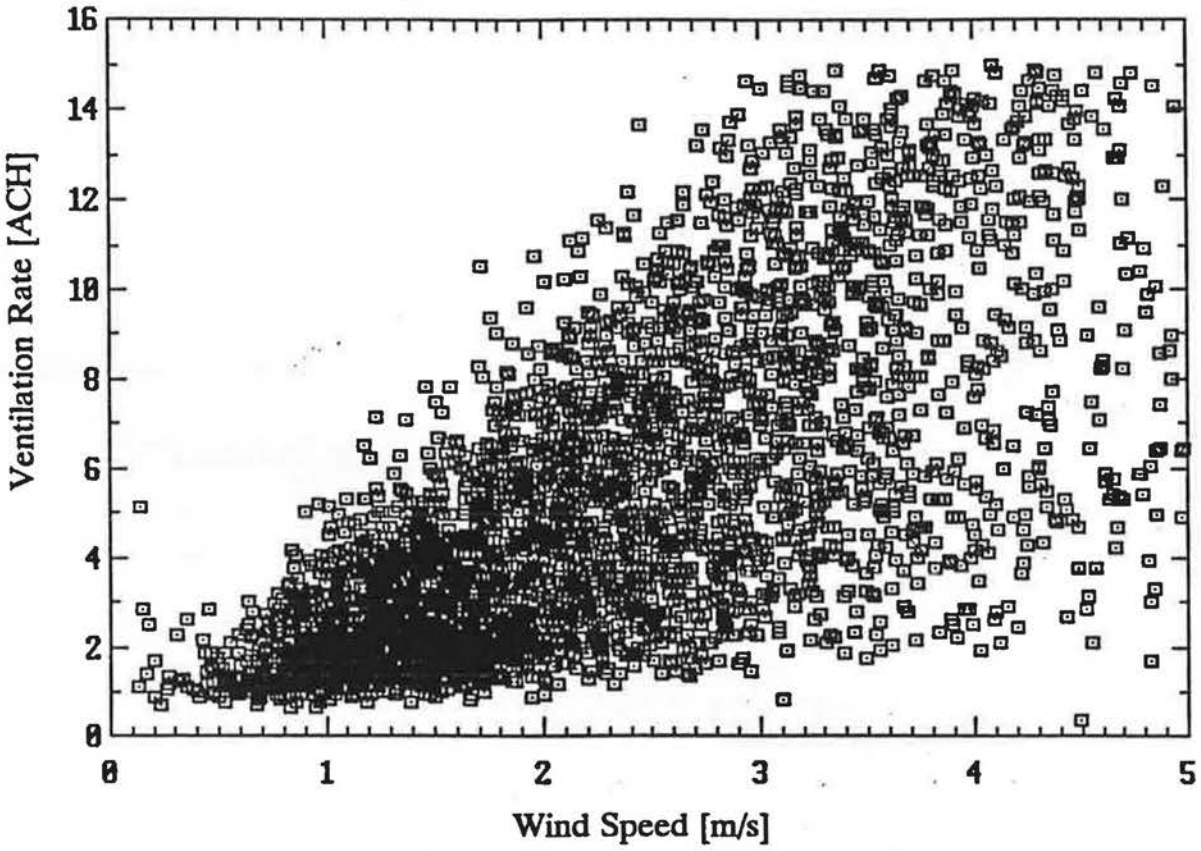

Figure 5-14B. Measured ventilation rates in attic 6 for windspeeds up to 5 m/s and all temperature differences (3522 data points).

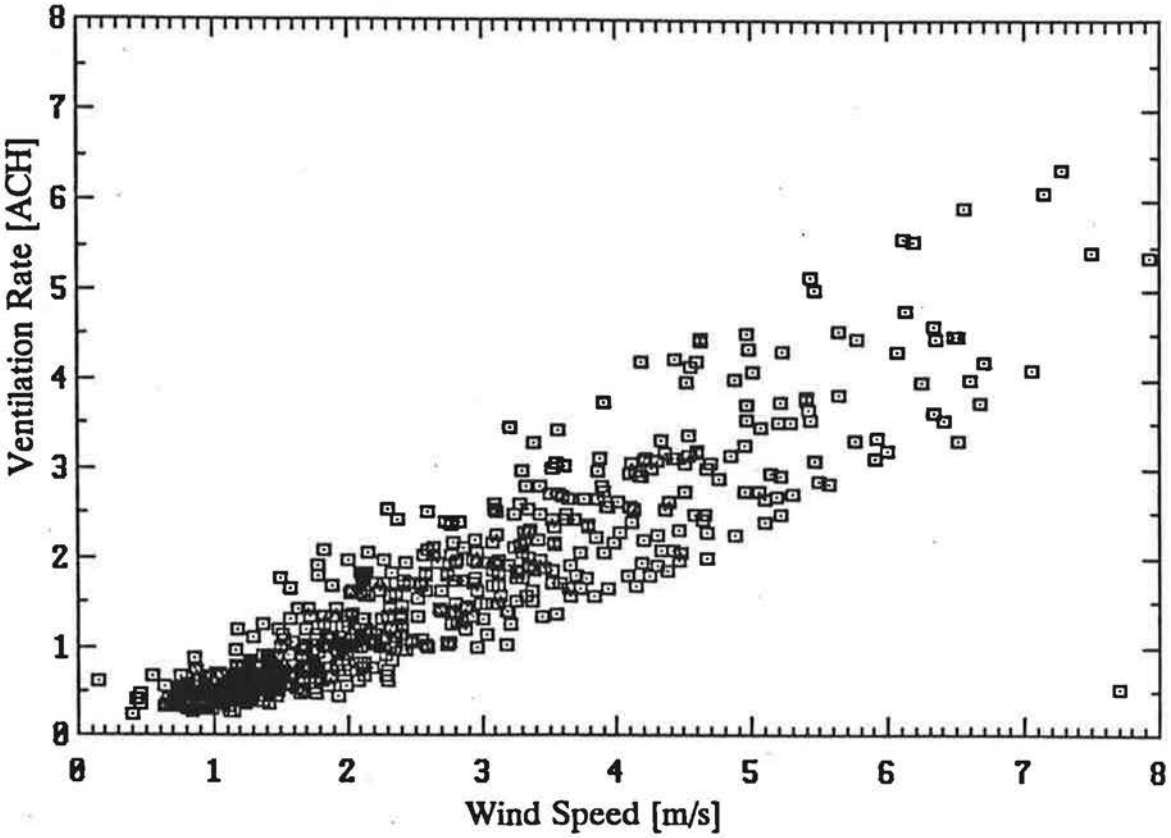

Figure 5-15A. Measured ventilation rates in attic 5 for south winds only (unsheltered) (641 data points).

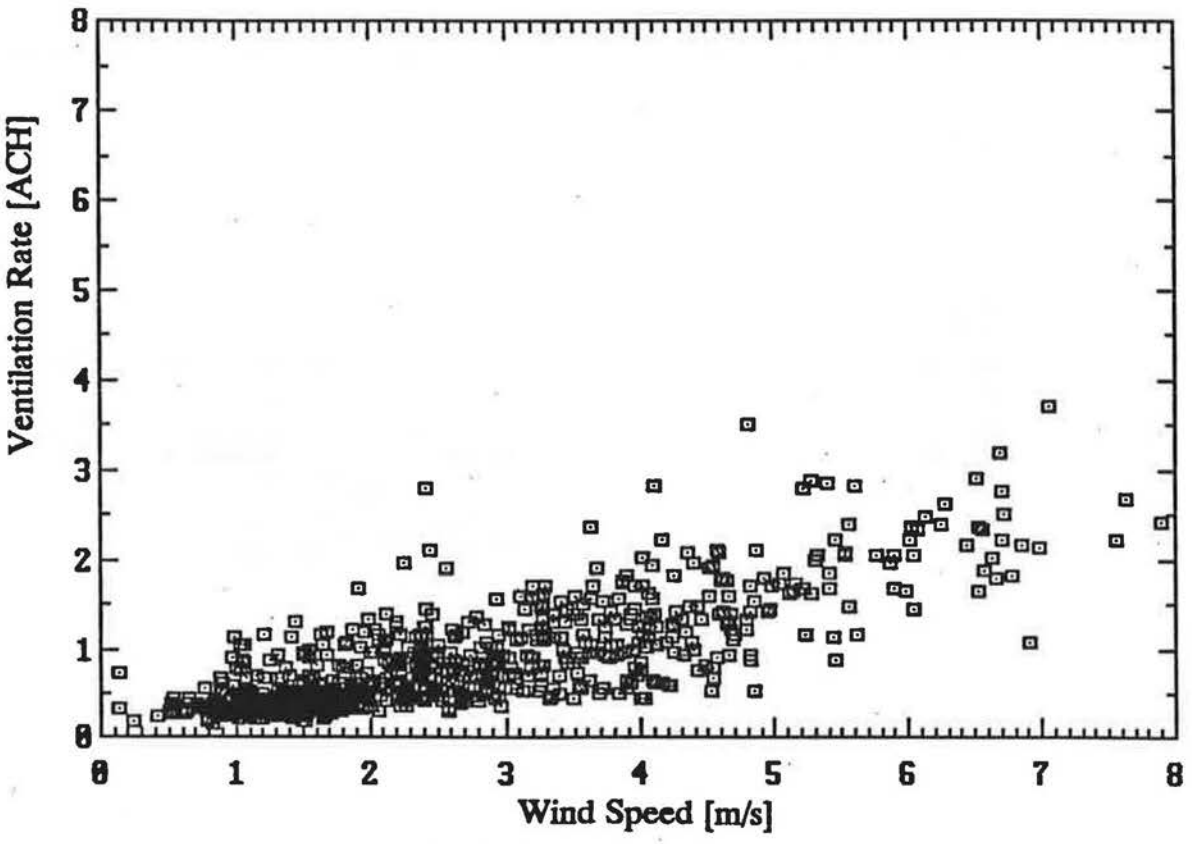

Figure 5-15B. Measured ventilation rates in attic 5 for west winds only (sheltered) (784 data points).

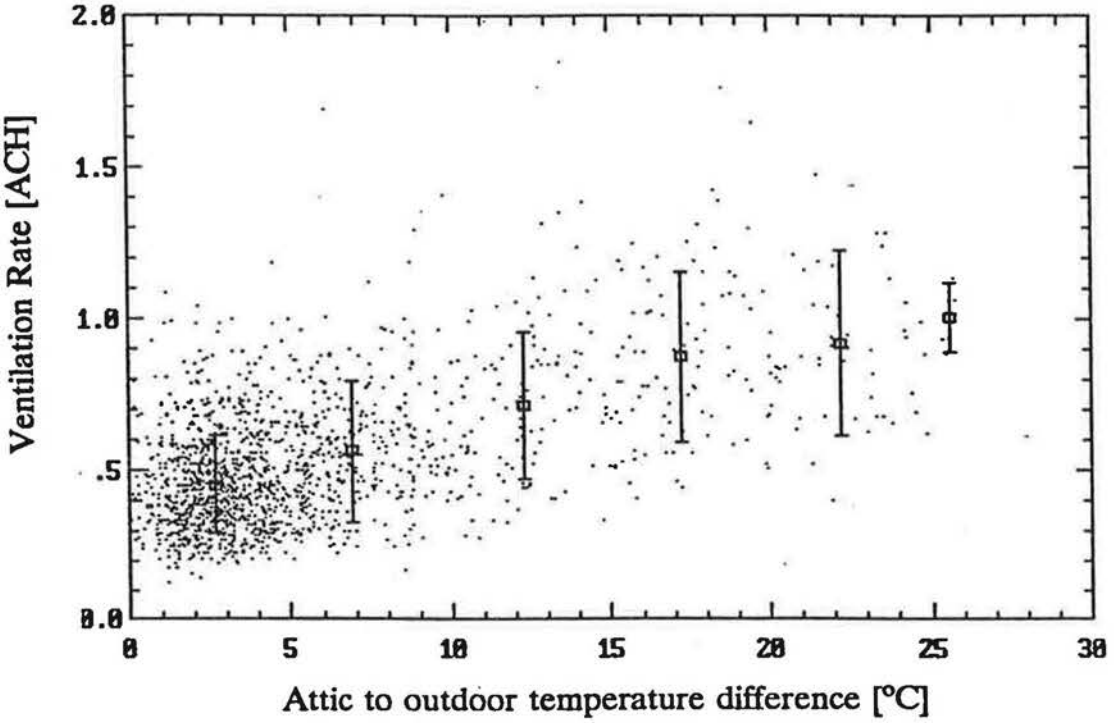

Figure 5-16A. Temperature dependence of measured ventilation rates in attic 5 for windspeeds less than 2m/s (1573 points).

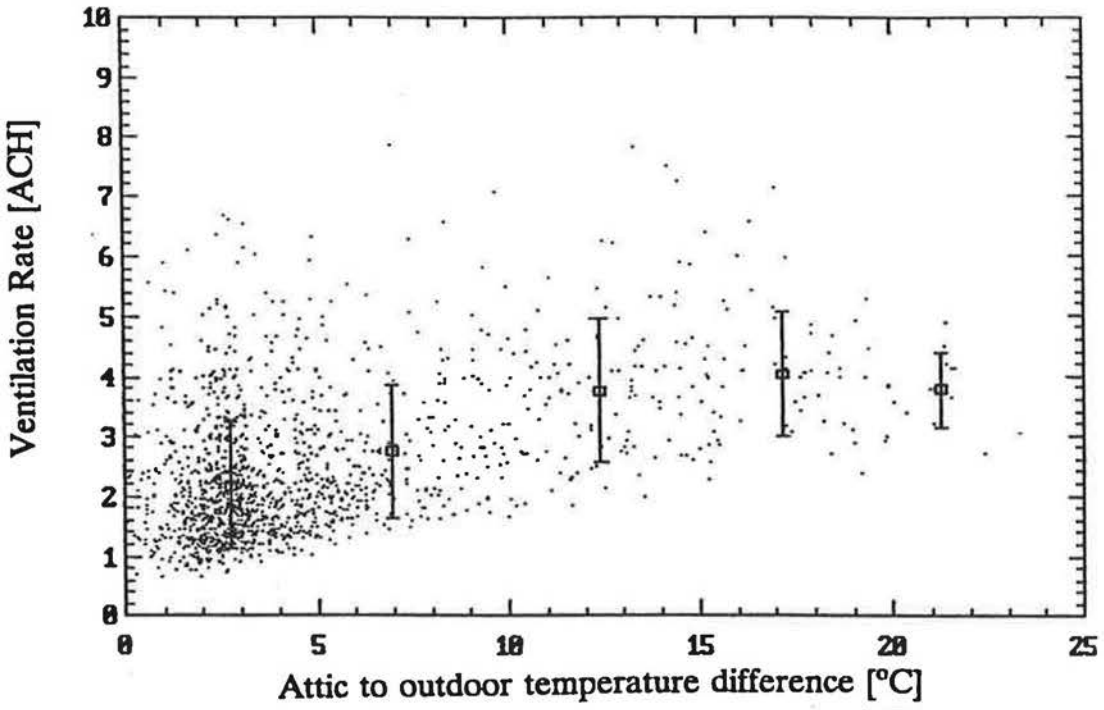

Figure 5-16B. Temperature dependence of measured ventilation rates in attic 6 for windspeeds less than 2m/s (1444 points).

mean is shown by the squares and the error bars represent the standard deviation in each bin. These data have been selected from the time period between December 1, 1990 and October 31, 1991 and include only those hourly-averaged ventilation rates when the wind speed was below 2 m/sec. Although the data show considerable scatter, there is a weak dependence of ventilation rate on attic-outdoor temperature difference with stack effect driven ventilation rates reaching approximately 1 ACH in attic 5 and 4 ACH in attic 6. Comparing Figure 5-14 to 5-16 for both attics indicates that stack effect driven ventilation is much less than ventilation generated by wind-induced pressure on the attic envelope.

One of the observations from the data presented in Figure 5-14 is that to see the expected increase in ventilation rate with increasing wind speed, a large number of measurements need to be taken. Figure 5-14A for attic 5 contains 3758 hourly averaged data points and Figure 5-15A contains 3522 data points. Data sets that contain a limited number of measurements could display any type of variation with wind speed, increasing, decreasing, or constant. To uncover true trends in the data a large number of measurements are therefore required. For this study over 5000 hours of attic ventilation data have been accumulated. With a large data set it becomes possible to sort for low windspeeds in order to examine the stack driven ventilation for the attic shown in Figure 5-16.

The effect of wind direction on ventilation rates was partially illustrated in Figure 5-15 for attic 5, where data was selected for sheltered and unsheltered wind directions. To better observe the effect of wind direction on ventilation rates, the data has been plotted as a function of wind angle (0° being north and positive angles measured in a clockwise sense). The measured results for attics 5 and 6 are presented in Figures 5-17 and 5-18, respectively. In each figure the upper plots show individual data points, while the lower plot shows the average and standard deviation of the measurements when data was sorted into 22.5° wind angle bins. This helps to accentuate the dependence of ventilation rates on wind direction and remove some of the scatter that can make the data difficult to interpret. To further reduce the considerable scatter that is evident in the figures, the data is normalized to factor out the variation of ventilation rate with wind speed for a given direction.

The range of ventilation rates at a given wind direction is mostly caused by the range of wind speeds. To remove the wind speed dependence each ventilation rate measurement is divided by windspeed to the power 2n because (as discussed earlier) ventilation rate is proportional to wind speed to the power 2n. This is done for each

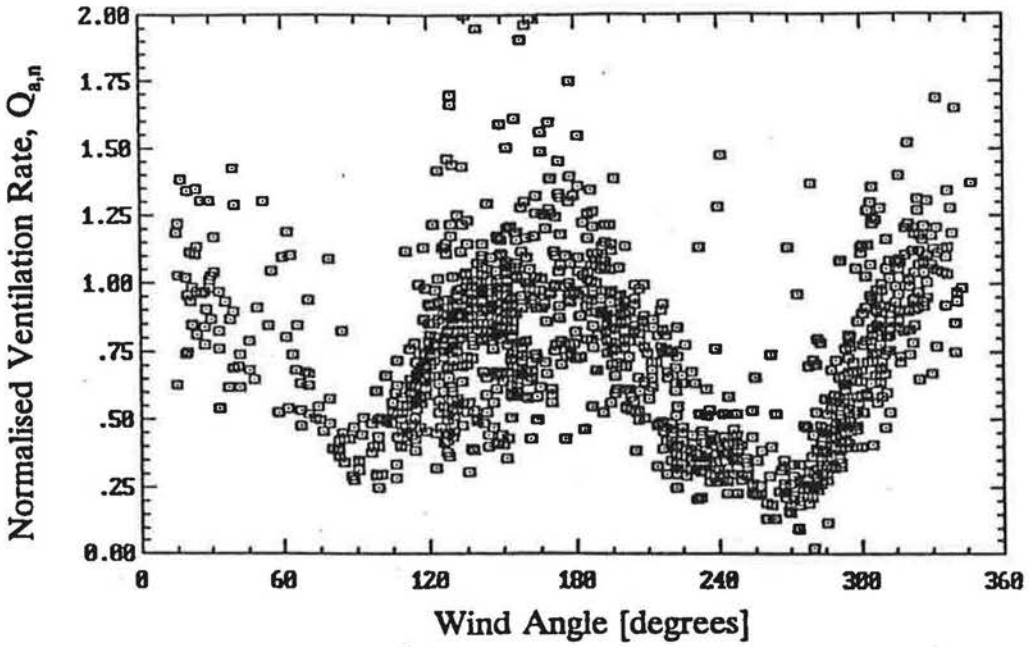

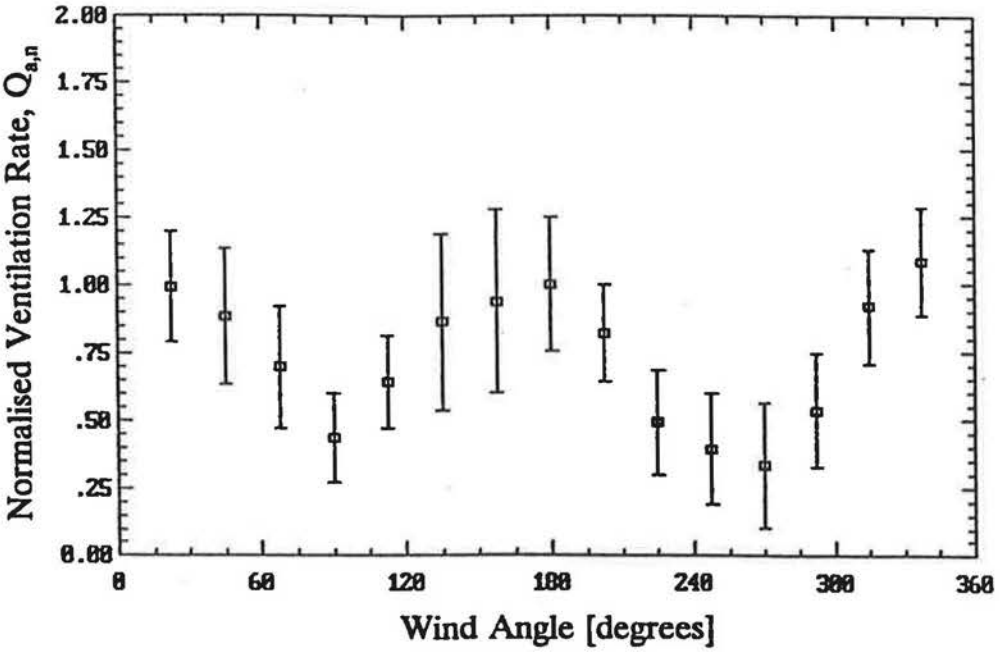

Figure 5-17. Effect of wind direction (wind shelter and pressure coefficients) on ventilation rate for attic 5 (1302 points).

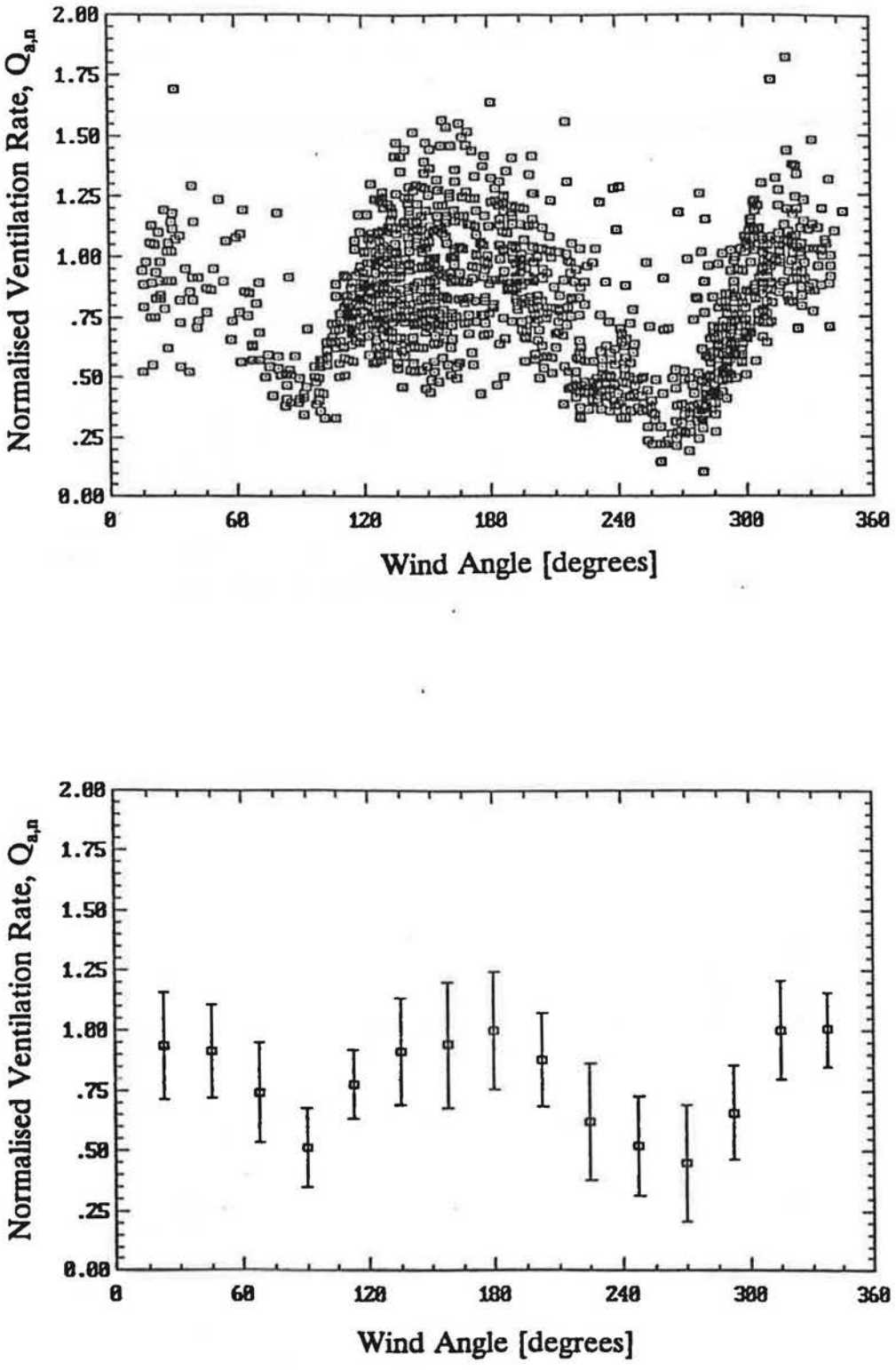

Figure 5-18. Effect of wind direction (wind shelter and pressure coefficients) on ventilation rate for attic 6 (1302 points).

individual data point, not the binned averages. These wind speed normalized ventilation rates are then divided by the mean wind speed normalised ventilation rate from the bin for south winds (180°). So the ventilation rate normalised for both wind speed and wind shelter effects, $Q_{a,n}$, (shown in Figures 5-17 and 5-18) is given by

$$Q_{a,n} = \frac{Q_a}{U^{2n}} \frac{1}{Q_{180}} \qquad (5\text{-}5)$$

where Q_{180} is the mean wind speed normalised ventilation rate for south winds. The southerly direction (180 degrees) was chosen because this direction contained a large amount of data and the houses experienced the least wind shelter.

Both data sets for attics 5 and 6 show a reduction in ventilation rate of approximately 50% for easterly winds (90°) and 70% for westerly winds (270°). The reduction in ventilation rates for westerly winds was slightly larger than for easterly winds and this small asymmetry is due to the air flow pattern over the houses which affects the surface pressure coefficients. For westerly winds, both attics 5 and 6 are sheltered by four identical houses. For easterly winds, attic 5 is sheltered by house 6 and attic 6 is only partly sheltered by the windbreak shown in Figure 5-1. The exact nature of the differing flow patterns and their effect on pressure coefficients would require detailed experimentation in a wind tunnel (or perhaps numerical simulation) and is beyond the scope of this study. Figures 5-17 and 5-18 show that the neighbouring houses provide a large amount of shelter for attics 5 and 6 that reduces ventilation rates by about a factor of three.

5.3.2 Attic fan ventilation

During the second year of testing, a ventilating fan was installed in attic 6 and tests were carried out for two modes of operation. The fan was operated depressurizing the attic (standard installation procedure) and then pressurizing the attic. As mentioned previously in section 5.1, the fan provided a maximum flow rate of 9.6 ACH and was cycled on between 10:00 am and 4:00 pm and off for the remaining portion of the day. The effect this has on ventilation rates in attic 6 can be seen in Figure 5-19A which covers a three day period from November 20 to 22, 1991. This period was selected because the ventilation rates for the first two days were relatively constant, while ventilation rates increased significantly on the third day due to increased wind speeds. For comparison purposes, the ventilation rates in attic

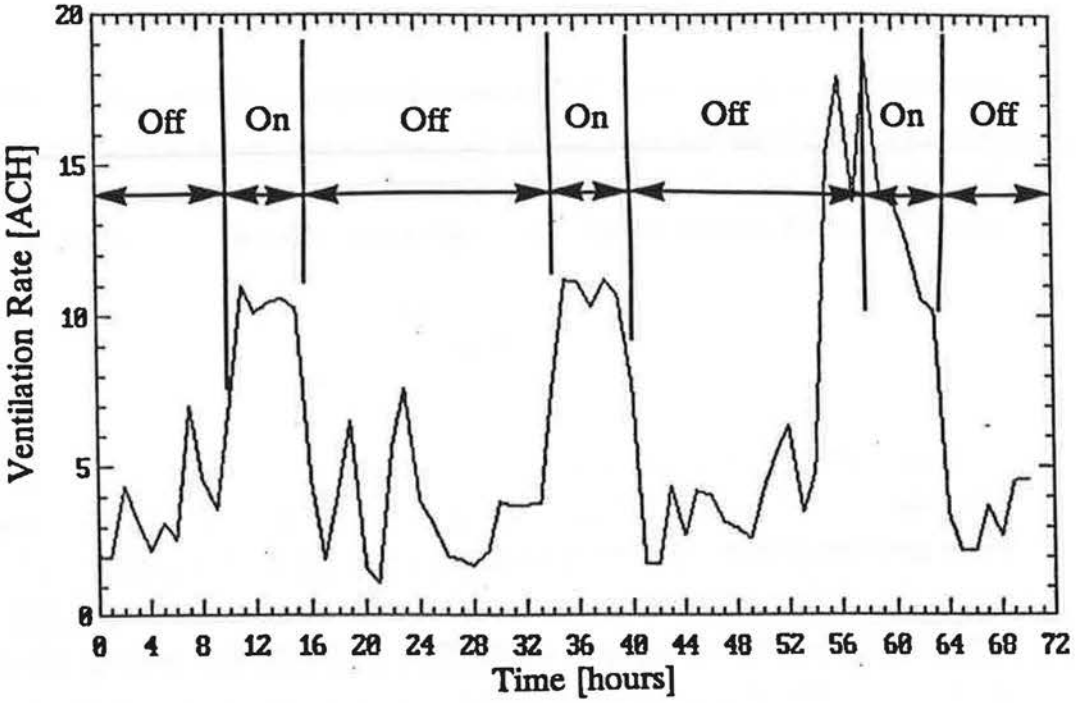

Figure 5-19A. Effect of ventilation fan on attic 6 ventilation rates.

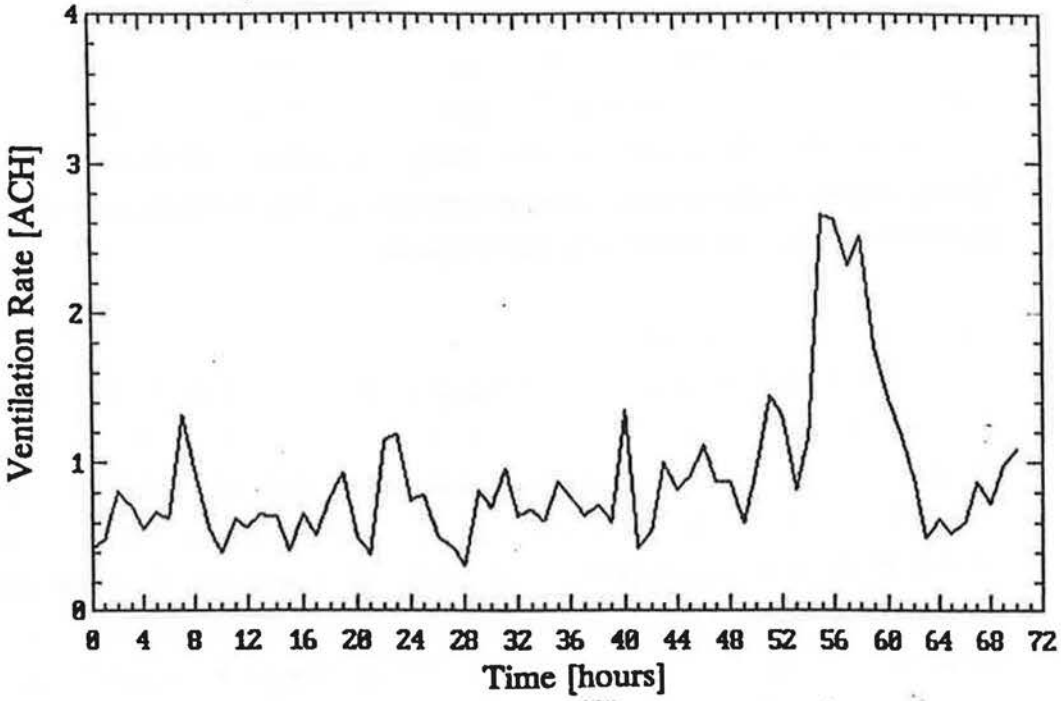

Figure 5-19B. Ventilation rates in attic 5 for the same time as Figure 5-19A, showing the increase in ventilation rates for the third day caused by increased wind speed.

5 over the same period are shown in Figure 5-19B and indicate relatively calm conditions the first two days with low ventilation rates and increased ventilation on the third day. When ventilation rates are low, the attic fan creates pressure differences across the attic envelope that are much larger than wind or stack effect pressure differences and for these situations attic ventilation rates are dominated by the fan. Over the first two days, the ventilation rates with the fan on averaged approximately 11 ACH and with the fan off, approximately 4 ACH. The fan contribution was therefore about 7 ACH, which is close to the maximum capacity of the fan. On the third day, the wind speed increased during the day resulting in an increase in the background ventilation rate to approximately 13 ACH while the measured rate was approximately 16 ACH. In this case, the fan did not increase the ventilation rate to the same extent as on the previous days because the wind-induced pressures on the attic envelope were relatively large.

5.3.3 Indoor to attic exchange rates through the ceiling

One of the important measurements obtained during the field monitoring program was the magnitude of the indoor-attic exchange rate and its dependence on outdoor weather conditions. Moisture is transported into the cool attic space when there is a sustained exchange of air from indoors to the attic and the interior heated space has a large relative humidity. During cold weather this moisture may deposit as frost which steadily accumulates. A sudden thaw will melt the frost with resultant water damage to the ceiling and an increase in sheathing and joist wood moisture content. Despite its importance, there are very few field measurements of the magnitude of this flow or its dependence on ambient weather conditions.

Measured indoor-attic exchange rates (expressed as ACH based on the attic volume) in attics 5 and 6 are shown in Figures 5-20A and 5-20B, respectively and are correlated with the indoor-outdoor temperature difference. As with previous temperature driven ventilation rate figures, the measurements have been selected for wind speeds less than 2 m/s to reduce the scatter. The individual hourly averages are shown as dots together with the average and standard deviation in each 5 °C wide bin. During extremely cold weather, there is a large sustained pressure difference across the ceiling due to the stack effect which results in exchange rates, on the order of 0.2 to 0.25 ACH (12 to 15 m^3/hr). This is approximately 60% of the total house ventilation rate (at the low ventilation rates induced by stack flow only). For stack dominated ventilation rate in the attics the ceiling flow rate represents about 10% of

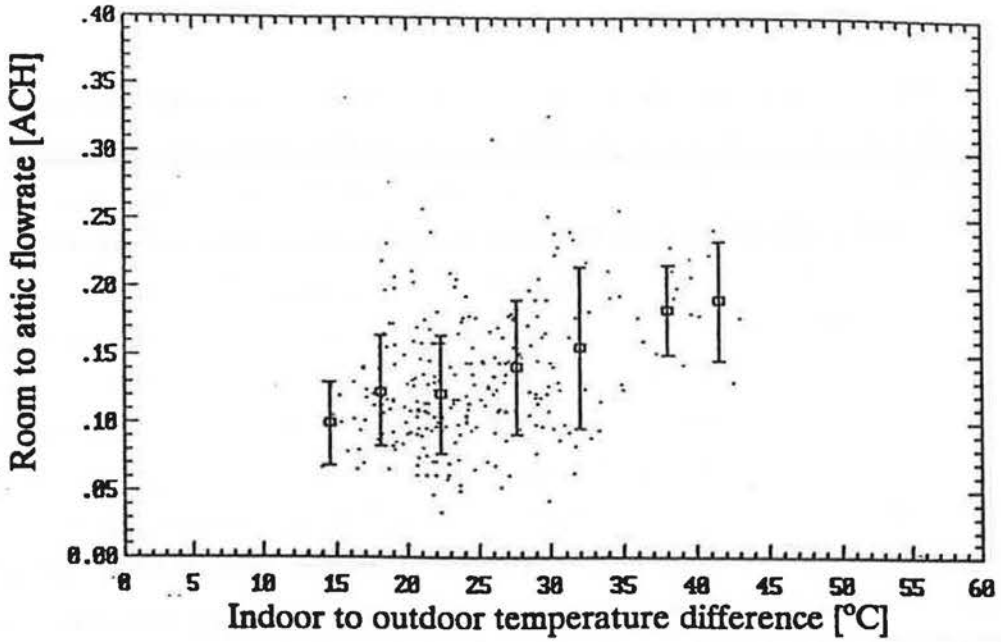

Figure 5-20A. Indoor-outdoor temperature difference effect on measured indoor to attic exchange rates for attic 5 for windspeeds less than 2m/s.

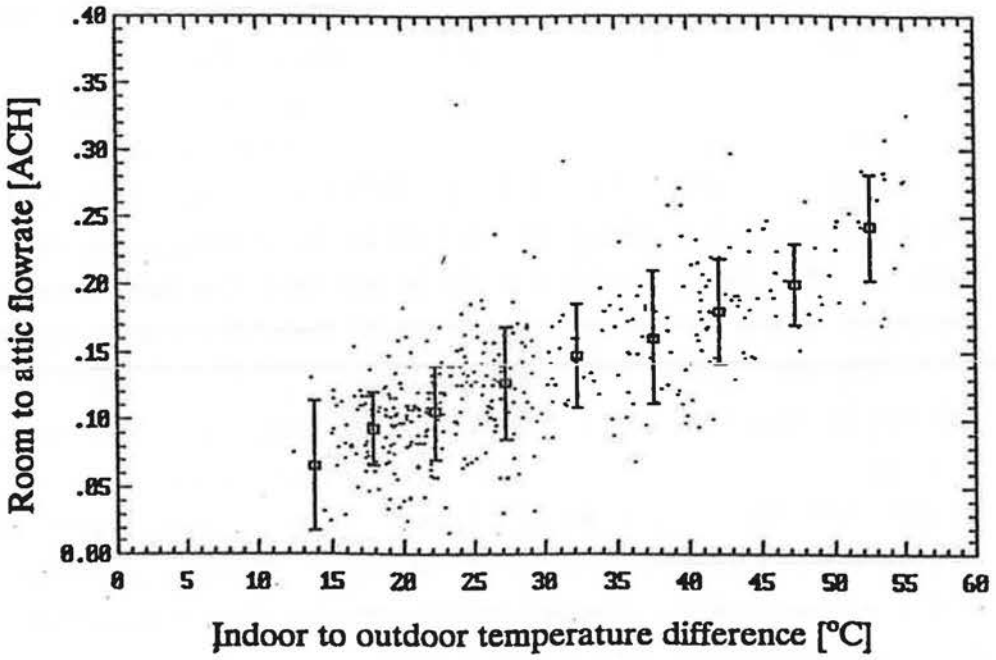

Figure 5-20B. Indoor-outdoor temperature difference effect on measured indoor to attic exchange rates for attic 6 for windspeeds less than 2m/s.

the total for attic 5 and only 2% for attic 6. When the wind speed is greater than 2 m/s the attic ventilation rates increase and the ceiling flow rate becomes difficult to measure because the attic concentration of SF_6 is too low. The ceiling flow rate is not a large fraction of the attic ventilation rate and results in the two zones for the ventilation model being only weakly coupled.

At the house interior conditions of 20°C and relative humidity of 40%, this maximum leakage flow will convect on the order of 100 grams of water per hour. The magnitude of the ceiling flow rates depends on the total ceiling leakage area and therefore these measured values are characteristic of test houses 5 and 6 at AHHRF. The indoor-attic exchange rates may also be correlated with wind speed. To look for this effect a typical set of measurements is shown in Figure 5-21 for attic 5 exposed to winds from the south (180°±45°). A relatively large wind angle bin was selected to provide enough data points. The data suggests that there is no obvious correlation of exchange rates with wind speed. The large scatter in the data probably obscures any correlation that may exist.

In a previous study by Cleary (1985), the room to attic exchange rates were measured on a single occasion. Cleary measured an exchange rate through the ceiling that was 25% of the total house ventilation rate and 3% of the total attic ventilation rate. Cleary's measurement shows that measured ventilation rates in other attics are similar to those found in this study.

5.3.4 Attic air and wood temperatures

The measured attic temperatures exhibit a strong diurnal cycle due to daytime solar gains and night time radiative losses. Figure 5-22 shows a spring day, where hour 1 is midnight, for attic 5. The south facing sheathing is heated the most and is more than 30°C higher than the outdoor temperature at its peak value at 2 p.m. (hour 15) in the afternoon. The truss and attic air temperatures are less than the sheathing temperature because they are not directly exposed to the radiative gains. The peak values do not occur at the same time due to the thermal masses involved and the attic air and the trusses lag behind the sheathing by approximately two hours. In addition, after the sun has set at about 7 p.m. (hour 19) the low thermal mass of the sheathing and its exposure to the cold sky temperature means that it cools faster than the attic air and the trusses. This is important because it implies that a steady state model of heat transfer that does not account for the thermal masses will not predict the correct magnitude or time variation of attic temperatures.

The night time cooling of attic sheathing due to radiation to the sky is

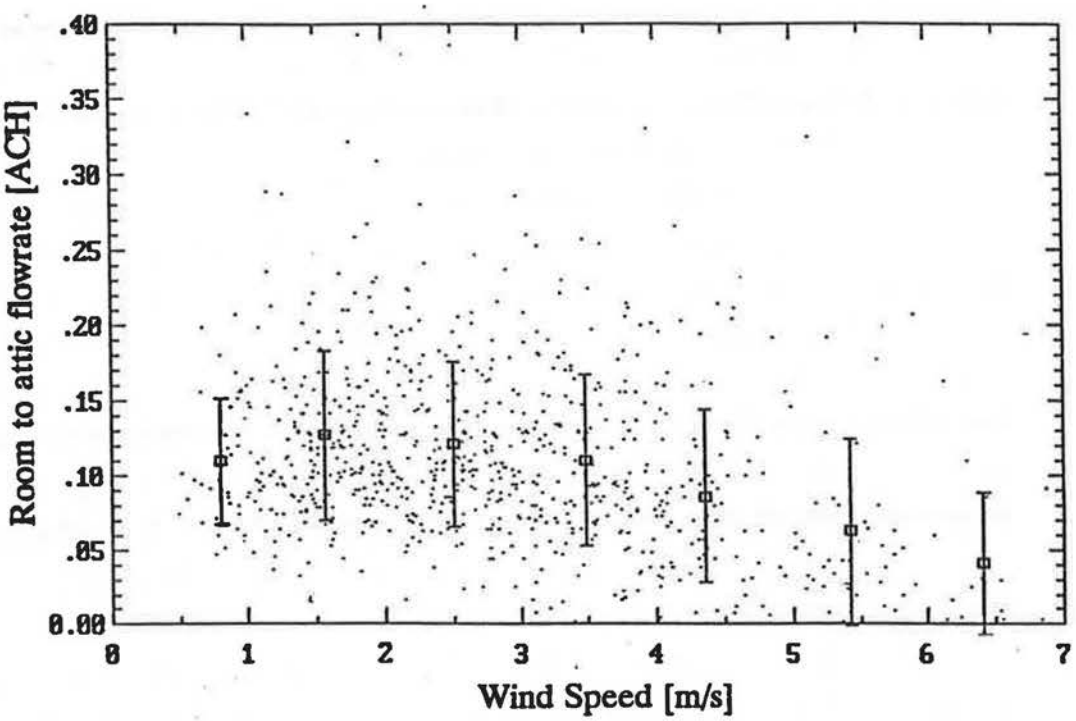

Figure 5-21. Effect of winsdpeed indoor to attic exchange rates for attic 5 for south winds (180°±45°).

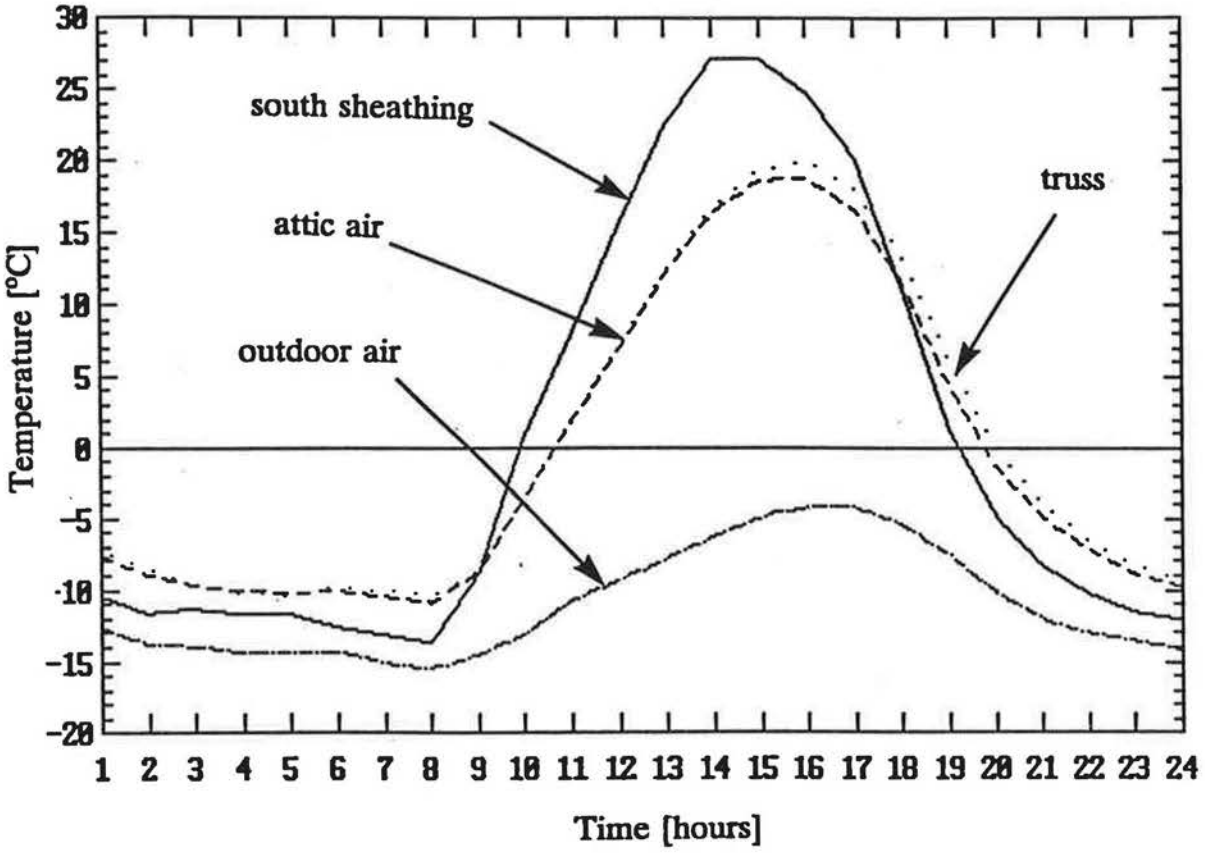

Figure 5-22. Diurnal variation of temperatures in attic 5 for March 12th 1991.

illustrated further in Figure 5-23 on a spring day for attic 6, where hour 1 is noon. The outer sheathing temperature drops 3 to 4 degrees below the ambient temperature and 4 to 5 degrees below the attic air. The inner sheathing shows less temperature depression of about 2 degrees below the attic air but is still the coldest attic surface. This is important for night time moisture deposition on the sheathing surfaces.

5.3.5 Wood moisture content

Typical results for wood moisture content are shown in Figure 5-24 for a heating season (5 months). The results shown in Figure 5-24 are for the north and south sheathing in attic 5. At the low values (below 7%) of wood moisture content shown in Figure 5-24, the wood moisture meter is at its operating limit and therefore all that can be realistically inferred about the measured values is that they are at or below about 7%. Because of the uncertainty in these low values of wood moisture content the small rise and fall of about 2% over the heating season does not imply any seasonal moisture storage in the sheathing. These low values are because the measuring pins for measuring wood moisture content are sealed below the surface and do not see the larger changes in moisture content at the wood surface. These measurements are useful for verification of the model predictions of the inner wood moisture contents as they should indicate that the wood remains dry as shown by this data. These measured values do not give any information about the moisture content of the surface layer. Therefore, it will not be possible to verify model predictions for the surface layer, except to see if moisture is condensed as frost (as was occasionally observed by visual inspection of the attics during winter months).

5.4 Summary of measurement program

The measurement program for this study was undertaken in order to find the range of factors influencing moisture transport in attics and to provide data for verification of the ventilation, heat transfer and moisture transport models developed in the preceding chapters. The measurements were hourly averages made in two attics at the Alberta Home Heating Research Facility. Attic ventilation rates were measured using a constant concentration tracer gas system. House to attic exchange rates were measured by the same system using two different tracer gasses for the house and the attic (SF_6 and R22 respectively). Temperatures were measured in both houses and attics using thermocouples. Relative humidity sensors monitored the moisture content of the air inside the houses and attics and outdoors. Wood

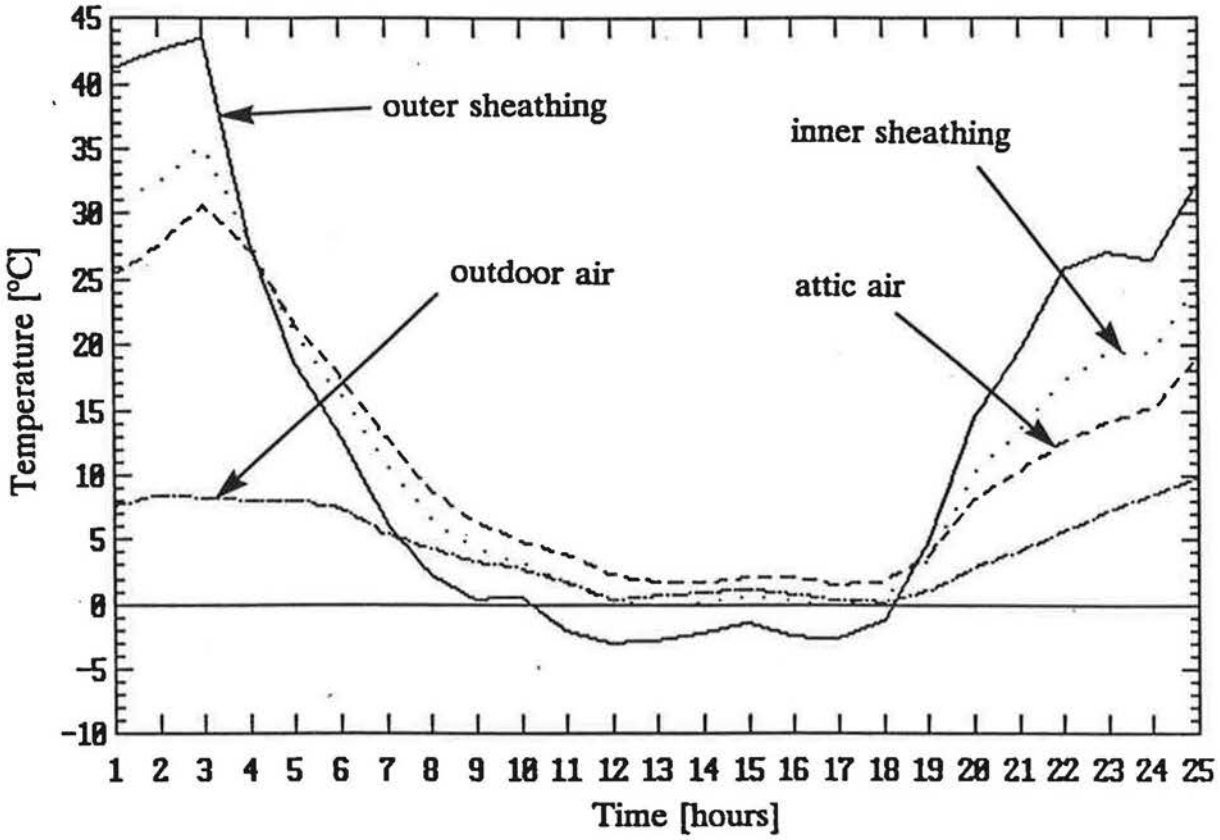

Figure 5-23. Diurnal variation of temperatures in attic 6 for April 9th and 10th 1991.

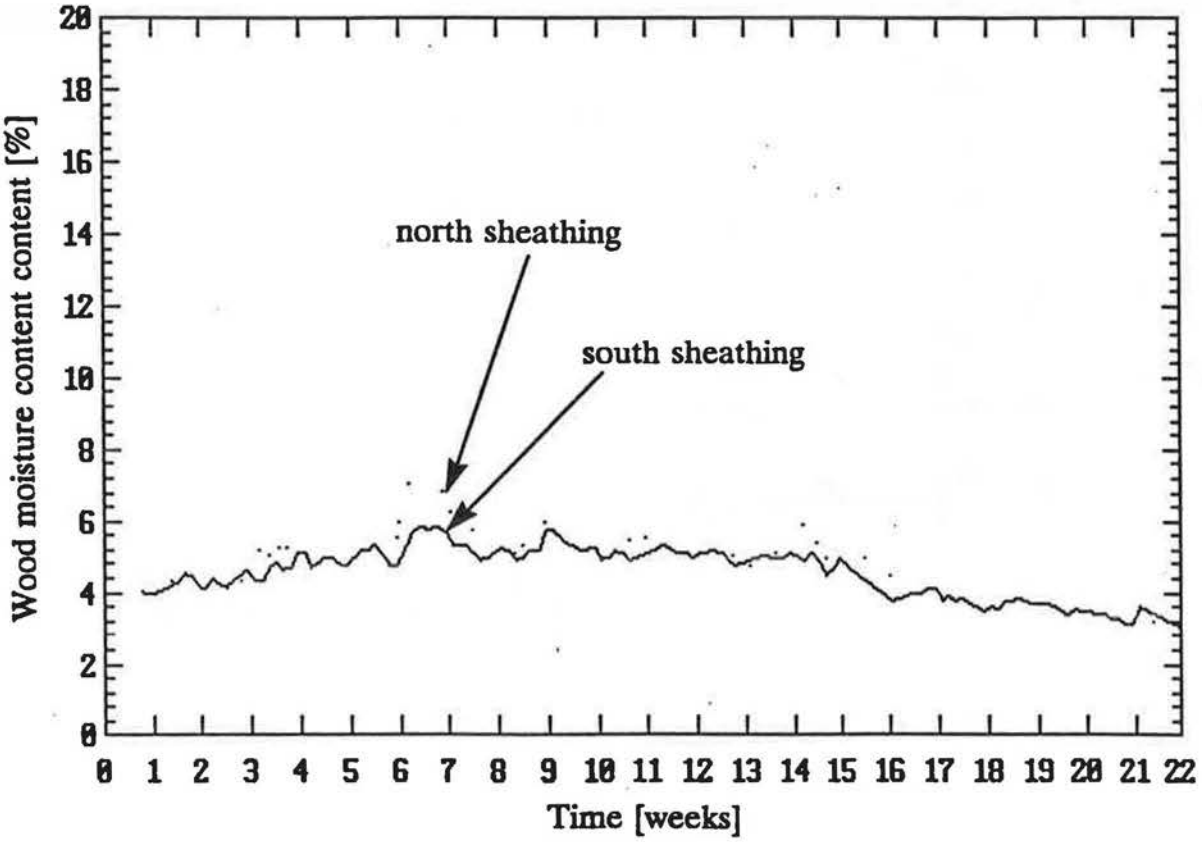

Figure 5-24. Measured wood moisture content in attic 5 over the heating season from December 1991 through April 1992.

moisture content was measured in the attic sheathing and trusses and joists using electrical wood resistance moisture meters. The ambient conditions of air temperature, wind speed, wind direction and solar radiation were measured to be used as inputs when validating the models.

The ventilation model requires the leakage areas of the attics, houses and ceiling to be known. The leakage areas were measured using a fan pressurization system that covered a wide range of pressure differences from zero to 100 Pa (or the maximum pressure difference attainable by the fan pressurization system). The fan pressurization results showed that a power law can be used to describe the pressure-flow relationship far all the measured leakage areas.

The two attics had different leakage configurations. Attic 5 had no soffits or roof vents and was ventilated by the distributed background leakage. Attic 6 had approximately four times the leakage area of attic 5 (with corresponding greater ventilation rates) due to its open soffits and roof mounted ventilators. In addition, attic 6 was also tested with a fan that supplied about 9.6 ACH. The fan has been tested in both supply and exhaust configurations. Including all configurations over 5000 hours of data has been taken over two heating seasons in both attics.

The attic ventilation rates and house to attic exchange rates are the most significant because previous studies have not systematically amassed as large an amount of data as this study. It has been shown that the scatter in measured ventilation rates means that a large amount of data needs to be taken in order to identify trends. An error analysis of the attic ventilation measurement system (given in detail in appendix B) has shown that the uncertainty in attic ventilation rates is about ±6% of the measured value. Most of this uncertainty is due to the error in mean tracer gas concentration over the hour. The largest problem with the ventilation monitoring system was uncertainty in measuring high ventilation rates. This was due to incomplete tracer gas mixing by fans installed in the attics. Investigation of this effect led to the adoption of a 20 ACH upper limit imposed on the ventilation measurements, above which the system tended to overpredict the ventilation rate.

The measurements of wood moisture content showed the importance of differentiating between the moisture content of the wood surface and the moisture content of the inner wood. The measurements performed for this study were of the inner wood and showed variations of only two to three percent moisture content over the length of the study. The inner wood moisture content remained uniformly low

(below about 7%) at all measurement locations. However, at various times during the winter the underside of the sheathing was observed to be damp and covered with a layer of frost, which implies that the surface layer of wood would be at a high moisture content. For improved verification of moisture transport models a method of measuring surface wood moisture contents needs to be developed.

The next chapter shows how the model predictions compare to the measurements discussed in this chapter.

Chapter 6. Model Validation

In this chapter the ventilation, heat transfer and moisture transport models will be validated by comparing their predictions to measured values. The measurements, made at AHHRF, were described in the previous chapter. Once the models have been validated they will be used to perform attic simulations, based on idealised weather conditions, as presented later in Chapter 7. The ventilation model will be verified first because the predicted ventilation rates are a required input for the heat transfer and moisture models. The effect of the interaction between the ventilation and heat transfer models will be examined by running the heat transfer model with either measured or predicted ventilation rates. Lastly, the moisture transport model will be tested using the ventilation rates and temperatures predicted by other models. The difference between predictions and measurements will be expressed using the following four error estimates:

- **Mean error** is the mean of the differences between each pair of measured and predicted data points. For binned data this is not the same as the difference in the average measured and predicted values for a bin.
- **Absolute error** is the mean of the absolute value of the differences between each pair of measured and predicated data points, i.e. positive and negative differences do not cancel. The absolute error is always larger than or equal to the mean error. The two error estimates are the same if the model either over predicts every hour or under predicts every hour.
- **Percent (%) error** is the mean of the percentage differences between each pair of measured and predicted data points
- **Absolute percent (%) error** is the mean of the absolute percentage differences between each pair of measured and predicted data points, i.e. positive and negative differences do not cancel.

6.1 Attic Ventilation Model

In this section the attic ventilation model predictions will be compared with measured values. This will include predictions of overall attic ventilation rate, house ventilation rates, house to attic exchange rates and ventilation rates with fans operating. The ventilation model uses measured values of wind speed, wind direction and indoor and outdoor temperatures to predict the pressures driving the ventilation flows. The ventilation flows also depend on the amount of leakage and its location. The background leakage was measured using fan pressurization tests as outlined in Chapter 5, section 5.2.

6.1.1 Attic ventilation rates

The attic ventilation model predictions of the total attic ventilation rate were verified by comparing model predictions to measured data (described in Chapter 5). The ventilation model requires both the amount and location of the house and attic leaks to be supplied. The total distributed leakage, as measured by the fan pressurization tests, is given in Table 5-2. In order to make predictions of ventilation rates in the two attics assumptions were made about the leakage distribution over the attic envelope. The assumed distribution of this leakage is summarised in Table 6-1, together with the additional vents for attic 6. The distribution was estimated by visual inspection by the author. In Table 6-1 the percentages are the fractions of background leakage estimated to be at the specified locations. The smallest amount of leakage considered in these estimates is 5% because it was not possible to make a more accurate estimate without detailed component leakage measurements in the attics. The total ventilation rate predicted by the attic ventilation model was relatively insensitive to the leakage distribution estimates provided that extreme values were not used e.g. all of the leakage at one location. Moving 5% of leakage between different locations changed the total predicted ventilation rate by less than 5%.

Table 6-1. Assumed distribution of background leakage area for attics 5 and 6 and location and size of attic 6 roof vents

Surface or Point on Attic Envelope	Attic 5		Attic 6	
	%	height above grade [m]	% (or area in bold)	height above grade [m]
eaves on roof surface 1	25	3	45	3
eaves on roof surface 2	25	3	45	3
gable - surface 3	5	distributed	0	-
gable - surface 4	5	distributed	0	-
roof surface 1	20	distributed	5	distributed
roof surface 2	20	distributed	5	distributed
vents on roof surface 1	-	-	**0.036 m^2**	4.5
vents on roof surface 2	-	-	**0.036 m^2**	4.5
roof peak	-	5	-	5

The numbered surfaces in Table 6-1 refer have the same numbering scheme as given for the ventilation model in Chapter 2. For the houses at AHHRF 1 is north, 2 is south, 3 is east and 4 is west. The roof peak height is the upper height limit for the distributed pitched roof surface (sheathing) leakage, and it is used to calculate the stack effect pressures at the top of the attic.

The ventilation model also computes the house ventilation rates and the flow between the house and attic through the ceiling. The distribution of house leakage used to perform these calculations is summarised in Table 6-2. As with the attic, these leakage distributions are estimated by inspection. The exception is the fraction of leakage in the ceiling which is calculated from the difference in leakage areas found from the pressurization tests for the house with the ceiling holes open and covered as shown in Table 5-2. The wall and floor level leakage is assumed to be equally distributed over the four sides of the building.

Table 6-2. Assumed leakage distributions and locations for house 5 and 6

Location on Building Envelope	House 5		House 6	
	%	height above grade [m]	%	height above grade [m]
Floor Level	20	0.6	15	0.6
Ceiling	15	3	15	3
Walls	65	distributed	70	distributed

The other inputs to the ventilation model are wind speed, wind direction (to calculate pressure coefficients and wind shelter), and house, attic and outdoor temperatures. The measured attic temperature was used for the data comparisons in this section so that the ventilation model may be tested independently of the heat transfer model. The temperature of the attic air changes the stack effect pressures driving ventilation and the air density used in the ventilation model mass flow balance.

To better identify which parts of the ventilation model may be contributing to differences between measured and predicted ventilation rates, the model predictions have been compared with both stack effect and wind effect dominated ventilation rates. The attic ventilation rate was not a strong function of the attic temperature as shown by Figures 6-1 and 6-2, for attic 5 and 6 respectively. In these figures the maximum temperature difference (stack) induced ventilation rate was only about 20%

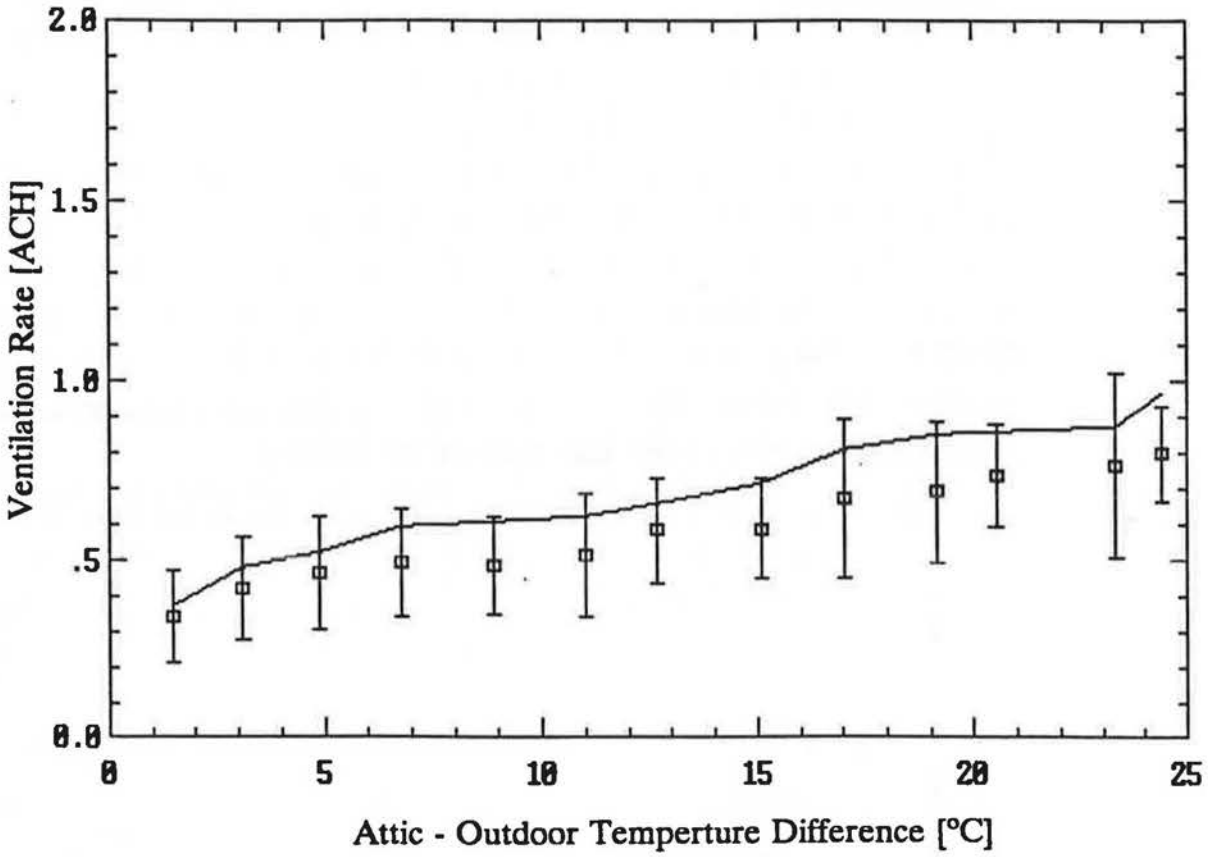

Figure 6-1. Temperature difference induced ventilation rates for attic 5 with windspeeds < 2 m/s (589 hours) showing mean and standard deviation of binned measured data and a line connecting the mean predicted values for each bin.

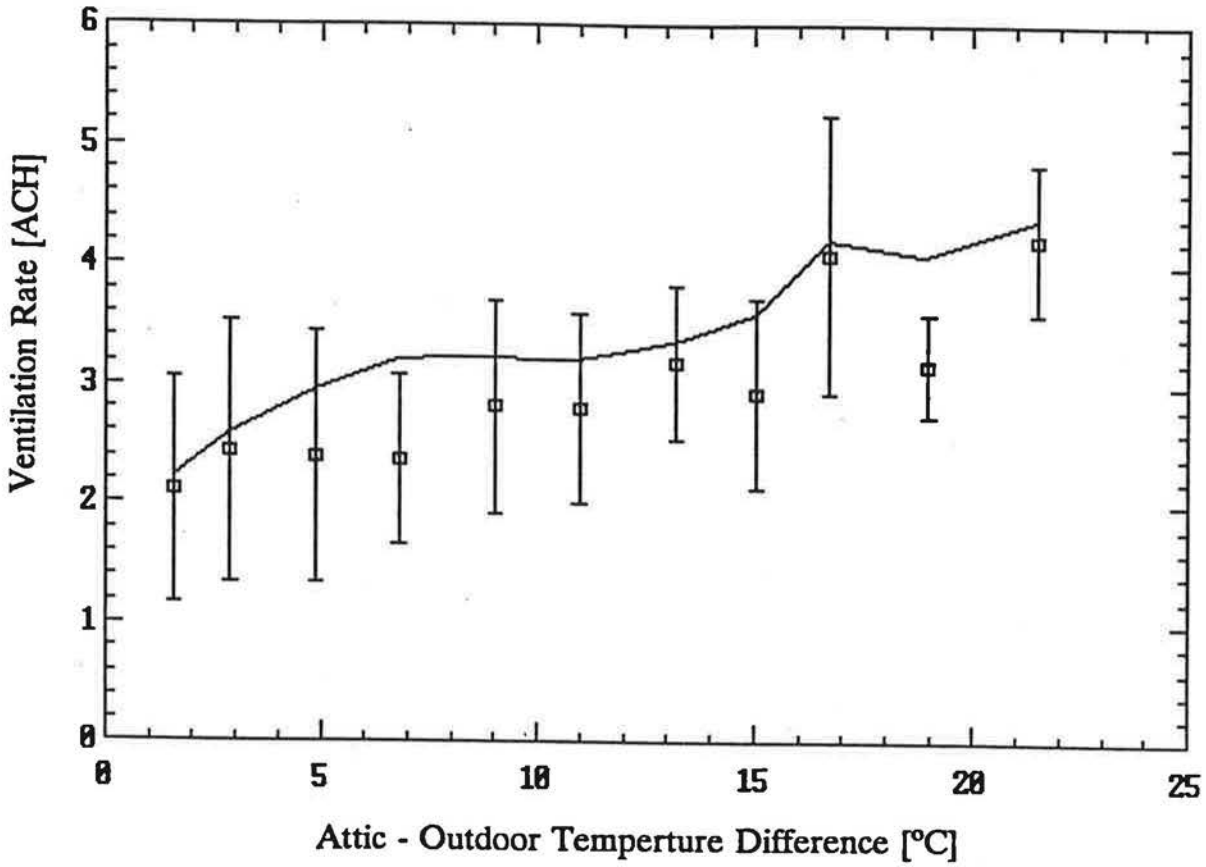

Figure 6-2. Temperature difference induced ventilation rates for attic 6 with windspeeds < 2 m/s (464 hours) showing mean and standard deviation of binned measured data and a line connecting the mean predicted values for each bin.

of that due to wind effects as shown in Figures 5-14, 6-3 and 6-4. In Figures 6-1 and 6-2 the measured data has been sorted for wind speeds less than 2m/s (to remove the higher wind speed effects) and binned every 2K of attic to outdoor temperature difference. Chapter 5, section 5.3 discusses the representation of binned data. The square indicates the mean value in the bin and the error bars show one standard deviation for the measured data. A solid line is used to connect the means of the predicted ventilation rates that are also averaged for each bin. Figures 6-1 and 6-2 show that the model tends to overpredict these stack driven ventilation rates. For attic 5 the mean error is 0.07 ACH (19%) and for attic 6 the mean error is 0.34 ACH (21%). The percentage errors are large for the stack driven ventilation rates because the ventilation rates are low. At windspeeds less than 2 m/s the following Figures 6-3 and 6-4 show that the wind produces flow rates that are the same magnitude as those shown for the stack effect only in Figures 6-1 and 6-2. Because the wind effect tends to be underpredicted the inclusion of some wind effect does not account for the systematic overprediction of stack effect ventilation rates and this requires further investigation. The wind produces maximum ventilation rates that are about five times greater than for stack effect which would reduce the percentage errors for the combined stack and wind driven ventilation.

Figures 6-3 and 6-4 show how the attic predictions compare to measured values for attic 5 and attic 6 respectively for all temperatures (this is the same measured data as shown in Figure 5-15). The maximum windspeed in Figure 6-4 for attic 6 was limited to 5 m/s because at 6 m/s (about 20 ACH) and higher the measured values were unreliable (as shown previously in Chapter 5, section 5.3.1 and in Figure 5-13). In order to compare measured values and predictions more clearly, the measured data was binned every 1 m/s of wind speed. The ventilation rates were predicted for every hour (3758 for Figure 6-3 and 3522 for Figure 6-4). Their mean values at the mean windspeed for each hour were connected by a straight line in the figures. The trend in increasing ventilation rate with windspeed shown by the measured values was followed by the model predictions with a general tendency towards underprediction. For attic 5 the mean error was -0.017 ACH (-9.3%) and for attic 6 the mean error is -0.5 ACH (+4.3%). Most of this underprediction occurred when the wind blew along the row of houses (as will be shown later in this section). The attic 6 mean percentage error was positive because its overpredictions occurred at lower ventilation rates where the percentage overprediction was high but the mean error in ventilation rate was relatively small. Considering the uncertainty

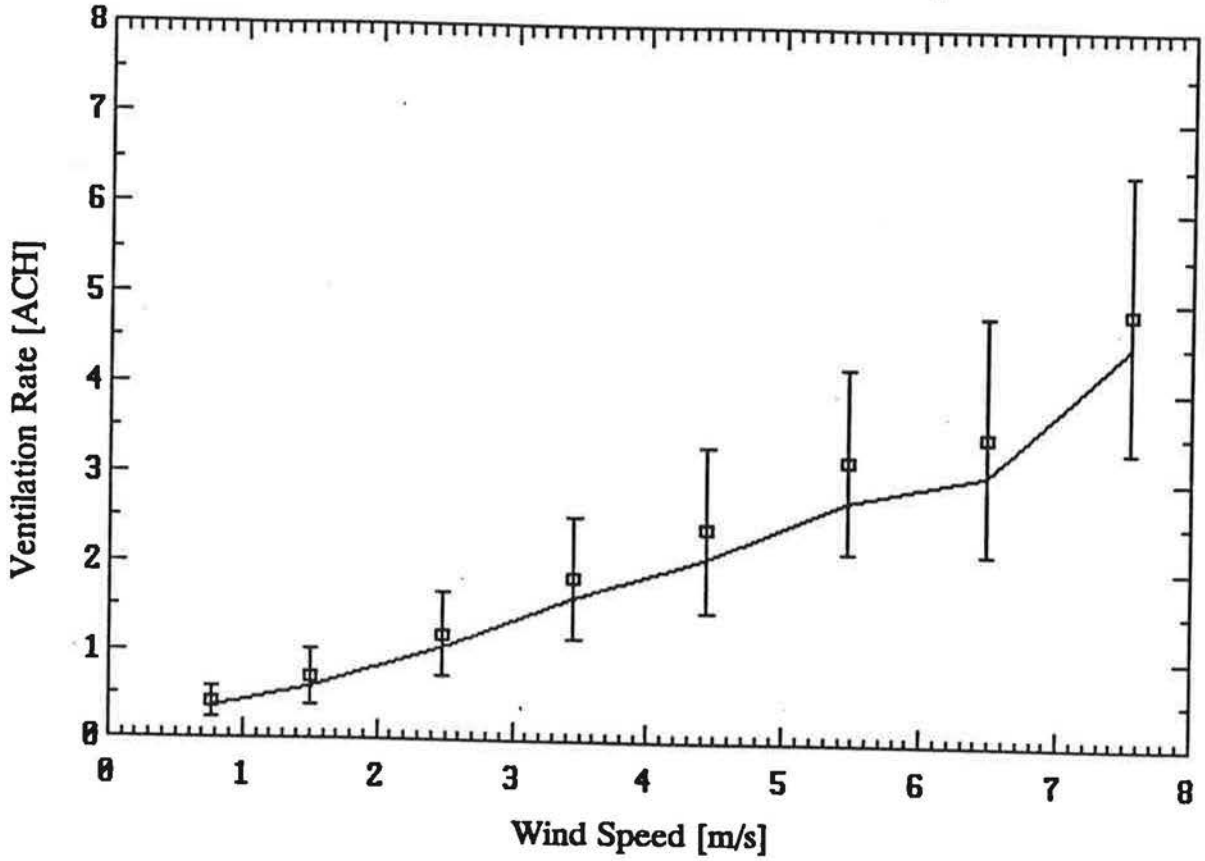

Figure 6-3. Measured binned Attic 5 ventilation data (3758 hours) with predicted line for all wind directions and temperatures.

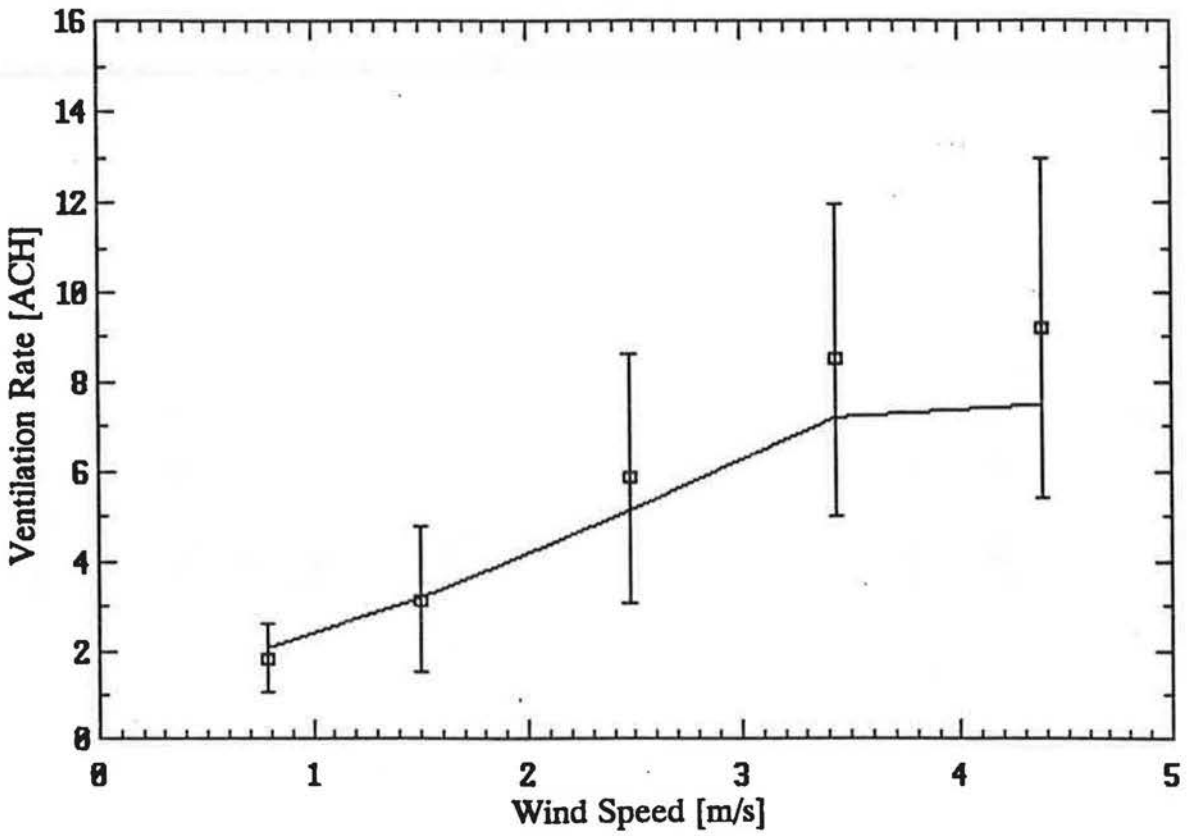

Figure 6-4. Measured binned Attic 6 ventilation data (3522 hours) with predicted line for all wind directions and temperatures.

in pressure coefficients, wind shelter and leakage distributions these errors were about as small as could be reasonably expected. The values of these parameters were not altered in order to reduce the errors. The model would then have been fitted to the measured data for the test houses and this procedure would not have validated the model in a general sense.

The wind direction has a strong effect on ventilation rate because it changes the wind pressure coefficients and wind shelter. The magnitude of this effect is about a factor of 4 at the test houses as shown by Figures 5-18 and 5-19. To test if the model has the correct variation of pressure coefficient and shelter the measured and calculated ventilation rates for attic 6 are shown in Figures 6-5 and 6-6 respectively. Both figures illustrate the same trends with lower ventilation rates for east and west winds (90° and 270°) than for north and south winds (0° and 180°). The large spread of data for a given wind direction is because a range of windspeeds and temperature differences are present. In addition, using an hourly averaged wind direction produces scatter with respect to wind direction in the results because the wind direction may change during the hour. The lower ventilation rates for a given direction correspond to lower windspeeds and temperature differences and the high ventilation rates to high windspeeds and temperature differences. There is less scatter in the predicted data because the measured data has included all the hourly variation in parameters such as wind speed, wind direction and temperatures that are not included in the hourly averages entered in the model.

To better observe the model performance the measured and predicted data were binned every 22.5° to provide 16 wind direction bins. The data were then normalised by dividing by U^{2n} to remove the effects of changing windspeed. In each bin the data were averaged and the measured standard deviation was calculated. A further normalisation was carried out by dividing all the binned averages by the mean ventilation rate from the bin for south winds. This bin was chosen because the test houses were completely exposed to winds from the south and there should be no wind shelter for that direction. This normalisation procedure was explained in more detail in section 5.3.1. Figures 6-7 and 6-8 show the results of this procedure for attic 5 and attic 6, respectively. For attic 5 the normalised air exchange rates are about 50% less for east and west winds than for north and south winds due to the sheltering effects of the neighbouring buildings. For attic 6 the sheltering effect is asymmetric with a reduction of almost 60% for west winds and only 40% for east winds. This is because attic 6 is sheltered by the row of houses for west winds but for east winds

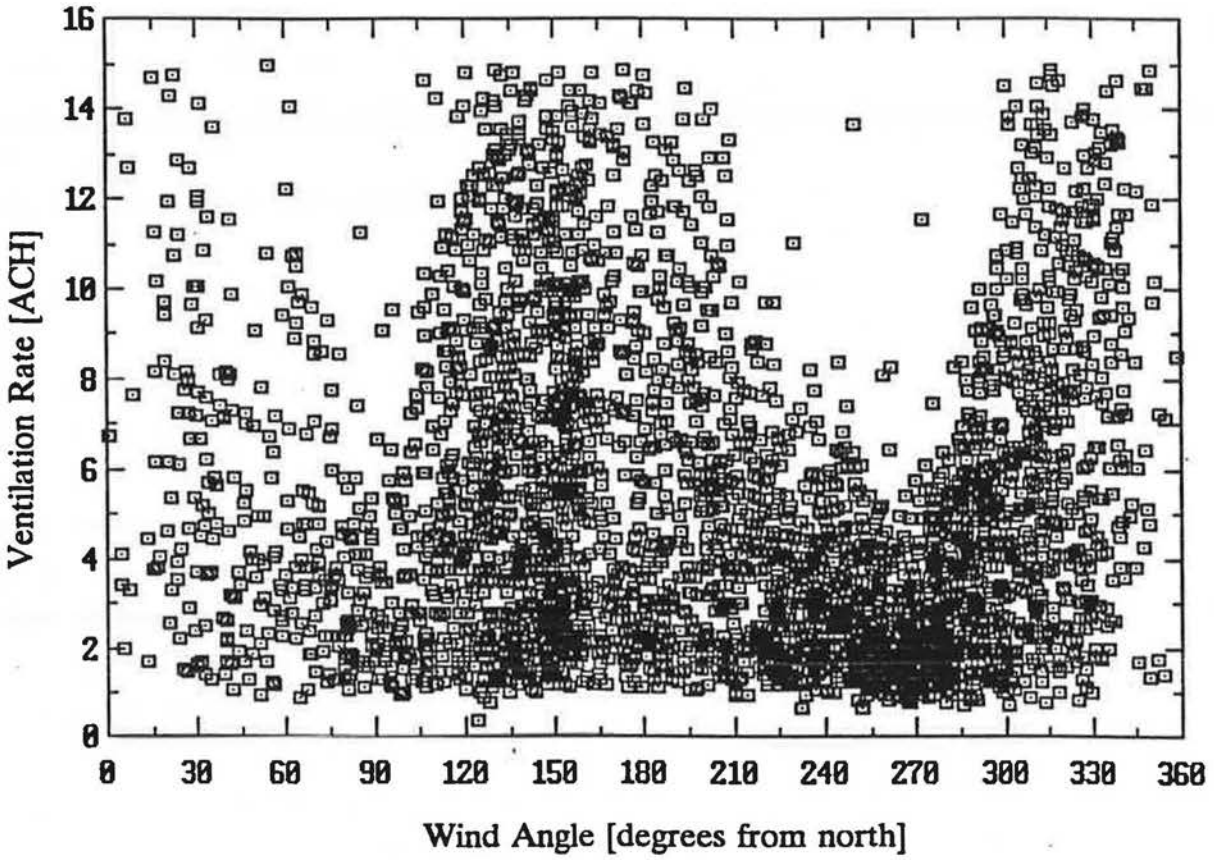

Figure 6-5. Variation of measured ventilation rates for attic 6 with wind direction (3522 hours).

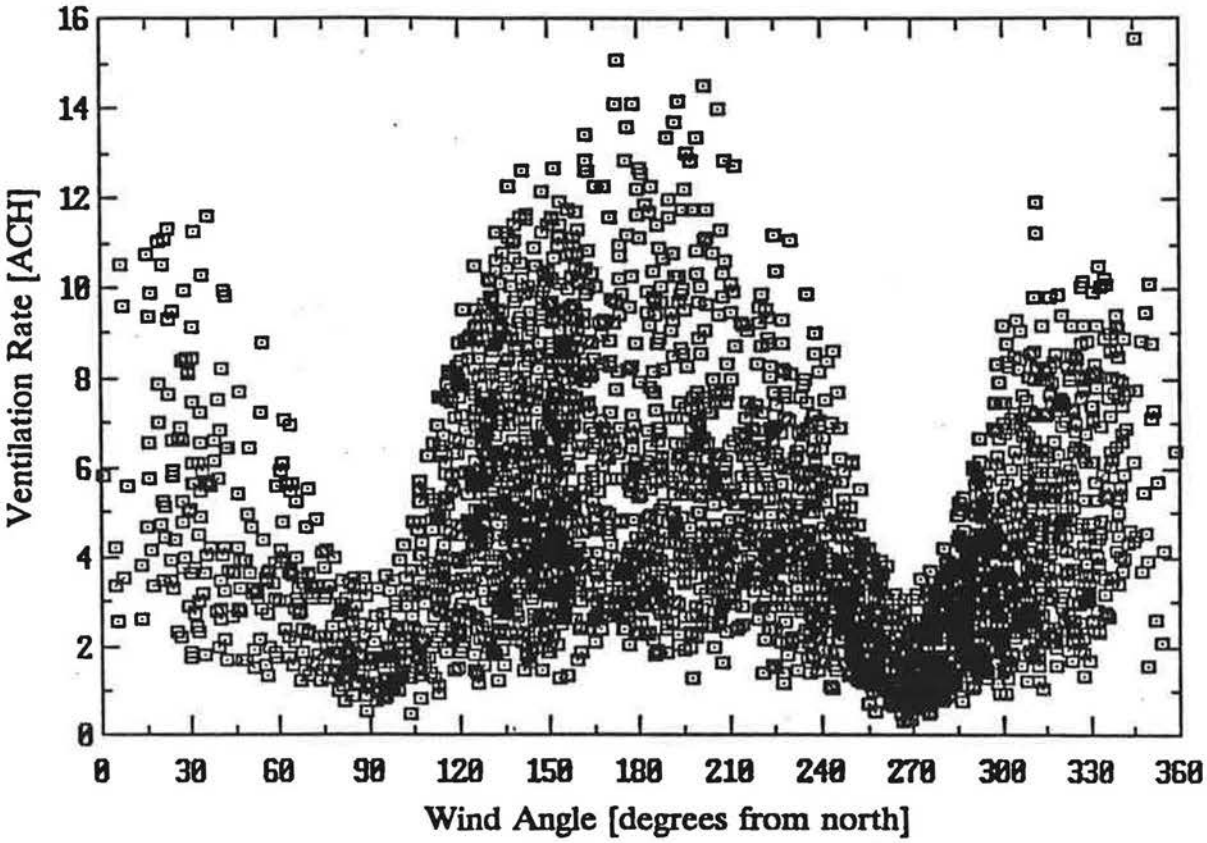

Figure 6-6. Variation of predicted ventilation rates for attic 6 with wind direction (3522 hours).

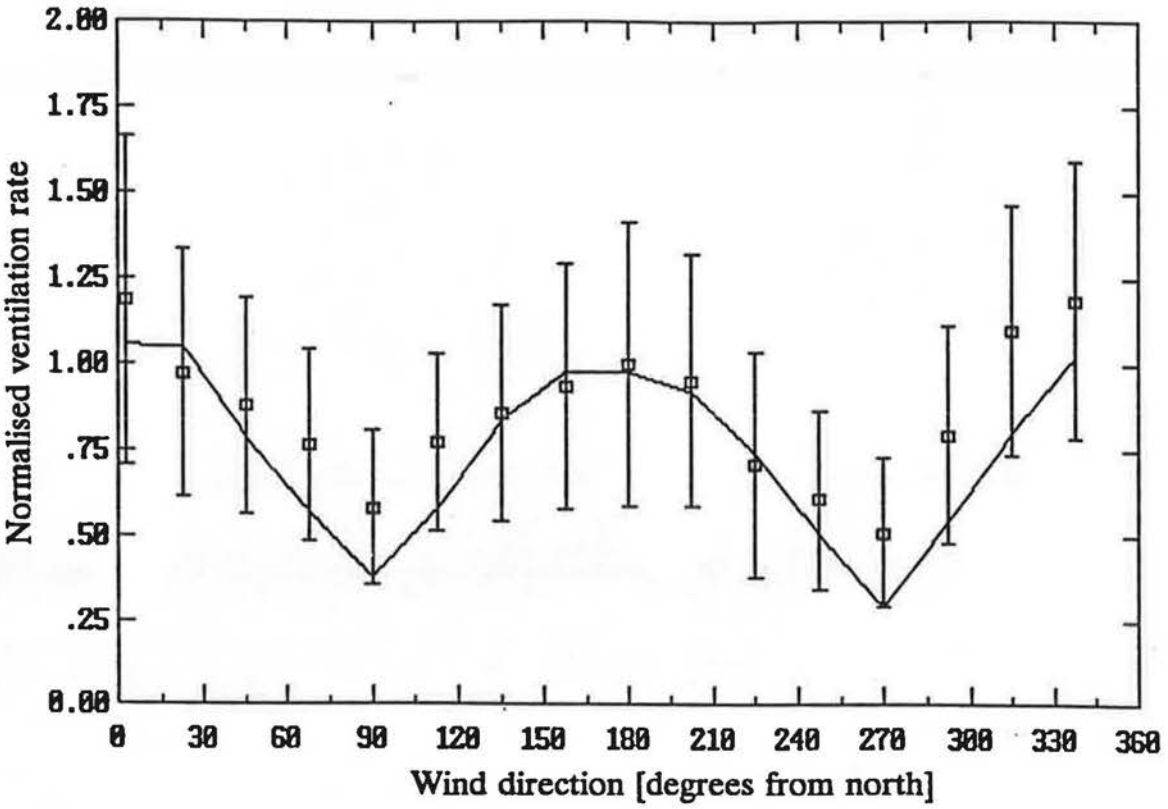

Figure 6-7. Comparison of predicted (line) and measured (binned) normalised ventilation rate as a function of wind direction for attic 5 (3758 hours) showing mean and standard deviation of binned measured data and a line connecting the mean predicted values for each bin.

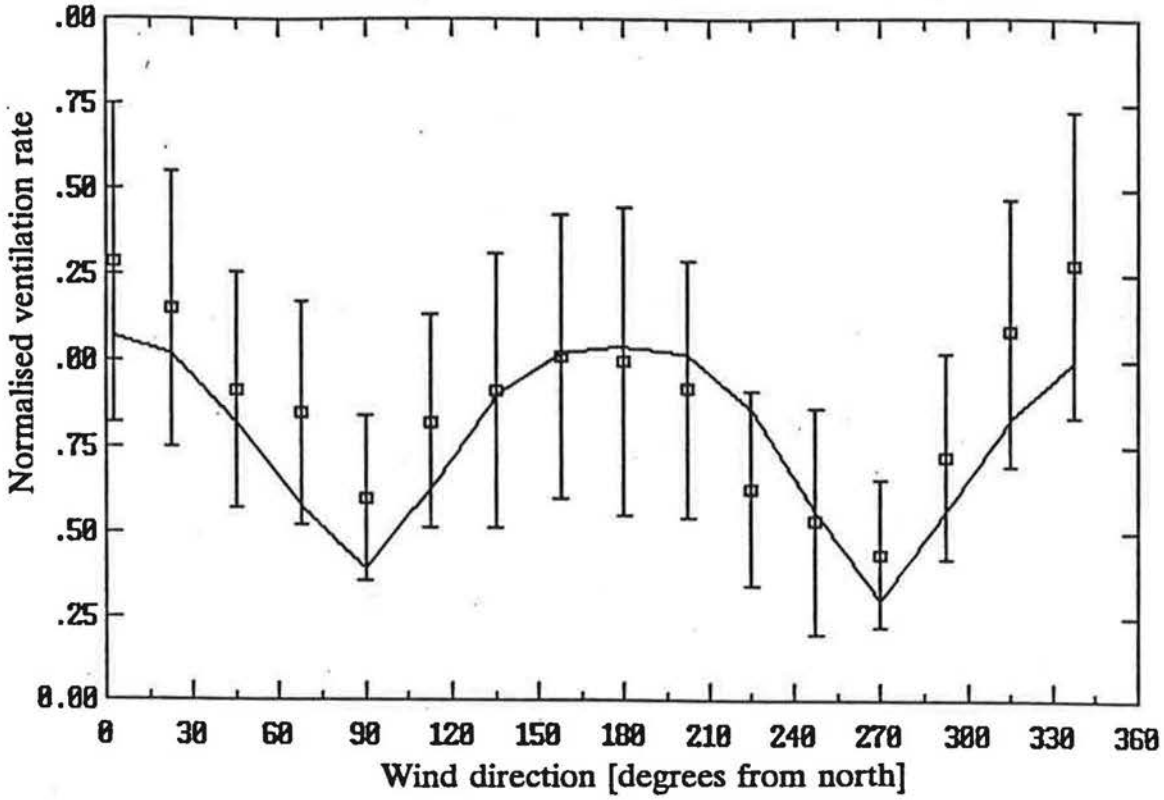

Figure 6-8. Comparison of predicted (line) and measured (binned) normalised ventilation rate as a function of wind direction for attic 6 (3522 hours) showing mean and standard deviation of binned measured data and a line connecting the mean predicted values for each bin.

only partial shelter is provided by a rectangular vertical wall 3.7m high and the same width as the houses. The data shows that this sheltering wall does not have the same shelter effect as an upwind house. This is for two main reasons. Firstly, the wall only extends 0.7m above eaves height of the house and leaves the rest of the attic exposed. Secondly, the flow pattern around the wall is different from that around a house due to flow separation at the sheltering wall edges.

The model follows the trends in normalised air exchange with wind direction and for both attics the largest error is an underprediction of about 25% when winds are from the east or west. This error is due to the combination of errors in estimating shelter factors and the error associated with assuming constant pressure coefficients over the surfaces of the attic. The shelter factors applied to the attics were developed for the houses but the attics are closer to the undisturbed air flow over the houses and thus may experience less shelter. In the real flow over the attic there will be spatial variation in the pressure coefficients that will create pressure differences and flow rates not accounted for in the ventilation model developed for this study. The ventilation model mean and percentage errors are summarised in Table 6-3 including the variation of error with wind angle.

Table 6-3. Mean and percentage errors of predicted ventilation rates for Attic 5 and 6

	Attic 5 Mean Error ACH (%)	Attic 6 Mean Error ACH (%)
For stack dominated ventilation	0.07 (19)	0.34 (21)
For wind dominated Ventilation All wind directions	-0.02 (-9.3)	-0.5 (+4.3)
North Winds Only	-0.04 (+2.2)	-1.7 (-14.1)
South Winds Only	0.15 (14.2)	0.08 (18.9)
East Winds Only	-0.24 (-25.8)	-1.50 (-27.1)
West Winds Only	-0.28 (-28.8)	-0.75 (-17.1)

6.1.2 House ventilation rates

Although this study concentrates on attic ventilation rates, the house ventilation rates were also calculated. The house ventilation rates are important because the balance of ventilation flows for the house in ATTICLEAK-1 determines

the flow rate through the ceiling. The house ventilation rates will not be discussed in detail here but a few results will be given to show that the ventilation model makes good predictions of house ventilation rates. A more thorough investigation of house ventilation rate predictions by the ventilation model used here is presented by Wilson and Walker (1991a). For house ventilation rates the air changes per hour (ACH) was based on the volume of the house (220 m^3 for the houses tested here). For the attic ventilation rates the air changes per hour (ACH) was based on the attic volume (61 m^3).

Figures 6-9 and 6-10 are typical results found by Wilson and Walker (1991a) for house 5 for stack and wind dominated ventilation. In Figure 6-9 data has been sorted for maximum wind speeds of 2 m/s to look at stack effect only. The mean error for the data shown in Figure 6-9 is 0.005 ACH (6.4%). In Figure 6-10 the data has been selected for wind speeds greater than 2 m/s to look at wind dominated ventilation (all wind directions are included). The error for the wind dominated ventilation rates shown in Figure 6-10 is -0.003 ACH (3%). In both Figures 6-9 and 6-10, the upper Figure shows the individual measured data points and the lower figure binned measured and predicted data.

6.1.3 House to attic exchange rates

For the heat transfer and moisture transport models the flow through the ceiling is an important parameter because this flow convects room temperature air and moisture into the attic. The ventilation model calculates this flow based on the leakage area attributed to the ceiling and the pressure differences between the house and attic. The measured house to attic exchange rates are calculated based on the concentration of SF_6 in the attic air using Equation 5-4. It was found that the house to attic exchange rate depends most strongly on the temperature difference between the house and the attic. The effect of windspeed is small because the mean pressures in both zones caused by the wind are approximately equal. The small windspeed effect was discussed earlier in Chapter 5, section 5.3.3, and shown in Figure 5-21. To reduce scatter the data was sorted for windspeeds less than 2 m/s. Model predictions are compared with measured data in Figures 6-11 and 6-12 for attics 5 and 6 respectively. These figures show good agreement between measured and predicted values considering how small these exchange rates are. The mean error for attic 5 is -0.015 ACH (4.5%) and for attic 6 it is 0.0014 ACH (14.3%). For both attics the peak exchange is about 0.25 ACH which is only a few percent of the total attic

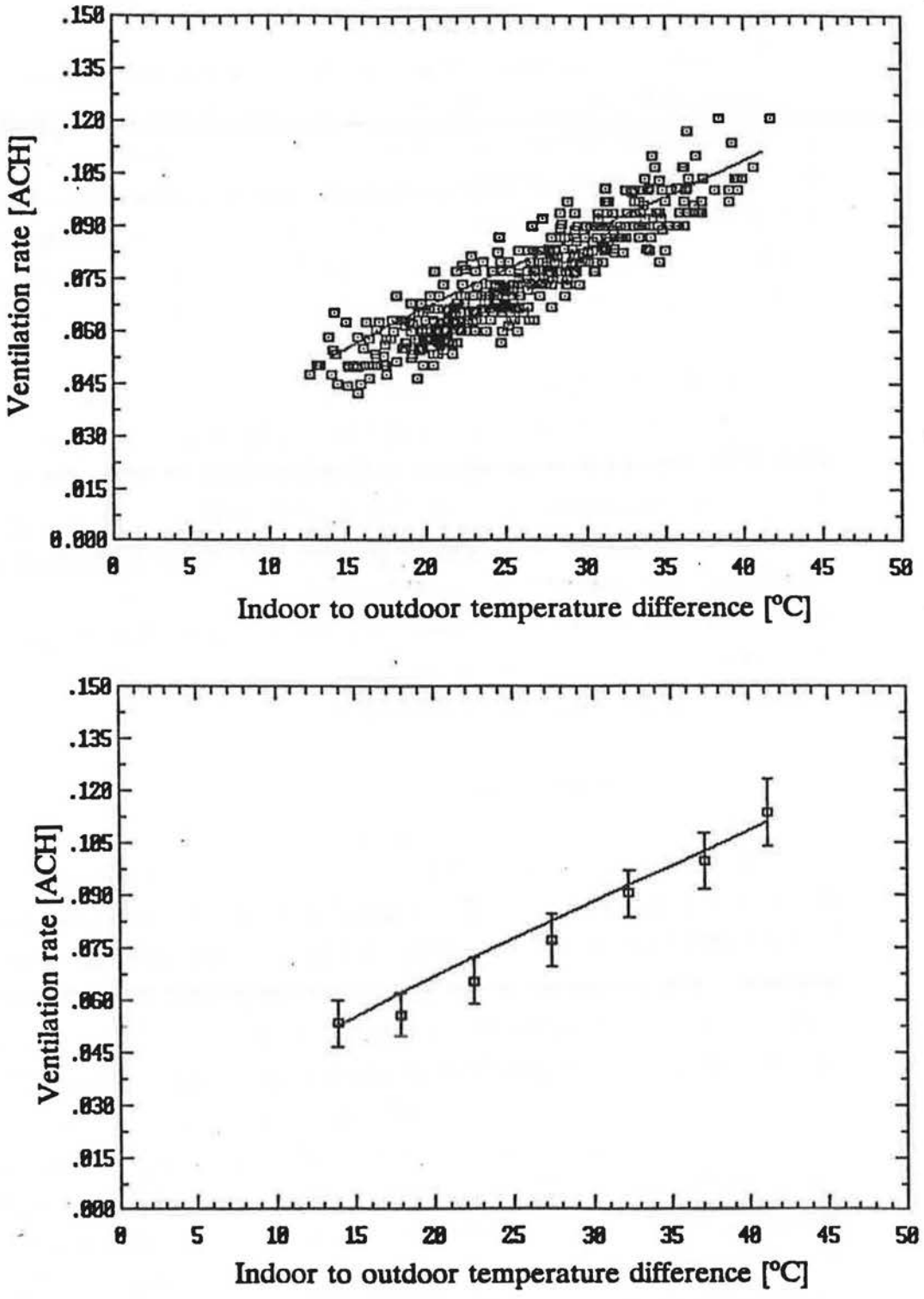

Figure 6-9. Comparison of measured and predicted stack effect ventilation rates for house 5 with wind speeds < 2 m/s (461 hours).

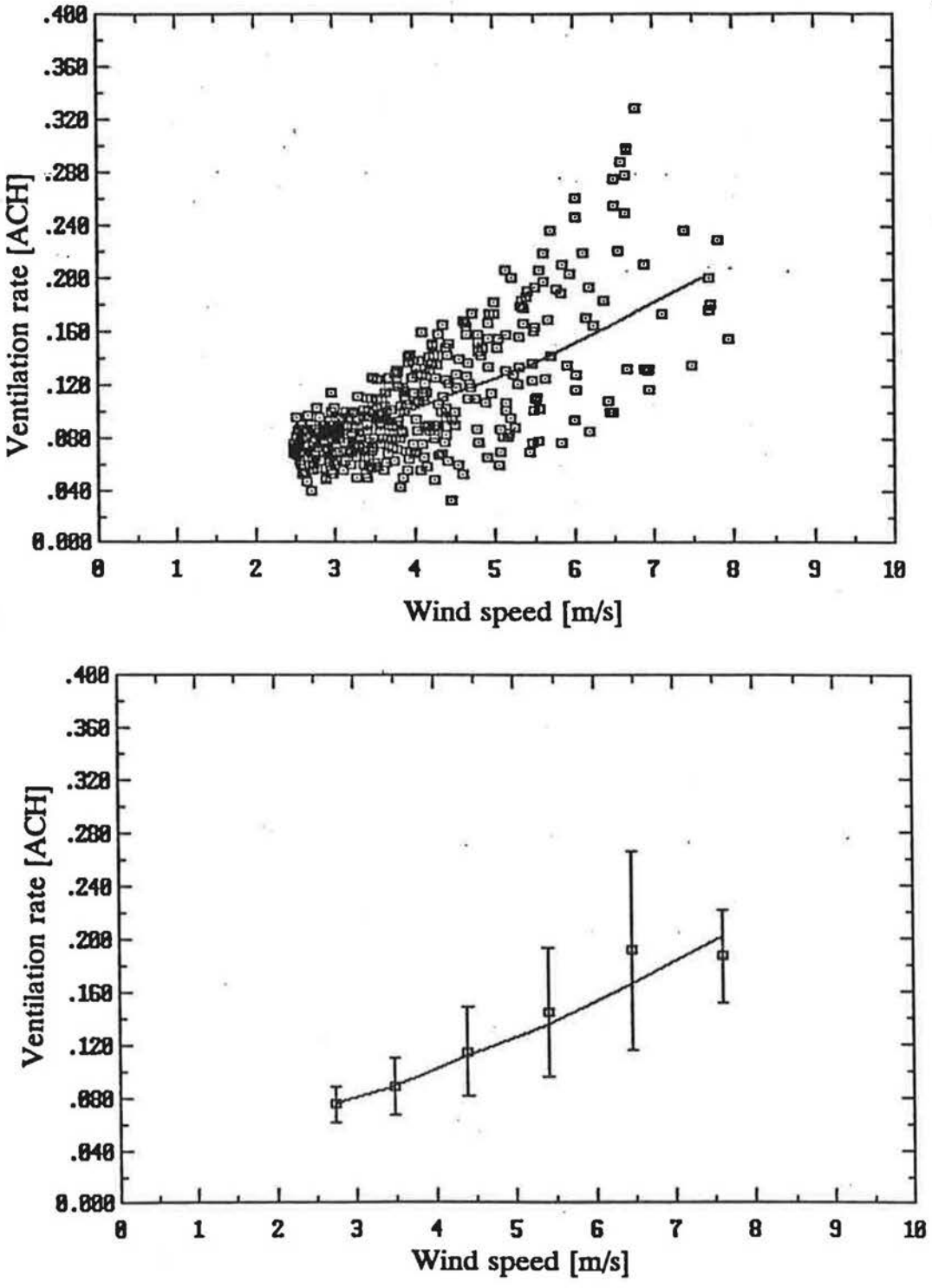

Figure 6-10. Comparison of measured and predicted wind effect ventilation rates for house 5 with wind speeds > 2 m/s (432 hours).

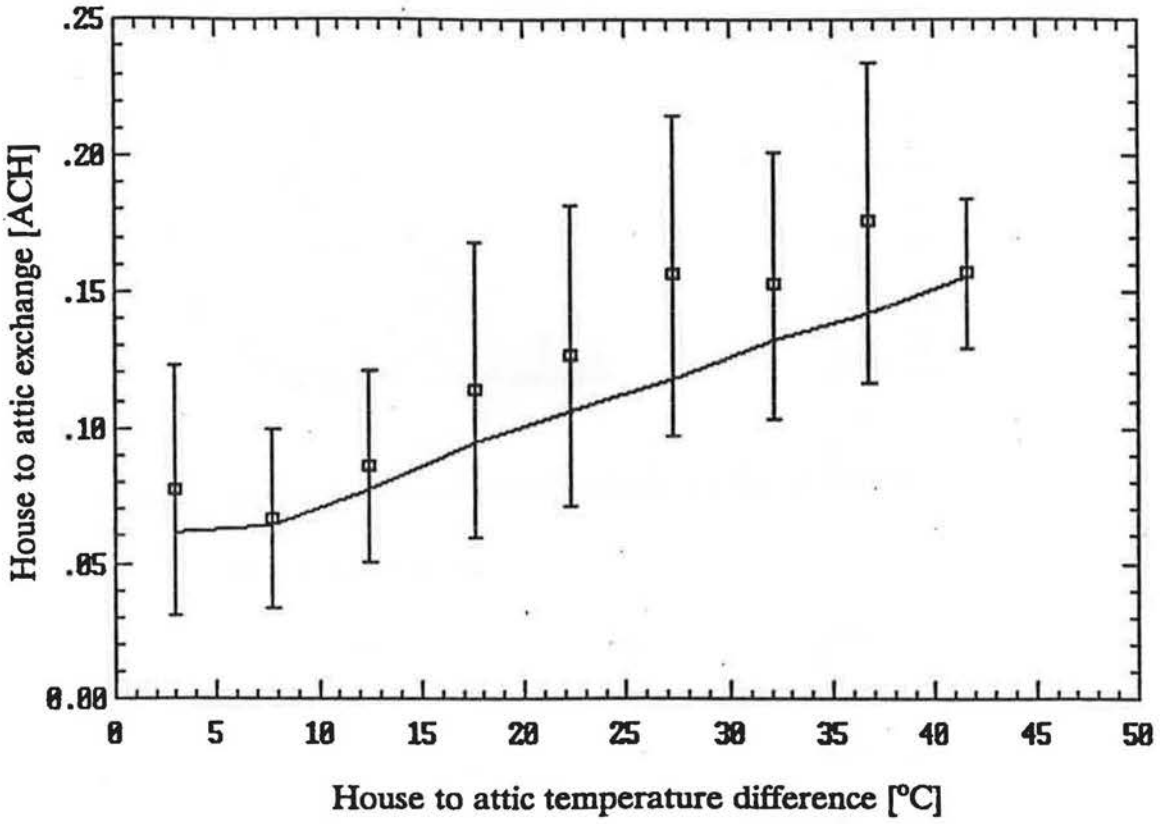

Figure 6-11. Comparison of measured (binned) and predicted (line) house to attic exchange rates for attic 5 for wind speeds < 2 m/s (990 hours) showing mean and standard deviation of binned measured data and a line connecting the mean predicted values for each bin.

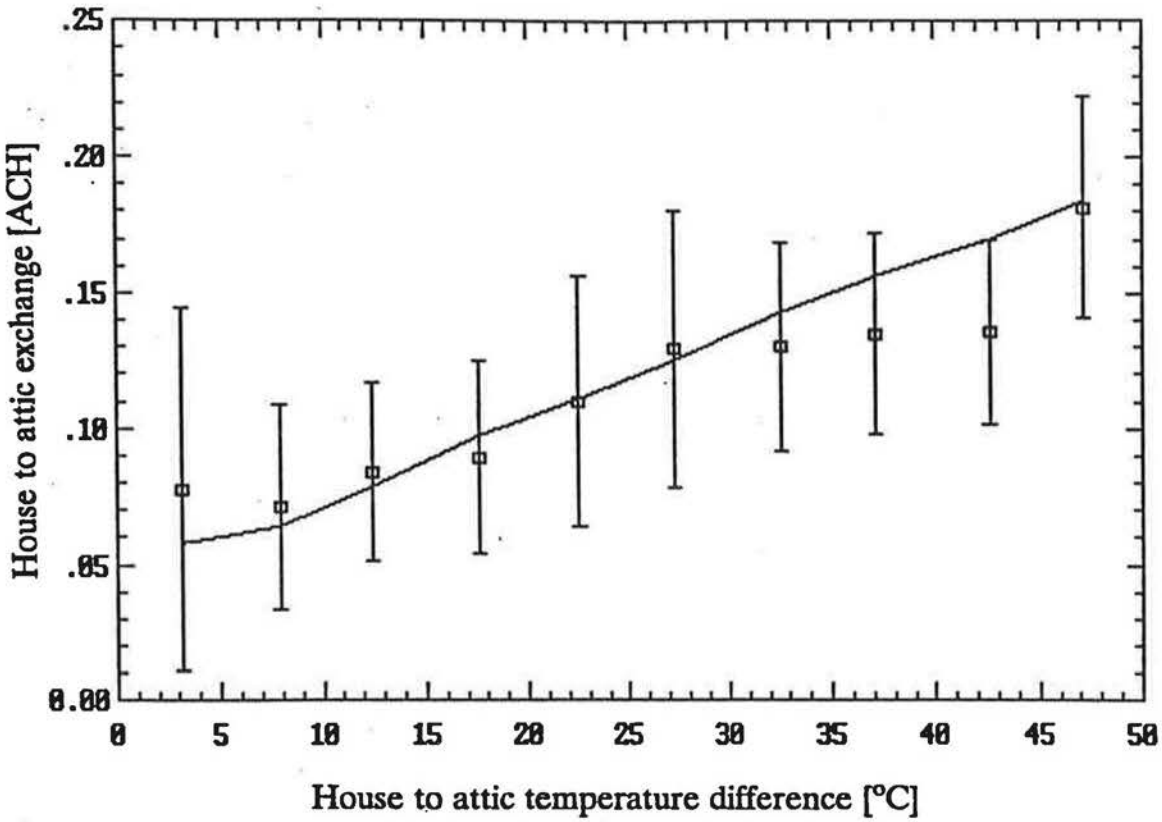

Figure 6-12. Comparison of measured (binned) and predicted (line) house to attic exchange rates for attic 6 for wind speeds < 2 m/s (722 hours) showing mean and standard deviation of binned measured data and a line connecting the mean predicted values for each bin.

ventilation rate. Typically the room to attic exchange is about 10% of the total for attic 5 and only 2% of the total for attic 6.

6.1.4 Attic ventilation rates with fans

For the winter of 1991-1992 attic 6 was equipped with a ventilation fan, described in section 5-1, to monitor the change in ventilation rate created by a fan. The fan was included in the ventilation model using a fan curve and the maximum flowrate and pressure difference generated by the fan as shown in Chapter 2, section 2.14.5. The maximum flowrate for the fan was 0.164 m^3/s (which corresponds to an attic ventilation rate of 9.6 air changes per hour (ACH) based on an attic volume of 61 m^3) and the maximum pressure difference that the fan can generate is 175 Pa. The fan was operated on a cycle, switching on at 10:00 a.m. and off at 4 p.m. Figure 6-13 shows four days of measured and predicted ventilation rates for the fan in extraction mode (depressurizing the attic). The predicted values follow the trend of increased ventilation when the fan is on. From November 1991 to February 1992 there were a total of 1035 hourly averaged ventilation measurements made, with 259 when the fan was on and 776 with the fan off. The mean error between measurements and predictions is -0.37 ACH (-6%) with the fan off, and -0.32 ACH (-3%) with the fan on. These results show that adding the fan does not introduce a systematic error in the predictions so that the model is combining the fan and natural ventilation rates correctly. The mean errors describe the model results as averages over the time period considered. On an hour by hour basis the errors are much larger. They are found by averaging the absolute error at each hour so that positive and negative errors do not cancel. The absolute errors are about 2 ACH with the fan both on and off. This translates into a typical absolute percentage error of 18% and 31% with the fan on and off respectively.

From March to June 1992 the fan was reversed an acted as a supply fan to pressurize the attic. A total of 1359 hours in ventilation data were measured; 326 hours with the fan on and 1033 with the fan off. Figure 6-14 shows four days of typical results chosen to show low natural ventilation for the first two days then higher natural ventilation rates for the last two days caused by an increase in wind speed. The magnitudes of the differences between measured and predicted ventilation rates are about the same as for the extractor fan and are summarised in Table 6-4.

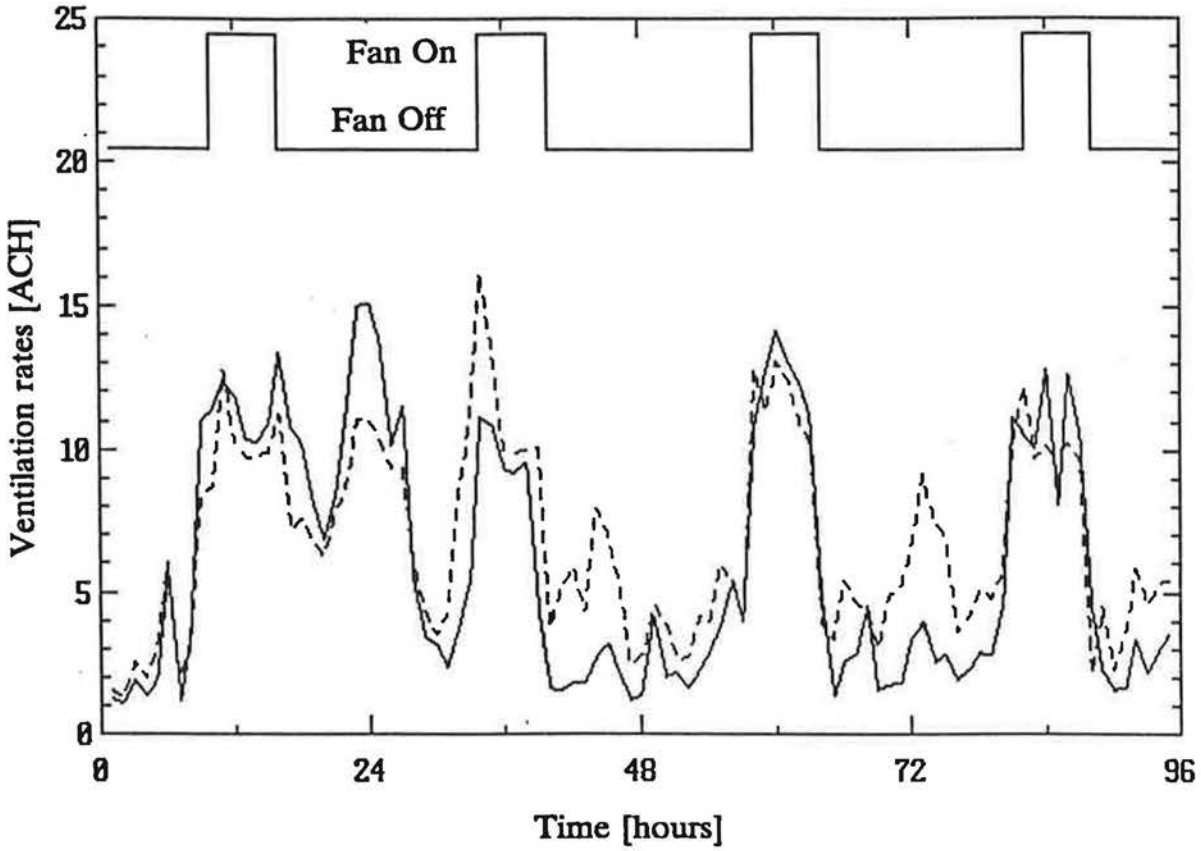

Figure 6-13. Measured (solid line) and predicted (dashed line) attic 6 ventilation rates with an exhaust fan providing about 9.6 ACH from 10 a.m. to 4 p.m. each day. January 17 to 20 1992.

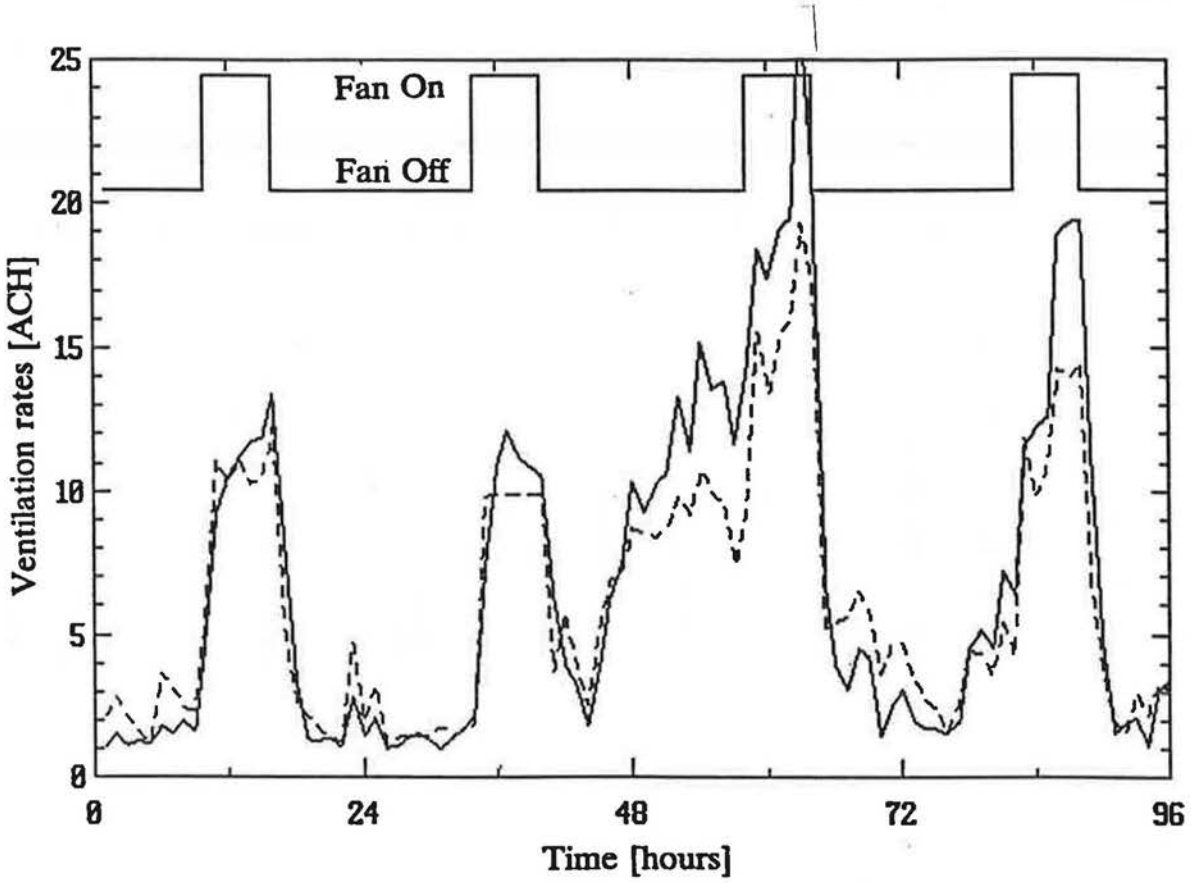

Figure 6-14. Measured (solid line) and predicted (dashed line) attic 6 ventilation rates with a supply fan providing about 9.6 ACH from 10 a.m. to 4 p.m. each day. March 13 to 16 1992.

Table 6-4. Summary of attic fan performance and model prediction errors

	Supply Fan		Exhaust Fan	
	ON	OFF	ON	OFF
Number of Hours	326	1033	259	776
Mean Measured [ACH]	12.22	5.38	11.16	6.04
Mean Predicted [ACH]	12.54	5.15	10.84	5.67
Mean Error [ACH] (%)	0.32 (2.6%)	-0.23 (-4.3%)	-0.32 (-2.9%)	-0.37 (-6.1%)
Absolute Error [ACH]	2.49	1.78	1.97	1.89
Absolute Error %	20.4%	33.1%	17.6%	31.3%

The results in Table 6-4 show that there is no systematic error in the model when fans are included. With and without the fan the mean errors are about the same. The increased ventilation rates with the fans on leads to the reduced percentage error. The percentage errors are reduced because the fan is a well defined leak in the model with little uncertainty in its flowrate.

6.2 Attic heat transfer model

The attic heat transfer model is described in Chapter 3. The model uses inputs of ambient weather conditions of temperature, solar radiation and cloud cover to predict attic wood and air temperatures. Additional inputs to the model are the area and mass of the wood in the attic, the attic air volume and density, and the thermal conductivity, specific heat and surface absorbtivity of the attic materials. As discussed earlier (in Chapter 3) the attic heat balance is also dependent on the attic ventilation rate. The heat transfer and ventilation models interact because the temperature of the attic air determines the stack effect for driving natural ventilation flows and also changes the attic air density for use in the attic mass flow balance. In this section, the heat transfer model will be tested using measured ventilation rates and then with predicated ventilation rates in order to find out if using the combined ventilation and heat transfer models introduces any systematic errors in temperature predictions.

6.2.1 Using measured ventilation rates

To test the heat transfer model independently from the ventilation model the first part of the verification procedure was performed using measured ventilation rates. The combined heat transfer and ventilation models will be tested later. To illustrate the model performance six days have been chosen (May 15 through 20, 1991) that cover a wide range of windspeeds and ventilation rates, and have a reasonable range of outdoor temperatures and high solar radiation gains in order to provide a range of model inputs. Figure 6-15 shows how the windspeed varies over the six days over a range of 0.8 m/s to 10 m/s and how rapidly the windspeed changes from hour to hour. The variation of outdoor temperature is shown in Figure 6-16 and has a diurnal cycle with peak temperatures in the afternoon 10 to 15 °C higher than at night. The measured solar radiation on the two pitched roof surfaces is shown in Figure 6-17 where the south face has greater solar gains than the north face. The third, fourth and fifth days show the effect of clouds which reduce the solar radiation and the long wave radiation losses to the cold night sky. The night sky is typically 30°C colder than the air temperature (see Chapter 3, section 3.1.3). Cloud cover was not measured at the test facility and for the model predictions it is assumed that the sky is half covered for all hours of the day and night. This assumption about cloud cover means that for clear skies the solar gains and night sky losses are under predicted and for cloud covered skies they are overpredicted by the model. The measured attic 5 ventilation rate and room to attic flow rate are shown in Figure 6-18. The room to attic flow has been multiplied by 10 in this figure to make its variations visible. The dependence of ventilation rate on wind speed is clearly seen by comparing Figure 6-18 to Figure 6-15. The increased ventilation rates correspond with increased wind speeds. The range of ventilation rates in attic 5 is about 0.5 ACH to 7.5 ACH and the ceiling flow rates range from about 0.01 ACH to 0.12 ACH.

Figure 6-19 shows the measured and predicted attic 5 air temperatures for this same time period. There is a much stronger diurnal variation than the outdoor temperatures in Figure 6-16, with temperatures up to 15 °C higher than outdoors during the day due to solar radiation gains. At night the attic air is not as cold as the outdoor air due to heat transfer through the ceiling. The model predictions follow the changing measured values very closely with a trend to under predict the air temperature. This is especially evident at night and could be due to excessive radiation to the cold night sky. This hypothesis was tested by running the heat

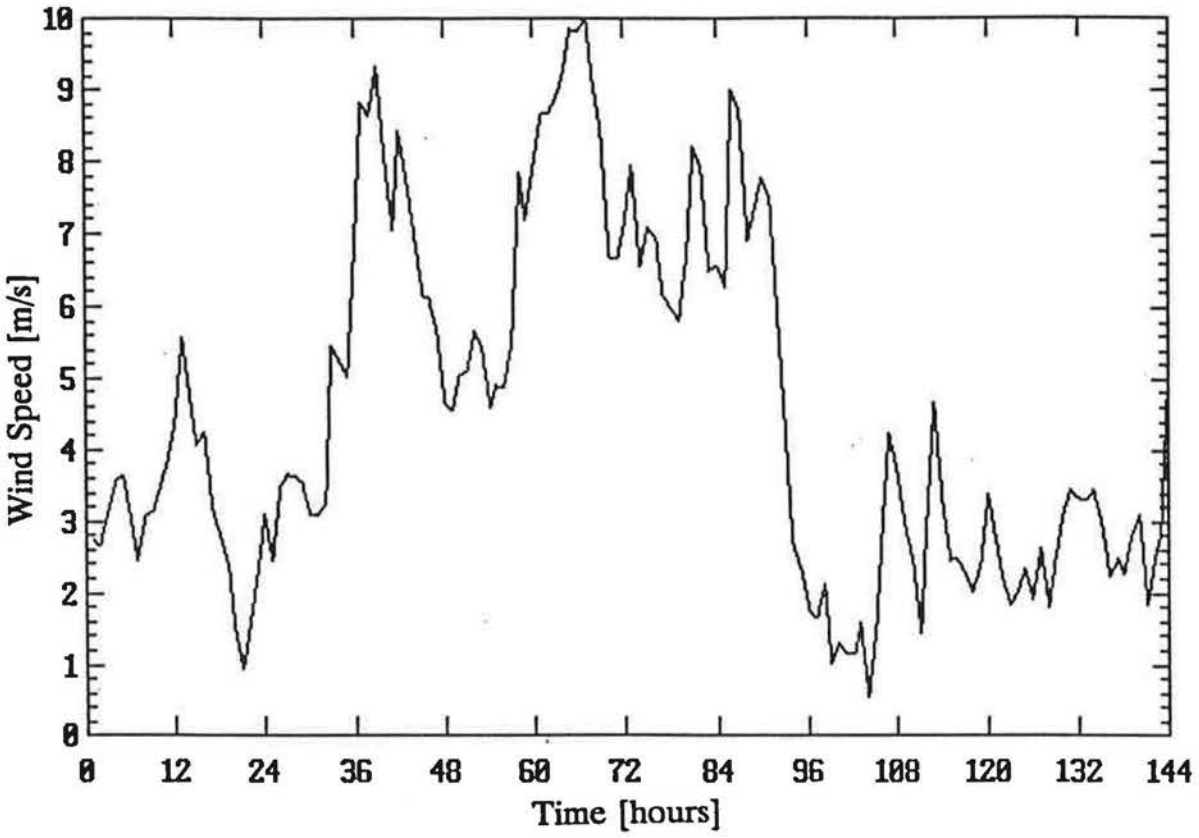

Figure 6-15. Variation of windspeeds used in heat transfer model verification. May 15 to 20 1991.

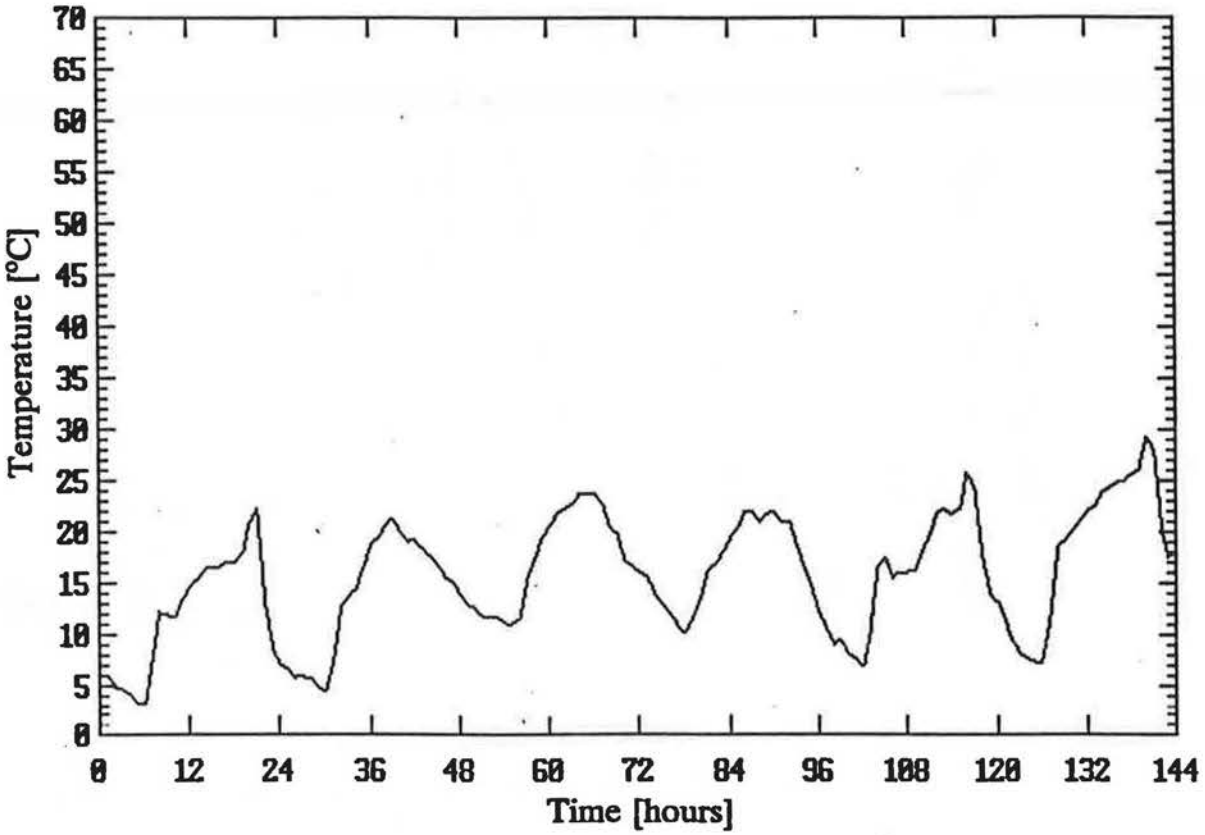

Figure 6-16. Diurnal variation of outdoor temperature used in heat transfer model verification. May 15 to 20 1991.

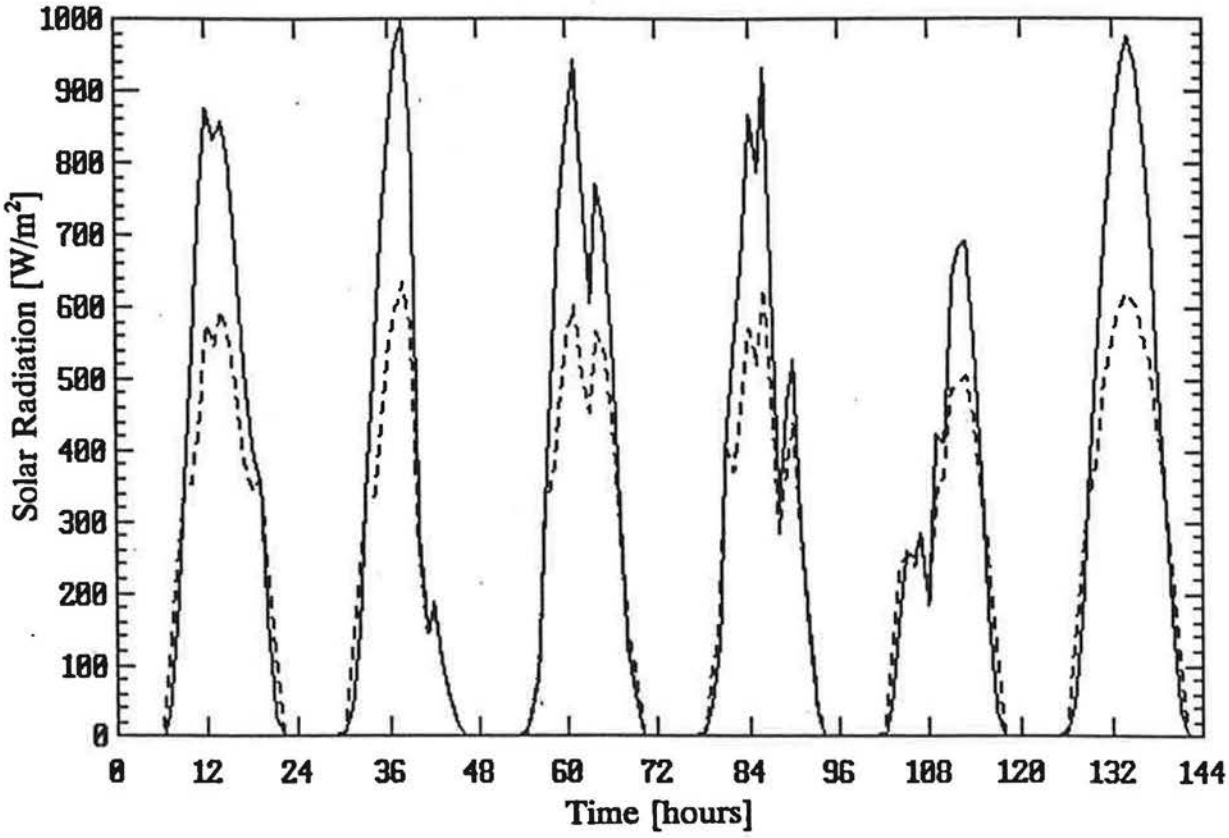

Figure 6-17. Measured incident solar radiation on the north (dashed line) and south (solid line) pitched roof surfaces. May 15 to 20 1991.

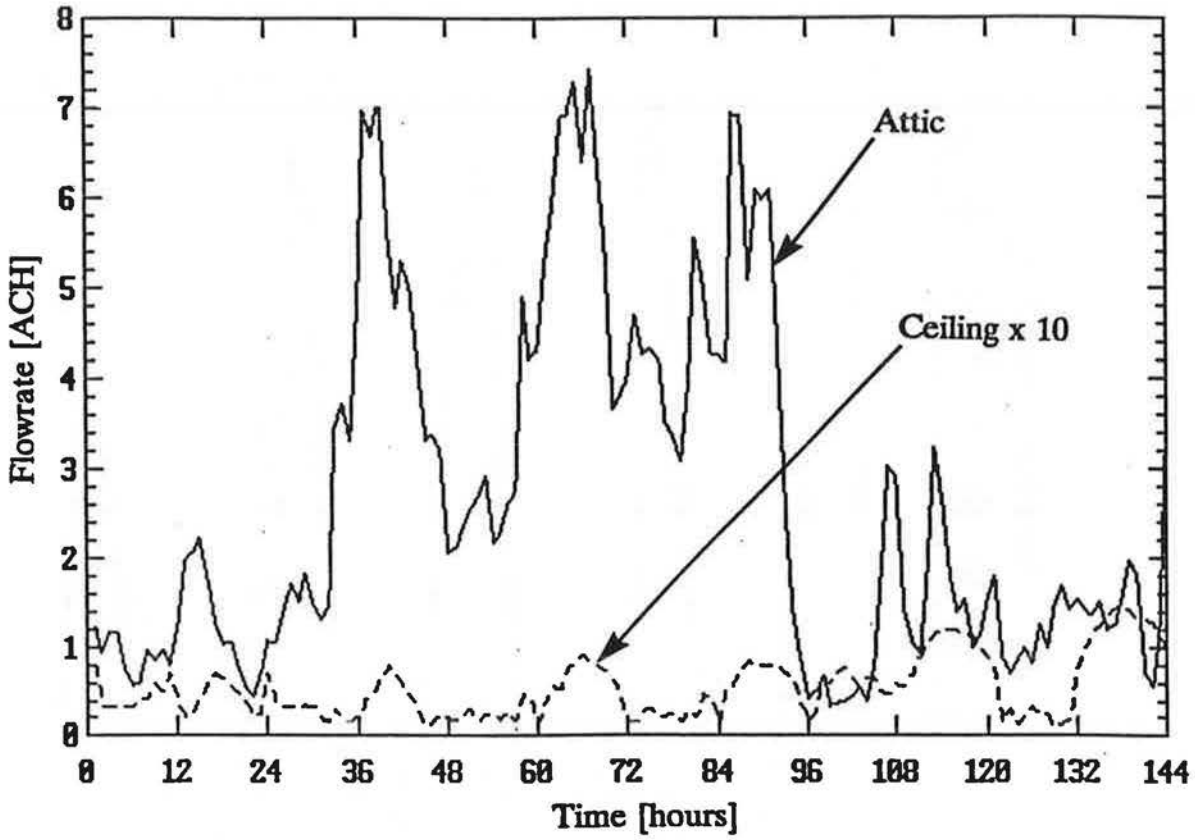

Figure 6-18. Measured attic 5 ventilation rate and flow rate through the ceiling (multiplied by 10). May 15 to 20 1991.

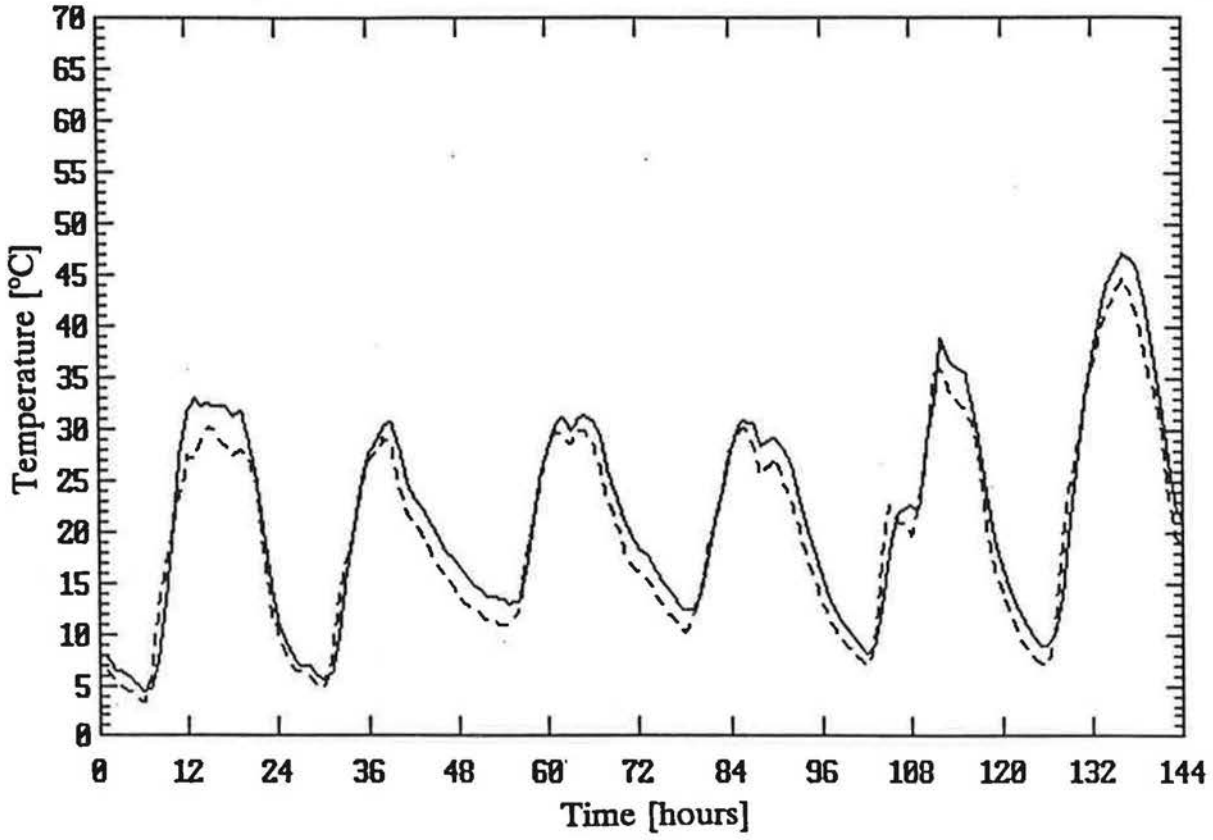

Figure 6-19. Measured (solid line) and predicted (dashed line) attic 5 air temperatures using measured ventilation rates. May 15 to 20 1991.

transfer model with the emissivity of the external sheathing surfaces (the shingles) reduced from 0.9 to 0.5. This reduced the under prediction of night time attic air temperatures by about 0.5 °C but did not make the predicted and measured values the same at night. This is a large and fairly unrealistic change to make in emissivity and it did not completely remove this error, so the emissivity was kept at 0.9 for the shingles. Another source of error is the assumption of the sky being half cloud covered. If night time skies were cloudy then the model would have excessive long wave radiation to the cold night sky resulting in cooler attic temperatures. However, clear skies would mean that the assumed cloud cover leads to over predicted temperatures. Because cloud cover was not measured this effect was not investigated.

Figures 6-20 and 6-21 show the measured and predicted inner and outer south sheathing temperatures, respectively. As expected, the sheathing has even larger diurnal variations with the most variation exhibited by the outer sheathing because it is directly exposed to daytime solar gains and night time radiation losses. The predictions tend to rise and fall more rapidly than the measured values and tend to underpredict the night time temperatures. This seems to indicate that the thermal mass at these nodes should be larger. These nodes in the model only include the mass of the wood and should probably have this increased to include the shingles. The shingles used at the test houses would add approximately 300 Kg of mass to both the sheathing surfaces. ASHRAE (1989), Chapter 37, gives the specific heat of tar and paper as 2500 and 1300 J/KgK, respectively. 2000 J/KgK will be used as an estimate of the specific heat of the shingles. The thermal mass of the sheathing was calculated based on a mass of 51.4 Kg of wood (see Table 4-1) with a specific heat of 1100 J/KgK (ASHRAE (1989), Chapter 37). In the original attic thermal model in Chapter 3, the thermal mass of the shingles was accounted for by simply doubling the thermal mass of the exterior of the sheathing. The values presented here show that this underestimates the thermal mass of the shingles by approximately a factor of 11. Running the thermal model with this increased thermal mass for the shingles has shown that it reduces the mean error in the predictions on average by only 0.03 °C for the sheathing and 0.002 °C for the attic air. The changes in absolute error are much more significant. The outer sheathing temperatures have their absolute error reduced from 3.7°C to 2.8°C by including the extra thermal mass of the shingles. This reduction in absolute error is because the sheathing temperatures do not have as large a diurnal variation when the extra thermal mass is included. Increasing the

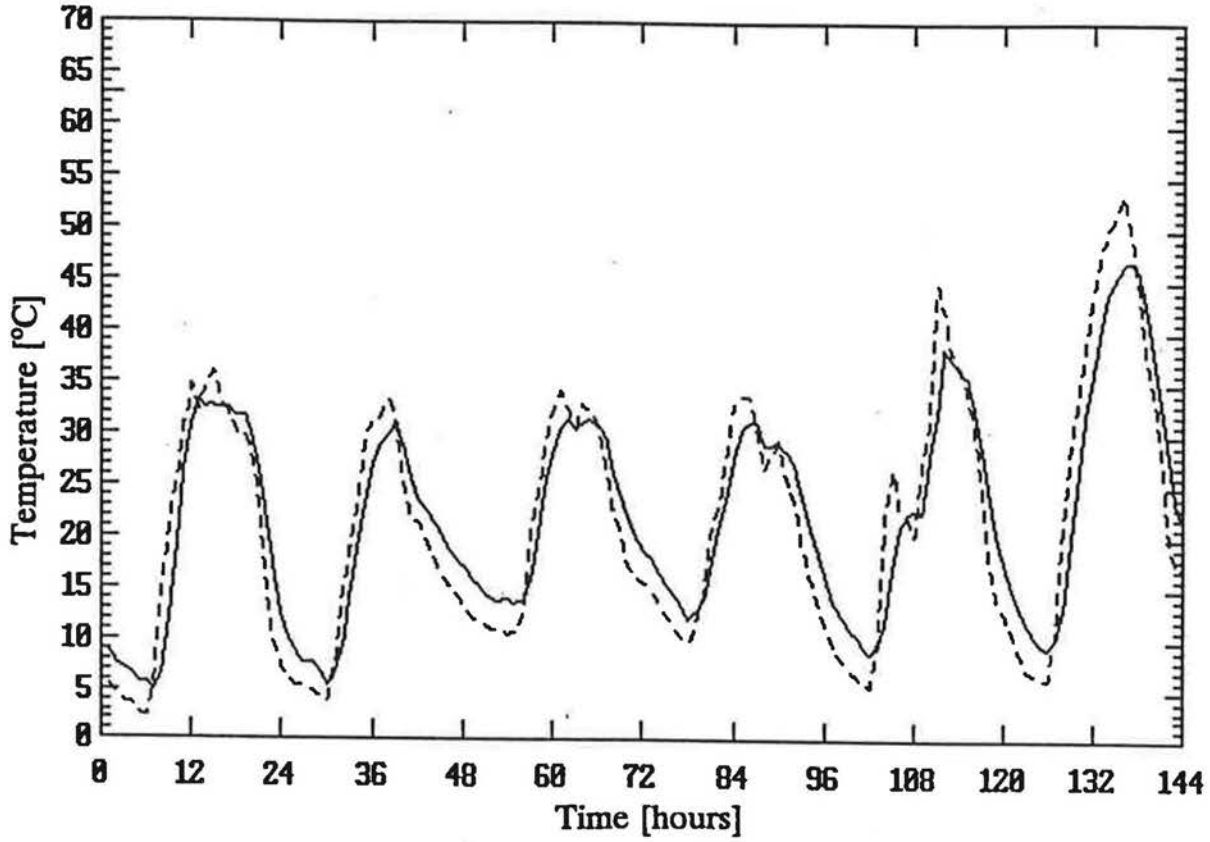

Figure 6-20. Measured (solid line) and predicted (dashed line) inner south sheathing temperatures for attic 5 using measured ventilation rates. May 15 to 20 1991.

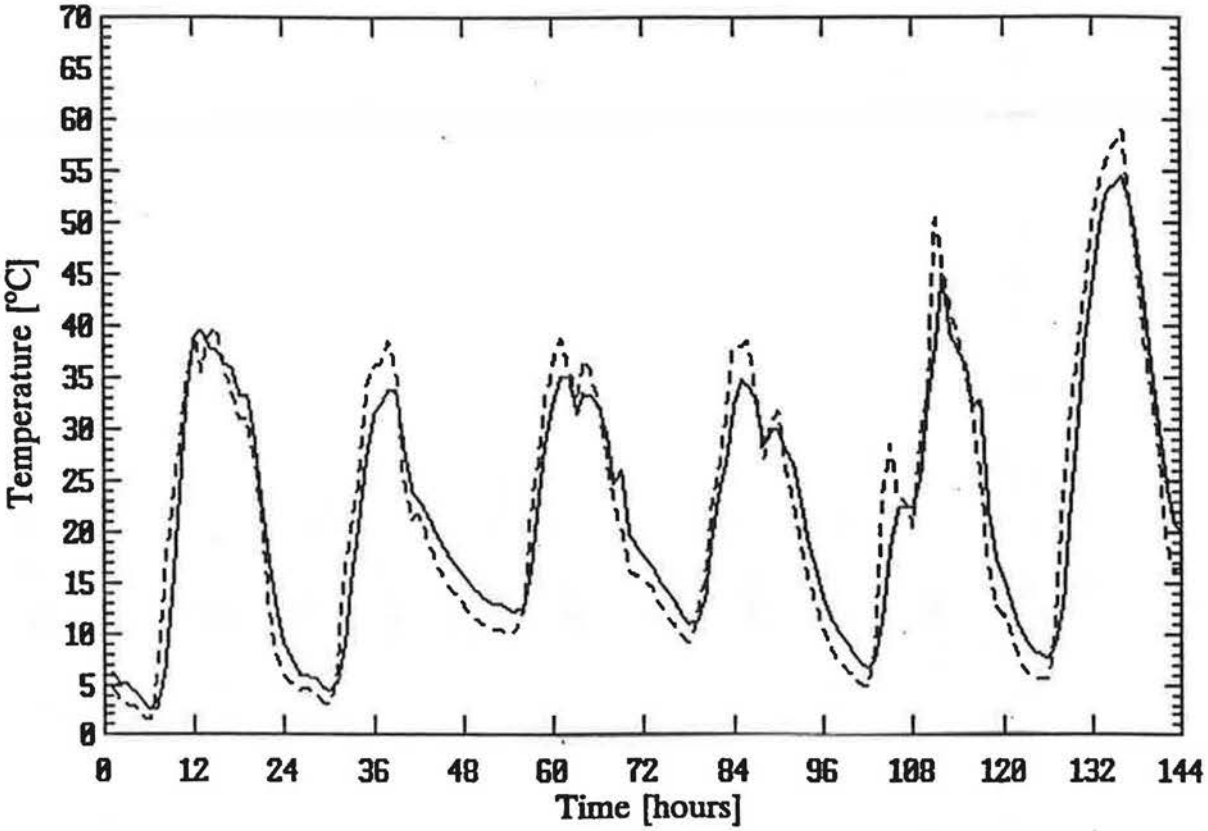

Figure 6-21. Measured (solid line) and predicted (dashed line) outer south sheathing temperatures for attic 5 using measured ventilation rates. May 15 to 20 1991.

thermal mass of the sheathing does not completely prevent the underprediction of night time attic temperatures but it does significantly improve the sheathing temperature predictions.

The north sheathing and the trusses and joists all exhibit similar behaviour and the mean error between measured and predicted temperatures is typically an underprediction of about 1 °C. The magnitude of this error is reasonable considering the assumptions in the model for cloud cover, surface emissivities and heat transfer coefficients. The values of all of these entered parameters and assumptions were not changed in order to make the model results fit the measured data better because the model would then only work for this attic. The mean errors for all node locations are summarised in Table 6-5.

The comparison of measured to predicted attic temperatures was repeated for attic 6. The higher ventilation rates (typically a factor of 4 to 5 larger than in attic 5), make the attic 6 temperatures closer to the outdoor temperature. Figure 6-22 shows measured and predicted values of attic 6 air temperature. These results show less diurnal variation then for attic 5 and the predictions follow the measurements more closely. This is due to the dominant effect of the ventilation rate as it becomes the largest term in the heat balance for the attic air. The attic air exchanges heat with the internal surfaces of the attic and by convective ventilation flows. From Chapter 3, section 3.5, a typical convective heat transfer is $6W/m^2$. The internal area of the attic is approximately $110m^2$ and so the total surface convection heat transfer is about 660W. The attic to outdoor temperature differences and attic ventilation rates measured over the test period shown in Figure 6-22 give ventilation heat transfers of about 500 W to 2000 W. This shows that the heat transfer due to ventilation is as big as or greater than all the surface heat transfer combined in attic 6 under typical conditions. Figures 6-23 and 6-24 show the inner and outer south sheathing temperatures for attic 6 that show the same trends as attic 5. The mean errors for the sheathing are similar to those for attic 5 as shown in Table 6-5.

6.2.2 Using predicted ventilation rates

In this section the combined ventilation and heat transfer models are used to predict attic temperatures. This is an iterative process where a calculated ventilation rate is used to find attic temperatures. The attic air temperature is then used to calculate a new attic air density and stack effect in the ventilation model. The ventilation rate is a weak function of attic temperature (see Chapter 5, section 5.3.1 and Figure 5-16) and the calculations seldom require more than five iterations.

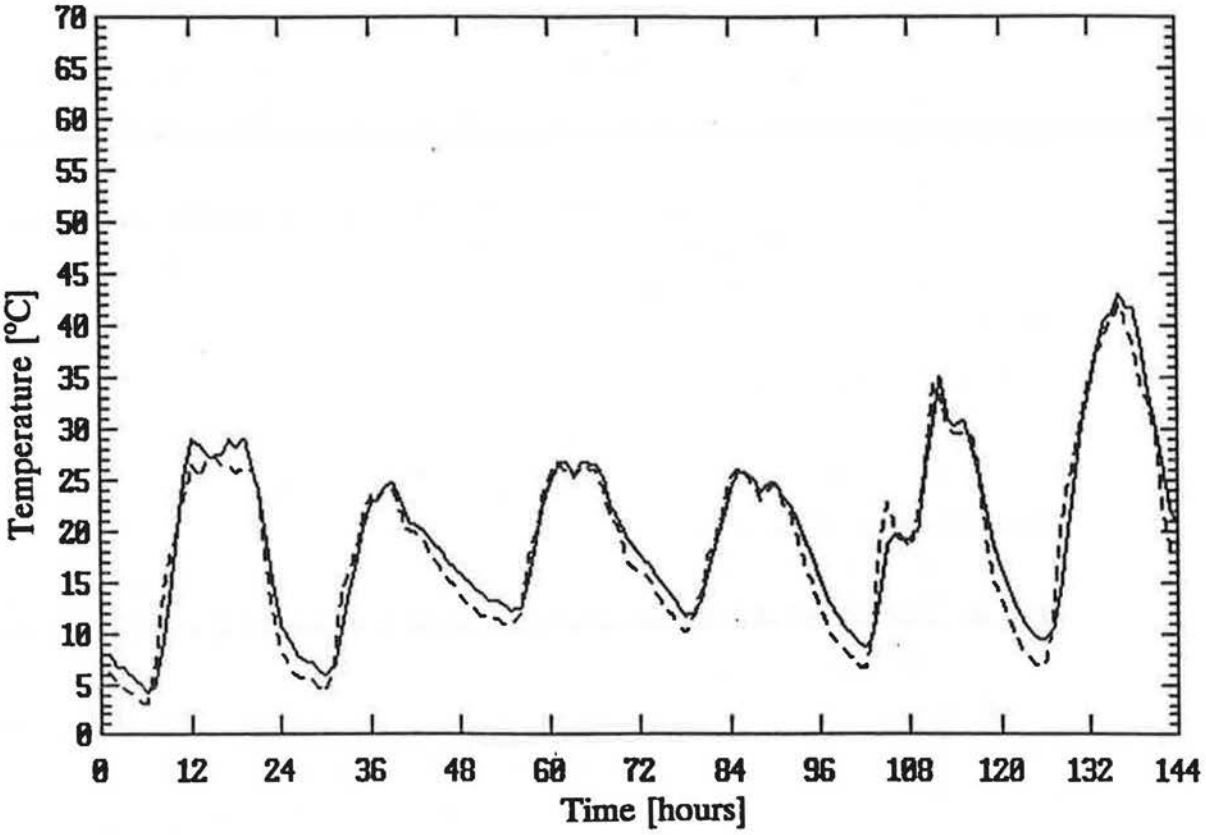

Figure 6-22. Measured (solid line) and predicted (dashed line) attic 6 air temperatures using measured ventilation rates. May 15 to 20 1991.

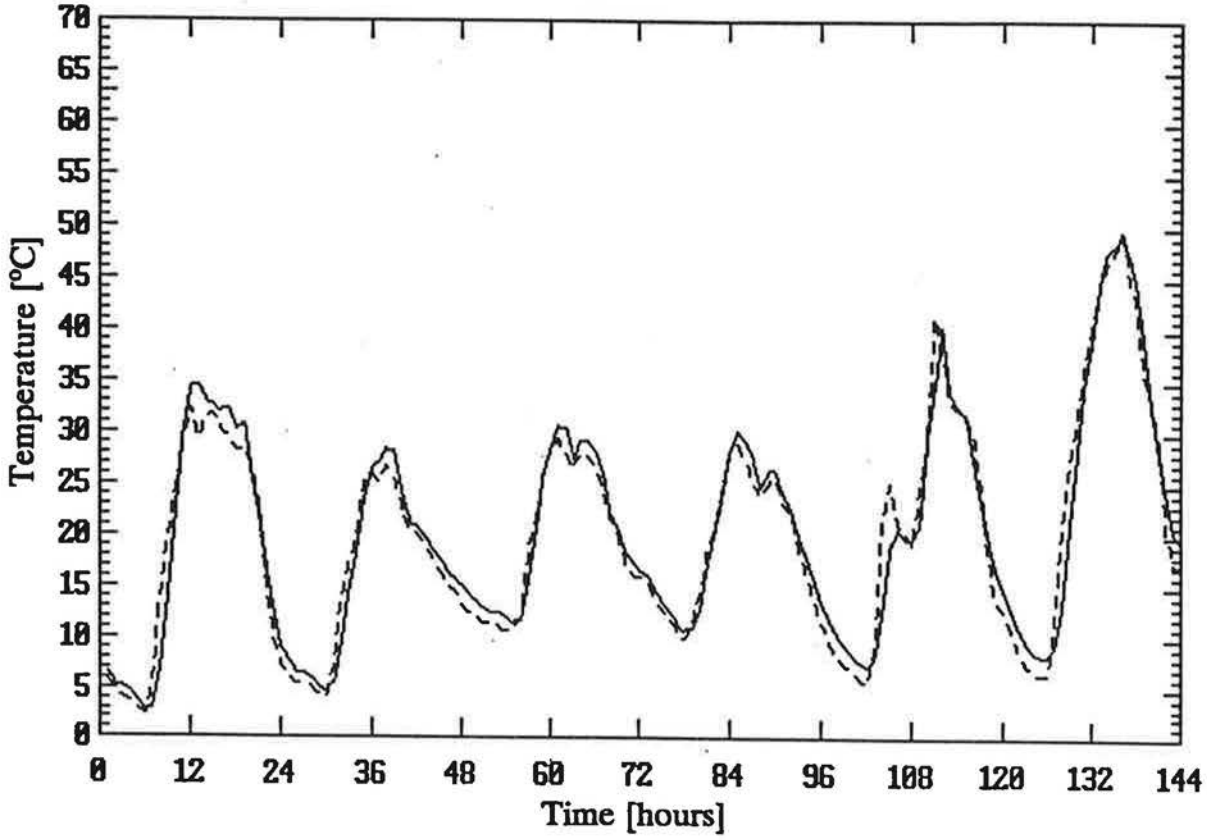

Figure 6-23. Measured (solid line) and predicted (dashed line) inner south sheathing temperatures for attic 6 using measured ventilation rates. May 15 to 20 1991.

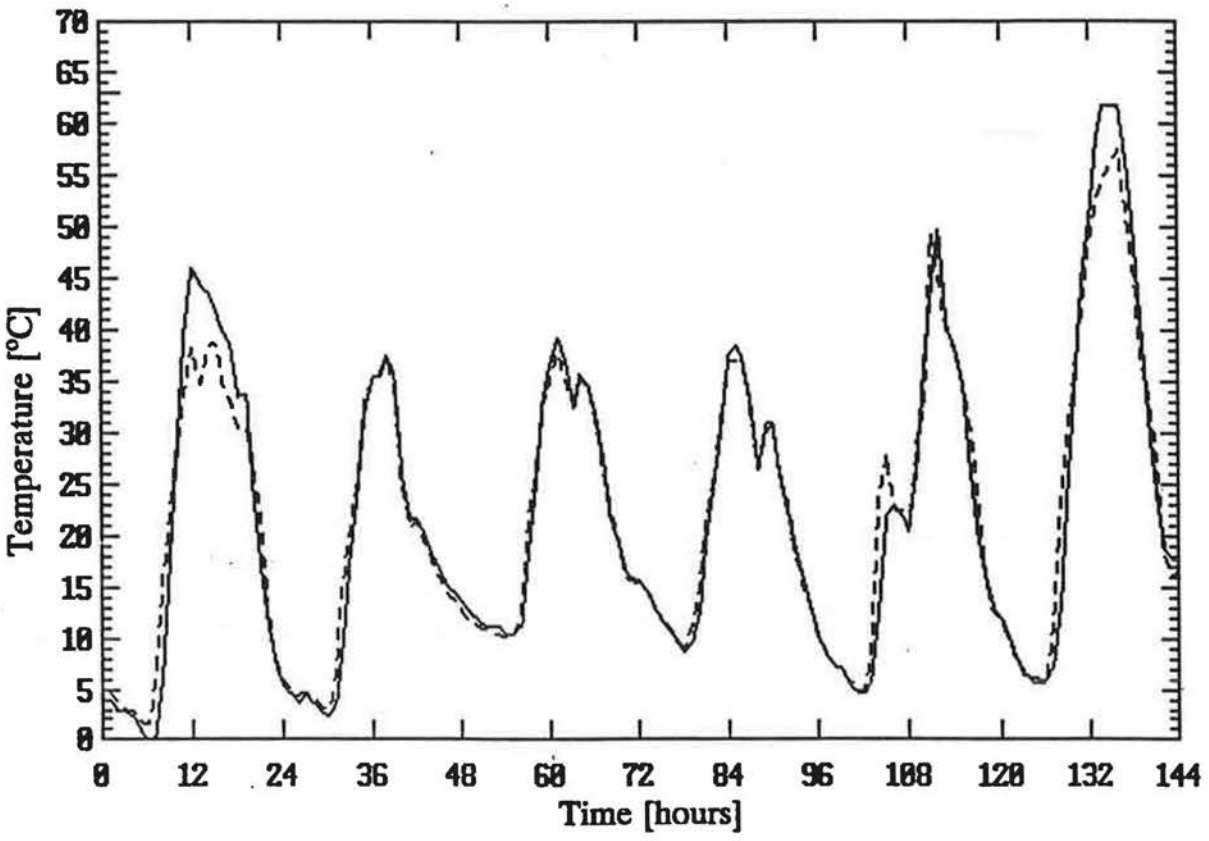

Figure 6-24. Measured (solid line) and predicted (dashed line) outer south sheathing temperatures for attic 6 using measured ventilation rates. May 15 to 20 1991.

Table 6-5. Errors for predicted temperatures from May 15 to 20, 1991, for attics 5 and 6.

Node Location	Using Measured Attic Ventilation Rates with $\epsilon = 0.9$	Using Measured Attic Ventilation Rates with $\epsilon = 0.5$	Using Predicted Attic Ventilation Rates, $\epsilon = 0.9$		Using Predicted Attic Ventilation Rates, $\epsilon = 0.9$ No thermal masses	
	Mean [°C]	Mean [°C]	Mean [°C]	Abs. [°C]	Mean [°C]	Abs. [°C]
Attic 5						
Air	-1.60	-0.90	-0.68	1.75	-0.70	3.57
Inside South Sheathing	-0.46	0.50	0.55	4.33	0.55	5.32
Outside South Sheathing	0.06	1.08	0.96	3.85	0.96	4.30
Inside North Sheathing	-2.04	-1.27	-1.14	2.75	-1.14	3.72
Outside North Sheathing	-0.96	-0.06	-0.23	4.15	-0.23	4.59
Truss	-1.60	-1.05	-0.74	1.80	-0.85	4.0
Attic 6						
Air	-0.79	-0.84	-0.51	-	-	-
Inside South Sheathing	-0.38	-0.79	1.10	-	-	-
Outside South Sheathing	-0.05	2.83	0.93	-	-	-
Inside North Sheathing	-0.56	0.43	0.61	-	-	-
Outside North Sheathing	-0.40	0.54	0.34	-	-	-
Truss	-0.68	-0.70	-0.46	-	-	-

Figure 6-25 shows predicted and measured attic 5 air temperatures using predicted attic ventilation rates. Comparing this figure to Figure 6-19 shows that predicted ventilation rates gave temperatures within about 1°C of those using measured ventilation rates. For all the temperature predictions made using predicted ventilation rates in attic 5 the mean absolute error has been calculated in addition to the mean error and are shown for each node location in Table 6-5. For the data in Figure 6-25 the mean error is -0.68°C and the absolute error is 1.75°C. Figures 6-26 and 6-27 show the measured and predicted temperatures for the inside and outside

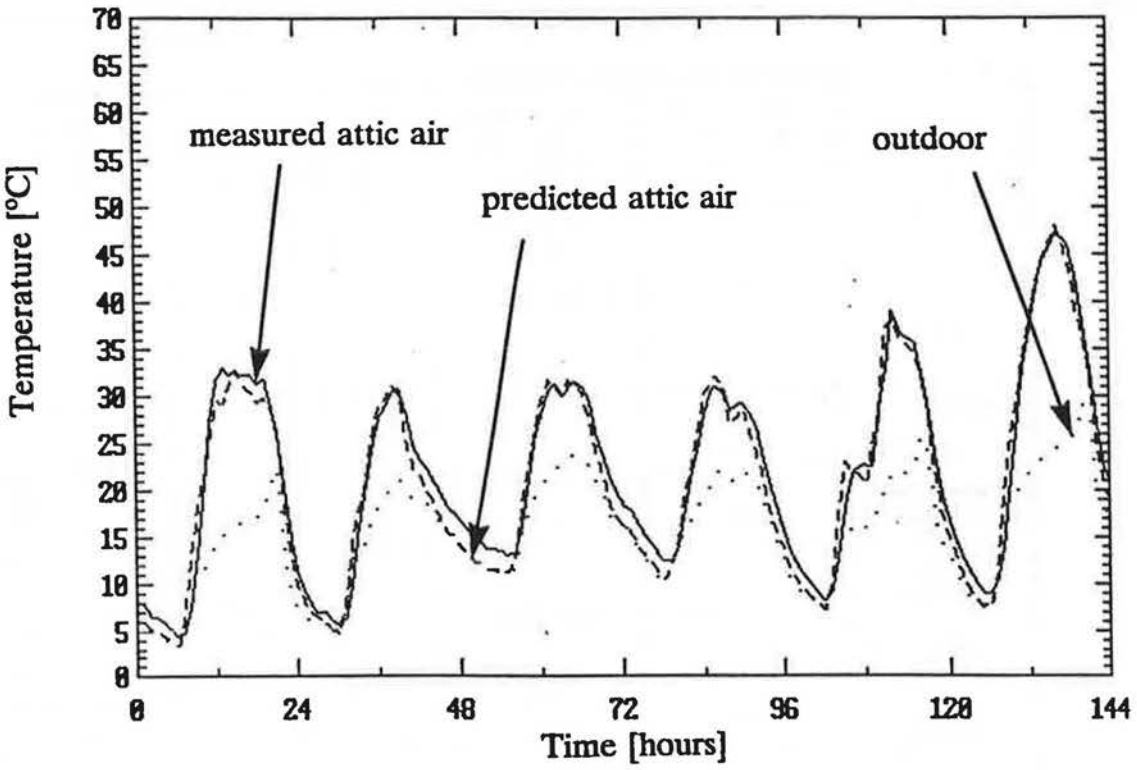

Figure 6-25. Measured (solid line) and predicted (dashed line) attic 5 air temperature and outdoor temperature (dotted line) using predicted ventilation rates. May 15 to 20 1991.

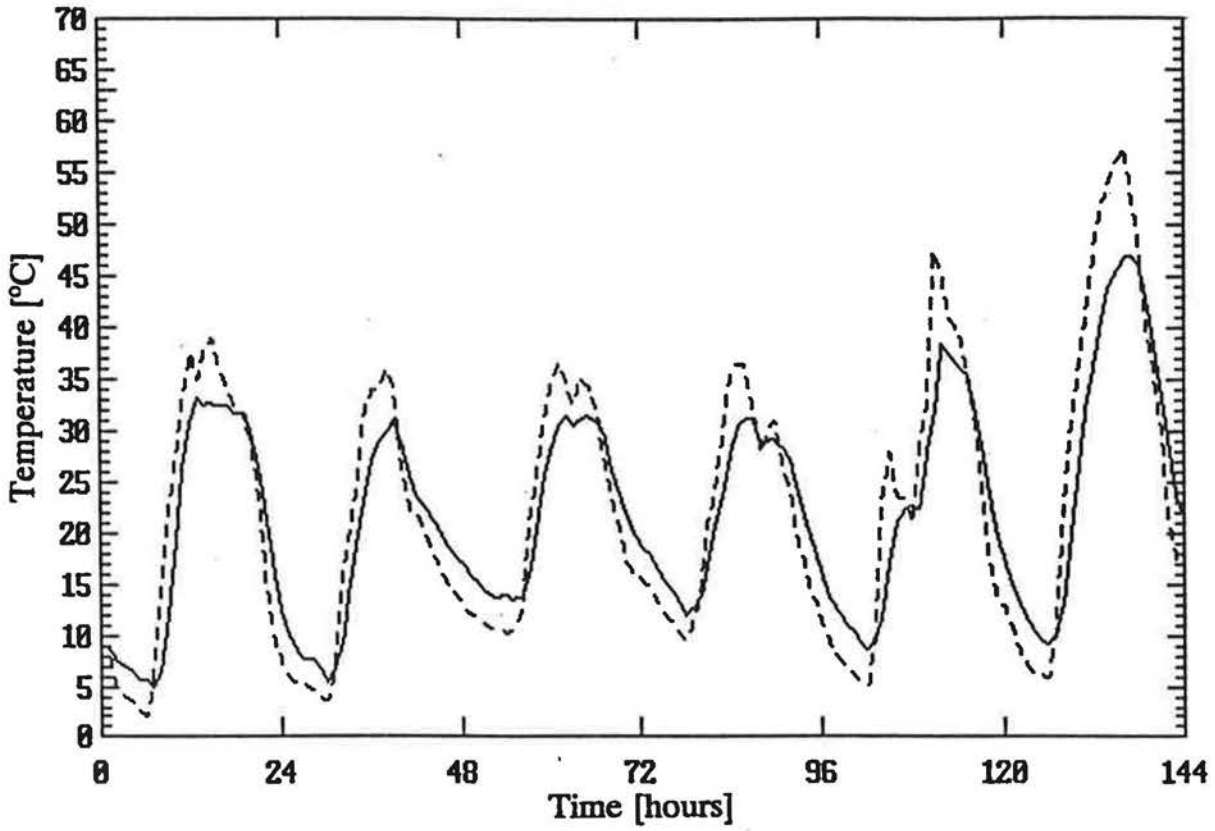

Figure 6-26. Measured (solid line) and predicted (dashed line) inner south sheathing temperatures for attic 5 using predicted ventilation rates. May 15 to 20 1991.

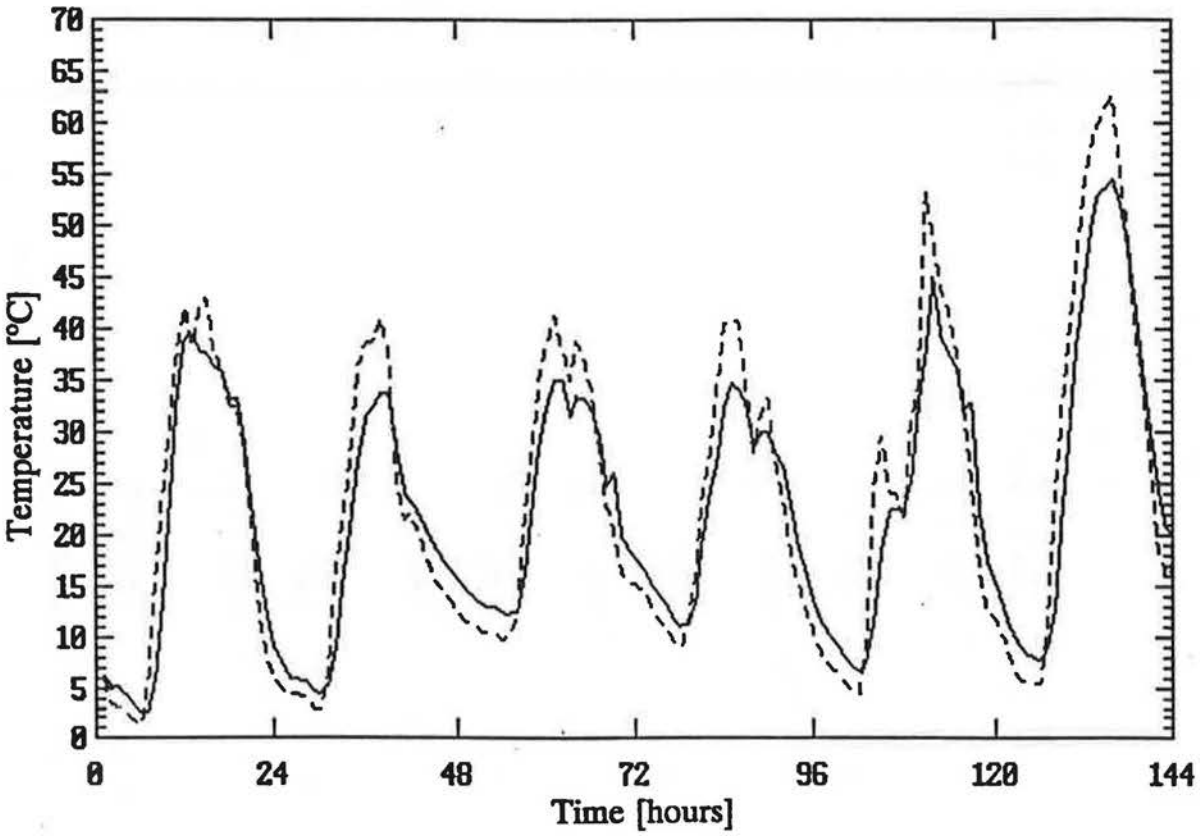

Figure 6-27. Measured (solid line) and predicted (dashed line) outer south sheathing temperatures for attic 5 using predicted ventilation rates. May 15 to 20 1991.

of the south sheathing respectively. These figures show that there is a greater variation in predicted temperatures during the day when using the predicted attic ventilation rate compared with the results shown in Figures 6-18 and 6-19 using measured ventilation rates. This is due to underprediction of attic ventilation rates during the test period that makes the ventilation term in the attic air heat balance and the surface heat transfer coefficients too small. This results in predicted temperatures that deviate more from the outdoor temperature. Figure 6-25 also includes the outdoor temperature. Although the outdoor temperature displays a diurnal cycle, the magnitude of the cycle is much less than for the attic air. This shows the skill of the combined ventilation and heat transfer model for predicting the difference between attic and outdoor air temperatures.

Figures 6-28 to 6-30 show the predicted and measured temperatures in attic 6 for the attic air and inside and outside south sheathing respectively using predicted attic ventilation rates. The results are similar to attic 5 where underestimation of attic ventilation rate causes larger diurnal variations in air and sheathing temperatures than when using measured ventilation rates. However, in attic 6 the measured ventilation rates are greater than 20 ACH for most of the middle three days. As discussed earlier in the measurements chapter, these ventilation rates are overpredicted by the measurement system. This measurement error will account for some of the difference between the temperatures calculated using measured and predicted ventilation rates in attic 6. The errors in predicting temperatures in attic 6 using measured ventilation rates are shown in Table 6-5.

The outdoor temperature is included in Figure 6-28. As with the attic 5 results shown in Figure 6-25 the diurnal cycle of outdoor temperature is less than the attic air. Because the ventilation rates are higher in attic 6, the attic air temperatures are closer to the outdoor temperature than for attic 5. Figure 6-28 shows how the combined ventilation and heat transfer model is able to predict the effect of changing attic leakage on attic air temperatures.

The thermal model has also been run for attic 5 with the thermal mass terms set to zero which is equivalent to assuming a steady-state solution. Table 6-5 shows that the mean errors are almost the same (within 0.02 °C) as with the thermal masses included, but the absolute error increases. The effect is largest for the nodes with the greatest thermal masses which are the attic air and the trusses where the steady state assumption more than doubles the absolute error. This increase in absolute error occurs because ignoring the thermal masses makes the diurnal swings in temperature

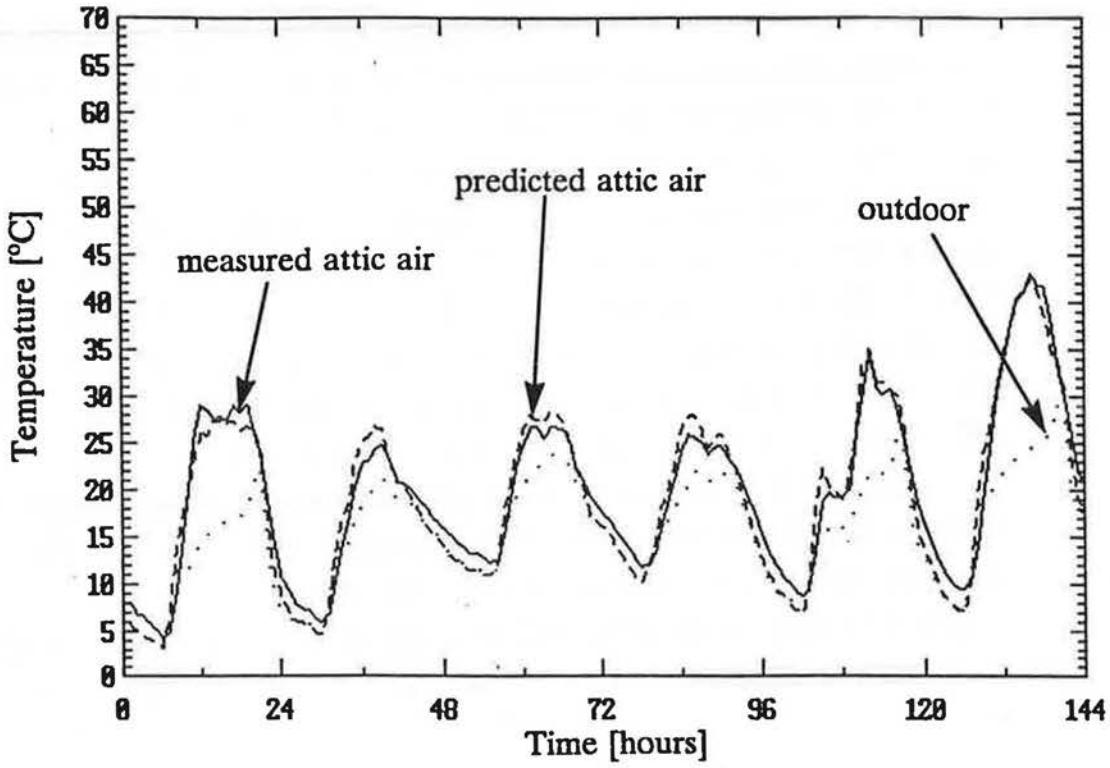

Figure 6-28. Measured (solid line) and predicted (dashed line) attic 6 air temperature and outdoor temperature (dotted line) using predicted ventilation rates. May 15 to 20 1991.

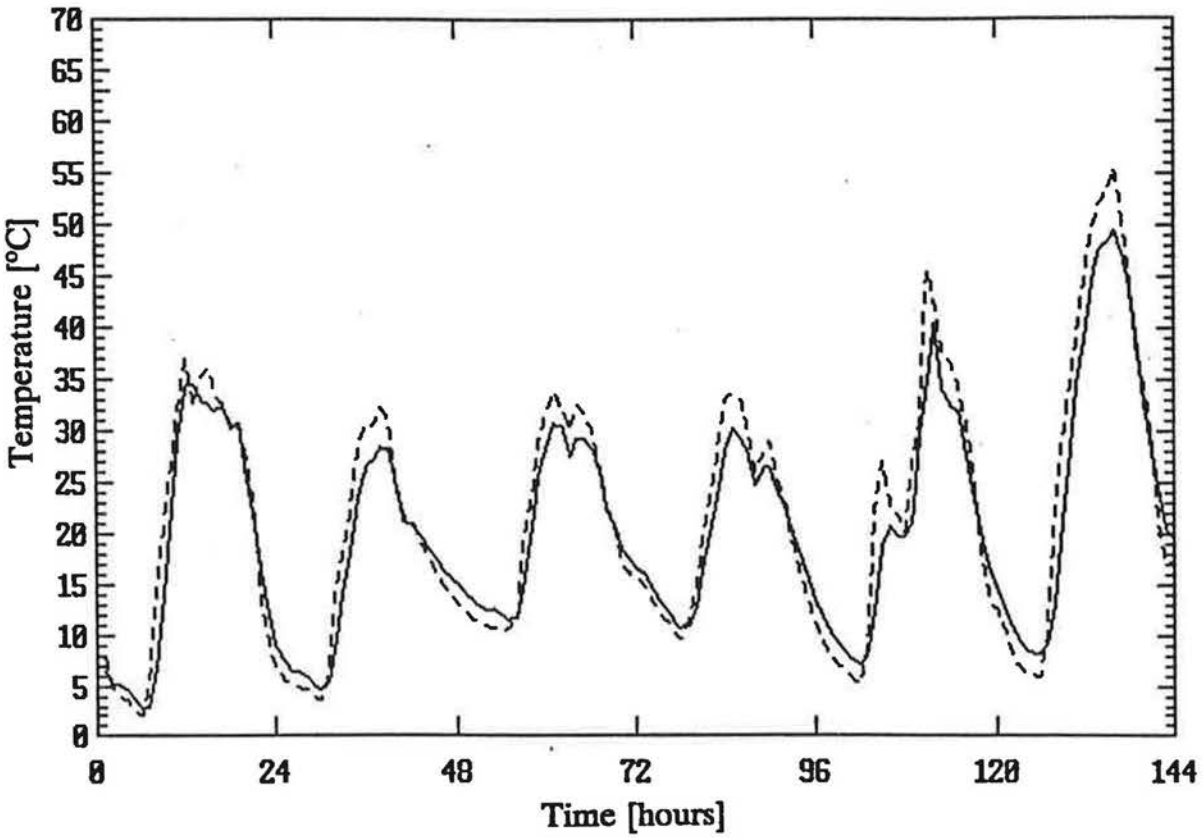

Figure 6-29. Measured (solid line) and predicted (dashed line) inner south sheathing temperatures for attic 6 using predicted ventilation rates. May 15 to 20 1991.

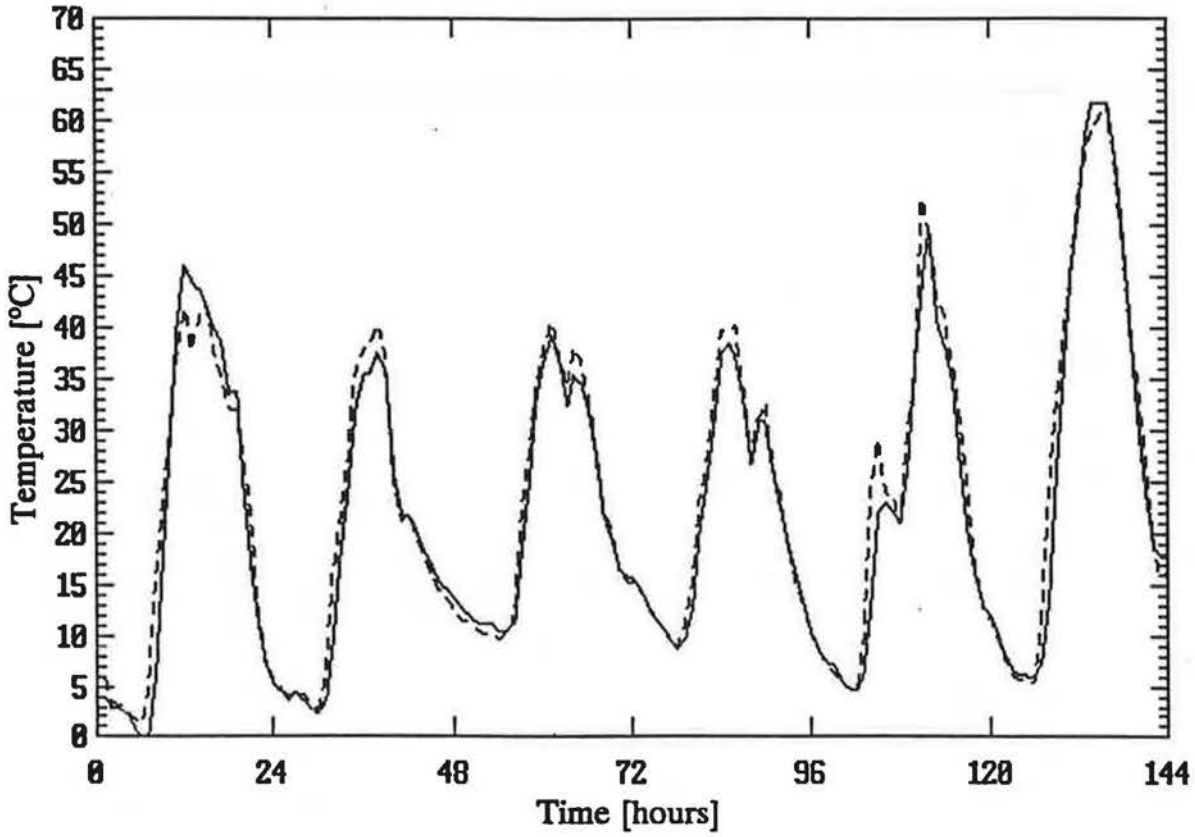

Figure 6-30. Measured (solid line) and predicted (dashed line) outer south sheathing temperatures for attic 6 using predicted ventilation rates. May 15 to 20 1991.

larger and also shifts the predictions forward in time since the nodes respond too rapidly to the changing thermal environment. This is illustrated in Figures 6-31 and 6-32 which show the diurnal variation in truss temperatures. The thermal mass term was included in the predictions in Figure 6-31 and with steady-state assumed in Figure 6-32.

6.3 Moisture transport model

Ideally the moisture transport model predictions for surface wood moisture content and condensation should be compared with measured values. As yet there is no reliable method of measuring these quantities with an automated data acquisition system so the verification of the moisture transport model will be based on comparisons to the measured attic air relative humidity (RH) (and the derived vapour pressure (P_w)) and the wood moisture content (W_{MC}) of the underlying wood. This is still a vigorous test of the model because the attic air is the most active node for moisture transport in the attic.

The moisture transport model uses the ventilation rates and the temperatures calculated by the ventilation and heat transfer models. Additional inputs include the ambient and house interior relative humidity, both of which were measured at the test site, and initial estimates of attic relative humidity, wood moisture content and condensed mass at each node. For the purposes of verification the initial moisture conditions for the inner wood nodes are given by the first measured value for each test. The initial condensed masses are set to zero for each surface. The initial relative humidity is taken from the first measured value. The surface wood moisture contents must be estimated because they were not measured. For winter conditions in attic 6 the initial surface wood moisture content is set equal to the inner wood moisture content and for spring or summer conditions an extra 5% wood moisture content is added to the inner wood moisture content. For attic 5, 5% is added to the inner wood moisture content to obtain estimates of the surface moisture content in all seasons. These values were chosen based on the providing the smallest initial transient when the model verifications were performed.

The effects of poor initial wood moisture content estimates are easily seen in the model predictions. For example, if an initial estimate of 20% wood moisture content is made for the surface layer in winter the vapour pressure, wood moisture content and temperature relationship used in this model shows that much of this moisture will condense out at low temperatures because the saturation wood moisture

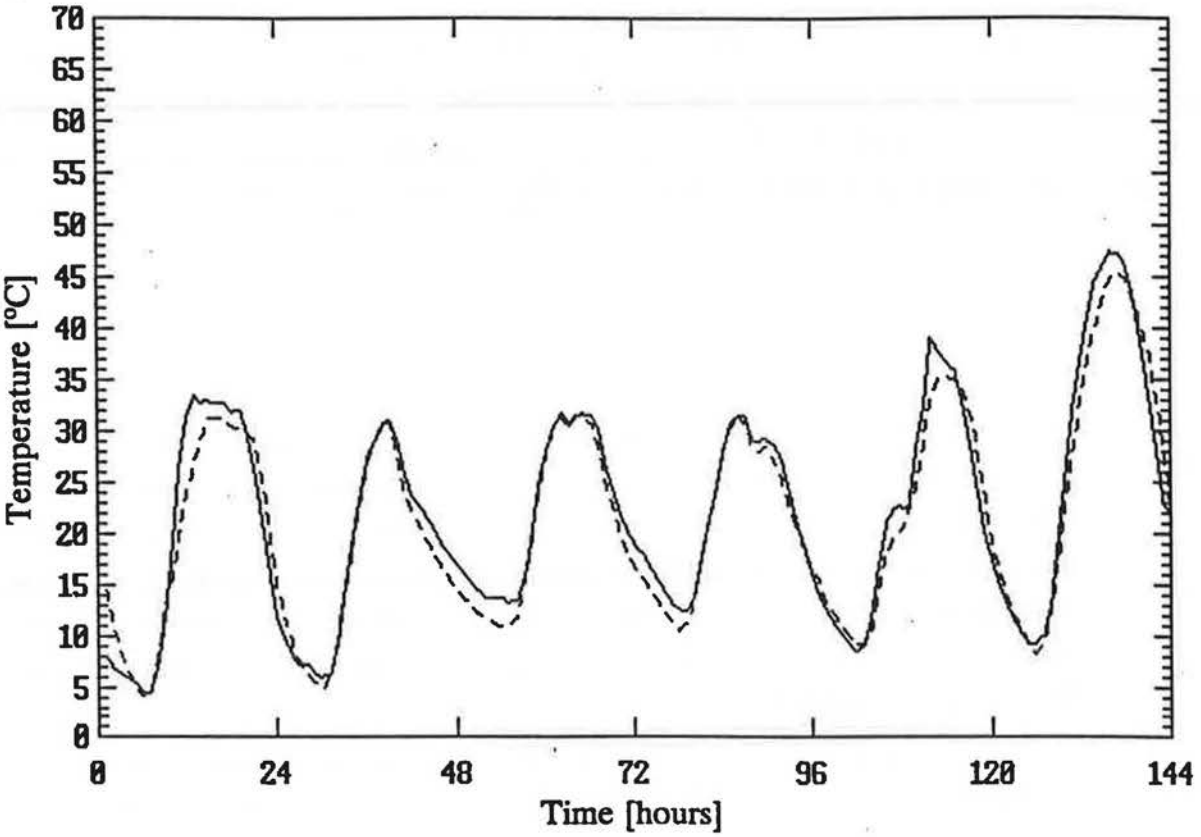

Figure 6-31. Measured (solid line) and predicted (dashed line) attic 5 truss temperatures including thermal masses. May 15 to 20 1991.

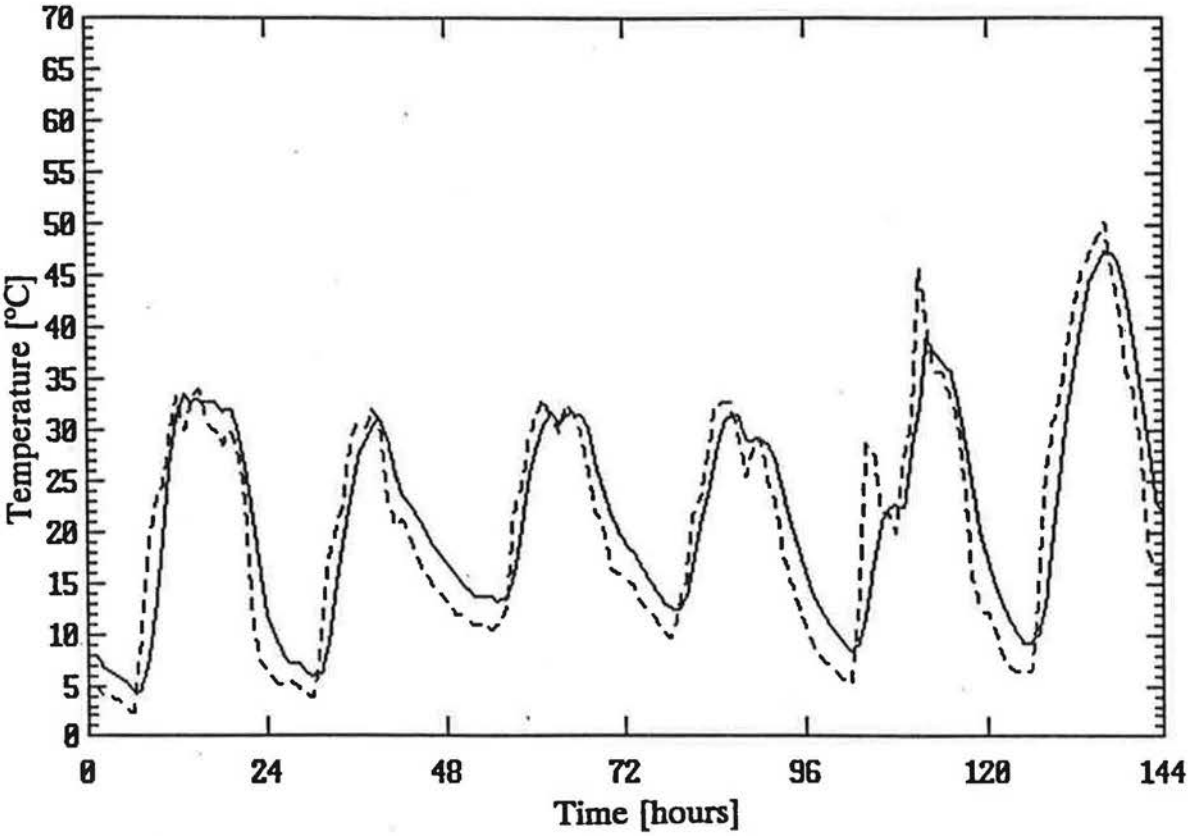

Figure 6-32. Measured (solid line) and Predicted (dashed line) attic 5 truss temperatures assuming steady state. May 15 to 20 1991.

content is about 10%. This condensed mass will evaporate over time and model simulations, performed later in Chapter 7, have shown that the model predictions are independent of the initial conditions after about one week. Smaller errors in estimating initial wood moisture will disappear over a shorter time so that an estimate within a couple of percent will have a negligible effect on model predictions. This shows that the verification procedure and model simulations (in Chapter 7) will not be systematically biased by initial wood moisture content estimates.

6.3.1 Internal wood moisture content

Figure 6-33 shows measured internal wood moisture content for north sheathing, south sheathing and for the joists in attic 5 for winter conditions where the average outdoor temperature is -24°C. All these measured moisture contents stay relatively constant between 5% and 7%. Due to the lower limit of the measuring instrument all that can be said about these values is that they are less than about 7%. These low values of measured wood moisture content for internal wood occur in all seasons in both attics. The only way this measured data can be used to verify the model is if the model always predicts low wood moisture content.

Figure 6-34 shows predicted internal wood moisture content in attic 5 for the same time period as Figure 6-33. These predicted wood moisture contents remain low and change very slowly. The model predicts that the inner wood remains at low wood moisture content for both attics over all weather conditions. This relatively constant low value of wood moisture content corresponds with the measured wood moisture contents but this does not verify any of the dynamic performance of the model.

6.3.2 Attic air relative humidity and vapour pressure

Attic relative humidity and temperature were measured at the test facility (AHHRF) and are used to calculate an equivalent vapour pressure that will be used here as the measured vapour pressure. In order to test the model over a wide range of conditions three sets of data were used to verify the relative humidity and vapour pressure predictions. The three sets of data are for summer, spring and winter conditions, with each set being six days long. The range of weather conditions covered by these data sets are summarised in Table 6-6 and show the wide range of mean outdoor temperatures from -24°C to 20°C. These are average values for the six days of each test. The diurnal temperature variation means that the total temperature range based on individual hours is -40°C to 30°C. A large range of measured ventilation rates is also covered ranging from 0.2 to about 60 ACH. As

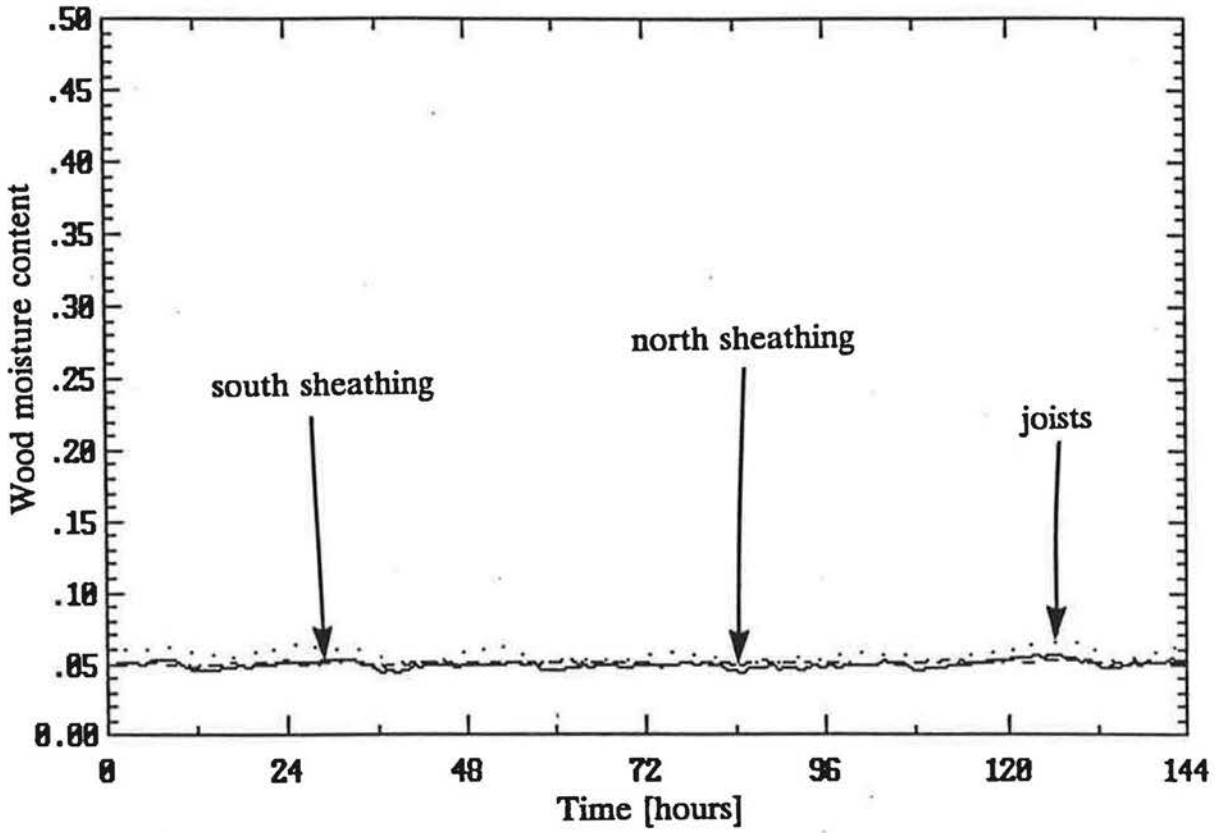

Figure 6-33. Measured internal wood MC for south sheathing (solid line), north sheathing (dashed line) and for the joists (dotted line) in attic 5 for winter conditions where the average outdoor temperature is -24°C. January 1 to 6 1991.

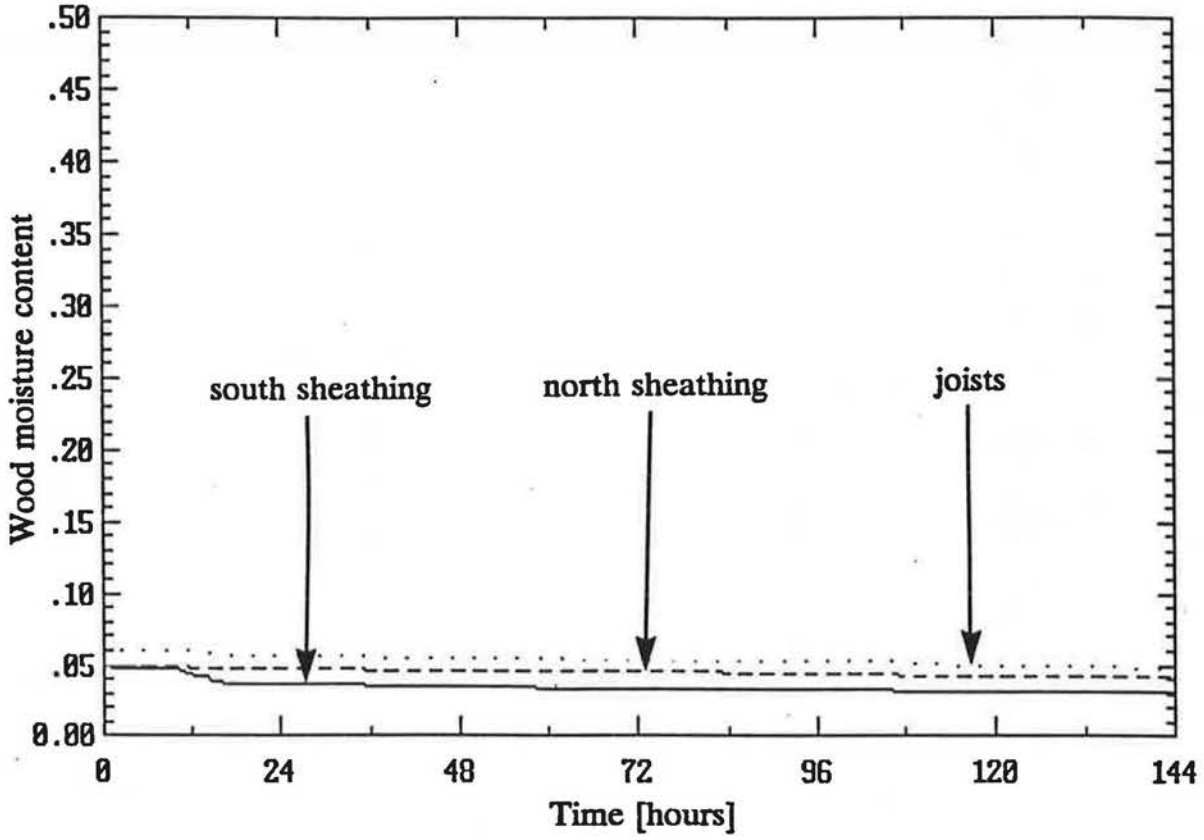

Figure 6-34. Predicted internal wood MC for south sheathing (solid line), north sheathing (dashed line) and for the joists (dotted line) in attic 5 for the same time period as figure 6-33 (January 1 to 6 1991).

discussed previously, in Chapter 5, the measured ventilation rates above about 20 ACH have a great deal of uncertainty due to incomplete mixing of the tracer gas so the maximum ventilation is more realistically about 30 ACH.

Attic air relative humidity

Figures 6-35, 6-36 and 6-37 show the measured and predicted attic air relative humidity for attic 5 for the summer, spring and winter data sets respectively. The sharp spikes in Figures 6-35, 6-38, 6-41 and 6-43 are due to data acquisition system errors. Both the summer and spring measured and predicted values show strong diurnal variations in attic air relative humidity because it is decreased by the higher attic air temperatures during the day. Both the vapour pressure and saturation pressure change during the day but the saturation pressure has a larger effect due to its strong temperature dependence. In order to highlight the measurements the individual measured data points for the spring (Figure 6-36) are shown in Figure 6-36B. In all the other figures in this section the individual data points are not shown and the measured values are connected by a solid line. For the winter data in Figure 6-37 the predicted relative humidity still shows a strong diurnal variation with the attic air becoming saturated (100% RH) for the last two nights of the test. The measured data in this figure do not show these same variations. This may be due to poor sensor response at low temperatures or weather conditions such as snow on the roof. Snow on the roof reduces the daytime solar gains due to reduced external surface absorbtivity and reduces night time losses because it forms an insulating blanket. The snow cover is not included in the model validations because snow depth on the roof was not measured. The effect of a snow layer on the roof will be examined using simulations in Chapter 7. The differences between measured and predicted relative humidity for the winter data set may also be because small errors in attic vapour pressure and temperature can cause large changes in relative humidity for winter data where vapour pressures are low. The mean error for attic 5 relative humidity predictions is about -2.5% RH with an absolute error of about 5% RH. These absolute errors do not include the larger errors from the winter data. The results of the attic 5 relative humidity predictions are summarized in Table 6-6.

Figures 6-38, 6-39 and 6-40 show the measured and predicted data for attic 6 in summer, spring and winter. There is more diurnal variation in relative humidity in attic 6 because the higher ventilation rate makes the attic air vapour pressure more like the outdoor air. This leads to less variation in vapour pressure. The combination of similar diurnal temperature and saturation pressure variations and

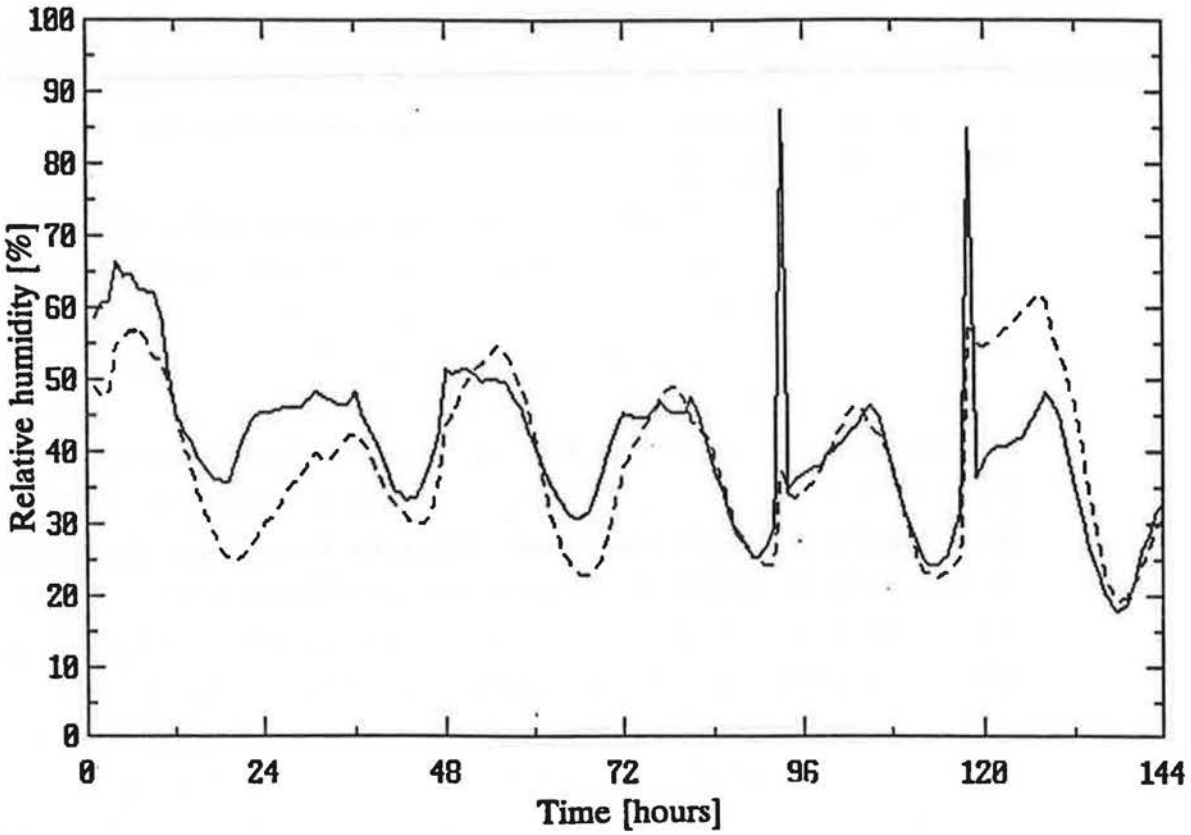

Figure 6-35. Measured (solid line) and predicted (dashed line) attic air relative humidity for attic 5 in the summer. August 13 to 18 1991.

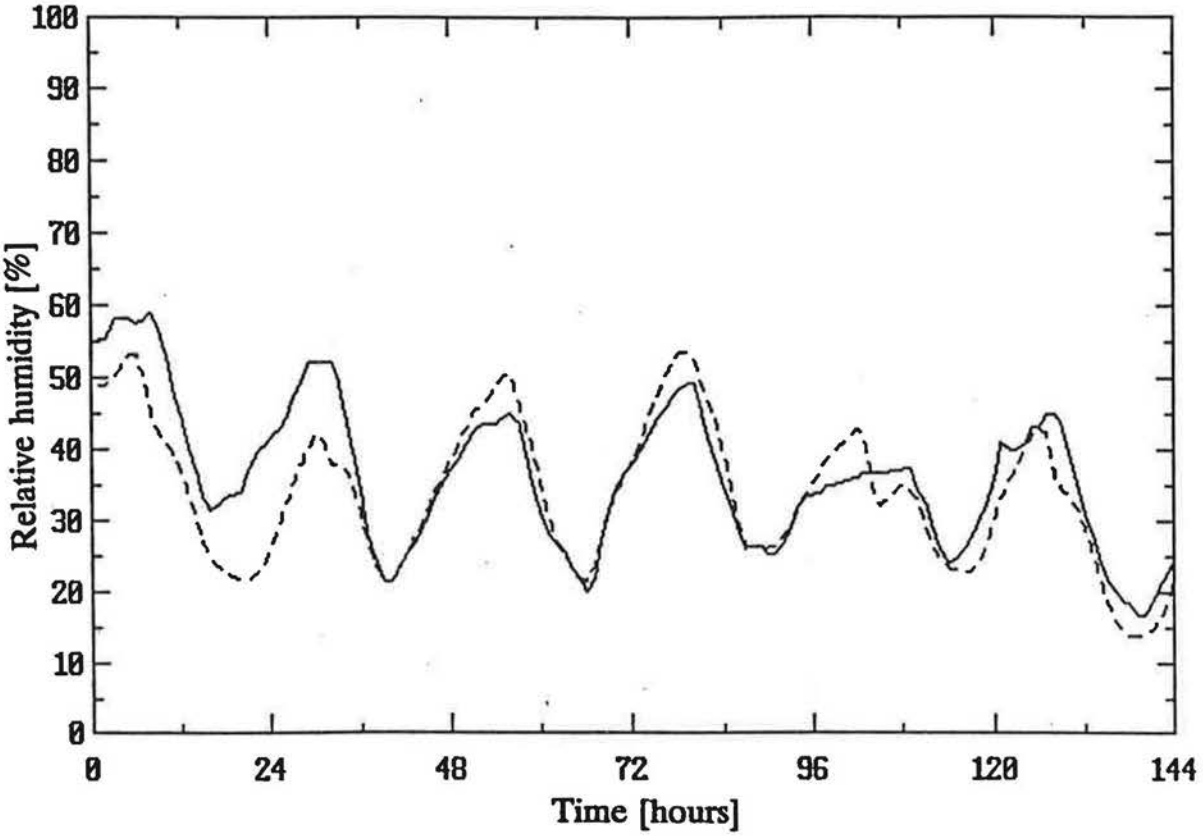

Figure 6-36. Measured (solid line) and predicted (dashed line) attic air relative humidity for attic 5 in the spring. May 15 to 20 1991.

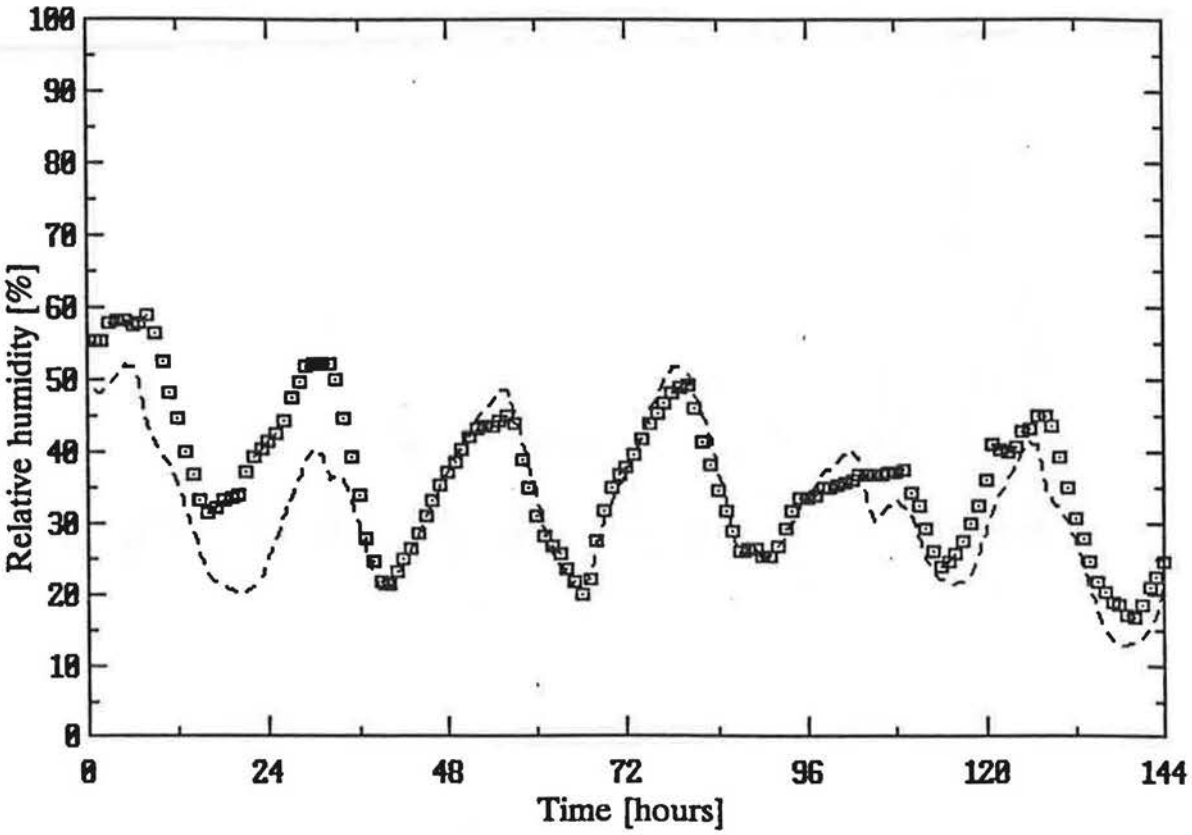

Figure 6-36B. Measured (points) and predicted (dashed line) attic air relative humidity for attic 5 in the spring showing individual data points. May 15 to 20 1991.

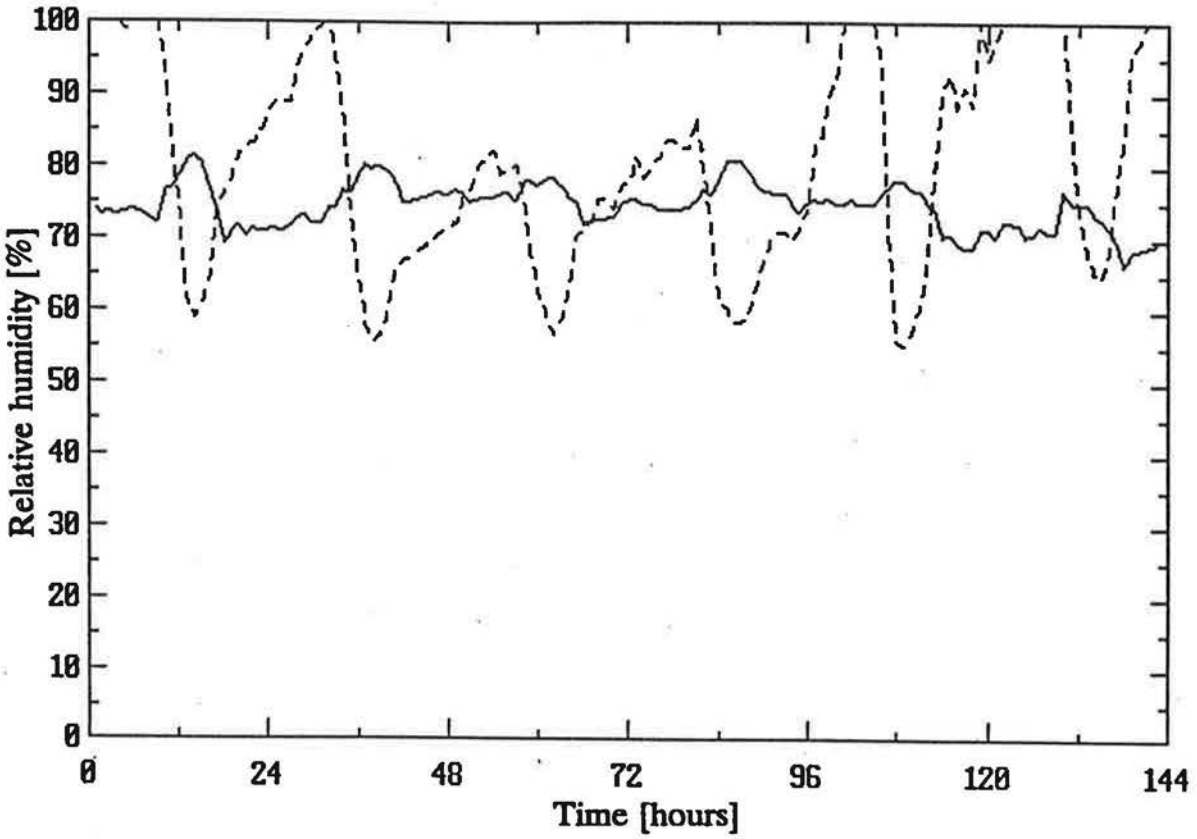

Figure 6-37. Measured (solid line) and predicted (dashed line) attic air relative humidity for attic 5 in the winter. January 1 to 6 1991.

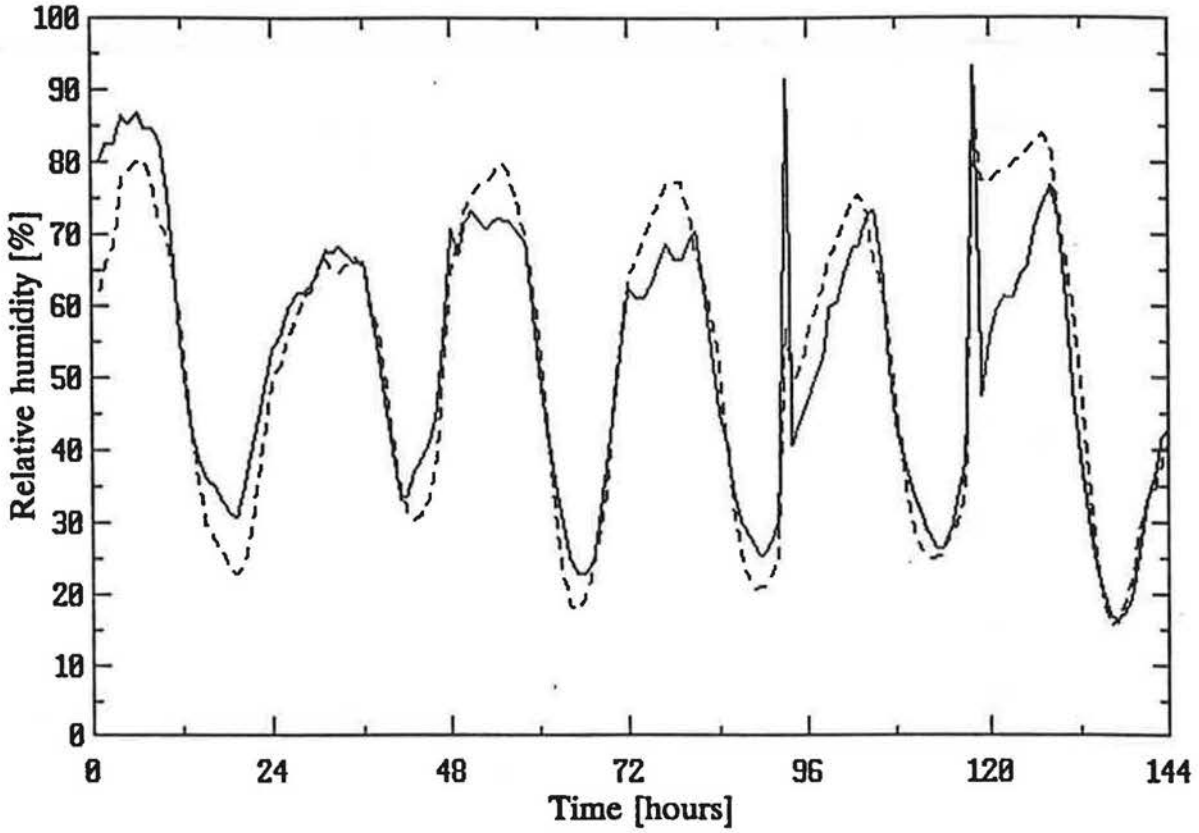

Figure 6-38. Measured (solid line) and predicted (dashed line) attic air relative humidity for attic 6 in the summer. August 13 to 18 1991.

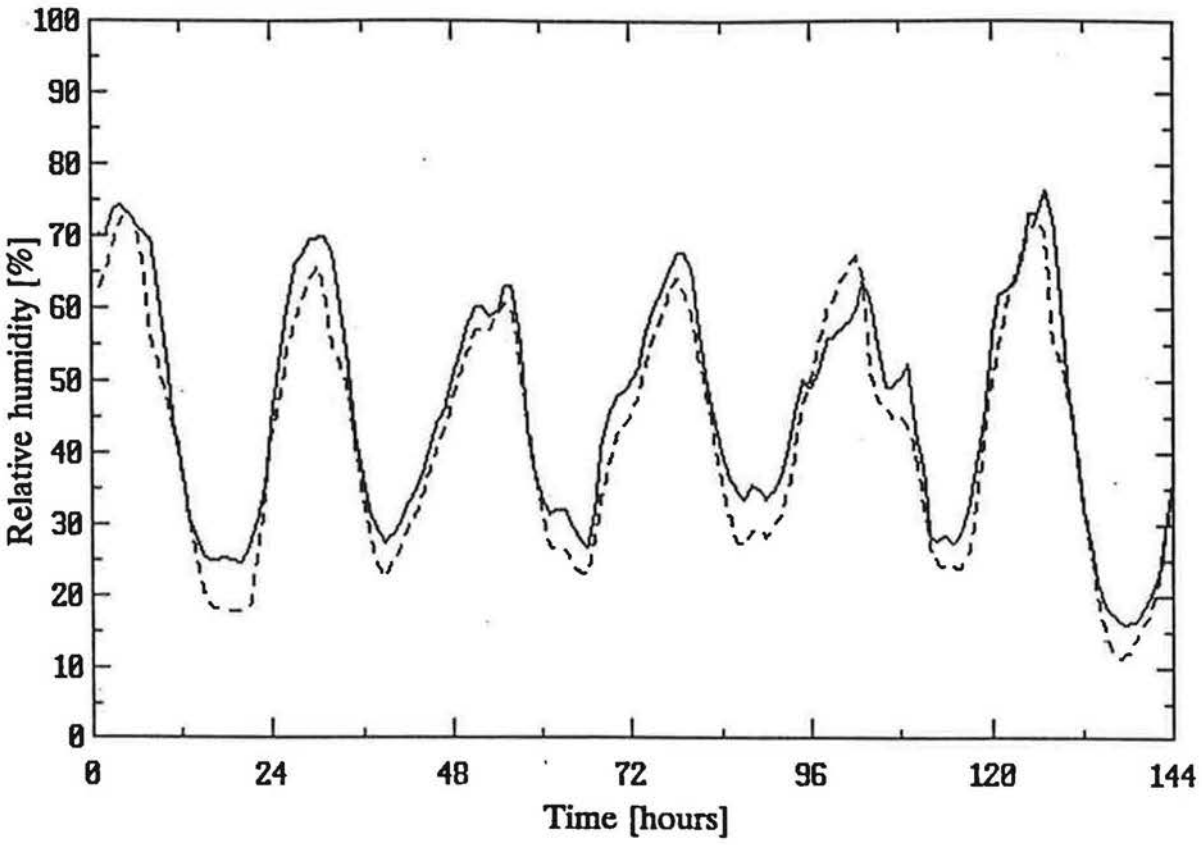

Figure 6-39. Measured (solid line) and predicted (dashed line) attic air relative humidty for attic 6 in the spring. May 15 to 20 1991.

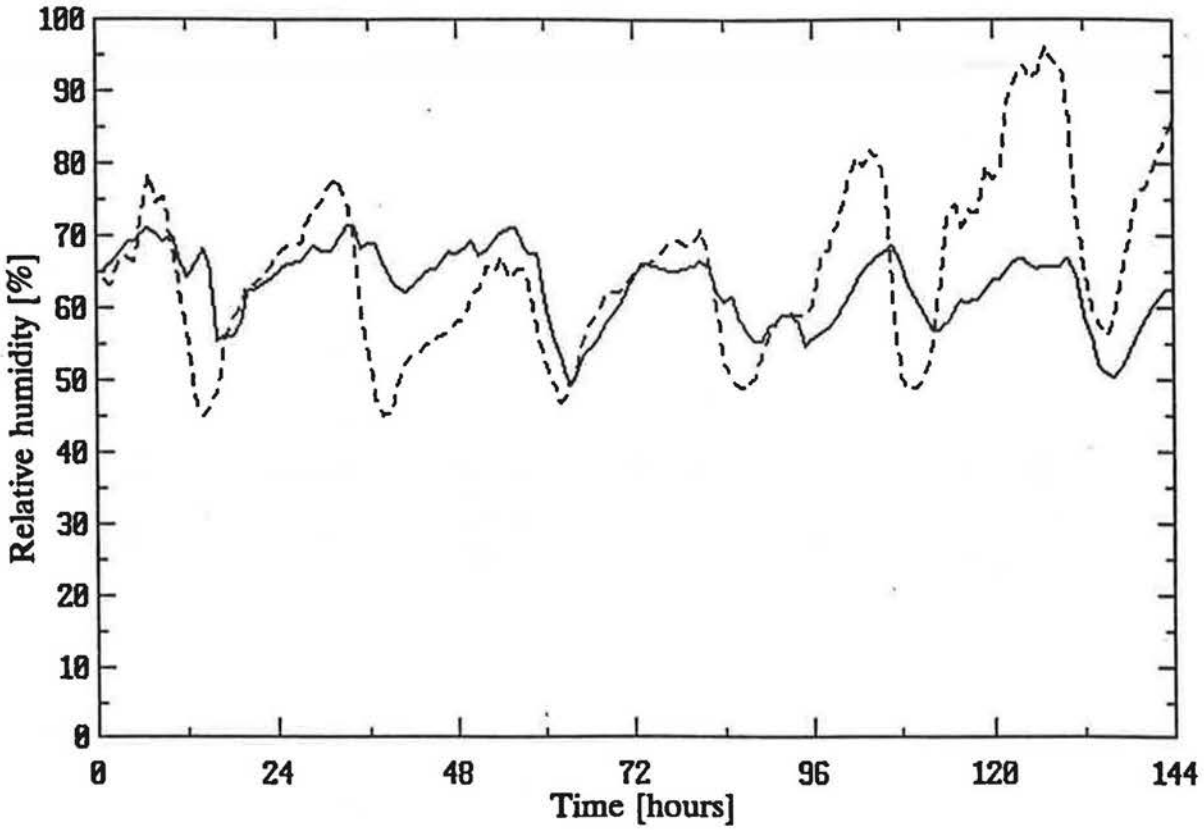

Figure 6-40. Measured (solid line) and predicted (dashed line) attic air relative humidity for attic 6 in the winter. January 1 to 6 1991.

less variation in vapour pressure makes the attic 6 relative humidity vary more than in attic 5. This is particularly noticeable for the winter data in Figure 6-40 where the measured values have a similar diurnal variation as the predicted values. In attic 5 for the same time period, Figure 6-36, the measured relative humidity displays little diurnal variation. The largest swing in attic 6 relative humidity is in the summer in Figure 6-38 where in the last 24 hours the measured RH drops from 80% to about 15% and the model predictions are able to follow this change. Generally the attic 6 prediction errors are similar to those in attic 5, with a mean error of about 3% Relative humidity and an absolute error of about 6%. The results of the attic 6 relative humidity predictions are summarized in Table 6-7.

Table 6-6. Range of test conditions for moisture model verification

	Mean Tout [°C]	Ventilation Rate [ACH]		
		Mean	Minimum	Maximum
Attic 5				
Summer	20	1.2	0.2	3.4
Spring	16	2.5	0.3	6.8
Winter	-24	0.8	0.4	2.3
Attic 6				
Summer	20	5.4	0.7	17.4
Spring	16	15.3	0.8	~30
Winter	-24	4.0	1.3	18.9

Table 6-7. Comparison of measured and predicted attic air relative humidity

	Figure Number	Mean Measured % RH	Mean Error		Absolute Error	
			% RH	%	% RH	%
Attic 5						
Summer	6-35	41	-2.3	-6	6.3	15
Spring	6-36	36	-2.5	-7	4.6	13
Winter	6-37	75	6.1	8	15	20
Attic 6						
Summer	6-38	52	0.3	0.6	5.8	11
Spring	6-39	46	-3.8	-8	4.4	10
Winter	6-40	63	2.4	4	8.9	14

Attic Air vapour pressure

The attic air vapour pressures for the same test periods as used for the comparison of relative humidities are shown in Figures 6-41 to 6-43 for attic 5 and 6-44 to 6-46 for attic 6. As with the relative humidities there are much stronger diurnal variations in summer compared with winter. For attic 5 these variations are about a factor of five in summer and only a factor of two in winter. These variations are not as strong in attic 6 where the higher ventilation rates mean that the attic air vapour pressure is closer to the outdoor vapour pressure. These figures show that the model is able to track the diurnal variation in vapour pressure as well as the seasonal changes. The magnitudes of vapour pressure cover a large range with summer peaks of about 4000 Pa and winter peaks as low as 100 Pa. The figures show that the model is able to track these changes in orders of magnitude. Table 6-8 contains a summary of the comparison of measured to predicted data for these tests.

Figures 6-41 and 6-44 also include the outdoor vapour pressure. These figures show that the outdoor vapour pressure does not experience the large diurnal cycles of the attic air. This is because the attic air has a larger temperature cycle (see Figures 6-25 and 6-28) and is exchanging moisture with the attic wood surfaces.

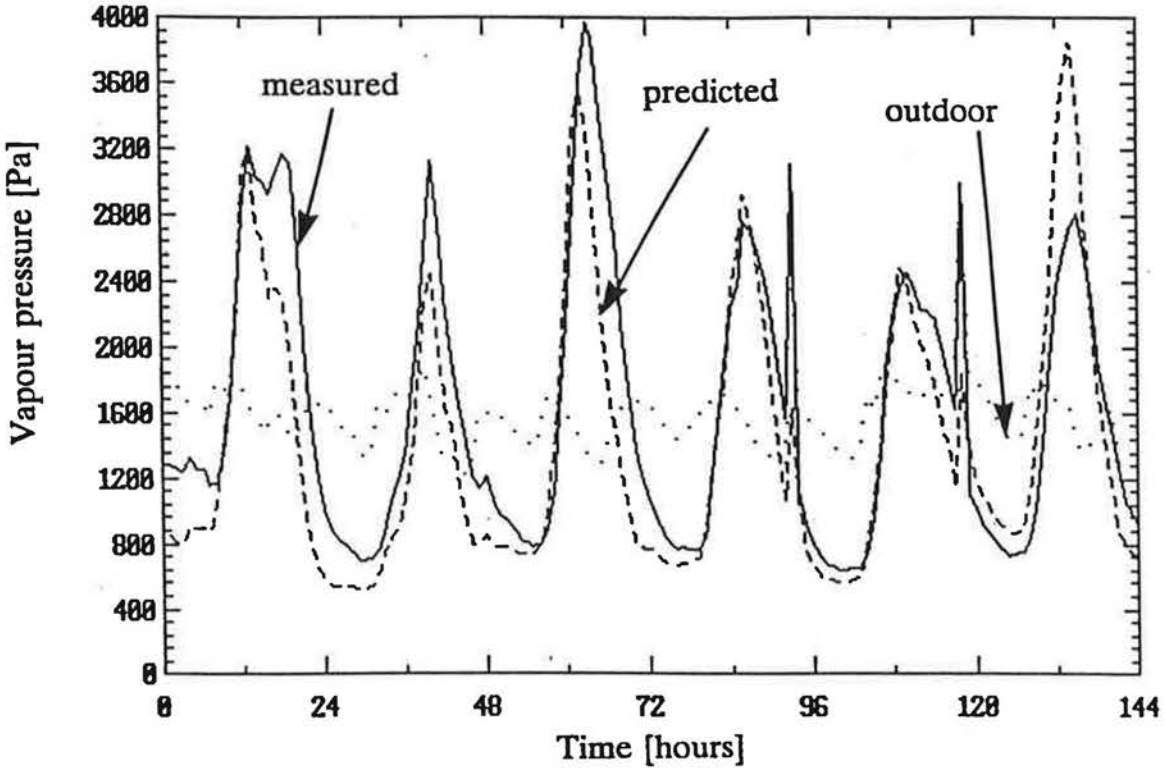

Figure 6-41. Measured (solid line) and predicted (dashed line) attic air vapour pressure and outdoor vapour pressure (dotted line) for attic 5 in the summer. August 13 to 18 1991.

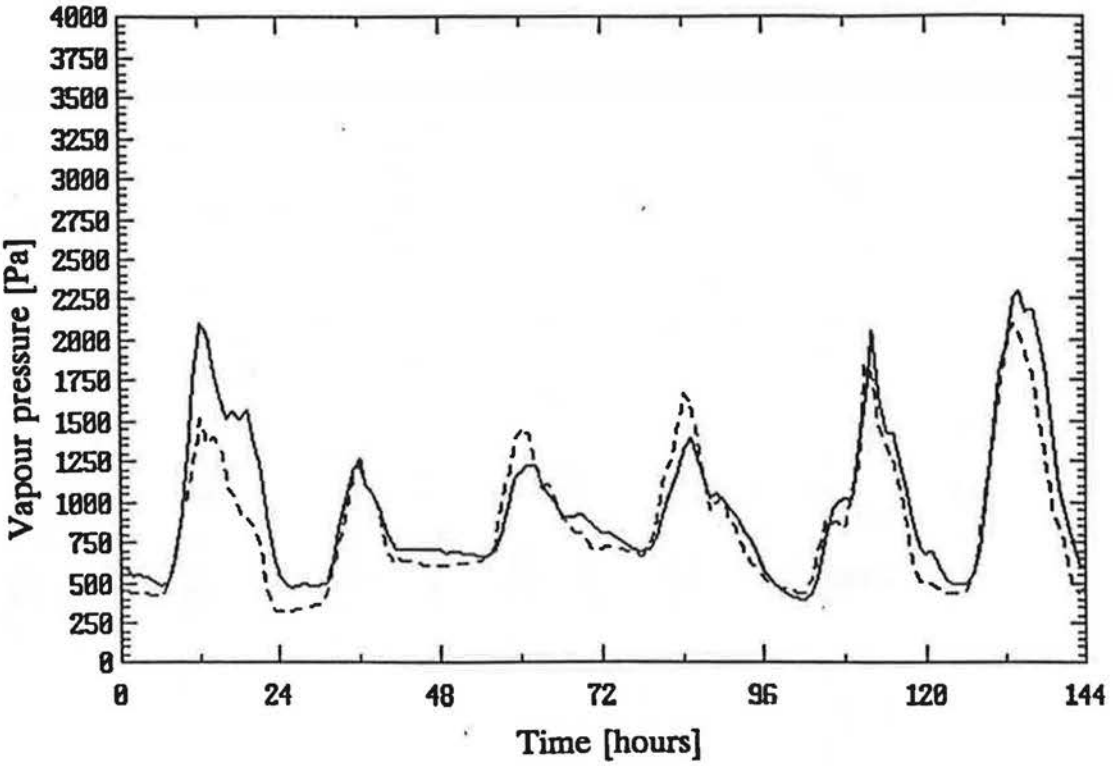

Figure 6-42. Measured (solid line) and predicted (dashed line) attic air vapour pressure for attic 5 in the spring. May 15 to 20 1991.

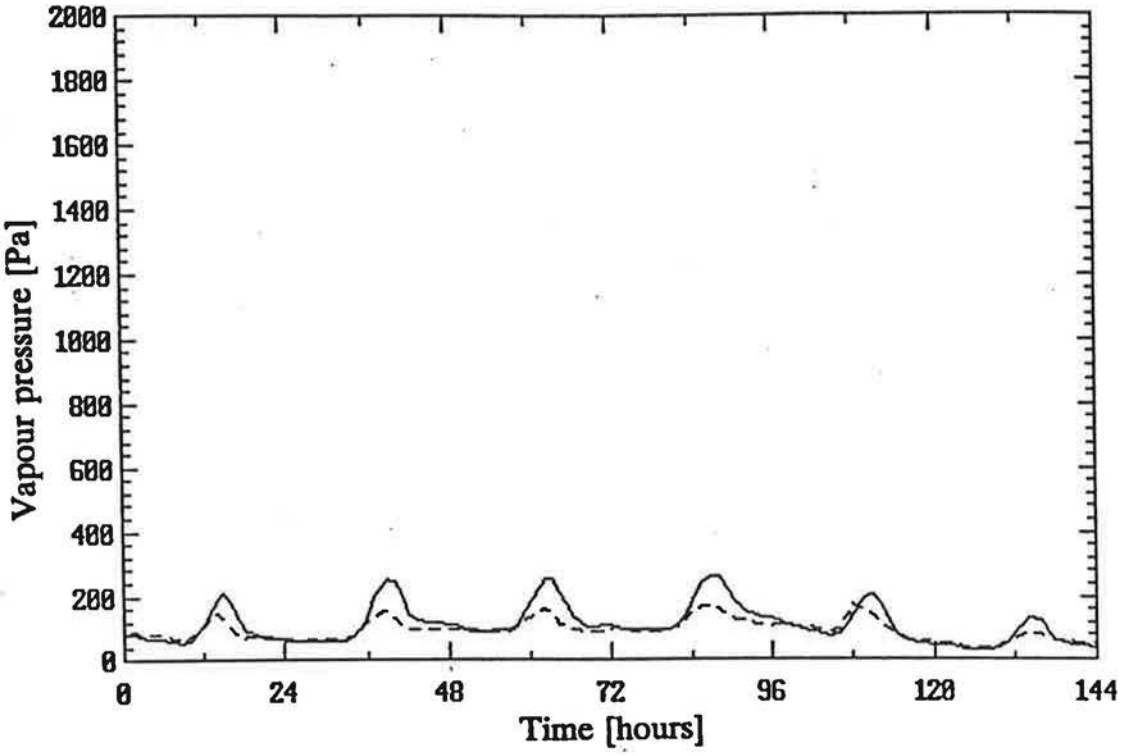

Figure 6-43. Measured (solid line) and predicted (dashed line) attic air vapour pressure for attic 5 in the winter. January 1 to 6 1991.

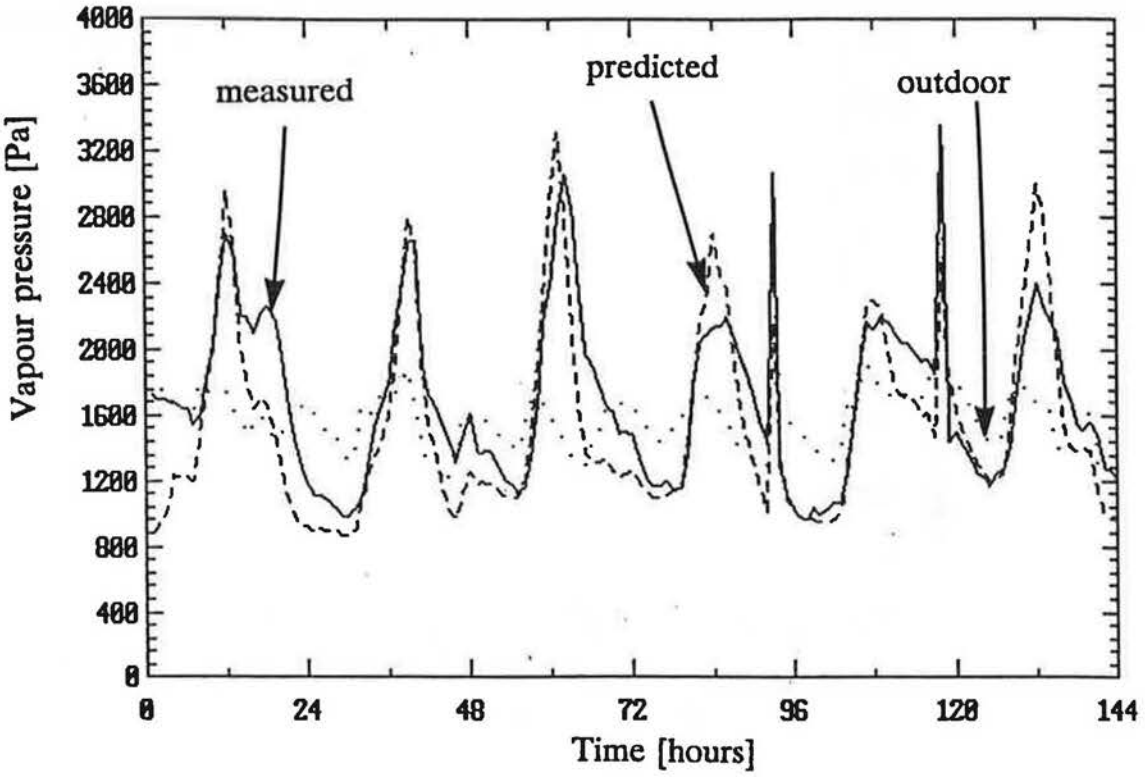

Figure 6-44. Measured (solid line) and predicted (dashed line) attic air vapour pressure and outdoor vapour pressure (dotted line) for attic 6 in the summer. August 13 to 18 1991.

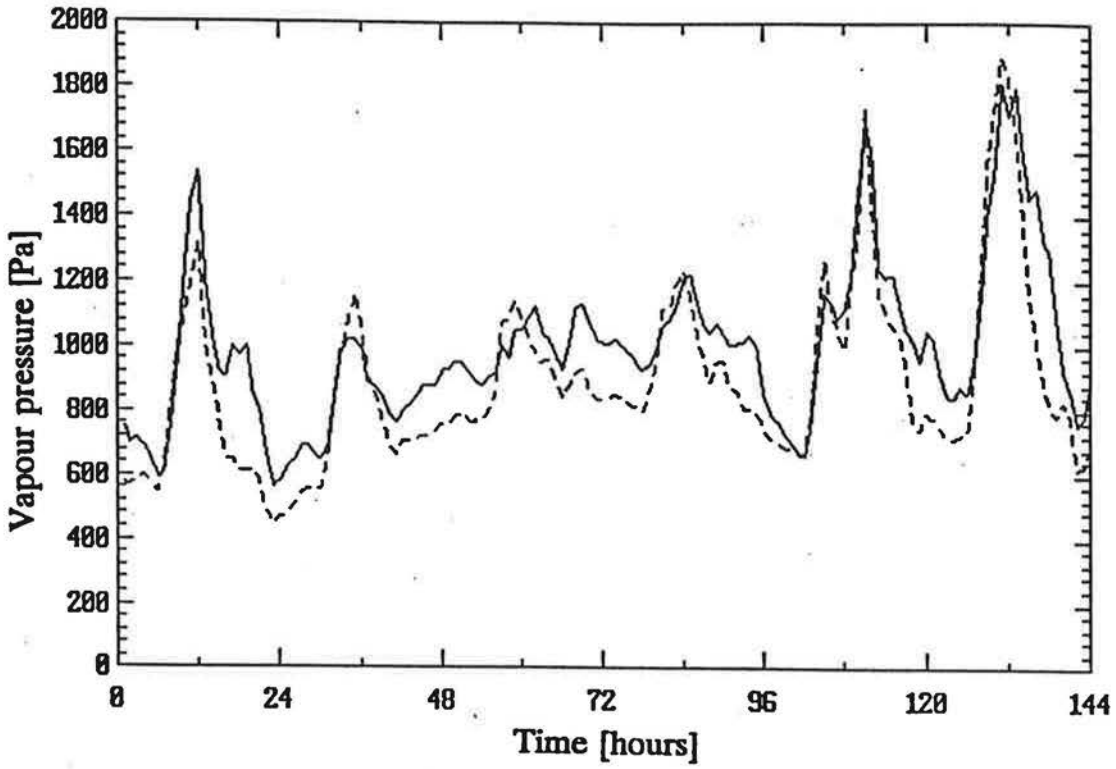

Figure 6-45. Measured (solid line) and predicted (dashed line) attic air vapour pressure for attic 6 in the spring. May 15 to 20 1991.

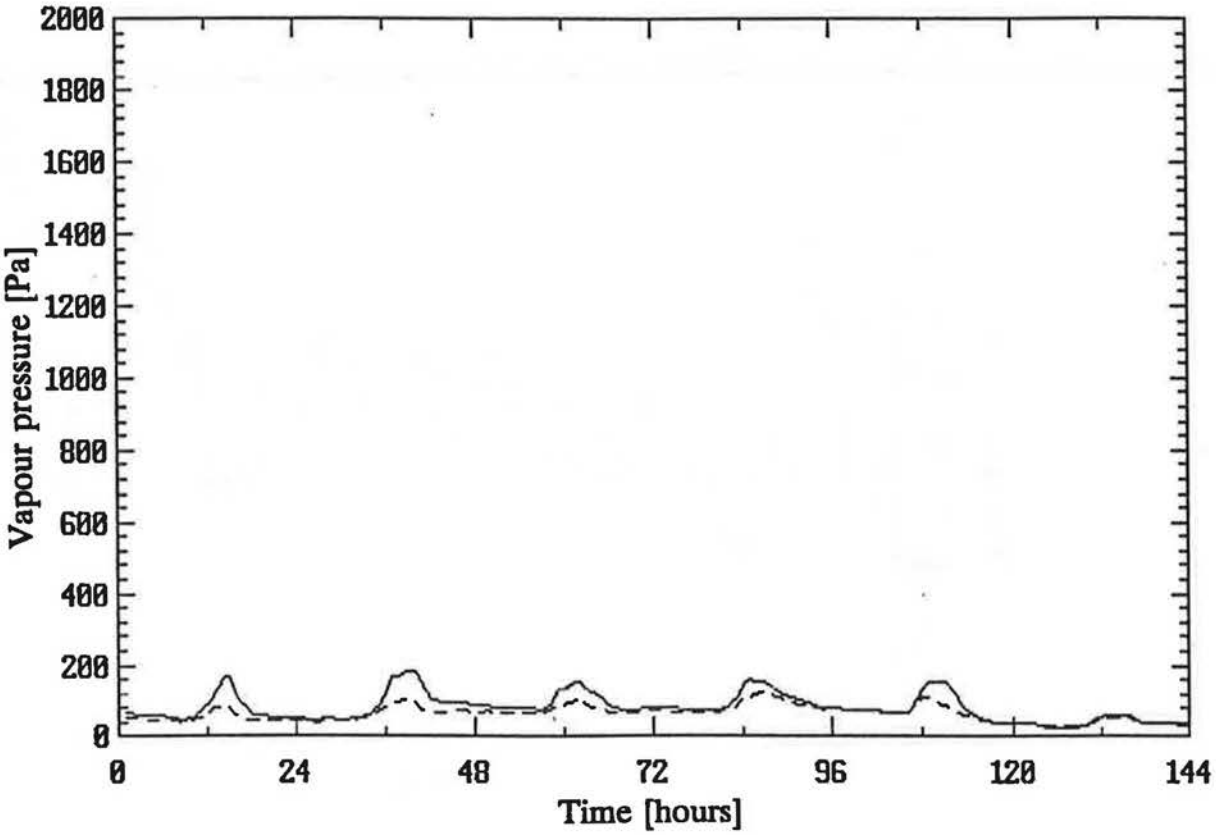

Figure 6-46. Measured (solid line) and predicted (dashed line) attic air vapour pressure for attic 6 in the winter. January 1 to 6 1991.

Figures 6-41 and 6-44 show the skill of the attic simulation model in predicting the differences between outdoor and attic vapour pressures. The increased ventilation rates in attic 6 make the attic 6 air vapour pressure closer to the outside vapour pressure, although there is still a marked difference between the two that the model must predict. The simulation model is able to account for changes in attic leakage and makes the predictions in Figure 6-44 more like the outside air when compared to the results in Figure 6-41 (for attic 5).

Table 6-8. Comparison of measured and predicted attic air vapour pressures

	Figure Number	Mean Measured P_v [Pa]	Mean Error		Absolute Error	
			Pa	%	Pa	%
Attic 5						
Summer	6-41	1632	-133	-8	318	19
Spring	6-42	970	-102	-11	152	16
Winter	6-43	111	-18	-16	23	21
Attic 6						
Summer	6-44	1692	-126	-7	247	15
Spring	6-45	995	-108	-11	134	13
Winter	6-46	82	-16	-20	17	21

In both attic 5 and attic 6 there is a tendency to underpredict the attic air vapour pressure with the error increasing from about 7% in summer to 20% to 30% in winter. These large percentage errors in winter must be kept in perspective because the vapour pressures in winter are extremely low and an error of only 16 Pa in vapour pressure corresponds to a 20% error. In addition, small errors in temperature of about 2°C at winter temperatures of -20°C will produce errors in saturation pressure of about 15%. The magnitudes of the errors shown in Tables 6-7 and 6-8 are acceptable considering the cumulative errors from the ventilation and heat transfer models used to predict the ventilation rate and attic temperatures that are entered in the moisture transport model.

6.3.3 The effect of assuming steady-state in the moisture transport model

If the rate of change of mass terms are set to zero in the mass balance

equations then the sum of the fluxes at a node is equal to zero and this implies an assumed steady-state solution for each hour. The inner and surface wood nodes will both have same moisture content. The resulting effect of ignoring the dynamic part of the moisture transport equations can be seen in Figures 6-47 and 6-48 which show the measured and predicted relative humidity and wood moisture content for attic 5 in the summer. The assumption of steady state makes the predictions extremely unrealistic with the attic air saturating every night and the wood having very high moisture content. In addition the wood becomes saturated each night resulting in large amounts of condensed mass at the wood nodes. As the measurements and observations have shown the inner wood in the attic is dry at all times, the attic air relative humidities are much lower than the steady-state predictions and there is no condensing mass during the summer. This implies that it is extremely important to not assume steady-state when predicting attic moisture transport.

6.4 Summary of model validation

The ventilation, heat transfer and moisture transport models developed for this study have been verified by comparing their predictions to measured hourly averaged data. The validation procedure has illustrated that a large amount of measured data is required in order to isolate individual parameters, e.g. selecting wind speeds below 2 m/s to look at temperature difference driven ventilation rates. The following sections discuss typical differences between measure and predicted values.

6.4.1 Ventilation model

The attic ventilation rates were found to be a weak function of the attic temperature. The maximum stack driven ventilation rates were only 20% of the wind driven ventilation rates. The typical mean error for stack driven attic ventilation rates is about 20%. The mean errors for the more dominant wind driven ventilation are less, typically 5 to 10% of the measured values. Because the wind driven ventilation is much larger than the stack driven ventilation the errors for wind driven ventilation are a better indicator of the overall ventilation model performance. The absolute errors are much larger, typically 20% to 30%. The mean errors are systematic errors due to uncertainty in leakage distribution, assumed wall averaged pressure coefficients and shelter factors. The absolute errors include the variability of ventilation rate during the hour due to changing wind speed, wind direction and temperatures.

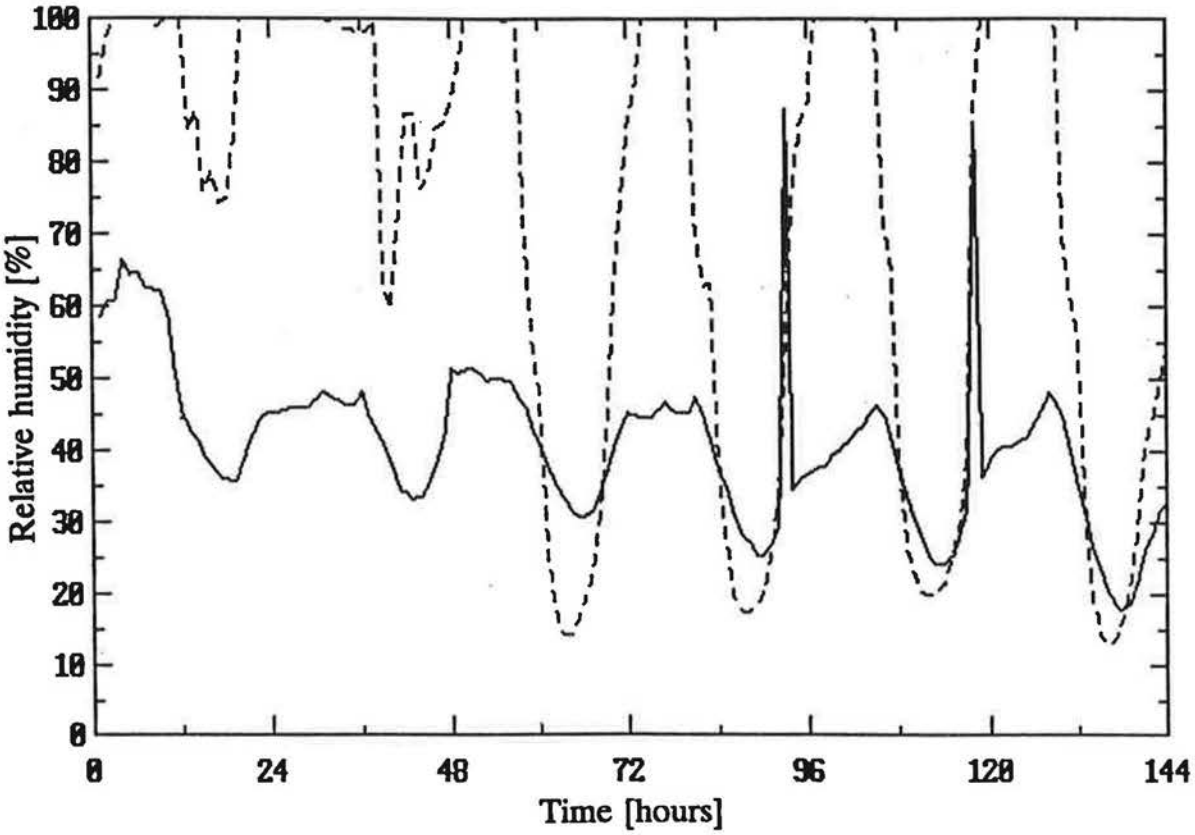

Figure 6-47. Measured (solid line) and predicted (dashed line) attic 5 relative humidity in the summer assuming steady-state. August 13 to 18 1991.

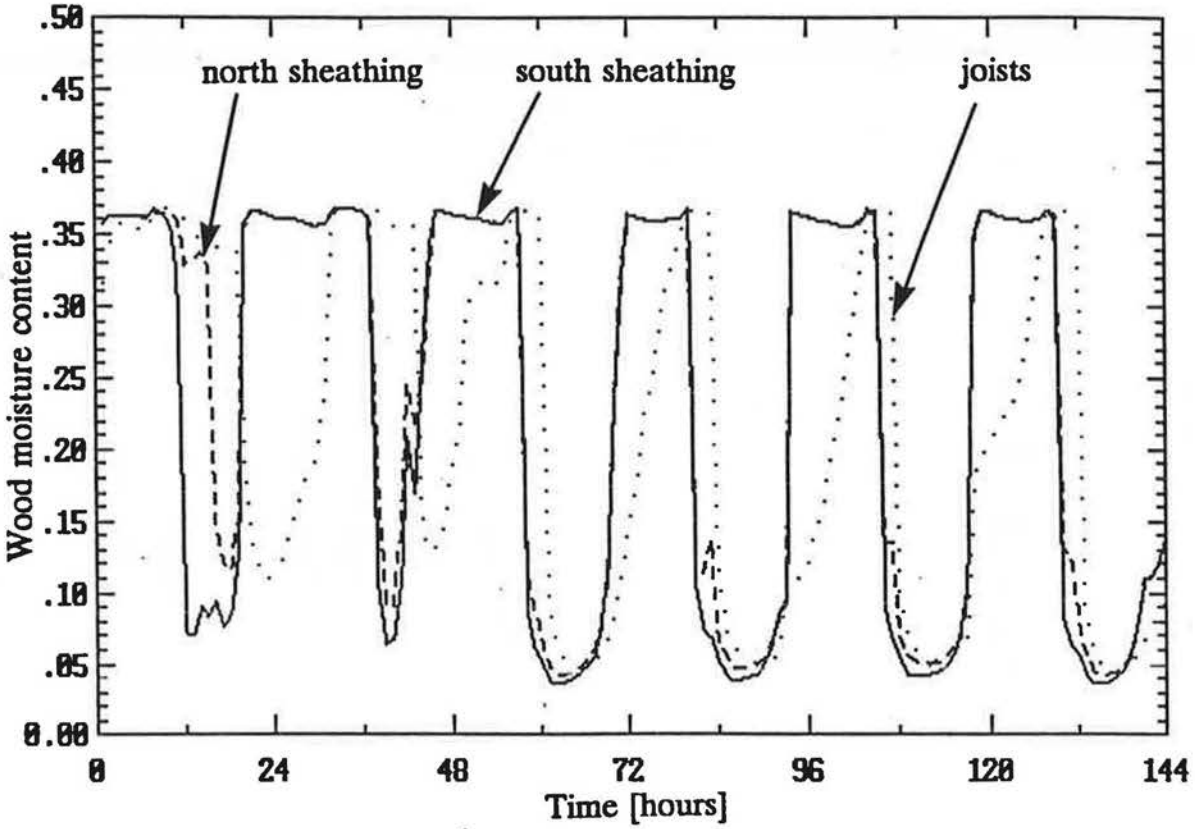

Figure 6-48. Predicted inner wood moisture content for south sheathing (solid line), north sheathing (dashed line) and for the joists (dotted line) for attic 5 in the summer assuming steady-state. August 13 to 18 1991.

Wind direction was found to create up to a factor of 3 change in ventilation rate due to shelter effects for the row of houses. The results showed that the greatest underprediction of ventilation rates occurred for winds blowing along the row of houses, when shelter effects are the most important. The mean errors were about -15% to -30% for these wind directions. This underprediction is due to a combination of the following factors: The shelter factors applied to the attics were developed for the houses but the attics are closer to the undisturbed air flow over the houses and thus may experience less shelter. The assumption of uniform pressure coefficients over large areas of the attic is critical when the wind blows along the row of houses and all the attic leaks have the same pressure coefficient. In the real three dimensional flow there are local variations in pressure coefficient that are not accounted for in this model. These local changes in pressure coefficient would create pressure differences across the attic leaks resulting in greater attic ventilation rates.

The house ventilation rates are described in more detail in Wilson and Walker (1991a) for a wide range of leakage configurations. For house typical mean errors for both wind and stack dominated ventilation is about 5%.

The flow of air from the house to the attic is very important for the moisture and heat transport models as it transports warm and moist indoor air into the attic space. The exchange of air between the house and the attic changes the energy balance for the attic air in the heat transfer model which is why an iterative procedure is used to solve the ventilation and heat transfer models. The magnitudes of the flow through the ceiling are small compared with the overall attic ventilation rates. The measured and predicted values indicate that the room to attic exchange is about 10% of the total ventilation rate for attic 5 and only 2% in attic 6. The maximum exchange rate is about 0.25 ACH in both attics. Considering what a small percentage of the total flow the house to attic exchange is, the ventilation model predicts the exchange very well with mean errors of 0.015 ACH (5%) for attic 5 and 0.0014 (15%) for attic 6. For attic 6 the mean error is actually smaller than in attic 5, but the mean percentage error is larger. This is because the overpredictions for attic 6 occur when the flowrate is low, which results in large positive percentage errors.

Tests with fans in both supply and exhaust mode for the attic gave similar results. There was found to be no systematic change in the mean error when the fans were added. This meant that the mean percentage errors decreased when fans were included because the mean ventilation rate is higher. The lower percentage errors

are because the fan is a well defined leakage site with very little uncertainty in its calculated flowrate.

6.4.2 Heat transfer model

The heat transfer model was run using measured and predicted ventilation rates as input data to see if using predicted ventilation rates would change attic temperature predictions. The validation tests showed that using measured or predicted ventilation rates made a difference of typically 1°C in attic air temperature. This indicates that the predicted ventilation rates do not introduce large errors into attic air temperature predictions. The same range of mean errors, typically 1°C, was found using both measured and predicted ventilation rates.

The absolute errors are important because they indicate what magnitude of error can be expected for a single hour. Using measured ventilation rates the absolute errors are typically a factor to 3 to 4 larger than the mean errors. This is because the predicted temperatures showed larger diurnal variations than the measured temperatures. The larger diurnal variations have been shown to be reduced by increasing the thermal mass of the sheathing nodes and reducing the surface emissivity of the external attic surfaces. Neither of these two changes were able to completely remove the excessive nighttime cooling of the attic.

The heat transfer model was also used with the thermal masses of each node set to zero. This was done in order to simulate assuming steady state heat transfer. This assumption had a negligible effect on mean errors but made the absolute errors worse by about 1°C compared with model predictions that included the thermal masses. These results show that it is important to include the thermal masses in an attic heat transfer model.

6.4.3 Moisture transport model

The moisture transport model uses the predictions of the ventilation model and the heat transfer model as inputs, and the moisture transport validation includes all three components. The moisture model predictions were compared with measured values of inner wood moisture content, and attic air relative humidity and vapour pressure. Predicted surface moisture contents could not be validated because surface moisture contents were not measured due to lack of a suitable measurement procedure.

The measured values of inner wood moisture content were always low and close to the measurement limit of the wood moisture meter used in the data acquisition system. This means that the model predictions can only be validated if

they are also below the same threshold (7% moisture content). The predictions show that the inner wood moisture content is always low and changes very slowly because it can only exchange moisture with the surface wood by diffusion. The measured data only validates the general trend of inner wood moisture predictions and does not allow the examination of the dynamic performance of wood moisture predictions.

The attic air is the most active node for moisture transport because it includes ventilation terms that remove and supply moisture from the attic space. The attic air relative humidity is an important factor because it shows how close to saturation the attic air is and describes the potential of the attic air for moisture absorbtion. The model predictions for both attics had mean errors of about 2.5% RH and absolute errors of about 5% RH. Included in the prediction of attic air relative humidity is the prediction of saturation vapour pressure. This is a strong function of temperature and so the errors in predictions of relative humidity include errors in prediction of temperature.

The driving potential for moisture transport is the vapour pressure. For the attic air the vapour has a range from 40 Pa in winter (for saturated air at -30°C) to 4000 Pa in summer (50% RH at 42°C). For both the attics the mean errors ranged from about 20 Pa (20%) in winter to 120 Pa (7%) in summer. The percentage errors are smaller in the summer because the mean values are proportionally higher. The absolute errors for all seasons in both attics was found to be about 17%. These errors in predicting attic air vapour pressure contain the cumulative errors from the ventilation and heat transfer models. Given the uncertainty in attic ventilation rates (absolute errors of 20% to 30%) and attic temperatures (absolute errors of about 3°C) the errors in predicting attic vapour pressure are reasonable.

These validated models will be used in the next chapter to perform simulations under controlled weather conditions. This allows for systematic evaluation of the parameters effecting attic moisture, e.g. climate, ventilation rate, attic leakage distribution and the effect of ventilation fans.

Chapter 7. Attic Moisture Simulations

In this chapter the models that have been developed and verified using measured data will be used in attic simulations so that the effect of important parameters for attic moisture accumulation and transport may be examined systematically. This allows the parameters that are most important for attic moisture to be evaluated independently of each other. This independent evaluation is difficult using measured data because the parameters change simultaneously. The simulations will be performed by running the combined ventilation, heat transfer and moisture transport models for one week (168 hours) and examining the resulting predictions. The parameters to be investigated were chosen by examining the measurement results in Chapter 5 and the validation results in Chapter 6.

The effect of the changing input parameters will be examined by looking at the predicted wood moisture contents, accumulated masses, attic air relative humidity, attic air temperature and ventilation rates.

7.1 Parameters examined in attic moisture simulations

7.1.1 Climatic zone.

The model was run with two extremes of outdoor winter weather, a dry prairie climate and a damp maritime climate:

- **Prairie climate.** Ambient temperature was assumed to vary sinusoidally over a 24 hour cycle from a minimum of -20°C at midnight to a maximum of 0°C at noon. Ambient vapour pressure also varied sinusoidally, from 100 Pa at midnight to 200 Pa at noon, corresponding to 97% RH and 33% RH respectively. These values were chosen as typical prairie values from the data measured at the test facility.
- **Maritime climate.** Ambient temperature was assumed to be constant throughout the day at -1°C. Ambient relative humidity was 100% and the corresponding vapour pressure was 563 Pa. These values were chosen as a typical Canadian maritime climate from weather data presented by CMHC (1988)(Figure 5.2, p.25) for Halifax, Nova Scotia in December, January and February.

7.1.2 Cloud cover and solar radiation.

The cloud cover was either one (complete cloud cover) or zero (clear sky) for the whole simulation period in order to examine the extremes of this effect. The cloud cover changed the short wave solar radiation to the roof and the long wave radiation from the roof to the to the ground and sky. When the sky was cloudy the

effective sky temperature was the air temperature. For clear skies the effective temperature was lower and the attic sheathing experienced temperature depressions at night. The cloud cover factor, S_c has a value of zero for clear skies and 1 for completely cloud covered skies.

The solar radiation for clear skies was assumed to be zero from 5 p.m. to 9 a.m. Between 9 a.m. and 5 p.m. the solar radiation varied sinusoidally from zero to a peak of 550 W/m^2 on the south sheathing and 60 W/m^2 on the north sheathing. These values were based on measurements taken on January 1, 1991 at AHHRF. For a cloudy day both sheathing surfaces were assumed to have the same peak solar radiation of 120 W/m^2 based on measurements taken on the 25,26 and 27 December 1990 at AHHRF. The roof ridge was assumed to be in an east-west line so that there was a south facing and a north facing sheathing surface and the simulated house had the same orientation as the AHHRF test houses.

7.1.3 Wind speed.

For the simulations three wind speeds were chosen: light winds of 0.5 m/s, average winds of 2.5 m/s and strong winds of 6 m/s. These wind speeds were based on the range of measured data at AHHRF. This range of wind speeds was chosen to produce a large range of ventilation rates. The house was assumed to be completely exposed to the wind and has no shelter. The wind direction for calculating wind pressure coefficients was assumed to be perpendicular to the roof ridge of the attic for all simulations.

7.1.4 Fans.

The effect of having extract, supply or balanced fans was tested for a sealed attic to see if fans can be used to alleviate moisture problems by increasing ventilation rates in low leakage attics. The balanced fan system had one fan supplying air to the attic and one fan extracting air from the attic. Each of the balanced fans had a rated flow rate of 7 ACH (75 l/s). The single fans had rated flow rates of 14 ACH. The sealed attic that the fans were used in for the simulations was described in section 7.2. A simulation was also included of the current practise for attics which is an extraction fan on a timer so that it only operates during the day. A range of fans sizes were simulated to determine if there is an optimum fan size to balance the effects of reduction of attic temperatures, which tends to increase moisture problems, and bringing dryer outdoor air into the attic to remove moisture.

7.1.5 Snow on the roof.

Heat exchange through a snow layer is a complex combination of conduction through the air and snow, radiation within the porous snow structure and convection through the pores in the snow. For simplicity, the heat transfer for the attic is assumed to be changed by having snow on the roof due to the following two effects:

- The snow changes the exterior surface radiation transfer. The short wavelength absorbtivity of snow is assumed to be about 0.5 (from Sellers (1965), p.21) based on the ratio of reflected to incident radiation. This is less than the value of 0.9 used for the shingles which means that less solar radiation is absorbed during the daytime. The emissivity of snow is assumed to be about 0.9 (from Sellers (1965), p.41) which is the same as for shingles. This results in the same nighttime radiation losses as for shingles with reduced daytime solar gains. Because snow is a complex, porous, three dimensional structure absorbtivity and emissivity can cover a wide range and may be different from the values assumed here.
- The snow provides an insulating blanket on the sheathing. The thermal conductivity of snow is given by Yen (1981)

$$k_{\Sigma}=0.22362\left(\frac{\rho_{\Sigma}}{1000}\right)^{1.885} \qquad (7\text{-}1)$$

where ρ_{Σ} is the density of the snow in Kg/m^3. The density of snow is 200 to 500 Kg/m^3 depending on its age and temperature history. Using this range of snow densities gives thermal conductivities of k_{Σ} from 0.11 to 0.60 W/mK. For simplicity in the simulations the thermal conductivity of snow is assumed to be an average value of 0.35 W/mK.

The thermal resistance of the snow layer, R_{Σ}, is given by

$$R_{\Sigma}=\frac{\Delta X_{\Sigma}}{k_{\Sigma}} \qquad (7\text{-}2)$$

where ΔX_{Σ} is the depth of the snow layer. The R_{Σ} is added to the thermal resistance of the sheathing surfaces thus reducing the heat transfer by conduction through the roof. For the simulations, the thickness of the snow layer is assumed to be 0.15m thus the additional thermal resistance is 0.43 m^2K/W compared with 0.2 m^2K/W for sheathing alone.

The assumed thermal conductivity of snow of 0.35 W/mK corresponds to a

snow density of 375 Kg/m^3 from Equation 7-1. The thermal model includes the extra mass of the snow by adding the mass of snow in the 0.15m layer with a density of 375 Kg/m^3 to the mass of the outer sheathing node. This adds about 1700 Kg of mass to the sheathing surfaces. Assuming that the snow and the sheathing have the same heat capacity means that this mass can simply be added to the mass of the sheathing.

7.1.6 Initial wood moisture contents.

Different initial wood moisture contents were examined to determine their effects on moisture accumulation and attic wood drying. The two wood moisture contents chosen for these simulations were: dry wood at 5% moisture content and damp wood at 15% moisture content. These different initial conditions were chosen to reflect different moisture histories of the wood. Initial conditions also produce a transient term that is superimposed on the stationary solution. The simulations will show how long the initial transient influences the model predictions.

7.2 Attics and houses used in simulations

The house used in the simulations was the same for all simulations. It's dimensions and leakage distribution were based on the test houses at AHHRF. Two different attic leakage configurations were tested; a standard attic that has soffit and roof vents and distributed leakage as same as attic 6 at AHHRF, and sealed attic sealed attic that has only 10% of the distributed leakage of a standard attic with no soffit or roof ventilators and is tested to represent tight attic construction.

7.2.1 Houses

The houses for all the attic simulations were similar to houses 5 and 6 at AHHRF in that they have the same dimensions and a full basement. The building dimensions are summarised in Table 5-1. The houses are assumed to have no furnace flue or fireplace leakage. This makes the flow from the house into the attic as large as possible because a furnace flue or fireplace would otherwise be the major air outflow site. Making the flow from the house to the attic as large as possible allows the exfiltrating warm and damp house air to have the maximum effect on the moisture load for the attic. The house air relative humidity and temperature were constant throughout the simulations at 50% RH and 20°C respectively. The four pascal leakage area is chosen to be 100 cm^2 with exponent n = 0.66 resulting in C = 0.0108 m^3/s(Pa)^n. These are values that would be typical for a house this size in Canada (see Sulatisky (1984)). This is a slightly larger leakage area than the AHHRF test houses because the AHHRF houses have been constructed with greater

care than typical houses. The leakage distribution is also assumed to be similar to the AHHRF houses with 20% of leakage in the ceiling, 20% at floor level and 60% in the walls, with the wall and floor leakage evenly distributed to the four sides of the building.

7.2.2 Standard attic

The standard attic had the same dimensions attic 6 at AHHRF, with background distributed leakage combined with soffit vents above the north and south walls (parallel to the roof ridge) and an additional ventilator on each pitched roof surface. The total leakage area was calculated based on the Canadian building code (NBCC (1990)). The code recommends that the leakage area of the attic is 1/300 of the floor area. This results in a total four pascal leakage area of 1900 cm^2. This leakage was separated into 55% for the distributed leakage in the soffits (50%) and pitched roof surfaces (5%) and 45% in the two ventilators. Assuming a leakage exponent, n, of 0.7 means that the leakage coefficient for the standard attic is 0.0798 m^3/sPa^n. Each of the two ventilators had a leakage area of 430 cm^2 corresponding to a leakage coefficient of 0.086 m^3/sPa^n for an assumed leakage exponent of 0.5. The standard attic differed from the attics used in the measurement program described in Chapter 5 because it did not have the roof raised above the floor of the attic. Therefore the roof peak height was only 4.3m and the attic volume is reduced to 38 m^3.

7.2.3 Sealed attic

A sealed attic was simulated because attics of this type are common in regions of Canada where blowing snow is a problem, e.g. in the arctic. The sealed attic is the same size as the standard attic but has no soffit vents of roof ventilators. It has only 10% of the background leakage of the standard attic but in these simulations the ceiling leakage is kept the same to maintain a moisture load on the attic that would reveal any moisture related problems. The four pascal leakage area of the attic is about 134 cm^2 with $n = 0.7$ and $C = 0.0096$ m^3/sPa^n.

7.3 Summary of simulations

The simulations were organised so that only one parameter at a time was changed from simulation to simulation. Table 7-1 contains a list of the simulations performed to examine the effects of the parameters discussed in sections 7.1 and 7.2. The effect of the changing input parameters will be examined by looking at the model predictions for wood moisture contents, accumulated masses, attic air relative humidity, attic air temperature and ventilation rates.

Table 7-1. List of attic simulations

Simulation	Attic Configuration	Initial Wood moisture content, %	Wind Speed m/s	Climatic Zone	Cloud Cover
1	Standard	5	0.5	Prairie (P)	0
2	Standard	5	2.5	P	0
3	Standard	5	6	P	0
4	Standard	5	0.5	P	1
5	Standard	5	2.5	P	1
6	Standard	5	6	P	1
7	Sealed	5	0.5	P	1
8	Standard	15	0.5	Maritime (M)	0
9	Standard	15	2.5	M	0
10	Standard	15	6	M	0
11	Standard	15	6	M	1
12	Standard	15	2.5	M	1
13	Standard	15	0.5	M	1
14	Standard	19	0.5	M	1
15	Standard	19	6	M	1
16	Standard	19	6	M	0
17	Sealed with Balanced Fans	15	6	M	0
18	Sealed with Extraction Fan	15	6	M	0
19	Sealed with Supply Fan	15	6	M	0
20	Sealed with Balanced Fans	5	6	P	0
21	Sealed	15	6	M	0
22	Sealed	5	6	P	0

23	Sealed with Balanced Fans	15	6	M	1
24	Sealed	15	6	M	1
25	Sealed with Extraction Fan 9 a.m. to 4 p.m.	15	6	M	1
26	Sealed with Extraction Fan 9 a.m. to 4 p.m.	15	6	M	0
27	Sealed with Supply Fan Tout = -5°C	15	6	M	0
28	Sealed with Supply Fan of 50 cfm	15	6	M	0
29	Sealed with Supply Fan of 100 cfm	15	6	M	0
30	Standard with Snow on Roof	15	0.5	M	0
31	Standard with Snow on Roof	15	6	M	0

7.4 Results of simulations

The simulations shown in Table 7-1 were all run for one week (168 hours), which was found to be sufficient for the predicted quantities to reach stationary values. For the predicted values that have strong diurnal values the high and low as well as the mean values were calculated. The mean, high and low values are taken over the last 48 hours to remove any initial transient effects. Table 7-2 summarises the results for the simulations given in Table 7-1. The effects of the various input parameters were determined by looking at the following results for the dependent quantities.

- **Ventilation rates.**

The mean values were calculated for the simulation period. They are a function of windspeed, outdoor temperature, attic leakage area and fan flows.

• **Ceiling flow rates.**

The mean value of ceiling flow over the simulation period depends on the same factors as the ventilation rates and is important in determining the moisture load on the attic. Negative ceiling flows imply flow out of the attic into the house.

• **Attic Air Temperature.**

The mean, high and low values over the simulation period control the dynamics of the moisture transport.

• **Attic air RH.**

The mean, high and low values describe how close the attic air is to saturation and what range of relative humidities occur that may deposit or remove moisture.

• **Moisture Content of South and North Sheathing.**

Only surface moisture contents are presented here because in all model predictions (and measurements) described in Chapters 5 and 6 the inner wood moisture content had no significant changes. Experimental results described in Chapters 5 and 6 have shown that the sheathing is the most critical part of the attic for moisture deposition. The mean values of wood moisture content for the sheathing describe how much moisture is deposited or removed from the attic over the simulation period. The high and low values show how much moisture is transported in and out of the wood surface over a 24 hour period due to diurnal variations in temperature and attic air moisture content.

• **Condensation.**

The amount of condensation on attic wood surfaces is critical because this condensed mass causes structural problems and growth of micro-organisms on wood surfaces. Condensation was found to either accumulate over time or may be periodic with deposition at night and evaporation during the day. For periodic deposition the peak value was calculated, and for accumulating condensation the average amount per day that accumulates was calculated.

Table 7-2. Summary of Attic Simulation Results

Simulation	Ventilation Rate, ACH Attic (Ceiling)	Attic Air Temp. °C Mean (Hi,Lo)	Attic RH % Mean (Hi,Lo)	W_{MC}% South Sheathing Mean (Hi,Lo)	W_{MC}% North Sheathing Mean (Hi,Lo)	Condensation
1	1.9 (0.3)	-8.9 (12,-20)	53 (90,25)	5 (7,4)	7 (8,7)	-
2	7.9 (0.3)	-8.9 (5,-20)	53 (78,35)	8 (9,7)	9 (9,8)	-
3	25 (0)	-9.4 (3,-20)	53 (76,32)	8 (10,7)	8 (10,7)	-
4	2.4 (0.3)	-5.3 (8,-15)	49 (70,36)	8 (9,7)	8 (9,7)	-
5	8 (0.3)	-7.5 (4,-16)	55 (72,37)	8 (9,7)	8 (9,7)	-
6	25 (0)	-8.8 (4,-18)	52 (72,32)	8 (9,7)	8 (9,7)	-
7	0.3 (0.3)	-4.5 (8,-14)	60 (75,45)	9 (10,9)	9 (10,9)	-
8	2 (0.25)	-0.8 (12,-5)	61 (75,47)	8 (11,6)	12 (13,11)	-
9	7.3 (0.2)	-0.4 (5,-2)	86 (93,79)	17 (22,13)	25 (26,24)	-
10	24 (-0.1)	-0.7 (2,-2)	94 (97,90)	25 (29,20)	29 (30,29)	0.1 Kg South periodic 0.6 Kg North Periodic
11	24 (-0.1)	-0.1 (1,-1)	91 (93,90)	26 (27,25)	26 (27,25)	-
12	7.4 (0.2)	0.9 (6,0)	86 (87,85)	21 (21,23)	21 (21,23)	-
13	1.9 (0.3)	2.8 (8,2)	71 (73,67)	14 (15,13)	14 (15,13)	-
14	1.9 (0.3)	2.8 (8,2)	71 (73,67)	14 (15,13)	14 (15,13)	-
15	24 (-0.1)	-0.1 (1,-1)	93 (94,92)	26 (27,25)	26 (27,25)	-
16	24 (-0.1)	-0.7 (2,-2)	95 (97,90)	25 (29,20)	25 (29,20)	0.1 Kg South periodic 0.6 Kg North Periodic
17	9 (0.8)	-0.2 (3,-2)	93 (97,91)	27 (30,23)	30 (32,28)	0.3 Kg South periodic 0.3 Kg North Periodic

18	17 (2.7)	0.3 (3,-5)	96 (97,95)	30 (32,27)	31 (33,30)	2.2 Kg South Periodic 2.2 Kg/Day North Accumulates
19	16.6 (-2.1)	-1.4 (2,-2.5)	97 (100,92)	27 (28,23)	29 (30,28)	2 Kg South Periodic 2 Kg North Periodic
20	9.4 (0.8)	-9 (4,-18)	72 (95,48)	11 (12,9)	11 (12,9)	-
21	0.7 (0.7)	0.6 (4,-0.5)	90 (92,88)	22 (25,19)	30 (32,29)	1 Kg North Periodic
22	0.8 (0.8)	-7.6 (5,-17)	87 (100,70)	14 (16,12)	15 (17,13)	1.7 Kg South Periodic 2.6 Kg North Periodic
23	9 (0.8)	0.6 (2,0)	95 (96,94)	29 (29,29)	29 (29,29)	-
24	0.7 (0.7)	1.5 (3,1)	97 (97,97)	32 (32,32)	32 (32,32)	1 Kg/Day Accumulates North and South
25	5.4 (1.3)	1.3 (3,1)	97 (99,96)	32 (33,32)	32 (33,32)	0.4 Kg/Day Accumulates North and South
26	5 (1.3)	0.3 (3,-0.5)	92 (95,90)	25 (27,18)	29 (30,29)	0.4 Kg North Periodic
27	17 (-2.1)	-5.4 (-2,-7)	98 (100,92)	21 (21,19)	22 (25,21)	1.3 Kg South Periodic 3 Kg North Periodic
28	3 (0.5)	-0.1 (3,-2)	90 (92,88)	23 (25,19)	27 (29,26)	-
29	5 (-0.1)	-0.5 (3,-2)	87 (91,85)	21 (23,18)	24 (26,23)	-
30	1.7 (0.2)	-3.2 (3,-5)	86 (92,78)	14 (16,12)	21 (27,19)	0.8 Kg/Day Accumulates North
31	24 (-0.1)	-1.1 (1,-1)	96 (97,95)	28 (30,25)	29 (31,29)	1 Kg South Periodic 2 Kg/Day Accumulates North

7.4.1 Moisture Dynamics

The diurnal cycles of solar gain, nighttime radiation, temperatures and relative humidity have significant effects on attic moisture transport. The simulations were run for 168 hours so as to capture seven complete diurnal cycles. The following

results for wood moisture content and condensing mass illustrate some of these effects.

Wood moisture content

The dynamics of wood moisture content are discussed for wood surfaces only. The inner wood nodes display no moisture dynamics because they are not exposed to the changing conditions of the attic air. The assumed relationship between wood moisture content, temperature and vapour pressure plays an important part in the moisture dynamics. For a given moisture content an increase in temperature increases the effective vapour pressure of the wood and a reduction in temperature will reduce vapour pressure. At night the temperature of the wood falls and so does its vapour pressure. This means that there will be a flow of water vapour to the wood from the attic air which is at a higher vapour pressure. Therefore, at night the wood moisture content will tend to increase due to this flow of water vapour into the wood. During the day when the wood is heated its vapour pressure rises above the attic air vapour pressure and so moisture is transferred form the wood to the attic air. The hotter the wood gets, the more it dries. This is why south facing sheathing surfaces are drier than north facing ones, because under clear skies they receive more solar radiation and thus have higher temperatures.

Figure 7-1a shows the wood moisture contents of the three surface wood layers for simulation 10 (standard attic in a maritime climate). During the night the wood moisture content of the south sheathing increases. When the sun comes up and heats this surface it rapidly loses this moisture, which is transferred to the attic air. This increases the vapour pressure in the air so that moisture is then transferred to the other two wood surfaces as shown by their increasing wood moisture content for the first couple of hours after the south sheathing starts to losc moisture. Later in the day the north sheathing and the trusses have increased temperatures and so they too lose moisture. The north sheathing reaches saturation after the first 48 hours of the simulation. The increase in wood moisture content during the first 48 hours shows how rapidly the wood surface nodes lose the effect of the initial assumed wood moisture content of 15%. The effect of the wood moisture content to temperature relationship for wood at saturation (as shown in Figure 4-4) can be seen because the increased daytime temperatures allow a higher wood moisture content at the saturation pressure. This additional mass that can be absorbed during the higher daytime temperatures is then condensed out at night as the sheathing cools as shown in Figure 7-2a.

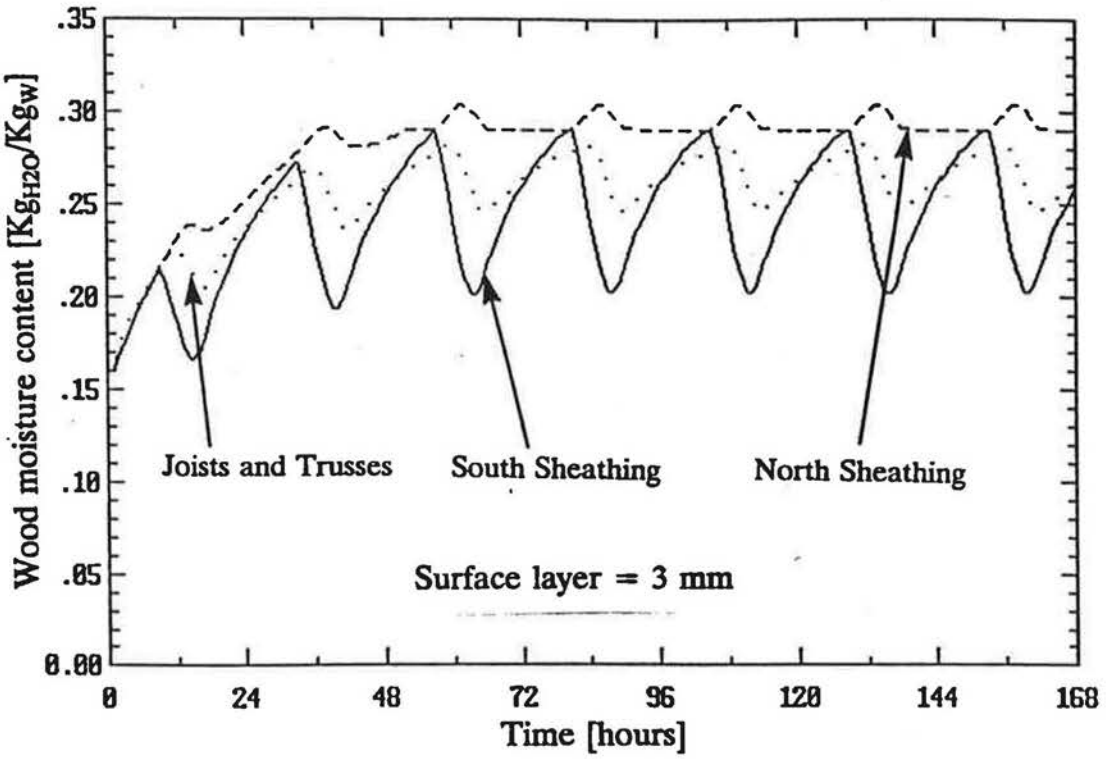

Figure 7-1a. Diurnal variation of wood surface MC for attic simulation 10. With the maritime climate, a ventilation rate of 24 ACH, clear skies, and standard wood surface layer thickness.

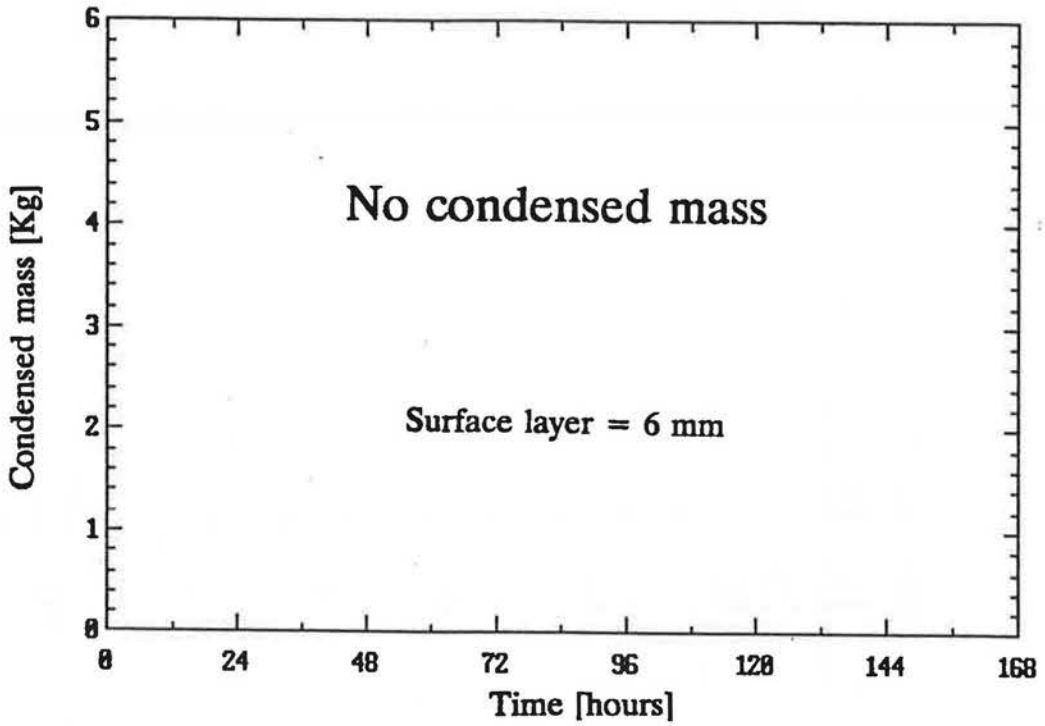

Figure 7-2b. Periodic condensation on attic sheathing for attic simulation 10. For a standard attic, maritime climate, a ventilation rate of 24 ACH, clear skies and double the surface wood layer thickness.

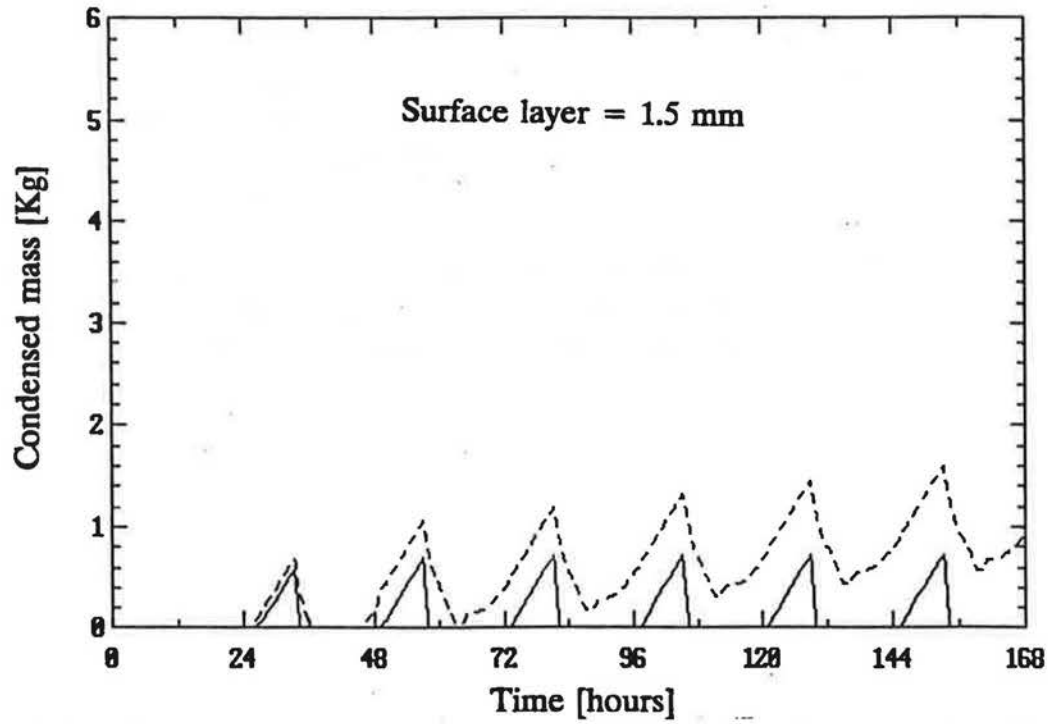

Figure 7-2c. Periodic condensation on attic sheathing for attic simulation 10. For a standard attic, maritime climate, a ventilation rate of 24 ACH, clear skies and half the surface wood layer thickness.

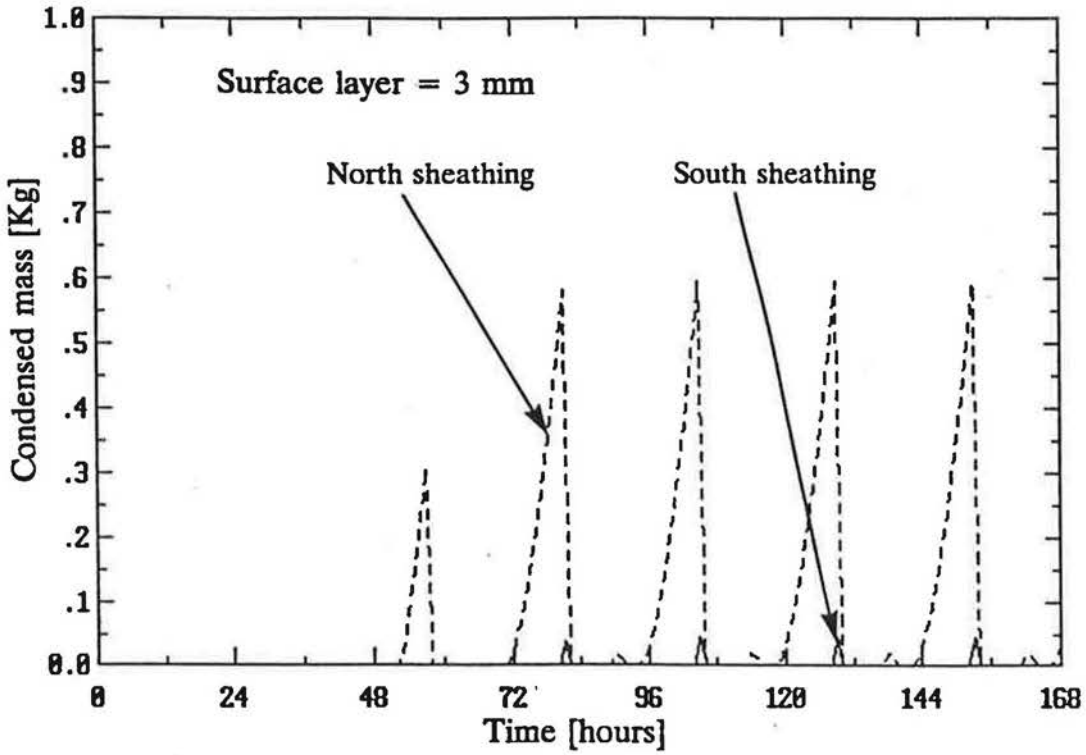

Figure 7-2a. Periodic condensation on attic sheathing for attic simulation 10. For a standard attic, maritime climate, a ventilation rate of 24 ACH, clear skies and standard surface wood layer thickness.

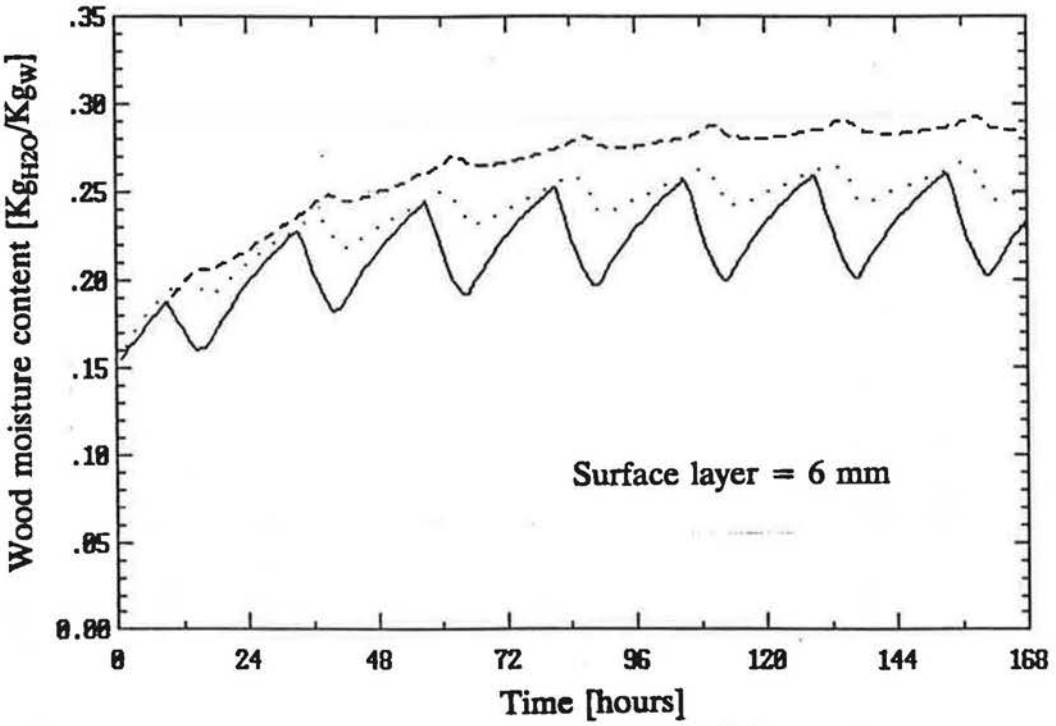

Figure 7-1b. Diurnal variation of wood surface MC for attic simulation 10. With the maritime climate, a ventilation rate of 24 ACH, clear skies, and double the surface wood layer thickness.

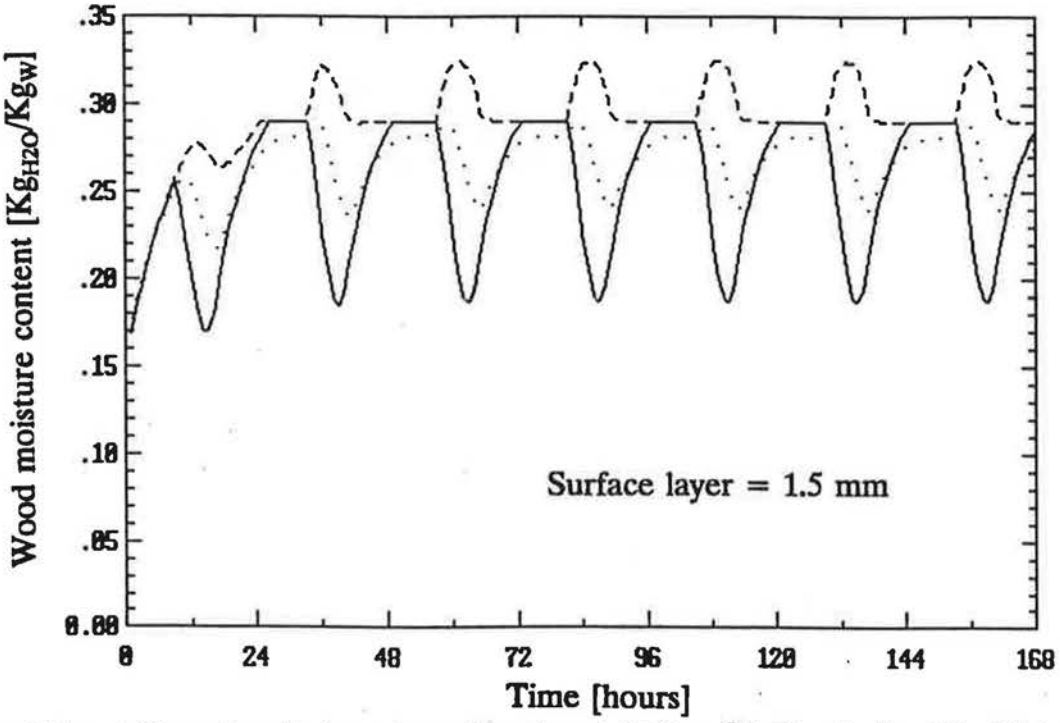

Figure 7-1c. Diurnal variation of wood surface MC for attic simulation 10. With the maritime climate, a ventilation rate of 24 ACH, clear skies, and half the surface wood layer thickness.

To examine the effect of changing the effective surface wood layer thickness simulation 10 was also performed with double and one half the wood surface layer thickness. For the standard tests shown in Figures 7-1a and 7-2a the sheathing surface layer thickness was 3mm. The results shown in Figures 7-1b and 7-2b are for a surface layer of 6mm (2/3 of the total sheathing),while Figures 7-1c and 7-2c are for a surface layer of 1.5mm (1/6 of the total sheathing). Comparing Figures 7-1a and 7-1b shows that increasing the surface layer thickness decreased the mean moisture content and also reduced the diurnal variations. Because the wood moisture content is not high enough for the wood vapour pressure to reach saturation there is no mass condensed for the 6mm thickness layer, as shown in Figure 7-2b. Halving the surface layer has the opposite effect as can be seen by comparing Figures 7-1a and 7-1c. The thinner surface layer has a higher mean moisture content and larger diurnal variations that result in the wood being at its saturation pressure for longer at night, as shown by the flat areas in the moisture content curves. Figure 7-2c shows that more mass is condensed on both sheathing surfaces, and is accumulating on the north facing sheathing. The trends shown in these results can be predicted by looking at a simple mass balance for the wood surface; for the same surface moisture flux, a node with a higher mass of wood will have a lower moisture content which affects the conditions under which condensed mass appears.

The results of examining the effect of surface layer thickness show that this is an important parameter for determining wood moisture content and the amount of condensed mass. Because the measurements of wood moisture content made for this study are an effective spatial average of the underlying wood they cannot be used to estimate appropriate surface layer thicknesses. To examine this problem more closely more experimental data are required. A simple experiment would be to perform a mass balance on samples of wood in a controlled environment (of temperature and vapour pressure). If measurements of surface condensation were made then an equivalent surface layer thickness could be found that would make the model predict the surface condensation.

Condensing mass

In some of the simulations mass condenses on the sheathing at night and is later evaporated during the day. An example of periodic condensation is shown in Figure 7-3 for simulation 22 which is for a sealed attic in a prairie climate with clear skies. The peak values are about 1.7 Kg on the north sheathing and 2.6 Kg on the south sheathing. The higher peak values for north sheathing are characteristic of

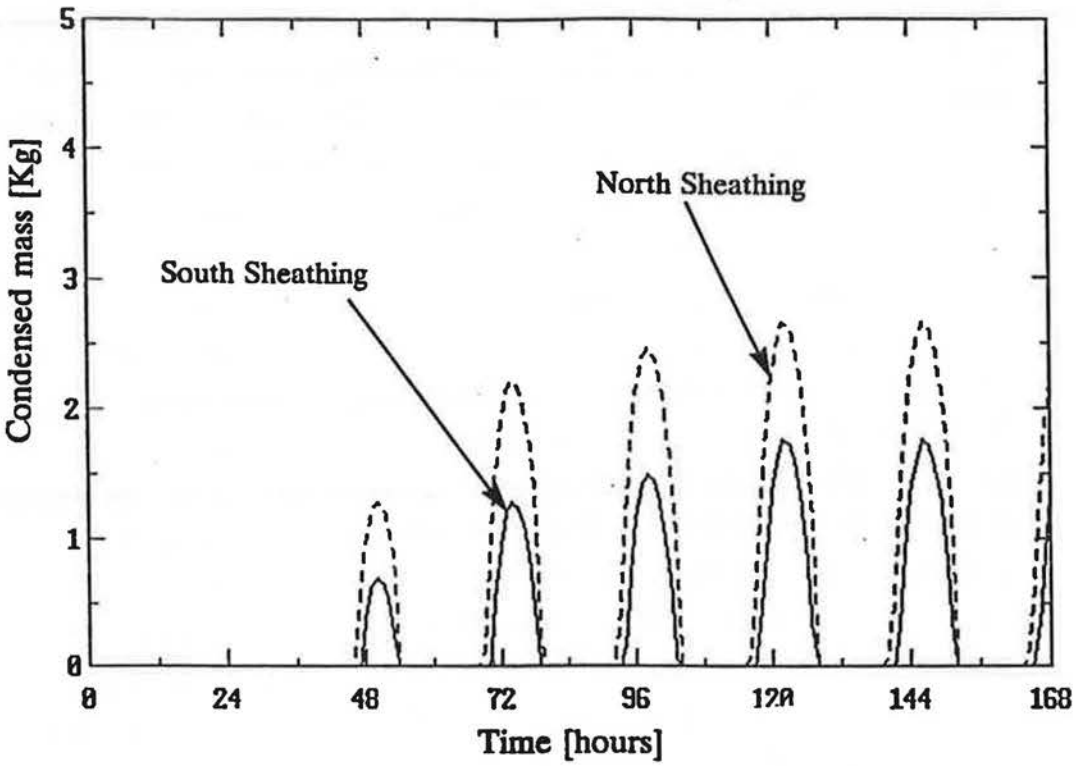

Figure 7-3. Periodic condensation on attic sheathing for attic simulation 22. For a sealed attic, prairie climate, a ventilation rate of 0.8 ACH and clear skies.

clear sky simulations because the north sheathing does not receive as much solar radiation during the day so its temperatures are lower, and less moisture is removed during the day.

In the worst cases not all the condensed mass is removed by daytime solar gains. This results in mass accumulation as shown in Figures 7-4a and 7-4b for two consecutive days of the same conditions : a sealed attic with an extractor fan on a timer with cloudy skies (simulation 25). The results in Figures 7-4a and 7-4b are for cloudy conditions where both sheathing surfaces experience the same radiation gains and losses and thus have the same temperatures and the same accumulating mass. The mass accumulates in a ratcheting fashion with deposition at night and evaporation during the day. The mass accumulates because the amount deposited exceeds the amount evaporated. The mass accumulates at a net rate of about 0.4 Kg/day on both sheathing surfaces.

For clear skies mass may accumulate on north sheathing but appear periodically on the south sheathing due to its higher daytime temperature. This is illustrated in Figure 7-5 which shows nighttime accumulation and daytime evaporation for both sheathing surfaces for simulation 18, a sealed attic with an extractor fan and clear skies.

7.4.2 Climatic zone

The maritime climate with the high ambient RH (and vapour pressure) produced much higher values of surface wood moisture content and attic air relative humidity. This can be seen by comparing the results of simulations 2 and 3 for the prairie climate to simulations 9 and 10 for the maritime climate. The maritime climate produced the worst case for the standard attic (simulation 10) with the only case of condensation on the sheathing. Over all the simulations the prairie climate the wood was always drier (never above 10% wood moisture content). The maritime climate produced higher relative humidity values that were often close to saturation. The exception is for low wind speeds that produce low ventilation rates (simulations 8 and 12). The decreased ventilation rate results in increased attic air temperatures, increased saturation pressure, and therefore lower relative humidities.

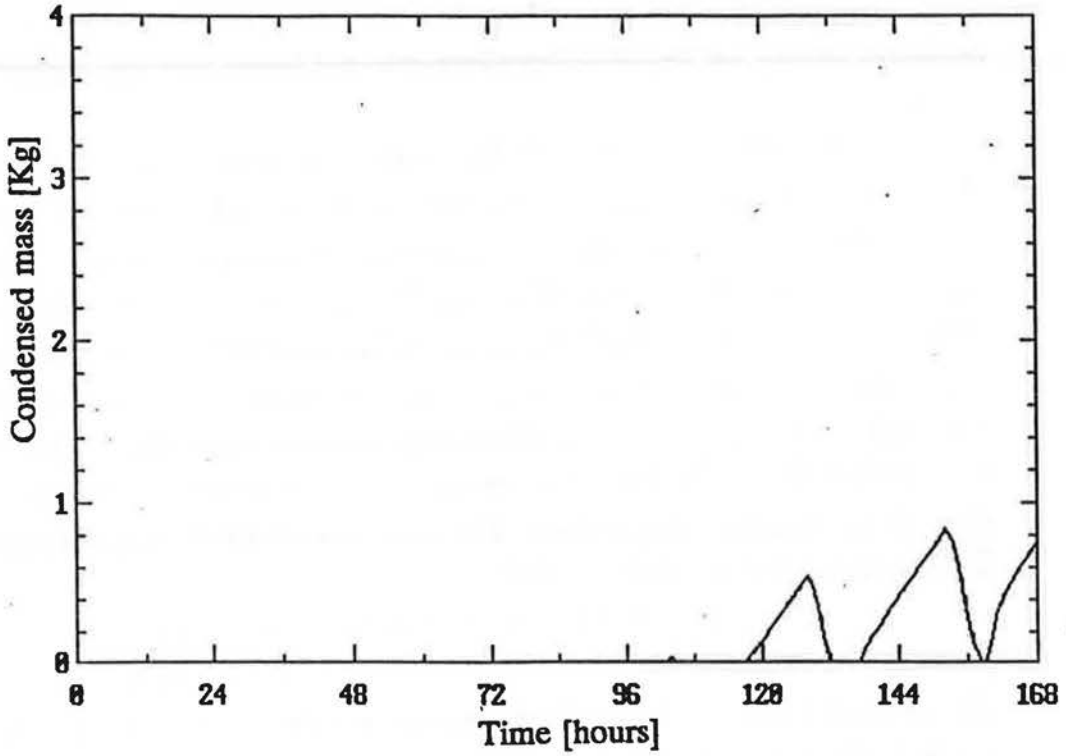

Figure 7-4a. Accumulating condensed mass on north and south sheathing for attic simulation 25 (week 1). For a sealed attic with an extraction fan on from 9 a.m. to 4 p.m., maritime climate and cloudy skies.

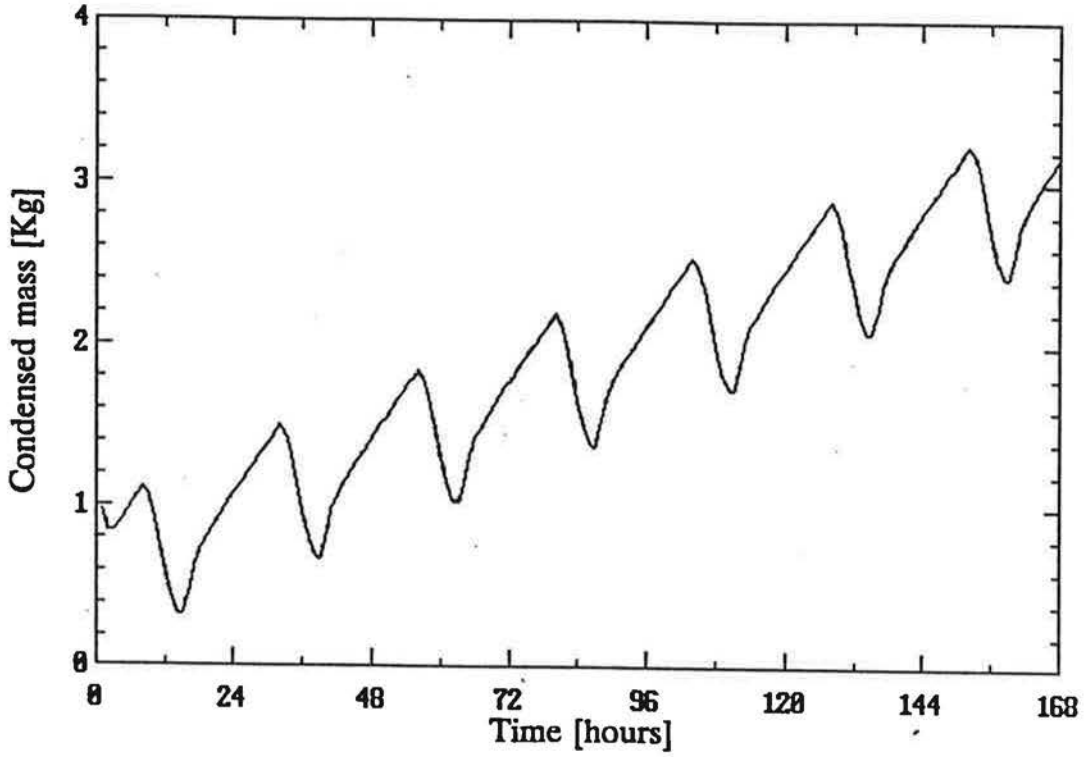

Figure 7-4b. Accumulating condensed mass on north and south sheathing for attic simulation 25 (week 2). For a sealed attic with an extractor fan on from 9 a.m. to 4 p.m., maritime climate and cloudy skies.

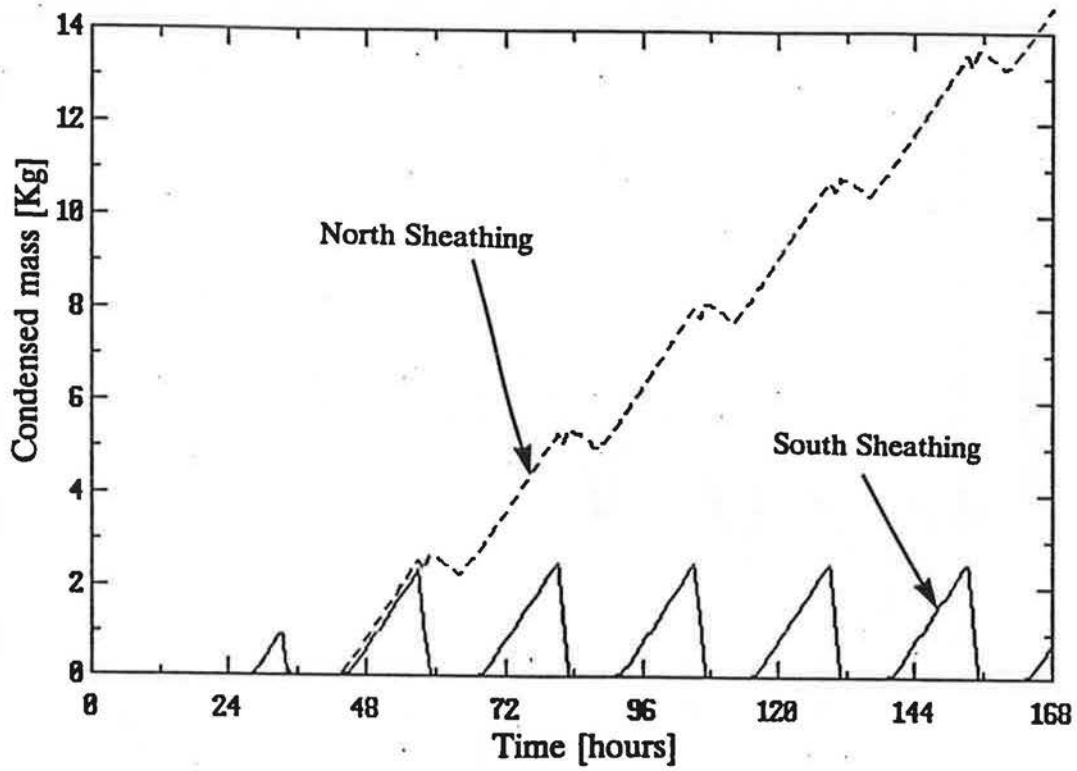

Figure 7-5. Accumulating condensation on north sheathing and periodic condensation on south sheathing for attic simulation 18. For a sealed attic with an extractor fan, maritime climate and clear skies.

7.4.3 Cloud cover

To best observe the results of changing cloud cover, compare simulations 1,2 and 3 for clear skies to simulations 4, 5 and 6 for cloudy skies. Clear skies produced larger extremes in all the predicted parameters due to the large change in temperatures from solar gains during the day and radiation to a clear sky at night. The most important effect for moisture deposition is the night time cooling of the sheathing that is greatest for clear skies. Measurements from Chapter 5 (see Figure 5-23) show that the outer sheathing temperature drops 3 to 4 degrees below the ambient temperature and 4 to 5 degrees below the attic air. The inner sheathing shows less temperature depression of about 2 degrees below the attic air, but it is still the coldest attic surface. Simulation 10 and simulations 16 through 19 show that clear skies produce condensation on the interior of the attic sheathing.

- The cooling of the sheathing due to night time radiation was found to be one of the most important factors in producing condensed mass accumulation.

7.4.4 Wind speed and ventilation rate

Because the wind dominates the calculation of ventilation rates and therefore the convective heat and mass transfer coefficients it had a significant effect on the simulations. For the standard attic simulations the ventilation rates ranged from about 2 ACH to about 24 ACH when changing from windspeeds of 0.5 m/s to 6 m/s. The effect of ventilation rate on the model predictions is shown by simulations 8, 9 and 10. The high ventilation rate in simulation 10 had the highest relative humidity (94% compared with 61%), the highest surface wood moisture content (29% compared with 12%) and condensing mass when the low ventilation rate simulation 8 had none. These results were due to increased ventilation rates acting to cool the attic and increase heat and mass transfer coefficients.

The flow through the ceiling was reduced by increased ventilation rates and wind speeds as shown by looking at groups of simulations where only the wind speed changes i.e. simulations 1,2 and 3, simulations 4, 5, and 6, simulations 8, 9, and 10 and simulations 11, 12 and 13. The significance of attic cooling, discussed above, is particularly important in light of the fact that the flow through the ceiling (and thus the moisture load from the house) decreases as ventilation rate increases. The maximum house to attic flow rate of 0.3 ACH represents a mass flow of 0.084 Kg/hour at indoor conditions of 20°C and 50% relative humidity. At the lowest ventilation rate of 2 ACH (simulation 8) the maritime outdoor climate of -1°C and

100% relative humidity supplies 0.263 Kg/hour of water vapour to the attic. This shows that even at low ventilation rates the flow of moisture from outside is more important than the flow through the ceiling for a standard attic. As will be shown later, the sealed attics that have all the inflow through the ceiling and fans that depressurize the attic are exceptions to the above result.

Figures 7-6 and 7-7 illustrate the effect of wind speed and ventilation rate on attic temperatures. Figure 7-6 is for simulation 1 where the windspeed was 0.5 m/s and Figure 7-7 is for simulation 3 where the windspeed was 6 m/s. The high windspeed (25 ACH) gave attic temperatures much closer to outdoor temperatures. Although the mean temperatures were only 0.5°C different, the low windspeed case had temperatures 10°C higher for a few hours in the middle of the day. The magnitude of the peaks in the sheathing temperature is even larger, as shown in Chapter 6. The high peak temperatures increase the vapour pressure in the wood thus driving moisture out of the wood. The lower relative humidities and wood moisture contents in the warmer, low ventilation rate attic simulations show that the higher peak temperature had a significant drying effect.

- In all the simulations increased ventilation never reduced attic moisture in terms of relative humidity, wood moisture content or condensation. The worst case results with respect to high moisture content and condensed mass were always at high ventilation rates (windspeeds).
- For standard attics the moisture flow through the ceiling is a small fraction (less than 1/3) of the total moisture transport into the attic.

7.4.5 Sealed attics

The sealed attic simulations (7, 21, 22 and 24) retained the same amount of ceiling leakage as the standard attics so that this leakage was a much greater proportion of the attic total. The simulations show that this made all of the inflow to the attic come through the ceiling. Having all the incoming air at a high moisture content (a humidity ratio of 0.00738 Kg_{H2O}/Kg_{air} compared with 0.00349 Kg_{H2O}/Kg_{air} for ambient maritime conditions) resulted in higher wood moisture content and more condensation problems. The sealed attic was the only one that produced condensation in a prairie climate (simulation 22). The wood moisture contents in this case were only 14% to 15% (fibre saturation is at about 30%) which shows the effect of the vapour pressure, wood moisture content and temperature relationship used in this model (see Chapter 4, section 4.3). This relationship calculates saturation

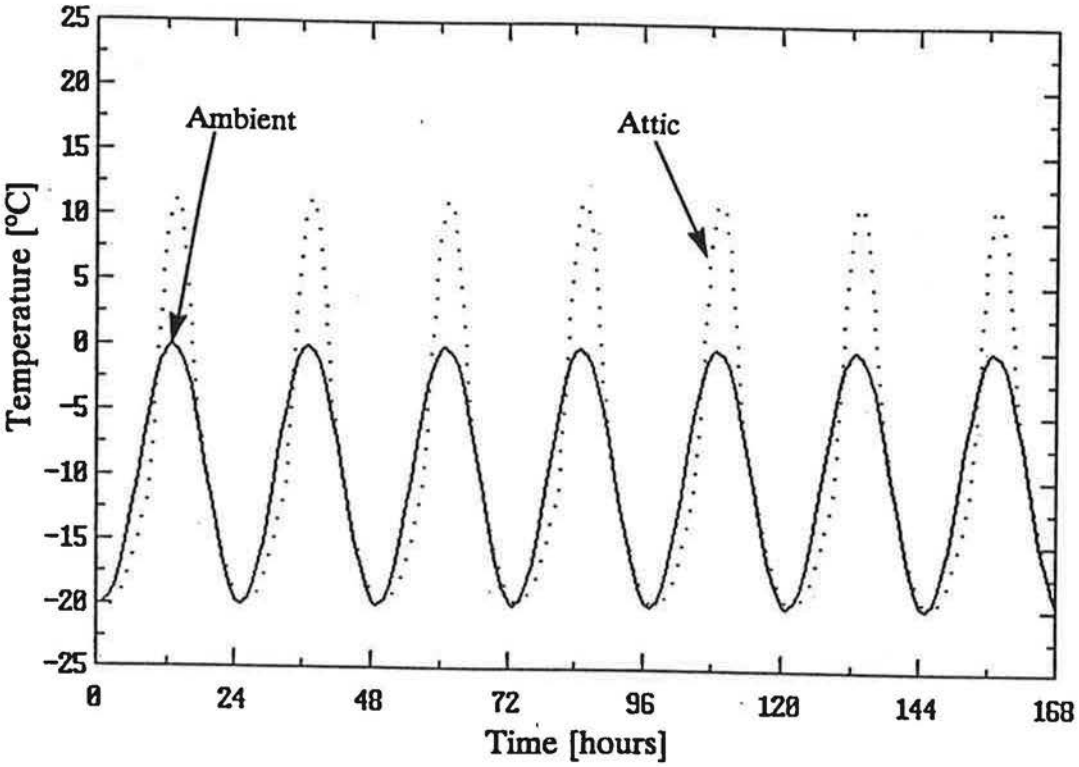

Figure 7-6. Diurnal variation of outdoor and attic air temperatures for the attic simulation 1. With the prairie climate, a ventilation rate of 1.9 ACH and mean attic temperature of -8.9°C.

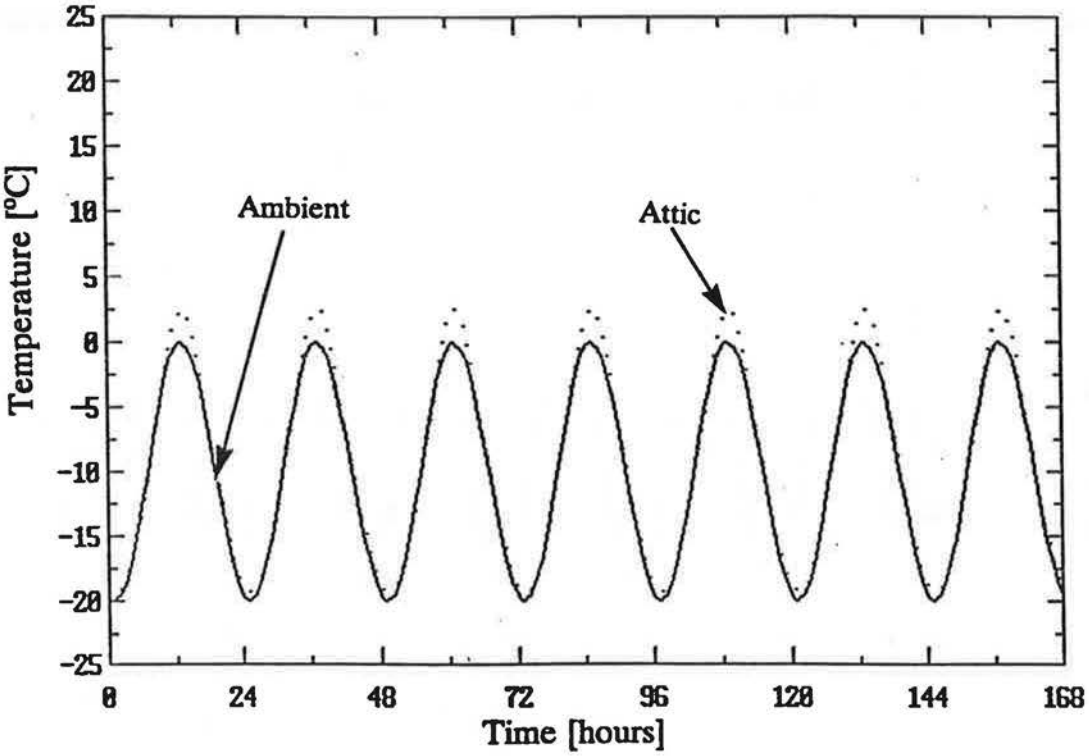

Figure 7-7. Diurnal variation of outdoor and attic air temperatures for the attic simulation 3. With the prairie climate, a ventilation rate of 25 ACH and mean attic temperature of -9.4°C.

pressures below fibre saturation point at low temperatures.

- These results show that sealing the attic leaks but not sealing the ceiling leaks produces worse moisture problems.

7.4.6 Balanced Fans

Compare simulation 17 for a sealed attic with a balanced fan to simulation 21 for the sealed attic without the fan system in the maritime climate. With the addition of a balanced fan system producing 7 ACH the attic ventilation rate increases from 0.7 ACH to 9 ACH. The flowrate through the ceiling only changes slightly from 0.7 to 0.8 ACH. This should have the effect of bringing more low moisture content air from outside into the attic, thus reducing moisture levels. The simulations show that using the balanced fan resulted in about 3% higher relative humidity and wood moisture content and similar condensed mass. This is because the increased ventilation rate reduces the attic temperatures and increases the surface heat and mass transfer coefficients. Simulation 23 is the same as simulation 17 but it has cloud covered skies instead of cloudy skies. The cloud covered sky limits the night time radiation losses that cool the attic sheathing. This increased sheathing (and overall attic temperature) prevents moisture condensation on the sheathing for this case. This shows how important it is to compare simulations that have the same cloud cover.

Simulations 20 and 22 in the prairie climate are for a sealed attic with and without a balanced fan respectively. These simulations show that the much drier prairie air with humidity ratios ranging from 0.00062 to 0.00125 Kg_{H2O}/Kg_{air} has a drying effect on the attic. The attic relative humidity is reduced from 87% to 72%, and the wood moisture contents are reduced by about 4%. More important is the prevention of attic air saturation and prevention of condensed mass on the sheathing.

- This result shows that balanced fans only remove moisture problems for a sealed attic if the outside air is sufficiently dry. i.e. in a prairie climate.

7.4.7 Extract and Supply Fans

The fans were added to a sealed attic to find out if they would reduce moisture problems. The extract and supply fans both had rated flows of 14 ACH (150 l/s), resulting in higher ventilation rates than for the balanced fan system. The fans were only tested for the maritime climate because the prairie climate produced no moisture problems with the sealed attic in these simulations. Simulations 18 and 19 show how a supply fan reversed the direction of flow through the ceiling because it pressurizes the attic instead of depressurizing (as the extraction fan does). For the

extraction fan (simulation 18) 2.7 ACH flowed from the house into the attic and for the supply fan (simulations 19) 2.1 ACH flowed from the attic to the house. This means that the moisture load on the attic due to ventilation flows is less with the supply fan. The simulation results show little difference between the two modes of operation. The relative humidities and wood moisture contents are only about 2% to 3% less with the supply fan. Mass condensed periodically in both attics but only accumulated in the attic with the extractor fan. These results are similar because of the extra cooling of the attic by the supply fan that draws more outside air into the attic instead of warmer indoor air. The cooling of the attic has a balancing effect that reduces the influence of reversing the flow direction through the ceiling.

Both the supply and extraction fans had worse results than the sealed attic with no fans shown in simulation 21. This is due to the extra cooling of the attic as a consequence of the increased ventilation rates. It is possible that smaller fans would have less of a cooling effect, however, they would also bring less fresh air into the attic for moisture removal. The effect of optimizing fan size will be discussed later.

The effect of lowering outdoor temperature for fan ventilated attics was examined in simulation 27. This simulation was for a supply fan in a maritime climate where the outside temperature was reduced to -5°C whilst keeping outdoor RH at 100%. Comparing to simulation 19, the lower temperatures resulted in about 6% lower wood moisture content and higher amounts of condensation on the north sheathing. In both simulations the wood is at its saturation pressure at night. The wood moisture content is lower at saturation for the lower temperature simulation due to the relationship between wood moisture content, vapour pressure and temperature used in the model. For the lower temperature simulation the wood is at saturation for a longer fraction of the day which results in the higher quantities of condensed mass.

- With a single fan it is better to install it as a supply fan to reduce moisture problems but the effectiveness is less than expected due to the extra attic cooling.

7.4.8 Extractor Fan on a Timer

Simulations 25 and 26 used the extractor fan on a timer from 9 a.m. to 4 p.m. This is a normal installation procedure for attics experiencing moisture problems. The greatest potential for moisture removal is when the attic air is at low relative humidity which occurs during warmer daytime hours. The fan on a timer produces

higher ventilation during the warmer daytime hours whilst not over ventilating during the cold night hours. As was shown in section 7.4.7, for the fans in continuous operation, overcooling of the attic at night can make moisture problems worse. At night the reduced ventilation with the fan off leads to higher attic temperatures and lower attic air relative humidities and less condensation.

Comparing simulations 26 to 18 shows that timed operation is an improvement over constant operation. The mean wood moisture contents are about 2% lower, there is five times less condensed mass on the north sheathing and no accumulation on the south sheathing. Comparing 26 to 19 shows that the fan on a timer was also an improvement over a constant supply fan.

- Fan ventilation worked best when the fan was only on during the day during which solar gains and attic temperatures are high. This is because moisture is removed form the wood during the warmer daytime hours.

7.4.9 Optimizing Fan Size

Simulations 19, 28 and 29 were performed to find if there is an optimum fan size that balances the moisture removal potential with the cooling effects (that increase moisture condensation) of a higher ventilation rate. The simulations were all performed for the maritime climate because the results of single fan simulations (discussed in section 7.4.7) have shown that the damp maritime climate requires fan size optimization. With too small a fan there would be no flow reversal at the ceiling and warm and moist indoor air enters the attic. With too large a fan the attic can be over ventilated, and therefore overcooled, which makes moisture problems worse. In the dry prairie climate it was shown that the extra moisture removal potential of the dry air compensated for the additional attic cooling by ventilation fans, and fan size optimization is not as crucial to good moisture removal performance. The fans were chosen to be supply fans as these gave the best results in continuous operation. Supply fans of 50, 100 and 300 cfm (0.024, 0.048 and 0.150 m^3/s and with maximum rated pressure differences of 32, 65 and 175 Pa) were used in simulations 28, 29 and 19 respectively. These fans produced mean attic ventilation rates of 3, 5 and 17 ACH, respectively.

The 50 cfm fan did not supply enough flow to completely pressurize the attic and stop the flow into the attic from through the ceiling. This resulted in slightly higher relative humidity and wood moisture content values than with the 100 cfm fan. Both smaller fans were better than the 300 cfm fan as they allowed higher attic temperatures due to their lower ventilation rates. The cooler attic resulting form the

high ventilation rates when using the 300 cfm suffered from condensation in the attic air, high wood moisture contents and mass condensation. The 100 cfm fan produced similar results to the standard attic in simulation 9. The advantage of the sealed attic with the supply fan is that the fan driven ventilation rate is independent of the weather conditions and so the attic will not be over or under ventilated at any time.

- It has been found that fan size can be optimized to reduce attic moisture problems. For the sealed attic in the maritime climate simulated here a fan providing 5 ACH in supply mode was found to result in the least moisture in the attic.

7.4.10 Snow on the roof

The last two simulations, 30 and 31, are for the standard attic with snow on the roof as described in section 7.1. Comparing the low wind speed simulations 30 and 8 (without snow), the reduced solar gains due to reduced absorbtivity mean that the attic temperature is about 2.5°C lower on average. The lower temperatures occur during the daytime where the reduced solar gain gives a peak temperature that is 9°C lower than the attic with no snow on the roof. The lower temperatures increased the mean relative humidity by 25% RH due to the reduced saturation pressure. In addition, the moisture content of the wood surfaces was increase by 6 to 9% and 0.8Kg/day of condensed mass appeared on the north sheathing. These results indicate that the reduction in solar gain has a greater effect than the increased thermal resistance provided by the covering of snow.

Comparing the high wind speed simulations 31 and 10 (at about 10 times the ventilation rate of simulations 30 and 8) the reduction in attic air temperature is much less than at low wind speeds and is only 0.4°C, and the snow covered attic has a mean relative humidity about 2% higher than the standard attic. The snow covered attic has surface wood moisture contents that are about 2% higher and the wood in both cases is near its saturation pressure all of the time. The condensed masses are increased with snow on the roof. On the south sheathing there is ten times (1 Kg peak) the amount of periodic condensation. On the north sheathing the amount of moisture that accumulates is increased from 0.2 to 0.6 Kg/day.

- Snow on the roof provides an insulating blanket and reduces external radiation gains during the day. The net effect is a colder attic with higher surface wood moisture content and more condensation problems.

7.4.11 Inner wood moisture content

In every simulation the inner wood nodes were observed to slowly dry out.

This is because inner wood nodes are not exposed to the high vapour pressure and relative humidity attic air at night (unlike the surface nodes) and they experience the highest daytime temperatures that dry the wood. This corresponds to the observations at AHHRF where low wood moisture contents were measured even when the surface was covered with a layer of frost.

For clear skies the south sheathing dried the fastest, coming to a steady value during the simulation, due to its greater daytime solar gain. The north sheathing and trusses responded much slower, drying by a few percent moisture content during the simulation. These results are illustrated in Figure 7-8 from simulation 9 in a maritime climate with clear skies, which shows how the drying occurs during the day with wood moisture content constant during the night.

The results for cloud covered skies are shown in Figure 7-9 for a maritime climate and the same wind speed (2.5 m/s) as in simulation 12 in Figure 7-8. Here the north and south sheathing have the same results as they experience the same solar gain. Both sheathing nodes dry faster than the trusses due to their solar gains, but all the attic wood dries slower than for clear sky conditions and have reduced their wood moisture contents by less than 5% at the end of the simulation.

7.4.12 Initial conditions

The initial assumption for wood moisture content imposes a transient at the beginning of the simulations as shown in Figure 7-1a. The effect of the initial condition was examined for a standard attic in the maritime climate for high wind speeds, low winds speeds, clear skies and cloudy skies. Simulations 14, 15 and 16 with the higher initial wood moisture content (19% instead of 15%) were compared with simulations 10, 11 and 13. There was negligible change in the stationary values of wood moisture content, relative humidity and condensing mass reached after 5 days. These values are summarized in Table 7-2. These results show that any reasonable assumption (within 20%) for initial wood moisture content in the attic will not affect the model predictions after a few days. Since the range of wood moisture contents is only from zero to approximately 30% (fibre saturation) it is easy to choose an initial wood moisture content that will only affect the model predictions for a few days. The only exception was the wood moisture content of the internal wood nodes whose time response is very slow, as shown earlier in Figures 7-8 and 7-9.

- The choice of initial conditions does not affect the model predictions after the first few days.

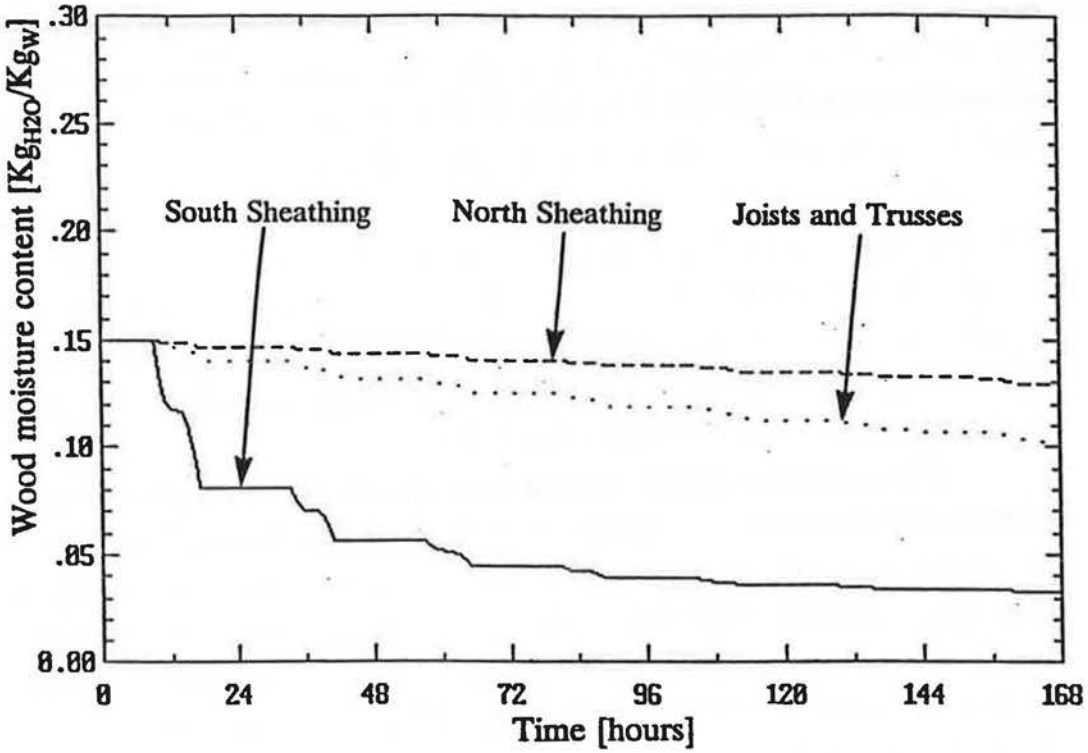

Figure 7-8. Drying of inner wood for clear skies attic simulation 9, maritime climate.

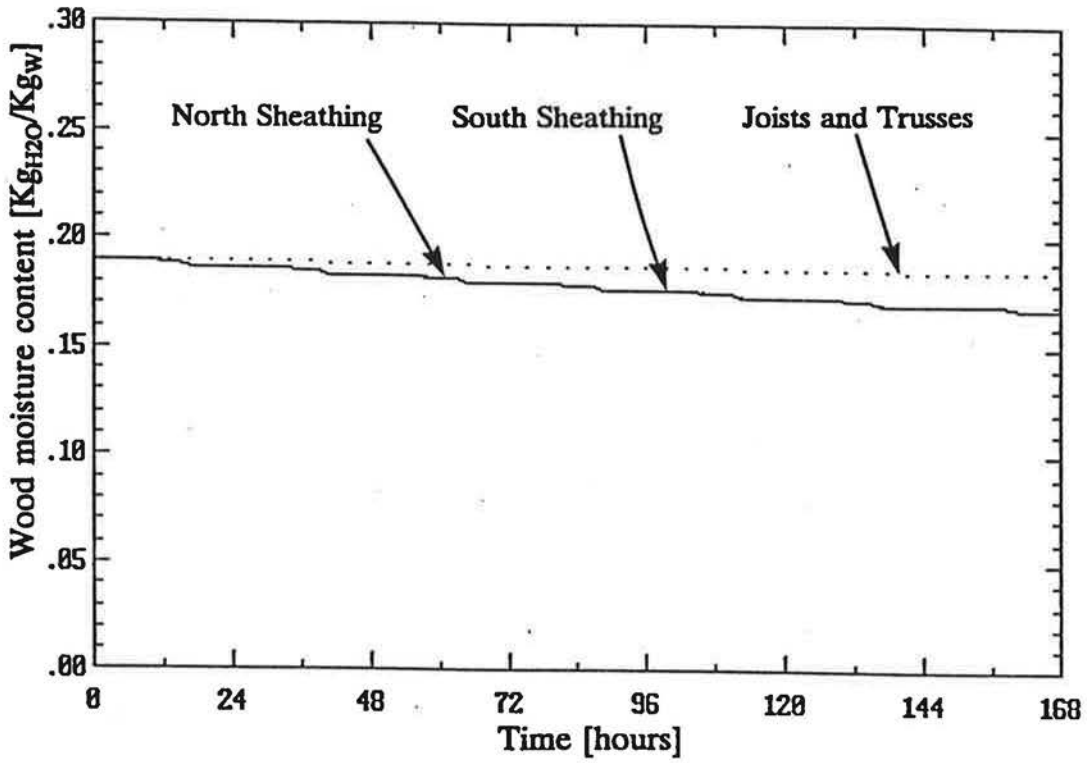

Figure 7-9. Drying of inner wood for cloudy skies for attic simulation 15, maritime climate.

7.5 Summary of attic moisture simulation results

A model for predicting attic wood moisture contents, relative humidities and condensing masses has been used for a range of attic moisture simulations. The moisture model includes a two zone attic and house ventilation model and an attic heat transfer model. These models, and their verification by comparison to measured data have been discussed in previous chapters. The simulations covered a range of ambient conditions for temperature, relative humidity, wind speed and cloud cover. In addition two different attic construction types were tested: a standard attic with leakage equal to that required by the Canadian Building Code (NBCC (1990)) and a sealed attic. The sealed attic was also tested with various fan combinations to examine the effect of fan ventilation. The following conclusions were drawn from the results of the simulations.

The choice of initial conditions does not affect the model predictions after the first few days so that good initial estimates of wood moisture content are not necessary. The maritime climate always produces worse moisture problems than the dryer prairie climate.

The cooling of the sheathing due to night time radiation was the dominant factor in producing condensed mass accumulation. The condensing masses tend to accumulate during the night and evaporate during the day. If the amount condensed at night exceeds that evaporated during the day then mass will accumulate at the surface. In every simulation the inner wood nodes were observed to slowly dry out. This corresponds to the observations at AHHRF where low wood moisture contents were measured even when the surface was covered with a layer of frost.

Increased ventilation did not reduce attic moisture in terms of relative humidity, wood moisture content or condensation, except for the single case of adding a ventilation fan to a sealed attic in a prairie climate. Generally, the worst case results were always at high ventilation rates (windspeeds). The exception to this is for the sealed attics with unsealed ceiling leakage. For these attics most of the air flowing into the attic came from the house and had a high moisture content and temperature. Having all the incoming air at a high moisture content resulted in higher wood moisture contents and more condensation problems than for standard attics even though the mean temperatures were higher. The sealed attic was the only one that produced condensation in a prairie climate because of the moisture entering the attic from the house. The wood moisture contents in this case were only 14% to 15% which is far below fibre saturation at about 30% moisture content. This result

shows the effect of the assumed relationship between vapour pressure, temperature and wood moisture content, because at low temperatures the wood moisture content at its saturation pressure is calculated to be below the fibre saturation point.

With a single fan it is always better to install it as a supply fan. The attic was slightly cooler than with an extractor fan, but had less moisture accumulating. Fan ventilation worked best when the fan was only on during the day when solar gains and attic temperatures are high because this is when moisture is forced out of the wood and can be convected away by the attic air. It has been found that fan size can be optimized to reduce attic moisture problems. In this case a fan providing 5 ACH in supply mode was found to result in the least moisture in the attic. With too small a fan there is no flow reversal at the ceiling and warm and moist indoor air enters the attic. With too large a fan the attic is over ventilated and therefore overcooled which makes moisture problems worse.

Snow on the roof provides an insulating blanket and reduces external radiation gains during the day. The net effect is a cooler attic with higher wood moisture content and more condensation problems. the simulations showed that the reduction in daytime solar gains (by about a factor of 2) had a greater effect than the additional insulation provided by the snow layer on the sheathing.

Chapter 8. Summary and Recommendations

8.1 Attic simulation models

An attic simulation model has been developed to predict attic ventilation rates, temperatures, wood moisture content and condensed masses. The model consists of the following three components:

- The first component is a ventilation model that predicts attic and house ventilation rates.
- The second part is a heat transfer model that predicts attic temperatures based on the previously calculated ventilation rates.
- The third component is a moisture transport model that uses the ventilation rates and temperatures calculated by the other models to predict attic wood moisture content and condensed masses.

The three model components have been verified using measured data taken in two attics and houses at the Alberta Home Heating Research Facility. After the models were verified they were used in simulations to test attic ventilation strategies for moisture control.

8.1.1 Ventilation model

The ventilation model is a two zone model. The two zones are the house and the attic. The interzonal flow is important because this flow transports warm and humid air into the attic space in winter. The ventilation model performs a mass balance on the two zones for the to find the ventilation flows. The flow rates are calculated based on house and attic characteristics such as leakage area, distribution of leakage and wind shelter due to upwind obstacles. The pressures that drive the ventilation flows are calculated from the ambient conditions of wind speed, wind direction and air temperatures. The major differences from previous work are as follows:

Both the house and the attic use the same method to find their ventilation rates and so the following comments apply to both zones.

- Wind shelter is based on a wind shadow wake method which gives numerical values of effective windspeed reduction for each building surface.
- Wind pressure coefficients are calculated as a continuous function of wind angle. Different pressure coefficient values are used for houses in a row to account for the change in flow pattern around the building. The wind pressure coefficients used in the model are surface averaged values from wind tunnel studies by other investigators.

- Mass flows are balanced instead of volume flows.
- Distributed leakage is combined with localised leakage to include the effects of flues and passive vents.
- Large openings such as doors and windows may have two-way counterflow with interfacial mixing.
- Fans are included using a fan performance curve so that if large natural pressures due to wind and stack effect occur at fan location then the fan flow will change.
- The indoor to attic exchange rate given by the interzonal flow through the ceiling is calculated. This is used to find the amount of heat and water vapour transferred from the attic to the house for the heat transfer and moisture transport models

8.1.2 Attic heat transfer model

The attic heat transfer model used here is based on that used by Ford (1982) and includes conduction, convection, and radiation. The energy balance for the attic is based on a lumped heat capacity analysis that allows the transient terms in the energy balance to be modelled. The attic is divided into nodes representing the attic air, the sheathing and the rest of the wood in the attic. An energy balance for each node results in a set of linear equations in temperature that are solved using gaussian elimination. The major differences from Ford's model are as follows.

- Attic ventilation and ceiling flow rates are calculated using a ventilation model instead of being a required input. This requires an iterative procedure because the attic ventilation and ceiling flow rates depend on the attic temperature and visa versa.
- An additional node is used to account for the mass of wood in joists and trusses in the attic.
- Forced natural convection heat transfer coefficients are used inside the attic instead of free convection coefficients.

8.1.3 Attic moisture transport model

The attic moisture transport model is based on a transient mass balance of water that includes ventilation flows, convective wood surface exchange and diffusion within the wood. The attic is divided into several nodes: the attic air, the wood surfaces and the interior of the wood. Mass balances are derived for each node by equating the mass change rate to the sum of the fluxes. The mass balance is

performed simultaneously for all the nodes. Major differences from previous attic moisture transport models are as follows.

The model developed for this study uses a relationship between vapour pressure, temperature and wood moisture content to calculate the rate of change of wood moisture content with time. This allows for the wood nodes and the attic air node vapour pressures to be solved for simultaneously, thus performing mass balance of water for the attic. Previous models by Ford (1982), Cleary (1985), and Gorman (1987) did not solve for the mass transfer at each node simultaneously. They balance the air flow mass transfers to find the attic air water vapour content which was then used to calculate mass transferred to and from the wood surfaces. The mass transfer at the wood surface was not included in their mass balance for the attic air and mass was not truly conserved for the attic.

The same relationship between wood moisture content, vapour pressure and temperature used above in the mass balance means that the transient terms in the mass balance at each node can be calculated. This means that it is not necessary to assume steady state conditions as assumed by previous authors. Removing the assumption of steady state is important because the surface wood moisture contents can change very rapidly making the assumption of steady-state difficult to justify.

The air flow through the attic to and from outside as well as the flow through the ceiling are different for each hour and are calculated using the attic ventilation model shown in Chapter 2. Previous models have either assumed a constant ventilation and ceiling flow rate or required them as measured inputs. Being able to predict the correct ventilation rate is important not only for the mass balance of water vapour, but also because the attic temperatures and surface heat and mass transfer rates are functions of the ventilation rate.

Mass condenses at the wood surfaces and appears as free water as well as being absorbed by the wood. Ford (1982) assumed that the wood was always saturated so that any mass flow to the wood appeared as condensation, and wood moisture contents were not calculated. Gorman (1987) assumed that there was no condensation until the wood reached fibre saturation (at 28% wood moisture content). A more sophisticated approach was taken for the model developed in this study. This approach uses the wood moisture content, vapour pressure and temperature relationship developed by Cleary (1985) to calculate the vapour pressure at a node given its temperature and moisture content. Condensation is assumed to occur when mass is transferred to a node that is at its saturation pressure. This

condensed mass is not included as moisture in the wood but is kept track of separately by the calculation procedure. If there is condensed mass at a node then the node remains at saturation pressure until all the condensed mass is removed from the node.

8.2 Measurements

The attic ventilation, heat transfer and moisture models, described in the previous chapters were verified with field data taken over the course of two heating seasons (1990-91 and 1991-92) at The Alberta Home Heating Research Facility. The two attics selected for this study had different venting arrangements. Attic 5 was selected as a low leakage attic where there were no intentional openings such as roof or soffit vents in the exterior portion on the attic envelope. The only leakage area in attic 5 was the unavoidable leakage associated with construction of the attic envelope. Attic 6 was fitted with continuous soffit vents along the north and south eaves and two flush-mounted attic vents. The measurement system monitored ventilation rates, room to attic exchange rates, temperatures, relative humidities and wood moisture contents in the attics. In addition, ambient conditions of wind speed, wind direction, temperature, relative humidity and solar radiation were measured for use as inputs to the models.

8.3 Measurement results

The measurements showed that the attic ventilation rates were dominated by wind and indoor-outdoor temperature difference has a weak effect. In attic 5 the ventilation rates reached a maximum of about 7 ACH (Air Changes per Hour) with an average of about 1.5 ACH. For attic 6 the maximum ventilation rate is limited by the measurement system to about 20 ACH and the mean is about 6 ACH. Wind shelter was also found to be important and reduced ventilation rates by up to 70% when the wind blew along the row and the attics were sheltered.

The indoor-attic exchange rates were found to be small, typically about 5% of the total ventilation rate for attic 5 and about 1% in attic 6. For both attics the measured indoor-attic exchange rates had a maximum value of about 0.25 ACH, with typical values about 0.15 ACH. This is an important result for the moisture load on the attic as the air coming from inside the house is warm and moist and can be a significant source of moisture.

Temperatures in the attic displayed a strong diurnal cycle much greater than that of the ambient air. This is due to daytime solar gains and nighttime radiative losses. The most significant result is the cooling of attic sheathing at night that results

in moisture deposition on theses surfaces.

The measured wood moisture contents were always low and near the operating limit of the wood moisture meter. This is because the moisture pins are below the surface and are not sensitive to the larger changes in wood moisture content at the wood surface.

8.4 Model verification

The models were verified by comparing their predicted values to those measured as outlined above.

8.4.1 Ventilation model

For attic 5 the underprediction is -0.017 ACH on average and for attic 6 it is -0.5 ACH. Most of this underprediction occurs when the wind blows along the row of houses. When expressed as an average percentage error the results are -9.3% and +4.3% for 5 and 6 respectively. The attic 6 percentage error is positive because its overpredictions occur at lower ventilation rates where the percentage overprediction is high but the ACH overprediction is relatively small. Considering the uncertainty in pressure coefficients, wind shelter and leakage distributions these errors are about as small as could be reasonably expected.

The shelter part of the ventilation model was found to reproduce the sheltering effect of adjacent buildings fairly well following the changes in measured ventilation with wind direction. The model tends to underpredict ventilation rates by about 25% when the wind blows along the row and the attic experiences the greatest shelter. This indicates that the shelter model overpredicts the shelter effects. This is because the very simple model used here cannot model the spatial variation of pressure coefficients over the attic surfaces that causes pressure differences not accounted for in the model.

For the room-attic exchange rates there is good agreement between measured and predicted values considering how small these exchange rates are in comparison to the total ventilation rates. The mean errors for house-attic exchange rates in attic 5 were -0.015 ACH (4.5%) and 0.0014 ACH (14.3%) in attic 6.

The attic ventilation model includes fans using a fan performance curve and this was found to work well as the errors with the fan on and off only differ by 0.05 ACH. This actually represents a reduction in the percentage error from 6% with the fan off to 3% with the fan on over the time period of the fan tests (November 1991 to February 1992). This is because the fan dominates the ventilation rate in most conditions because it supplies about 9 ACH which is much greater than the average

natural ventilation rates.

8.4.2 Heat transfer model

The temperature predictions of the heat transfer model were compared with measured values over a one week period that exhibited strong diurnal variations in input parameters of outdoor temperature and solar radiation and a large range of ventilation rates and windspeeds that produce large changes in surface heat transfer coefficients. This was done to exercise the model over as wide a range of parameters as possible.

The heat transfer model has been run in combination with the ventilation model in an iterative process because the heat transfer (and resulting attic air temperature) and ventilation rate are not independent. Because ventilation is a weak function of attic air temperature then this process seldom requires more than two or three iterations. The mean errors in temperatures for both attics are typically about 1°C. In attic 5 the mean absolute error was also calculated as this gives an estimate of the error expected for a single hour rather than a weekly average where positive and negative errors cancel out. This error is always greater than or equal to the mean error. The mean absolute errors ranged from 1.8 to 4.3 °C over all the nodes in the attic.

8.4.3 Moisture transport model

Ideally the moisture transport model predictions for surface wood moisture content and condensation should be compared with measured values. As yet there is no reliable method of measuring these quantities with an automated data acquisition system so the verification of the moisture transport model will be based on comparisons to the measured attic air relative humidity and the internal wood moisture content of the wood.

For the internal wood moisture content all the measured values stayed relatively constant between 5% and 7%. Due to the lower limit of the measuring instrument all that can be said about these values is that they are less than about 7%. These low values of measured wood moisture content for internal wood occur in all seasons in both attics. The only way this measured data can be used to verify the model is if the model also predicted low wood moisture contents. The model predicted that the inner wood remains at low moisture content for both attics over all weather conditions. The predicted values of wood moisture content corresponded with the measured wood moisture contents, however, this does not verify any of the

dynamic performance of the model. The mean error for both attic 5 and 6 relative humidity predictions is about -2.5% RH with an absolute error of about 5% RH.

8.5 Attic moisture simulations

After the verification of the models had been carried out they were used in simulations to study the effects of individual parameters on the moisture build up in attics. The simulations covered a broad range of windspeeds, ventilation rates, temperature differences and solar gains. To examine the effects of fan ventilation a sealed attic configuration was used so that the fans would dominate the ventilation rates. The following results and conclusions were made:

8.5.1 General model performance

The cooling of the sheathing due to night time radiation was found to be a dominant factor in producing condensed mass accumulation. This is because the coldest wood surface in the attic will tend to have the lowest vapour pressure and hence the greatest flow of moisture from the attic air. In addition, the coldest surface will also reach its saturation vapour pressure first. The condensing masses tend to accumulate during the night and evaporate during the day. If the amount condensed at night exceeds that evaporated during the day then mass will accumulate at the surface.

The choice of initial wood moisture contents was found to have a negligible effect on the model predictions after the first few days. This means that when running simulations the results will be unbiased by the chosen initial conditions.

The maritime climate always produces worse moisture problems than the dryer and colder prairie climate. This is because the potential for moisture removal by the moist maritime air is less than with the dry prairie air.

Snow on the roof provides an insulating blanket and reduces external radiation gains during the day. The net effect is a cooler attic with higher wood moisture content and more condensation problems. the simulations showed that the reduction in daytime solar gains (by about a factor of 2) had a greater effect than the additional insulation provided by the snow layer on the sheathing.

In every simulation the inner wood nodes were observed to slowly dry out. This corresponds to the observations at AHHRF where low wood moisture contents were measured even when the surface was covered with a layer of frost.

The diurnal cycles of ambient temperature, relative humidity and solar gain produce diurnal cycles in wood moisture content, attic relative humidity and condensed masses. The diurnal cycles are complex and require modelling of transient

terms in the heat transfer and moisture transport analyses as well as the use of a relationship between wood moisture content, vapour pressure and temperature for the wood. The diurnal temperature cycle of the sheathing can cause condensed mass to appear at the surface as it cools at night even though there is no net mass transfer to the surface as moisture is forced out of the wood according to the wood moisture content, vapour pressure and temperature relationship discussed in sections 4.2 and 4.3 in chapter 4. The condensing masses tend to accumulate during the night and evaporate during the day. If the amount condensed at night exceeds that evaporated during the day then mass will accumulate at the surface.

8.5.2 Effects of attic leakage configuration

Increased ventilation did not reduce attic moisture in terms of attic air relative humidity, wood moisture content or condensation, and the worst case results were always at high ventilation rates (windspeeds). This is mainly because the higher ventilation rates reduced attic temperatures and made the sheathing cooler and closer to saturation. The sealed attics had higher temperatures but all the incoming air was from the house and at a high vapour pressure. This resulted in higher wood moisture contents and more condensation problems. This shows that if an attic is sealed to raise its temperature to reduce moisture condensation on the sheathing then the ceiling is the most important area to seal. The sealed attic was the only one that produced condensation in a prairie climate. The wood moisture contents in this case were only 14% to 15% which is well below the fibre saturation point of about 30%). This shows the effect of the assumed vapour pressure, wood moisture content and temperature relationship.

8.5.3 Effects of fan ventilation

The simulations using balanced fans showed that the outdoor air conditions are an important consideration in fan installation. In a prairie climate it was found that the balanced fans resulted in reduced wood moisture contents but the damper maritime air resulted in increased wood moisture contents. With a single fan the simulations showed that it is always better to install it as a supply fan because this reverses the direction of the flow through the ceiling that is a source of moisture for the attic. Fan ventilation worked best when the fan was only on during the day when solar gains and sheathing temperatures are high because this is when moisture is forced out of the wood.

It was found that fan size can be optimized to reduce attic moisture problems. Supply fans were chosen for optimization testing because they can reverse the

direction of flow through the ceiling. Increased ventilation rates have two counteracting effects. There is potential for more moisture removal but the cooling effect increases the wood moisture content. The optimum fan size will balance these effects so as to remove the most moisture without over cooling the attic. In addition, the supply fan should pressurize the attic enough to prevent flow from the house into the attic. In this case a fan providing 5 ACH in supply mode was found to result in the least moisture in the attic.

8.6 Recommendations for Future Research

Measurements of static pressure, mean and turbulent windspeeds in the near wake of buildings are required to improve models of shelter for ventilation calculations. Other improvements in attic ventilation modelling could be obtained with more complete pressure coefficient measurements over a range of building shapes and roof pitch angles. Measurement of cloud cover for estimating external radiation heat transfer is required to improve attic heat transfer modelling.

Measurements of surface moisture in attics are required to verify attic model predictions. Current measurements give either the wood moisture content of the inner bulk wood or some combined value of surface and inner wood moisture content if the measuring pins are not isolated from surface condensation. These measurements need to separate the wood moisture content of the wood surface and the condensed mass on the surface. The results of these measurements could also be used to determine the appropriate surface wood layer thickness for use in the moisture transport model.

The number of nodes that each section of the attic wood is divided into could be increased. This would make the lumped heat and moisture capacity assumption at each node more valid and would reveal the temperature and moisture profiles within the wood. Another addition that could be made to the model is the inclusion of the porous attic insulation in the moisture balance. The insulation could be included in the same way as the attic wood, with a surface node that exchanges moisture with the attic air and an internal node for moisture storage.

The results of the simulations showed the importance of the relationship between wood moisture content, vapour pressure and temperature. Not only does the relationship determine the vapour pressure used to calculate the flows of water vapour to and from the wood surface, but it also gives low wood moisture contents at saturation pressure. The wood moisture content at saturation decreases with decreasing temperature so that a reduction in temperature leads to moisture leaving

the wood and appearing as condensed mass. This means that condensed mass may appear at a wood surface without there being a flux of moisture to the surface from the air. The relationship used in this study was developed by Cleary (1985) for wood moisture contents greater than 0°C. This relationship has been extrapolated to lower temperatures for use in attic simulations . To increase confidence in the model predictions severe winter conditions, this relationship needs to be verified at lower temperatures.

8.7 Major contributions made by this study

In this study a new method of simulating ventilation, heat and mass transfer in attics has been developed where ventilation, heat transfer and moisture transport have been combined into a single model. The main developments and important contributions of this study are:

- the development of a two zone attic ventilation model that calculates the house, attic and interzonal (ceiling) flow. The ventilation model calculates wind shelter using a new wind shadow method and calculates the shelter and wind pressure coefficients as continuous functions of wind direction.
- the coupling of heat transfer and ventilation models.
- the use of a complete transient mass balance for the attic moisture that includes the attic wood.
- the use of combined models. Ventilation and heat transfer models are used to calculate inputs for the moisture model so that ventilation rates and temperatures do not have to be measured or entered by the user.
- calculation of ventilation rates, temperatures and moisture levels using envelope leakage, indoor temperature and relative humidity, and outdoor weather conditions.
- the development of a large data base of measurements for evaluating attic models and identifying important parameters for attic moisture accumulation.

REFERENCES

References

Abrantes, V., (1985), "Thermal Exchanges Through Ventilated Attics", Proc. ASHRAE/DOE/BTECC Conf. on the Thermal Performance of the Exterior Envelopes of Buildings III, Clearwater Beach.

Akins, R.E., Peterka, J.A., and Cermak, J.E., (1979), "Averaged Pressure Coefficients for Rectangular Buildings", Wind Engineering, Vol. 1, Proc. 5th Int. Conf. on Wind Engineering, pp.369,380.

ASHRAE, (1989), Handbook of Fundamentals, ASHRAE, Atlanta, Georgia.

ASTM, (1982), "Measuring Air Leakage by the Fan Pressurization Method", Annual Book of ASTM Standards, part 18, pp.1484-1493.

Brown, W.G. and Solvason, K.R., (1962), "Natural Convection through rectangular Openings in Partitions. 1 - Vertical Partitions", Int. J. Heat and Mass Transfer, Vol.5, pp.859-868.

Burch, D.M., (1980), "A Mathematical Model for Predicting Attic Ventilation Rates Required for Preventing Condensation on Roof Sheathing", ASHRAE Trans. 1980, Vol.86, Part 1, pp.201-212.

Burch, D.M., (1980b), "Infrared Audits of Roof Heat Loss", ASHRAE Trans., Vol.89, p.209.

Burch, D.M., Lemay, M.R., Rian, B.J., and Parker, E.J., (1984), "Experimental Validation of an Attic Condensation Model", ASHRAE Trans., Vol. 90, Part 2A, pp.59-78.

Burch, D.M., and Luna, D.E., (1980), "A Mathematical Model for Predicting Attic Ventilation Rates Required For Prevention of Condensation on Roof Sheathing", ASHRAE Trans. Vol. 86, p.201.

Castro, I.P, and Robbins, A.G., (1977), "The Flow Around A Surface Mounted Cube in Uniform and Turbulent Streams", J. Fluid Mech., Vol. 79, Part 2, pp.307-335.

CGSB Standard 149.10-M86, (1986), "Determination of the Airtightness of Building Envelopes by the Fan Depressurization Method", Canadian General Standards Board.

Choong, E.T., and Skaar, C., (1969), "Separating Internal and External Resistance to Moisture Removal in Wood Drying", Wood Science, Vol.1, No.4, pp. 200-202.

Choong, E.T., and Skaar, C., (1972), "Diffusivity and Surface Emissivity in Wood Drying", Wood and Fiber, Vol.4, pp. 80-86.

Cleary, P.G., (1985), "Moisture Control by Attic Ventilation - An In Situ Study", ASHRAE Trans. 1985, Vol.91, Part 1.

CMHC, (1988), "CMHC/CHBA Task Force on Moisture Problems in Atlantic Canada", Canada Mortgage and Housing Corporation.

Cockroft, J.P., and Robertson, R., (1976), "Ventilation of an Enclosure Through a Single Opening", Building and Environment, Vol.11, pp.29-35.

Crommelin, R.D., and Vrins, E.M.H., (1988), "Ventilation through a single opening in a scale model", Air Infiltration Review, Vol. 9(3), pp.11-15.

Counihan, J., Hunt, J.C.R., and Jackson, P.S., (1974), "Wakes Behind Two-Dimensional Surface Obstacles in Turbulent Boundary Layers", J. Fluid Mech., Vol.64, Part 3, pp.529-563.

Cunningham, M.J., (1990), "Modelling of Moisture Transfer in Structures -II. A Comparison of a Numerical Model, an Analytical Model and some Experimental Results", Building and Environment, Vol.25, No.2, pp.85-94.

Dale, J.D. and Ackerman, M, Y, (1993), "The Thermal Performance of a Radiant Panel Floor-Heating System", To be published in ASHRAE Transactions 1993, Vol.99, Part 1.

Davies, M.E., Quincey, V.G., and Tindall, S.J., (1980), "The Near-Wake of a Tall Building Block in Uniform and Turbulent Flows", Proc. 5th Int. Conf. on Wind Engineering, Vol. 1, pp.289-298.

Fairey, P.W., (1983), "Effect of Infra-red Radiation Barriers on the Effective Thermal Resistance of Building Envelopes", Proc. ASHRAE/DOE Conf. on the Thermal Performance of the Exterior Envelopes of Buildings II.

Feustal, H.E., and Raynor-Hoosen, A., (1990), "Fundamentals of the Multizone Model - COMIS", Air Infiltration and Ventilation Centre Technical Note 29, AIVC, Coventry, U.K.

Ford, J.K., (1982), "Heat Flow and Moisture Dynamics in a Residential Attic", PU/CEES Report #148, Princeton University.

Forest, T.W., and Walker,I.S., (1993), "Attic Ventilation Modelling and Verification", CMHC report in preparation.

Fuji, T., and Imura,, H., (1972), "Natural-Convection Heat Transfer from a Plate with Arbitrary Inclination", Int. J. Heat and Mass Transfer, Vol.15, pp.755-767.

Gilpin, R.R., Dale, J.D., Forest, T.W. and Ackerman, M.Y., (1980), "Construction of the Alberta Home Heating Research Facility and Results for the 1979-1980 Heating Season", Department of Mechanical Engineering Report #23, University of Alberta, Edmonton, Canada.

Gorman, T.M., (1987), "Modelling Attic Humidity as a Function of Weather, Building Construction and Ventilation Rates", Ph.D. Dissertation, College of Environmental Science and Forestry, State University of New York.

Haghighat, F., Rao,J. and Fazio,P., (1991), "The Influence of Turbulent Wind on Air Change Rates - a Modelling Approach", Building and Environment, Vol. 26, No.2, pp.95-109.

Haysom, J.C., and Swinton, M.C., (1987), "The Influence of Termination Configuration on the Flow Performance of Flues", CMHC Report, Scanada Consultants Limited.

Holman, J.P., (1981), "Heat Transfer - 5th Ed.", McGraw - Hill.

Hunt, J.C.R., (1971), "The Effect of Single Buildings and Structures", Phil. Trans. Royal Soc. London, Part A, Vol. 269, pp.457-467.

Hunt, J.C.R., (1974), "Wakes Behind Buildings", Proc. of Atmospheric Environment Committee, Aeronautical Research Council, October 1974.

Hunt, J.C.R., Abell, C.J., Peterka, J.A., and Woo, H.G.C., (1978), "Kinematical Studies of the Flows Around Free or Surface-Mounted Obstacles; Applying Topology to Flow Visualisation", J. Fluid Mech., Vol.86, Part 1, pp.179-200.

Irwin, J.S., (1979), "A Theoretical Variation of the Wind Profile Power Law Exponent as a Function of Surface Roughness and Stability", Atmospheric Environment, Vol.13, pp.191-194.

James, M.L., Smith, G.M., and Wolford, J.C, (1977), "Applied Numerical Methods for Digital Computation with FORTRAN and CSMP -Second Edition", Harper and Row, pp.345-348.

Kiel, D.E., and Wilson, D.J., (1986), "Gravity Driven Flows Through Open Doors", Proc. Seventh Air Infiltration and Ventilation Centre Conference, AIVC, Coventry, pp. 15.1 - 15.16.

Kiel, D.E., Wilson, D.J., and Sherman, M.H., (1985), "Air Leakage Flow Correlations for Varying House Construction Types", ASHRAE Trans. 1985, Vol. 91, Part 2.

Lemberg, R., (1973), "On the Wakes Behind Bluff Bodies in a Turbulent Boundary Layer", University of Western Ontario Report BLWT-3-73.

Liddament, M.W., (1986), "Air Infiltration Calculation Techniques - An Applications Guide", Air Infiltration and Ventilation Centre.

McAdams, W., (1954), "Heat Transmission - 3rd Ed.", McGraw-Hill, p.249.

Modera, M., and Wilson, D.J., (1989), "The Effects of Wind on residential Building Leakage Measurements", Special Technical Publication of the ASTM Symposium on Air Change Rate and Air Tightness in Buildings, April 1989, Atlanta, GA.

National Building Code of Canada (NBCC), (1990), p.253.

NRC, (1984), "Humidity, Condensation and Ventilation in Houses", Proceedings of Building Science Insight '83, Division of Building Research, National Research Council Canada, Ottawa, Canada.

Newman, A.B., (1931), "The Drying of Porous Solids : Diffusion Calculations", Trans. Am. Inst. Chem. Eng., Vol.27, pp.310-333.

Ogniewicz, Y., and Tien, C.L., (1981), "Analysis of condensation in porous insulation", Int. J. Heat and Mass Trans. 1981, Vol. 24, p.421.

Panofsky, H.A. and Dutton, J.A., (1986), "Atmospheric Turbulence", John Wiley and Sons, p.160.

Parmelee, G., and Aubele, W., (1952), "Radiant Energy Emission of Atmosphere and Ground", ASHVE Trans., Vol. 58, p.85.

Peavy, B.A., (1979), "A Model for Predicting the Thermal Performance of Ventilated Attics", Summer Attic and House Ventilation, NBS Special Publication 548, pp.119-145.

Peterka, J.A., Meroney, R.N., and Kothari, K.M., (1985), "Wind Flow Patterns About Buildings", J. Wind Eng. and Ind. Aero., Vol. 21, pp.21-38.

Pfaff, F., and Garrahan, P., (1986), "New Temperature Correction Factors for the Portable Resistance-type Moisture Meter", Forest Products Journal, Vol.36, pp.28-30.

Sellers, W.D., (1965), "Physical Climatology", University of Chicago Press, Chicago, p.21 and p.41.

Sforza, P.M., and Mons, R.E., (1970), "Wall Wake: Flow Behind A Leading Edge Obstacle", AIAA Journal, Vol.8, December 1970, pp.2162-2167.

Shaw, B.H., and Whyte, W., (1974), "Air Movement Through Doorways. The influence of temperature and its control by forced airflow", Building Services Engineer, Vol.42(12), pp.210-218.

Sherman, M.H., (1980), "Air Infiltration in Buildings", Ph.D. Thesis, Energy and Environment Division, Lawrence Berkeley Laboratories, University of California.

Sherman, M.H., and Grimsrud, D.T., (1980), "The Measurement of Infiltration using Fan Pressurization and Weather Data", Report # LBL-10852, Lawrence Berkeley Laboratories, University of California.

Siau, J.F., (1984), "Transport Processes in Wood", Springer Verlag.

Spiegel, M.R., (1968), "Mathematical Handbook of Formulas and Tables", Shaum's Outline Series, McGraw-Hill.

Sulatisky, M., (1984), "Airtightness Tests on 200 New Houses Across Canada: Summary of Results", BETT publication No. 84.01, Energy, Mines and Resources Canada.

Tao, Y.-X., Besant, R.W., and Rezkallah, K.S., (1990), "Heat and Moisture Transport through a Glass-Fiber Slab with One Side Subject to a Freezing Temperature", Water in Exterior Walls: Problems and Solutions, ASTM STP 1107, American Society for Testing and Materials, Philadelphia.

Walker, I.S., (1989), "Single Zone Air Infiltration Modelling", M.Sc. Thesis, Department of Mechanical Engineering, University of Alberta, Edmonton, Canada.

Walker, I.S., (1992), "Pressure Coefficients on Sheltered Buildings", Air Infiltration Review, Vol.13, No.4, Air Infiltration and Ventilation Centre, Coventry, U.K.

Walker, I.S. and Wilson, D.J., (1990a), "AIM-2 The Alberta Infiltration Model", Department of Mechanical Engineering Report #71, University of Alberta, Edmonton, Canada.

Walker, I.S. and Wilson, D.J., (1990b), "Including Furnace Flue Leakage in a Simple Air Infiltration Model", Air Infiltration Review, Vol. 11, No. 4, September 1990, AIVC, Coventry, pp.4-8.

Walker, I.S. and Wilson, D.J., (1993), "Evaluating Models for Superposition of Wind and Stack Effect in Air Infiltration", to be published in Building and Environment 1993.

Wieringa, J., (1980), "Representativeness of wind observations at airports", Bulletin Am. Met. Soc., No. 61, pp.962-971.

Wilkes, K.E., (1983), "Dynamic Thermal Performance of Walls and Ceilings/Attics", Proc. ASHRAE/DOE Conf. on the Thermal Performance of the Exterior Envelopes of Buildings II, pp.131-159

Wilkes, K.E., (1989), "Model for the Thermal Performance of low-sloped Roofs", Proc. ASHRAE/DOE/BTECC/CIBSE Conf. on the Thermal Performance of the Exterior Envelopes of Buildings IV, Orlando, Florida.

Wilson, D.J., (1979), "Flow Patterns Over Flat-Roofed Buildings and Application to Exhaust Stack Design", ASHRAE Trans., Vol. 85, Part 2, pp.284-295.

Wilson, D.J. and Walker, I.S., (1991a), "Passive Ventilation to Maintain Indoor Air Quality", Department of Mechanical Engineering Report #81, University of Alberta, Edmonton, Canada.

Wilson, D.J. and Walker, I.S., (1991b), "Wind Shelter Effects on a Row of Houses", Proc. 12th AIVC Conf., Ottawa, Canada.

Wilson, D.J. and Walker, I.S., (1992), "Feasibility of Passive Ventilation by Constant Area Vents to Maintain Indoor Air Quality", Proc. Indoor Air Quality '92, ASHRAE/ACGIH/AIHA Conf., San Francisco, October 1992.

Wiren, B.G., (1985), "Effects of Surrounding Buildings on Wind Pressure Distributions and Ventilation Losses for Single Family Houses : Parts 1 and 2", National Swedish Institute for Building Research Report M85:19.

Wollenweber, G.C., and Panofsky, H.A., (1989), "Dependence of Velocity Variance on Sampling Time", Boundary Layer Meteorology, No.47, pp.205-215.

Woo, H.G.C., Peterka, J.A., and Cermak, J.E., (1977), "Wind Tunnel Measurements in the Wakes of Structures", NASA Contractor Report NASA CR-2806.

Wood Engineering Handbook, (1982), U.S. Forest Products Laboratory, Prentice-Hall, p.3-8.

Yen, Y-C., (1981), "Review of Thermal Properties of Snow, Ice and Sea Ice", CRREL Report 81-10, U.S. Cold Regions Research and Engineering Laboratory, Springfield, Va.

APPENDIX A

Appendix A: Example calculations for integrated ventilation flows

A.1 Example Calculations for Wall Flow

Consider the case where $T_{in} > T_{out}$ with counterflow where $H_{NL} > H_f$. For the section of the wall below H_{NL}

$$M_{w,j,in} = \frac{\rho_{out} C_{w,j}}{(H_e - H_f)} \int_{H_f}^{H_{NL}} \left(\Delta P_I + S_{U,j}^2 C p_i P_U - z\ P_T'\right) dz \tag{A-1}$$

Let

$$\Gamma(z) = \Delta P_I + S_{U,j}^2 C p_i P_U - z P_T' \tag{A-2}$$

then

$$d\ \Gamma = -P_T'\ dz \tag{A-3}$$

Substituting equations A-2 and A-3 in A-1 gives

$$M_{w,j,in} = -\frac{\rho_{out} C_{w,j}}{(H_e - H_f) P_T'} \int_{\Gamma(z=H_f)}^{\Gamma(z=H_{NL})} \Gamma^n d\,\Gamma \tag{A-4}$$

Integrating equation A-4:

$$M_{w,j,in} = -\frac{\rho_{out} C_{w,j}}{(H_e - H_f) P_T'} \frac{1}{(n+1)} \Gamma^{(n+1)} \Big|_{\Gamma(z=H_f)}^{\Gamma(z=H_{NL})} \tag{A-5}$$

Substituting Γ back into equation A-5:

$$M_{w,j,in} = -\frac{\rho_{out} C_{w,j}}{(H_e - H_f) P_T'} \frac{1}{(n+1)} \left(\Delta P_I + S_{U,j}^2 C p_i P_U - z P_T'\right)^{(n+1)} \Big|_{z=H_f}^{z=H_{NL}} \tag{A-6}$$

Evaluating A-6 at the limits:

$$M_{w,j,in} = -\frac{\rho_{out} C_{w,j}}{(H_e - H_f) P_T'} \frac{\left(\Delta P_I + S_{U,j}^2 C p_i P_U - H_{NL} P_T'\right)^{(n+1)} - \left(\Delta P_I + S_{U,j}^2 C p_i P_U - H_f\ P_T'\right)^{(n+1)}}{n+1} \tag{A-7}$$

The first term is zero by definition of the neutral level in equation 2-19 and equation

A-7 becomes

$$M_{w,i,in}=\frac{\rho_{out}C_{w,i}}{(H_e-H_f)P_T'}\frac{1}{(n+1)}\left(\Delta P_I+S_{U,i}^2 Cp_i P_U-H_f P_T'\right)^{(n+1)} \qquad \text{(A-8)}$$

Using the definition of the pressure at the bottom of the wall, ΔP_b, from equation 2-56 equation A-8 becomes

$$M_{w,i,in}=\frac{\rho_{out}C_{w,i}}{(H_e-H_f)P_T'}\frac{\Delta P_b^{(n+1)}}{(n+1)} \qquad \text{(A-9)}$$

which is the same as equation 2-64.

A.2 The six possible cases for wall flow when $T_{in} \neq T_{out}$

For convenience the definitions given by equations 2-56 and 2-57 for ΔP_t and ΔP_b are used here.

For $T_{in} > T_{out}$. There are three possible cases for integrating equation 2-62:

Case 1. All wall above H_{NL} - all flow out

$$M_{w,i,in} = 0$$

$$M_{w,i,out}=\frac{\rho_{in}C_{w,i}(\Delta P_t^{n+1}-\Delta P_b^{n+1})}{(H_e-H_f)P_T'(n+1)} \qquad \text{(A-10)}$$

Case 2. All wall below H_{NL} - all flow in

$$M_{w,i,out} = 0$$

$$M_{w,i,in}=\frac{\rho_{out}C_{w,i}(\Delta P_t^{n+1}-\Delta P_b^{n+1})}{(H_e-H_f)P_T'(n+1)} \qquad \text{(A-11)}$$

Case 3. H_{NL} on the wall with flow in below H_{NL} and flow out above H_{NL}.

$$M_{w,i,out}=\frac{\rho_{in}C_{w,i}\Delta P_t^{n+1}}{(H_e-H_f)P_T'(n+1)} \qquad \text{(A-12)}$$

For $T_{in} < T_{out}$. There are also three possible cases:

$$M_{w,i,in}=\frac{\rho_{out}C_{w,i}\Delta P_b^{n+1}}{(H_e-H_f)P_T'\ (n+1)} \qquad \text{(A-13)}$$

Case 1. All wall above H_{NL} - all flow in

$$M_{w,i,out} = 0$$

$$M_{w,i,in}=\frac{\rho_{out}C_{w,i}(\Delta P_b^{n+1}-\Delta P_i^{n+1})}{(H_e-H_f)P_T'\ (n+1)} \qquad \text{(A-14)}$$

Case 2. All wall below H_{NL} - all flow out

$$M_{w,i,in} = 0$$

$$M_{w,i,out}=\frac{\rho_{in}C_{w,i}(\Delta P_b^{n+1}-\Delta P_i^{n+1})}{(H_e-H_f)P_T'\ (n+1)} \qquad \text{(A-15)}$$

Case 3. H_{NL} on the wall with flow out below H_{NL} and flow in above H_{NL}.

$$M_{w,i,out}=\frac{\rho_{in}C_{w,i}(-\Delta P_b)^{n+1}}{(H_e-H_f)P_T'\ (n+1)} \qquad \text{(A-16)}$$

$$M_{w,i,in}=\frac{\rho_{out}C_{w,i}(-\Delta P_i)^{n+1}}{(H_e-H_f)P_T'\ (n+1)} \qquad \text{(A-17)}$$

A.3 Example calculation for flow through open doors and windows

Kiel and Wilson (1986) determined the flows through open doors and windows by integrating the vertical velocity profile in the opening. The velocities were found by applying Bernoulli's equation to streamlines passing through the opening. This assumes steady, irrotational and incompressible flow.

The different inside and outside air densities mean that the reference density used for the flow changes depending on the flow direction. Both inflow and outflow cases are derived below.

A.3.1 Flow into opening

For flow into the opening the flow density is ρ_{out} and the inflow velocity is given by Kiel and Wilson as

$$U_{in}=\left(\frac{2(P_{out,z}-P_{in,z})}{\rho_{out}}\right)^{\frac{1}{2}} \qquad \text{(A-18)}$$

where $P_{out,z}$ is the outside pressure, $P_{in,z}$ is the inside pressure, U_{in} is the flow velocity into the opening. The pressure difference driving the flow ($P_{out,z}$ - $P_{in,z}$) is found using equation 2-18. Because both $P_{in,z}$ and $P_{out,z}$ depend on height, z, the inflow velocity is also a function of z. The total mass flow, M_{in}, must therefore be found by integrating U_{in} with height, z, over the area of inflow.

$$M_{in}=\rho_{out}KW\int U_{in}dz \qquad \text{(A-19)}$$

where W is the width of the opening and K is the flow coefficient for the opening that includes turbulent mixing effects. K is found using equation 2-73. The limits of integration for equation A-19 depend on the location of the opening with respect to the neutral level H_{NL}. The example calculation here is for inflow below H_{NL} where $T_{in} > T_{out}$ where H_{NL} falls within the opening. The limits of integration are then the height of the bottom of the opening, H_b, and the neutral level, H_{NL}. Substituting equation 2-18 for the pressure difference (and assuming that air is an ideal gas so that the density differences are expressed in terms of temperature differences) and equation A-18 in equation A-19 gives

$$M_{in}=\rho_{out}KW\int_{z=H_b}^{z=H_{NL}}\left(CpS_U^2U^2-\frac{2gz(T_{in}-T_{out})}{T_{in}}+\frac{2\Delta P_I}{\rho_{out}}\right)^{\frac{1}{2}}dz \qquad \text{(A-20)}$$

Let

$$\Gamma(z)=CpS_U^2U^2-\frac{2gz(T_{in}-T_{out})}{T_{in}}+\frac{2\Delta P_I}{\rho_{out}} \qquad \text{(A-21)}$$

then

$$d\,\Gamma = -\frac{2g(T_{in}-T_{out})}{T_{in}}dz \qquad \text{(A-22)}$$

Substituting equations A-21 and A-22 into A-20

$$M_{in} = -\rho_{out} KW \frac{T_{in}}{2g(T_{in}-T_{out})} \int_{\Gamma(z=H_b)}^{\Gamma(z=H_{NL})} \Gamma^{\frac{1}{2}} d\,\Gamma \qquad \text{(A-23)}$$

Integrating equation A-23 gives

$$M_{in} = -\rho_{out} KW \frac{T_{in}}{2g(T_{in}-T_{out})} \frac{2}{3}\Gamma^{\frac{3}{2}} \Big|_{\Gamma(z=H_b)}^{\Gamma(z=H_{NL})} \qquad \text{(A-24)}$$

Substituting Γ back into equation A-24 yields

$$\begin{aligned} M_{in} = &-\rho_{out} \frac{KWT_{in}}{3g(T_{in}-T_{out})}\left(CpS_U^2U^2 - \frac{2gH_{NL}(T_{in}-T_{out}))}{T_{in}} + \frac{2\Delta P_I}{\rho_{out}}\right)^{\frac{3}{2}} \\ &+\rho_{out} \frac{KWT_{in}}{3g(T_{in}-T_{out})}\left(CpS_U^2U^2 - \frac{2gH_b(T_{in}-T_{out})}{T_{in}} + \frac{2\Delta P_I}{\rho_{out}}\right)^{\frac{3}{2}} \end{aligned} \qquad \text{(A-25)}$$

where the first term is zero by definition of H_{NL} in equation 2-19. The final equation for flowrate is

$$M_{in} = \rho_{out} \frac{KWT_{in}}{3g(T_{in}-T_{out})}\left(CpS_U^2U^2 - \frac{2gH_b(T_{in}-T_{out})}{T_{in}} + \frac{2\Delta P_I}{\rho_{out}}\right)^{\frac{3}{2}} \qquad \text{(A-26)}$$

A.3.2 Flow out of opening

In this case the density of the flow is ρ_{in} and equation A-18 becomes

$$U_{in} = \left(\frac{2(P_{out,z}-P_{in,z})}{\rho_{in}}\right)^{\frac{1}{2}} \qquad \text{(A-27)}$$

For flow out of the opening $P_{in,z} > P_{out,z}$ and the sign of the pressure difference term is negative. Therefore U_{in} will also be negative which implies outflow. This agrees with the convention applied to the other ventilation model leaks where inflow is

positive and outflow is negative. The pressure difference driving the flow, ($P_{out,z}$ - $P_{in,z}$), is found using equation 2-18. The total mass flow, M_{out}, is found by integrating U_{in} over the area of inflow.

$$M_{out}=\rho_{in}KW\int U_{in}dz \qquad \text{(A-28)}$$

The limits of integration for equation A-28 depend on the location of the opening with respect to the neutral level H_{NL}. The example calculation here is for inflow above H_{NL} where $T_{in} > T_{out}$ where H_{NL} falls within the opening. The limits of integration are H_{NL} and the top of the opening, H_t. Substituting equation 2-18 for the pressure difference (and assuming that air is an ideal gas so that the density differences are expressed in terms of temperature differences) into equation A-27 for velocity and then using this in equation A-28 gives

$$M_{out}=\rho_{in}KW\int_{z=H_{NL}}^{z=H_t}\left(\frac{\rho_{out}}{\rho_{in}}CpS_U^2U^2-\frac{\rho_{out}}{\rho_{in}}\frac{2gz(T_{in}-T_{out})}{T_{in}}+\frac{2\Delta P_I}{\rho_{in}}\right)^{\frac{1}{2}}dz \qquad \text{(A-29)}$$

Unlike the inflow case the densities do not cancel in the wind and stack pressure terms.

Let

$$\Gamma(z)=\frac{\rho_{out}}{\rho_{in}}CpS_U^2U^2-\frac{\rho_{out}}{\rho_{in}}\frac{2gz(T_{in}-T_{out})}{T_{in}}+\frac{2\Delta P_I}{\rho_{in}} \qquad \text{(A-30)}$$

then

$$d\,\Gamma=-\frac{\rho_{out}}{\rho_{in}}\frac{2g(T_{in}-T_{out})}{T_{in}}dz \qquad \text{(A-31)}$$

Substituting equations A-30 and A-31 into A-29

$$M_{out}=-\rho_{in}KW\frac{\rho_{in}}{\rho_{out}}\frac{T_{in}}{2g(T_{in}-T_{out})}\int_{\Gamma(z=H_{NL})}^{\Gamma(z=H_t)}\Gamma^{\frac{1}{2}}d\,\Gamma \qquad \text{(A-32)}$$

Integrating equation A-32 gives

$$M_{out} = -\rho_{in} KW \frac{\rho_{in}}{\rho_{out}} \frac{T_{in}}{2g(T_{in}-T_{out})} \frac{2}{3} \Gamma^{\frac{3}{2}} \Big|_{\Gamma(z=H_{NL})}^{\Gamma(z=H_t)} \qquad \text{(A-33)}$$

Substituting Γ back into equation A-33 yields

$$M_{out} = -\rho_{in} \frac{\rho_{in}}{\rho_{out}} \frac{KWT_{in}}{3g(T_{in}-T_{out})} \left(\frac{\rho_{out}}{\rho_{in}} CpS_U^2 U^2 - \frac{\rho_{out}}{\rho_{in}} \frac{2gH_t(T_{in}-T_{out}))}{T_{in}} + \frac{2\Delta P_I}{\rho_{in}} \right)^{\frac{3}{2}}$$
$$+\rho_{in} \frac{\rho_{in}}{\rho_{out}} \frac{KWT_{in}}{3g(T_{in}-T_{out})} \left(\frac{\rho_{out}}{\rho_{in}} CpS_U^2 U^2 - \frac{\rho_{out}}{\rho_{in}} \frac{2gH_{NL}(T_{in}-T_{out})}{T_{in}} + \frac{2\Delta P_I}{\rho_{in}} \right)^{\frac{3}{2}} \qquad \text{(A-34)}$$

where the second term is zero by definition of H_{NL} in equation 2-19. The final equation for flowrate out of the opening is

$$M_{out} = (\rho_{out}\rho_{in})^{\frac{1}{2}} \frac{KWT_{in}}{3g(T_{in}-T_{out})} \left(CpS_U^2 U^2 - \frac{2gH_t(T_{in}-T_{out})}{T_{in}} + \frac{2\Delta P_I}{\rho_{out}} \right)^{\frac{3}{2}} \qquad \text{(A-35)}$$

A.4 The seven possible cases of door/window flow

P_b and P_t are flow coefficients based on the pressures at the bottom and the top of the opening and are defined in equations 2-69 and 2-70.

For $T_{in} > T_{out}$ there are three possible cases.

Case 1. All opening above H_{NL} - all flow out

$$M_{in} = 0$$

$$M_{out} = (\rho_{out}\rho_{in})^{\frac{1}{2}} \frac{KWT_{in}}{3g(T_{in}-T_{out})} \left(P_t^{\frac{3}{2}} - P_b^{\frac{3}{2}} \right) \qquad \text{(A-36)}$$

Case 2. All opening below H_{NL} - all flow in

$$M_{out} = 0$$

$$M_{in} = \rho_{out} \frac{KWT_{in}}{3g(T_{in}-T_{out})} \left(P_b^{\frac{3}{2}} - P_t^{\frac{3}{2}} \right) \qquad \text{(A-37)}$$

Case 3. H_{NL} in the opening with flow in below H_{NL} and flow out above H_{NL}.

$$M_{out}=(\rho_{out}\rho_{in})^{\frac{1}{2}}\frac{KWT_{in}}{3g(T_{in}-T_{out})}P_t^{\frac{3}{2}} \qquad \text{(A-38)}$$

$$M_{in}=\rho_{out}\frac{KWT_{in}}{3g(T_{in}-T_{out})}P_b^{\frac{3}{2}} \qquad \text{(A-39)}$$

For $T_{out} > T_{in}$ there are three possible cases.

Case 1. All opening above H_{NL} - all flow in

$$M_{out} = 0$$

$$M_{in}=\rho_{out}\frac{KWT_{in}}{3g(T_{in}-T_{out})}\left(P_t^{\frac{3}{2}}-P_b^{\frac{3}{2}}\right) \qquad \text{(A-40)}$$

Case 2. All opening below H_{NL} - all flow out

$$M_{in} = 0$$

$$M_{out}=(\rho_{out}\rho_{in})^{\frac{1}{2}}\frac{KWT_{in}}{3g(T_{in}-T_{out})}\left(P_b^{\frac{3}{2}}-P_t^{\frac{3}{2}}\right) \qquad \text{(A-41)}$$

Case 3. H_{NL} in the opening with flow out below H_{NL} and flow in above H_{NL}.

$$M_{out}=(\rho_{out}\rho_{in})^{\frac{1}{2}}\frac{KWT_{in}}{3g(T_{in}-T_{out})}(-P_b)^{\frac{3}{2}} \qquad \text{(A-42)}$$

$$M_{in}=\rho_{out}\frac{KWT_{in}}{3g(T_{in}-T_{out})}(-P_t)^{\frac{3}{2}} \qquad \text{(A-42)}$$

For $T_{in} = T_{out}$

In this case there is wind effect only and H_{NL} is undefined. It is not necessary to integrate a velocity profile over the opening height and an orifice flow equation is used to compute the flow through the opening.

$$M=\rho K_D W(H_t-H_b)\sqrt{\frac{2\Delta P}{\rho}} \qquad \text{(A-44)}$$

where $\rho = \rho_{in}$ for outflow and $\rho = \rho_{out}$ for inflow, and $\Delta P = P_{out,z} - P_{in,z}$. The sign of ΔP determines if the flow is in or out. Following the same convention as for other leaks, a positive ΔP results in inflow and a positive mass flow, M. The pressure difference, ΔP, across the opening is found using equation 2-18. Then

$$M=\rho K_D W(H_t-H_b)\left(CpS_U^2U^2+\frac{2\Delta P_I}{\rho_{out}}\right)^{\frac{1}{2}} \qquad \text{(A-45)}$$

where W is the width of the opening and K_D is a flow coefficient assumed to be 0.6.

A.5 The seven possible cases of attic pitched roof surface flow

For $T_a = T_{out}$

$P'_{T,a} = 0$ and there are wind pressures only. $H_{NL,r}$ is undefined and for each roof pitch

$$\Delta P_r=P_{I,a}+S_U^2CpP_U \qquad \text{(A-46)}$$

and

$$M_r=\rho\frac{C_r}{2}(\Delta P_r)^{n_r} \qquad \text{(A-47)}$$

where $M_r = M_{r,in}$ and $\rho = \rho_{out}$ for inflow (ΔP_r positive)

$M_r = M_{r,out}$ and $\rho = \rho_{in}$ for outflow (ΔP_r negative).

For $T_a \neq T_{out}$

To find the total flow through each roof pitch the flow must be integrated to allow for the change in pressures. The limits of integration for pressure are found at the roof peak height, H_p, and eave height, H_e and are

$$\Delta P_p = \Delta P_{L,a} + CpS_U^2 P_U - H_p P'_{T,a} \quad \text{(A-48)}$$

$$\Delta P_e = \Delta P_{L,a} + CpS_U^2 P_U - H_e P'_{T,a} \quad \text{(A-49)}$$

For $T_a > T_{out}$ there are three possible cases:
Case 1. All roof pitch above $H_{NL,r}$ - all flow out

$$M_{r,in} = 0$$

$$M_{r,out} = \frac{\rho_a \frac{C_r}{2}(\Delta P_p^{(n_r+1)} - \Delta P_e^{(n_r+1)})}{(H_p - H_e)P'_{T,a}(n_r+1)} \quad \text{(A-50)}$$

Case 2. All roof pitch below $H_{NL,r}$ - all flow in

$$M_{r,out} = 0$$

$$M_{r,in} = \frac{\rho_{out} \frac{C_r}{2}(\Delta P_p^{(n_r+1)} - \Delta P_e^{(n_r+1)})}{(H_p - H_e)P'_{T,a}(n_r+1)} \quad \text{(A-51)}$$

Case 3 $H_{NL,r}$ on the pitched surface with flow in below $H_{NL,r}$ and flow out above $H_{NL,r}$.

$$M_{r,out} = \frac{\rho_a \frac{C_r}{2}\Delta P_p^{(n_r+1)}}{(H_p - H_e)P'_{T,a}(n_r+1)} \quad \text{(A-52)}$$

$$M_{r,in} = \frac{\rho_{out} \frac{C_r}{2}\Delta P_e^{(n_r+1)}}{(H_p - H_e)P'_{T,a}(n_r+1)} \quad \text{(A-53)}$$

For $T_{out} > T_a$ there are three possible cases:

Case 1. All roof pitch above $H_{NL,r}$ - all flow in.

$$M_{r,out} = 0$$

$$M_{r,in} = \frac{\rho_{out}\frac{C_r}{2}(\Delta P_e^{(n_r+1)} - \Delta P_p^{(n_r+1)})}{(H_p - H_e)P'_{T,a}(n_r+1)} \quad \text{(A-54)}$$

Case 2. All roof pitch below $H_{NL,r}$ - all flow out.

$$M_{r,in} = 0$$

$$M_{r,out} = \frac{\rho_a\frac{C_r}{2}(\Delta P_e^{(n_r+1)} - \Delta P_p^{(n_r+1)})}{(H_p - H_e)P'_{T,a}(n_r+1)} \quad \text{(A-55)}$$

Case 3. $H_{NL,r}$ on the pitched surface with flow out below $H_{NL,r}$ and flow in above $H_{NL,r}$.

$$M_{r,out} = \frac{\rho_a\frac{C_r}{2}(-\Delta P_e)^{(n_r+1)}}{(H_p - H_e)P'_{T,a}(n_r+1)} \quad \text{(A-56)}$$

$$M_{r,in} = \frac{\rho_{out}\frac{C_r}{2}(-\Delta P_p)^{(n_r+1)}}{(H_p - H_e)P'_{T,a}(n_r+1)} \quad \text{(A-57)}$$

APPENDIX B

Appendix B: Attic tracer gas system error analysis

The basic equation for calculating ventilation rate for the tracer gas system used in this error analysis is based on equation 5-3. Neglecting the temperature correction equation 5-3 can be written as

$$Q_a = \frac{NV_{inj}}{\Omega^a_{R22}} \qquad \text{(B-1)}$$

where Q_a = attic ventilation rate [m^3air/s]

N = number of injection per hour [inj/hour]

V_{inj} = average quantity of R22 released per injection [m^3R22/inj]

Ω^a_{R22} = mean concentration of R22 tracer gas in the attic over one hour [m^3R22/m^3air]

The uncertainty in ventilation rate is given by

$$\frac{e_Q}{Q_a} = \sqrt{\left(\frac{e_N}{N}\right)^2 + \left(\frac{e_{V_{inj}}}{V_{inj}}\right)^2 + \left(\frac{e_{\Omega^a_{R22}}}{\Omega^a_{R22}}\right)^2} \qquad \text{(B-2)}$$

where the ϵ's are the errors for each parameter. The error in injection is one injection so $\epsilon_N = 1$. The error in the amount of R22 released per injection can be estimated from repeated calibrations. The number of injections for the injector in attic 6, which has a volume of approximately 7.4cm^3, to fill a one litre volumetric flask is 135 ± 1. Taking this as the standard deviations then the one standard deviation uncertainty is 0.5/135 = 0.0037. The standard deviation of averages of 135 samples is related to the uncertainty of a single injection as follows: The error for an average of several injections is equal to the error for a single release divided by the square root of the number of injections, thus

$$0.0037 = \frac{\frac{e_{V_{inj}}}{V_{inj}}}{\sqrt{135}} \qquad \text{(B-3)}$$

and for a single release

$$\frac{e_{V_{inj}}}{V_{inj}}=0.043 \qquad \text{(B-4)}$$

then for equation B-2 the uncertainty in the average volume per injection over a one hour period with N injections is

$$\frac{e_{V_{inj}}}{V_{inj}}=\frac{0.043}{\sqrt{N}} \qquad \text{(B-5)}$$

The error in mean concentration depends on the standard deviation of the set of readings taken during an hour. For the attic system there are usually 12 readings in an hour taken to find Ω^a_{R22}. Because the attic ventilation rates are relatively high and sensitive to wind fluctuations the standard deviation may be as high as 1ppm in 5ppm, thus measurements taken over an hour have standard deviation of $\pm(1/12)^{.5}$ which is approximately 0.289, and

$$\frac{e_{\Omega^a_{R22}}}{\Omega^a_{R22}}=\frac{0.289}{5}=0.058 \qquad \text{(B-6)}$$

Substituting these estimates into equation B-2 gives

$$\frac{e_Q}{Q_a}=\sqrt{\left(\frac{1}{N}\right)^2+\left(\frac{0.043}{\sqrt{N}}\right)^2+(0.058)^2} \qquad \text{(B-7)}$$

from which it can be seen that a large number of injections reduces the error.

For an example calculation the following values were used. The attics at AHHRF have a volume of $61m_3$, the injector volume is $7.4cm^3$ and a typical air change rate for attic 6 is 10 ACH. Sustituting these values into equation B-1 and solving for the number of injections gives N = 412 injections. N is then substituted into equation B-7 to yield an error of $\pm 35m^3$/hour or 6% of the ventilation rate. Because the attic ventilation rates are high and a large number of injections are

required at all times the error in mean concentration is more important than the injection resolution and the variability in injected volume. The estimated error for attic ventilation rates can be taken as ±6% over the whole range of ventilation rates.